

**Establishing a novel platform for phycobiliprotein assembly:
biosynthesis of the pink pigment phycoerythrobilin in
*Synechocystis***

vom Fachbereich Biologie

der Rheinland-Pfälzischen Technischen Universität Kaiserslautern-Landau

zur Verleihung des akademischen Grades Dr. rer. nat. genehmigte

Dissertation

von

Steffen Heck, M. Sc., geb. in Karlsruhe

Mündliche Prüfung: 14.01.2025

Dekan:

Prof. Dr. Stefan Kins

Promotionskommissionsvorsitzender:

Prof. Dr. Michael Schroda

Berichterstattende:

Prof. Dr. Nicole Frankenberg-Dinkel

Prof. Dr. Matthias Hahn

Table of Contents

Table of Contents	I
Abbreviations	IV
1. Introduction	1
1.1. Cyanobacteria and cryptophytes	1
1.2. Oxygenic photosynthesis and carbon fixation.....	4
1.3. Phycobilisomes and phycobiliproteins.....	7
1.4. Phycobiliprotein assembly by phycobiliprotein lyases	14
1.5. Bilin biosynthesis	17
1.6. Objectives of this work	21
2. Materials and methods	22
2.1. Microbial strains, materials, and chemicals	22
2.1.1. Microbial strains.....	22
2.1.2. Plasmids.....	23
2.1.3. Oligonucleotides	26
2.1.4. Chemicals	27
2.1.5. Culture media and supplements.....	27
2.1.6. Kits, enzymes and antibodies.....	29
2.1.7. Equipment and consumables	30
2.1.8. Sterilization.....	31
2.2. Molecular biological methods.....	32
2.2.1. Preparation of plasmid DNA	32
2.2.2. Determination of nucleic acid concentrations	32
2.2.3. Agarose gel electrophoresis.....	33
2.2.4. Polymerase chain reaction (PCR).....	33
2.2.5. Purification of linear DNA.....	34
2.2.6. Restriction endonuclease digestion of nucleic acids	34
2.2.7. Ligation of DNA fragments.....	34
2.2.8. Colony PCR.....	34
2.2.9. Site-directed mutagenesis	35

2.2.10.	Gibson Assembly®	35
2.2.11.	Golden Gate assembly and modular cloning (MoClo)	36
2.2.12.	Sequencing of DNA	38
2.3.	Microbiological methods.....	39
2.3.1.	Cultivation of microorganisms	39
2.3.2.	Cyanobacterial growth experiments	39
2.3.3.	Cryopreservation of microorganisms	40
2.3.4.	Preparation of chemically competent <i>E. coli</i> cells	40
2.3.5.	Transformation of chemically competent <i>E. coli</i> cells	41
2.3.6.	Conjugation of cyanobacteria via triparental mating	41
2.3.7.	Confocal laser scanning microscopy	42
2.3.8.	Light response curves and oxygen formation	42
2.4.	Biochemical and biophysical methods	44
2.4.1.	Production and isolation of recombinant proteins in <i>E. coli</i>	44
2.4.2.	Isolation of phycocyanin from <i>Synechocystis</i>	50
2.4.3.	Purification of recombinant proteins from <i>Synechocystis</i>	52
2.4.4.	Tryptic digestion in solution	53
2.4.5.	Tryptic in-gel digestion.....	54
2.4.6.	Separation of chromopeptides by RP-HPLC.....	55
2.4.7.	Desalting of peptides via STAGE tips	55
2.4.8.	Liquid Chromatography-Mass spectrometry (LC-MS) analysis	56
2.4.9.	Isolation of intact phycobilisomes from <i>Synechocystis</i>	57
2.4.10.	Protein precipitation	57
2.4.11.	Determination of protein concentration	58
2.4.12.	SDS-polyacrylamide gel electrophoresis (SDS-PAGE).....	58
2.4.13.	Western Blot and immunodetection of recombinant proteins	60
2.4.14.	Zinc-enhanced fluorescence.....	61
2.4.15.	Chlorophyll a extraction from cyanobacterial cells.....	62
2.4.16.	Determination of glycogen content.....	62
2.4.17.	Quantification of phycobiliproteins.....	63
2.4.18.	UV-Vis spectroscopy	63

2.4.19.	Fluorescence spectroscopy.....	64
3.	Results	65
3.1.	The putative PBP lyase CpcX of <i>Guillardia theta</i>	66
3.2.	Phycoerythrobilin biosynthesis in <i>Synechocystis</i>	68
3.2.1.	Biomass formation under modified phycobilin biosynthesis	69
3.2.2.	Photosynthetic activity and nutrient accumulation.....	70
3.2.3.	PEB production induces PBP diffusion in <i>Synechocystis</i>	75
3.2.4.	Modified PBPs are not incorporated into intact PBSs	78
3.2.5.	PEB binds to phycocyanin.....	82
3.2.6.	PEB is covalently attached to cysteine 84 of CpcA.....	83
3.3.	Assembly of phycoerythrin from <i>P. marinus</i> MED4	87
3.3.1.	Heterologous expression of phycoerythrin biosynthesis genes	87
3.3.2.	Production of <i>PmCpeB</i> and <i>PmCpeS</i>	89
3.3.3.	Heterologous phycoerythrin assembly	93
4.	Discussion	96
4.1.	Phycobiliprotein assembly in heterologous hosts.....	96
4.2.	Modified phycobilin biosynthesis in <i>Synechocystis</i>	100
4.2.1.	The physiology of <i>Synechocystis</i> under heterologous PEB biosynthesis ..	100
4.2.2.	Assembly of modified phycobiliproteins.....	104
4.3.	Assembly of the <i>P. marinus</i> MED4 phycoerythrin in <i>Synechocystis</i>	106
5.	Summary	109
6.	Zusammenfassung.....	111
	References.....	113
	<i>Curriculum vitae</i>.....	138
	Eidesstattliche Erklärung	139
	Darlegung des Eigenanteil.....	140
	Darlegung aller benutzten Hilfsmittel und Hilfestellungen.....	141
	Danksagung	142

Abbreviations

A	absorption
ACN	acetonitrile
Amp	ampicillin
AP	alkaline phosphatase
APC	allophycocyanin
APS	ammonium persulfate
BCIP	5-bromo-4-chloro-3-indoxyl phosphate
bp	base pairs
BSA	bovine serum albumin
BV	biliverdin
Cb	carbenicillin
CDS	coding sequence
Chl	chlorophyll
CLSM	confocal laser scanning microscopy
CV	column volume
Da	dalton
DEAE	diethylaminoethyl
DHBV	dihydrobiliverdin
DMF	dimethylformamide
DMSO	dimethyl sulfoxide
DTT	dithiothreitol
ESI	electrospray ionization
FA	formic acid
Fd	ferredoxin
FDBR	ferredoxin-dependent bilin reductase
FPLC	fast protein liquid chromatography
Glu	glutamic acid
HL	high light
HO	heme oxygenase
HPLC	high performance liquid chromatography
IPTG	Isopropyl- β -D-thiogalactopyranoside
Kan	kanamycin
LB	lysogenic broth Luria Bertani
LL	low light
MeOH	methanol
MQ	milliQ water, ultra-pure water
MS	mass spectrometry
MW	molecular weight
MWCO	molecular weight cut off
NBT	nitro blue tetrazolium chloride
OD _{x nm}	optical density at a wavelength of x nm
PAM	pulse amplitude modulation
PBP	phycobiliprotein
PBS	phycobilisome
PC	phycocyanin
PCB	phycocyanobilin
PCR	polymerase chain reaction
PE	phycoerythrin
PEB	phycoerythrobilin
PebA	15, 16-dihydrobiliverdin:ferredoxin-oxidoreductase
PebB	phycoerythrobilin:ferredoxin-oxidoreductase
PebS	phycoerythrobilin synthase
PEC	phycoerythrocyanin
PS	photosystem
PUB	phycourobilin
PVDF	polyvinylidene fluoride
P Φ B	phytochromobilin
RBS	ribosome binding site
ROS	reactive oxygen species
RP-HPLC	reversed phase high performance liquid chromatography
Rpm	revolutions per minute
RT	room temperature

sdm	site-directed mutagenesis
SDS	sodium dodecyl sulfate
SDS-PAGE	sodium dodecyl sulfate polyacrylamide gel electrophoresis
SEC	size exclusion chromatography
Sp	spectinomycin
TEMED	N,N,N',N'-tetramethylethane-1,2-diamine
TFA	trifluoroacetic acid
TOF	time of flight
UV/Vis	ultra violet/visible
v/v	volume per volume
VC	vector control
w/v	weight per volume
WT	wild type
X-Gal	5-bromo-4-chloro-3-indolyl- β -D-galactopyranoside

1. Introduction

1.1. Cyanobacteria and cryptophytes

Cyanobacteria

Cyanobacteria, formerly called blue-green algae, are a diverse group of prokaryotic organisms found in almost every ecosystem ranging from terrestrial to marine and freshwater environments. They are also found in extreme habitats like hot springs (Ward *et al.*, 1998), Antarctic environments (Pandey *et al.*, 2004) and lakes with broad ranges of pH and salinity (Dadheech *et al.*, 2013). Probably based on the ability to survive in such versatile environments, the lineage of cyanobacteria evolved into a group of diverse morphology and physiology. In terms of morphology, they are mostly divided into unicellular and filamentous strains as *Synechocystis* sp. PCC 6803 (hereafter *Synechocystis*) and *Spirulina platensis*, respectively (Figure 1).

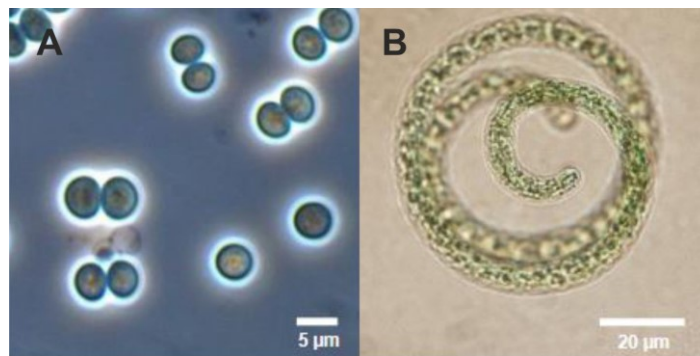


Figure 1: Microscopic images of cyanobacterial cells. (A) Unicellular *Synechocystis* cells with a diameter of three to four μm . (B) Filament of edible *Spirulina* cells. Adapted from Kachel (2021).

In accordance with their morphology, cyanobacteria are metabolically versatile, dynamic and responsive. They all share the capability to perform oxygenic photosynthesis by utilizing light-energy to convert carbon dioxide (CO_2) into chemical substitutes. Cyanobacteria have been found in fossils more than 3.5 billion years ago and are proposed to be the earth's first oxygen-forming organisms (Blank 2004) leading to the creation of the oxygen-rich atmosphere we breathe today (Bengtson 1994). Many species have the ability to fix atmospheric nitrogen, the second-most important element for any living organisms. Nitrogen is required for amino acid biosynthesis and reflects a fundamental component for DNA- as well as RNA biosynthesis. Ironically, reduction of elemental nitrogen by the nitrogenase is highly sensitive to oxygen (Gallon 1981). Cyanobacteria developed a set of strategies to overcome this circumstance. A number of filamentous cyanobacteria form so-called heterocysts which lack photosystem II

(PS II). In the case of nonheterocystous cyanobacteria, nitrogen fixation is performed at night, when photosynthetic activity is reduced. Based on the ability to fix CO₂ and nitrogen, cyanobacteria play an important role in the biogeochemical carbon- and nitrogen cycle and therefore also in the earth's climate regulation (Galloway *et al.*, 2004, Moisaner 2017, Zwirgmaier *et al.*, 2008). Approximately 20 – 30 % of the organic carbon is originating from cyanobacterial carbon fixation. Marine *Synechococcus* and *Prochlorococcus* species occur in almost every oceanic habitat and reflect the most abundant photoautotrophic organisms on earth. *Synechococcus* species mostly occupy coastal waters, coexist in ecological niches with *Prochlorococci* but also extend their habitat to arctic regions. In contrast, *Prochlorococci* are mainly found in warm oceanic ecosystems as in the Indian sea and the east Pacific Ocean in depths of 100 to 200 m. Both groups contribute approximately 25 % to the primary production and their abundance within ecological niches seems to be regulated by seasonal changes (Chisholm 1992, Flombaum *et al.*, 2013).

Cyanobacteria are intriguing not only from an ecological point of view, some species are used as a platform in basic research to study oxygenic photosynthesis. The amenability of some cyanobacterial species to genetic engineering promoted the wide use of these organisms for the investigation of gene functions and the utilization as chassis for biotechnological purposes. Following its isolation from a freshwater lake in 1968 (Stanier *et al.*, 1971), *Synechocystis* became one of the most extensively studied cyanobacterial model organism. Based on its ability to grow auto- and heterotrophically, it provides a solid basis for the investigation of the photosynthetic electron transport chain by genetic modification which could be lethal in species lacking such metabolic properties. Consequently, the impairment of photosynthesis-derived carbon fixation by genetic modifications can be compensated by providing sugars as an energy source (Williams 1988). Within the last decades, using such cyanobacterial platforms unravelled a vast number of molecular mechanisms of several biological pathways involved in, e.g. nitrogen- (Katayama & Osanai 2024, Lin *et al.*, 2023) and carbon metabolism (Lu *et al.*, 2023, Ortega-Martínez *et al.*, 2022) as well as photosynthesis (Bolte *et al.*, 2008, Wang *et al.*, 2010). Besides the research of fundamental biological processes, *Synechocystis* is commonly used for biotechnological applications. A variety of biofuels have been produced with this platform including isobutanol (Varman *et al.*, 2013) and molecular hydrogen (Kossalbayev *et al.*, 2020). Moreover, commodity chemicals were also synthesized as the commonly used solvent acetone (Zhou *et al.*, 2012) or ethylene (Ungerer *et al.*, 2012) and isoprene (Lindberg *et al.*, 2010), important precursors for the production of polymers and rubbers. In conclusion, *Synechocystis* is becoming

progressively intriguing for its potential in heterologous biosynthesis of target compounds, owing to its metabolic versatility as a cyanobacterium, genetic accessibility and straightforward culturing capabilities in laboratory environments. The development of *Synechocystis* as such a platform is further promoted by a recently published, standardized toolbox for the preparation of DNA constructs used for genetic modification (Vasudevan *et al.*, 2019). Here, characterized genetic elements (as promoters and terminators) were introduced to a standardized DNA assembly strategy based on Golden Gate cloning, known as MoClo, which was originally invented for the preparation of constructs for the genetic modification of plants (Engler *et al.*, 2014, Weber *et al.*, 2011).

Cryptophyte algae

Besides the metabolic capabilities of cyanobacteria in biotechnology and their influence on global biogeochemistry, they contributed to the evolution of plants as well as red, green and cryptomonad algae. Cryptomonad species are unicellular, eukaryotic algae formed by two events of endosymbiosis. Only one genus of the cryptomonads pursues a heterotrophic lifestyle, while all other representatives perform oxygenic photosynthesis and are therefore able to live phototrophic (Kugrens & Lee 1992, Martin-Cereceda *et al.*, 2010).

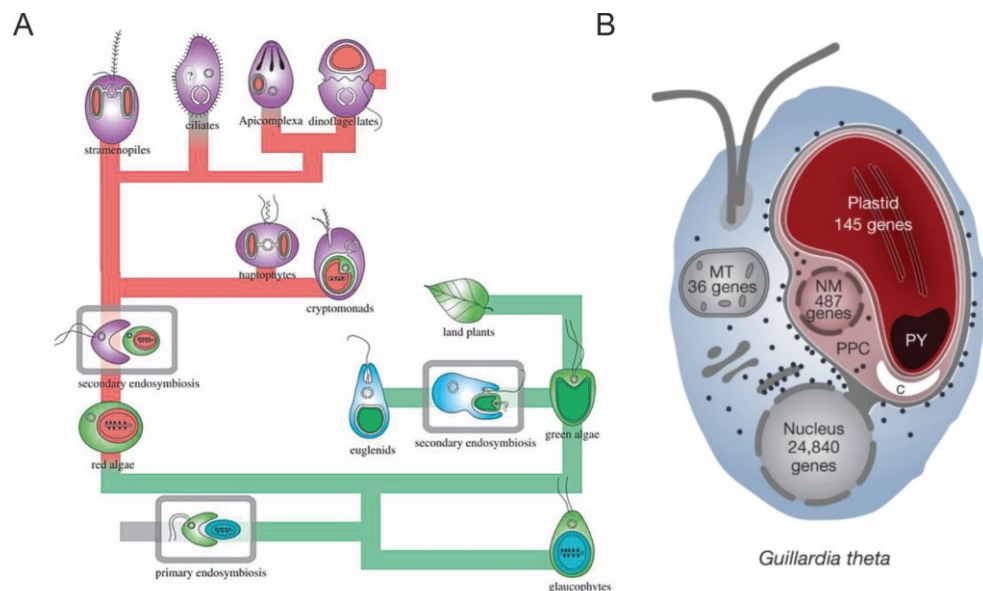


Figure 2: Endosymbiosis in the evolution of cryptophytes. (A) Plastid lineages of plants and green algae (green line) as well as red algae (red). Events of endosymbiosis are labelled in boxes. A single event of primary endosymbiosis led to the development of three lineages (glaucophytes, green- and red algae). Adapted from Farhat (2020). (B) Genome architecture of the cryptophyte *G. theta*. Based on secondary endosymbiosis, cryptophytes possess four genomes: the nucleus, the mitochondrial genome (MT), the former red algae nucleus called nucleomorph (NM) and the plastid genome. Cryptophytes have plastids surrounded by four membranes. The outer plastid membrane forms a continuous membrane network with the envelope of the nucleus. The complex surface is covered with ribosomes, which co-translationally transport proteins into the inner compartment of the organelle. PPC: periplastidial compartment, C: carbohydrate, PY: pyrenoid. Adapted from Curtis *et al.*, (2012).

Initially, in a primary endosymbiosis event, a eukaryotic host cell engulfed a cyanobacterial cell leading to the generation of plants, Chlorophyta (green algae), Rhodophyta (red algae) and Glaucophyta (Howe *et al.*, 2008, Palmer *et al.*, 2004) (Figure 2A). During evolution, an event of secondary endosymbiosis took place leading to the development of cryptomonads, which are also called cryptophytes (Burki *et al.*, 2012, Keeling 2009). Here, a rhodophyte cell was incorporated by another heterotrophic eukaryotic ancestor cell and the remaining of the red algae was continuously reduced to a more complex plastid with a degenerate nucleus, the nucleomorph (Stoebe & Maier 2002). Based on the evolution of cryptophytes, they possess four different genomes (Figure 2B). While the mitochondrial and plastid genome originate from prokaryotic ancestors (Hauth *et al.*, 2005, Rogers *et al.*, 2006), the nuclear and nucleomorph genomes derive from eukaryotes (Curtis *et al.*, 2012, Lane *et al.*, 2007). The presence of four different genomes led to the relocation of genes from the mitochondrion, the plastid and the nucleomorph to the nucleus via horizontal gene transfer (Timmis *et al.*, 2004). Consequently, a multitude of proteins require an elaborate protein transport network using signal- and transit sequences to overcome the complexity of the cryptophytic architecture (Bolte *et al.*, 2009, Douglas *et al.*, 2001).

1.2. Oxygenic photosynthesis and carbon fixation

The evolution of oxygenic photosynthesis constitutes the most important metabolic innovation providing the basis for almost all life on earth. It allowed life to generate energy by conversion of solar power and water into chemical substitutes. A multitude of organisms like plants, algae and cyanobacteria perform photosynthesis as they are capable of capturing light and CO₂ via cascades of oxidation-reduction reactions by utilizing nicotinamide adenine dinucleotide phosphate (NADP⁺) as the terminal electron acceptor (Cheng & Fleming 2009). These cascades indirectly lead to the conversion of light-energy into an electrochemical proton gradient, which generates a proton-motive force to drive ATP formation by the ATP synthase. The photosynthetic machinery is embedded in a system of internally folded membranes, the so-called thylakoid membranes (Figure 3).

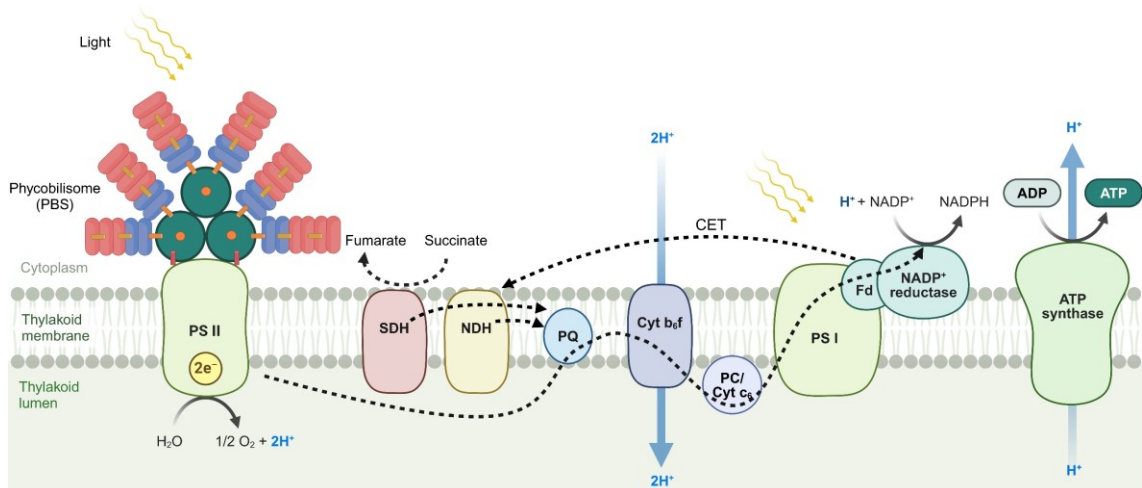


Figure 3: Photosynthetic electron transport chain of cyanobacteria. Shown is the cyanobacterial phycobilisome (PBS) and the thylakoid membrane with embedded protein complexes responsible for different routes of electron transfer (dashed arrows) across the membrane. In the linear electron transfer, electrons for reductant generation (NADPH) are derived from water hydrolysis at PSII. They are forwarded to PSI via plastoquinone (PQ), cytochrome b_6f (Cyt b_6f) and either plastocyanin (PC, encoded by *petE*) or the cytochrome c_6 (Cyt c_6). Both PC (*petE*) and Cyt c_6 are located in the thylakoid lumen and pass on the electrons to ferredoxin (Fd), but are regulated by the availability of copper and iron (Raven *et al.*, 1999). Eventually Fd provides an NADP⁺ reductase with the electrons for NADPH formation. The transport of electrons produces a hydrogen gradient across the thylakoid membrane, which drives the ATP-synthase to synthesize ATP from ADP. In cyanobacteria, different routes for electron transfer are present. While electron transfer routes from photosynthesis and respiration are separated in plants, both pathways are linked in cyanobacteria via electron carriers as e.g. Cyt b_6f and PQ. Hence, the succinate dehydrogenase (SDH) can introduce electrons derived from respiration in the thylakoid membrane electron transport chain (Cooley & Vermaas 2001). In addition, cyanobacteria are able to perform cyclic electron transfer (CET) from Fd to NADPH dehydrogenases (NDH) to further regulate ATP and reductant generation. Created with BioRender.com.

The chlorophyll molecules in the reaction centres of PS I and II are excited by photons of light. This allows the utilization of electrons derived from water hydrolysis by the PS II associated oxygen evolving complex, while generating protons and O₂ as byproducts (Vinyard *et al.*, 2013). The electrons released by water hydrolysis are transported via the PS II, plastoquinone (PQ), cytochrome b_6f (Cyt b_6f , [E.C. 7.1.1.6]), plastocyanin (PC encoded by *petE*) or cytochrome c_6 , and PS I to the ferredoxin (Fd) (Durán *et al.*, 2004, Jordan *et al.*, 2001, Kurisu *et al.*, 2003). The reduced ferredoxin supplies the Ferredoxin-NADP⁺-reductase (FNR) [E.C. 1.18.1.2] with electrons to generate the reductant NADPH which is, in addition to ATP, necessary for the cellular metabolism and the biosynthesis of energy-rich compounds derived from the CO₂ fixation in the Calvin-Benson-Bassham (CBB) cycle (Nagarajan & Pakrasi 2016). The CO₂ fixation reflects an electron sink for the reductants generated during oxygenic photosynthesis. If the sink capacity of the CBB cycle is saturated, the photosynthetic electron transport chain (PETC) potentially gets excessively reduced, which leads to the formation of reactive oxygen species (ROS). Disproportionate reduction of the PETC and generation of ROS can cause severe damage to the PSs demanding the development of alternative electron transport pathways as the cyclic electron transfer from Fd to PQ via NADPH

dehydrogenases [E.C. 1.6.99.1] (Battchikova *et al.*, 2011). In combination with electrons provided by, e.g. cellular respiration via the succinate dehydrogenase SDH [E.C. 1.3.5.1], these routes control the ratio of the proton-motive force for ATP generation and reductant formation or in short, the redox balance of the cell (Mullineaux 2014).

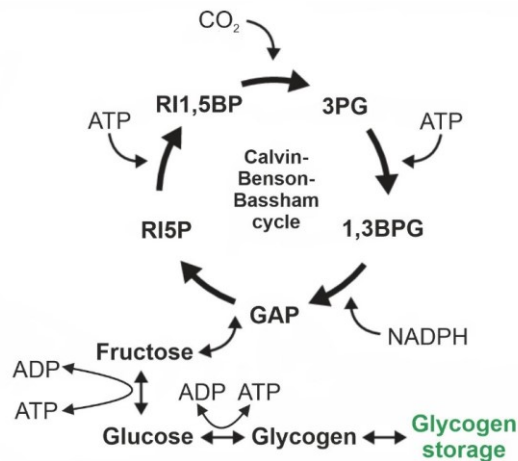


Figure 4: Calvin-Benson-Bassham cycle and glycogen accumulation. Shown is a simplified version glycogen synthesis derived from CO₂ fixation in the CBB cycle. The enzyme RuBisCO performs the carboxylation of ribulose-1,5-bisphosphate (RI1,5BP) using CO₂ to form two molecules of 3-phosphoglycerate (3PG). 3PG is then phosphorylated by the ATP-dependent phosphoglycerate kinase to yield 1,3-bisphosphoglycerate (1,3BPG). 1,3BPG is subsequently reduced to glyceraldehyde-3-phosphate (GAP) by a dehydrogenase using electrons from NADPH. Six GAP molecules are necessary to produce one usable GAP, since the remaining five molecules are utilized to regenerate the CO₂ acceptor RI1,5BP in an ATP-dependent reaction cascade. The residual GAP is then employed for fructose-, glucose and glycogen biosynthesis. Glycogen, the major carbon-storage compound derived from photosynthesis, is accumulated as a deeply branched molecule. NADPH and ATP required for all reactions in the CBB are derived from the photosynthetic electron transport chain. Adapted from Wijffels *et al.*, (2013).

The majority of carbon for biomass formation in cyanobacteria is accumulated by the CBB cycle (Figure 4) (Iñiguez *et al.*, 2020, Machingura & Moroney 2018). The first enzyme for carbon fixation via the CBB, namely Ribulose-1,5-bisphosphate carboxylase/oxygenase (RuBisCO) [E.C. 4.1.1.39], is an enzyme with two functions. It is catalysing both the carboxylation and oxygenation of ribulose-1,5-bisphosphate (RI1,5BP). Carboxylation of RuBisCO is the first step of carbon fixation in the CBB. Here, CO₂ is linked to one molecule of RI1,5BP, which dissociates into two molecules of 3-phosphoglycerate (3PG). Following phosphorylation of 3PG by using ATP, the formed 1,3-bisphosphoglycerate (1,3BPG) is then reduced to glyceraldehyde-3-phosphate (GAP) by electrons derived from NADPH. To generate one usable molecule of GAP, six molecules need to be formed by the CBB. Subsequently, one molecule GAP is introduced into different pathways responsible for carbohydrate biosynthesis as fructose, glucose, sucrose and the storage compound glycogen, the equivalent of starch in plants. Through a series of enzymatic reactions, the remaining five molecules GAP are utilized for the regeneration of the CO₂ acceptor ribulose-1,5-bisphosphate (RI1,5BP) via the intermediate ribulose-5-phosphate (RI5P). The energy and reductants required for the

biosynthesis of these carbon-rich compounds derive from ATP and NADPH produced via the photosynthetic electron transport chain. In contrast, the carboxylase activity leads to the accumulation of the toxic intermediate 2-phosphoglycolate, which needs to be rapidly metabolized by photorespiration (Farquhar *et al.*, 1980).

Photosynthetic electron transport, and therefore also carbon fixation, are not only influenced by the regulation of cyclic and linear electron transport, but also by the light-harvesting capacity of phototrophic organisms. A variety of photosynthetic organisms employ light-harvesting complexes containing chlorophyll *a* (Chl) as a chromophore, which are responsible for the absorption of blue- (400 nm – 500 nm) and red-light (600 nm – 700 nm). Based on environmental factors, phototrophs as cryptophytes, red algae and cyanobacteria developed accessory light-harvesting antenna proteins, the PBPs (Apt *et al.*, 1995). These PBPs extend the organisms ability of light-harvesting by filling the so called “green gap” between 490 nm and 650 nm (Csatorday *et al.*, 1987, Kehoe 2010, Searle *et al.*, 1978). They absorb the range of visible light insufficiently covered by Chl and transfer the light-energy to the PSs by radiation-free energy transfer to enhance photosynthetic activity (Glazer 1977, Grossman *et al.*, 1993, Steiner *et al.*, 2003). In cyanobacteria, such as *Synechocystis*, these accessory pigments are arranged in rod-shaped antenna complexes, called phycobilisomes (PBSs) which are associated with the cytosolic surface of the thylakoid membrane.

1.3. Phycobilisomes and phycobiliproteins

PBPs are multi-subunit pigment-protein complexes commonly found in cryptophytes, red algae and cyanobacteria. They constitute up to 50 % of the soluble protein content of the cell and funnel the incoming light-energy to enhance oxygenic photosynthesis. In most cyanobacteria and red algae, these accessory pigments are arranged in special light-harvesting complexes, the PBSs. The well-known PBS model of *Synechocystis* consists of the core-forming allophycocyanin (APC), which is surrounded by up to six rods of phycocyanin (PC), giving the PBS its hemidiscoidal shape (Figure 5A). The APC core consists of three cylinders, each composed of four trimeric APC discs. The PBS rods are formed by three stacks of PC and every individual stack consists of two trimeric discs. In some marine strains of *Synechococcus*, however, the PBS rods additionally harbour the PBP phycoerythrin (PE) on distal side of the PBS (Six *et al.*, 2007) (Figure 5B).

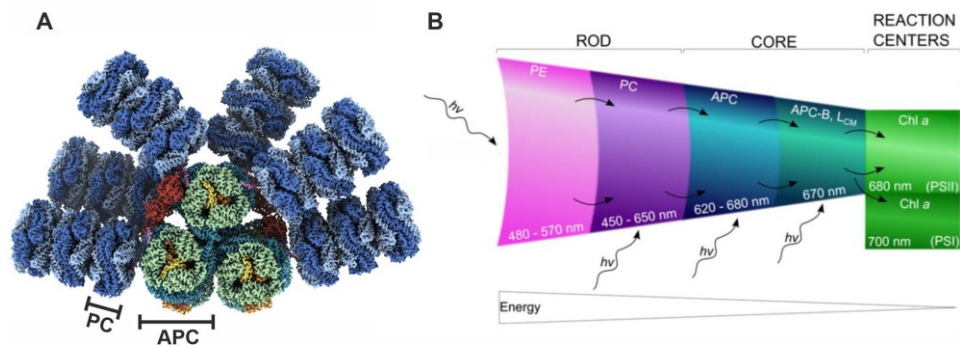


Figure 5: Structure of the PBS in *Synechocystis* and utilization of solar energy in PBSs containing both PE and PC PBPs in the PBS rods. (A) Phycobilisome structure of *Synechocystis* derived from cryo-EM density maps. The macromolecular structure is composed of three cylindrical APC trimers as the PBS core and six peripheral rods each consisting of three phycocyanin hexamers. Adapted from Dominguez-Martin *et al.*, (2022). **(B)** Funneling of light-energy by the PBS complex containing both PC and PE PBPs in the PBS rods. Based on the PBP content in PBSs, high-energy green light (480 nm – 570 nm) is absorbed by phycoerythrins (PE), which is passed down by phycocyanins (PC), allophycocyanins (APC) and eventually the terminal emitters APC-B and L_{cm} to the PS reaction centres via radiation-free energy transfer. Adapted from Pittera (2015).

The antenna complex captures solar energy through the absorption of high-energy light by the distal PBPs. This energy is then hierarchically transferred via radiation-free energy transfer to the proximal PBPs, the APC core, and ultimately to the Chl in the photosynthetic reaction centres, where charge separation drives the photosynthetic electron transport chain (Figure 5B). The chromophores of PBPs, which are responsible for the absorption of light, refer to a subspecies of linear tetrapyrroles, the so-called phycobilins. They are connected via thioether bonds to the PBP subunits and provide the proteins with spectral properties. Based on the phycobilin-chromophores' energy levels, cyanobacterial PBPs primarily are categorized into three different classes (Sui 2021). The first class absorbs high-energy light and consists of PEs or phycoerythrocyanins (PECs) at the core-distal ends of the rods. PEs covalently bind phycoerythrobilin (PEB) and, in some cases, phycourobilin (PUB), which gives the proteins the capability to absorb light-energy between 480 nm and 570 nm. In contrast, PECs contain the bilins phycoviolobilin (PVB) and phycocyanobilin (PCB) providing them with spectral properties between 565 nm and 600 nm. The second class consists of the PBS rod protein PC with attached PCB chromophores for light-harvesting of intermediate light-energy in a range of 620 nm and 650 nm. And lastly, APCs with bound PCB phycobilins as the main component of the core, which absorbs low-energy light between 650 nm and 680 nm. In contrast to the PBS rods, the structure of the APC core is more complex. As already mentioned, the PBS core consists of three cylinders of APCs. The cylinder-forming discs thereby contain varying subunits of APC. While the top cylinder in the PBS core consists of the subunits ApcA and ApcB with a small core linker protein forming a short-wavelength APC ($\lambda_{max} = \sim 650$ nm), the composition of the two

asymmetrically arranged bottom cylinders is more complex. Both bottom cylinders contain modified APC discs in addition to the regular trimers assembled by the α -subunit ApcA and the β -subunit ApcB. Either the α -subunit is replaced by ApcD (Peng *et al.*, 2014) or the β -subunit is substituted by ApcF (Calzadilla *et al.*, 2019), the latter is interacting with the chromophorylated core-membrane linker ApcE (Figure 5B, APC-B, L_{CM}). All three components harbour single PCB chromophores which provides the proteins with red shifted spectral properties ($\lambda_{max} = \sim 670 \text{ nm} - 680 \text{ nm}$) to fill the gap in energy transfer between the upper core cylinder and the chlorophyll in the photosynthetic reaction centre. Based on their function, they are designated as the terminal emitters of the PBS.

The PBS consists of chromophorylated, disc-shaped PBPs and a series of species-specific linker polypeptides, the latter serve several functions within the PBS. They enable, e.g. assembly of PBS subcomplexes, determine the position of particular PBPs in the macromolecular structure, modulate the spectral properties of PBPs to promote unidirectional light-energy transfer and serve as the scaffolding proteins to form the 7 MDa to 15 MDa large light-harvesting antenna complex (Figure 6). In *Synechocystis*, two copies of the major scaffolding protein ApcE (orange) connect the two bottoms with the top APC cylinders to stabilize the PBS core complex (Domínguez-Martín *et al.*, 2022). The rod core linker (CpcG1 in pink) facilitates attachment of the PBS core to the first stack of the rod-forming PC (Kondo *et al.*, 2005). Arrangement of two further PC discs is specified by the rod linkers CpcC1 (light pink) and CpcC2 (purple), which connect the second and the third disc to the PBS substructure, respectively (Arteni *et al.*, 2009). Eventually, the distal stack of PC is capped by CpcD (light purple).

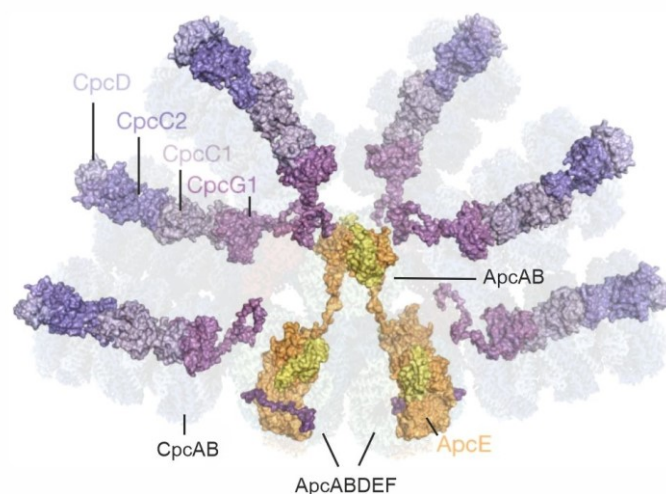


Figure 6: Linker proteins necessary for PBS assembly in *Synechocystis*. The major scaffolding protein ApcE links the two bottoms (2x ApcABDEF) with the upper APC cylinder (ApcAB) to form the PBS core. While the rod-core linker CpcG1 connects the APC core with the first stack of PC, the remaining two linkers CpcC1 and CpcC2 connect the first with the second and the second with the third stack of PC, respectively. Eventually, the last stack of PC is capped by CpcD. Adapted from Dominguez-Martin *et al.*, (2022).

Prior to the assembly of the antenna complex, the chromophorylation of the PBP subunits and their assembly to disc-shaped $(\alpha\beta)_3$ trimers or $(\alpha\beta)_6$ hexamers is required. Each of the PBP subunits typically binds one to three phycobilins, covalent linkage thereby proceeds in a specific order (Carrigee *et al.*, 2021, Zhao *et al.*, 2007). The chromophore attachment sites including the respective phycobilins are shown in Figure 7. In *Synechocystis*, PC binds three PCB molecules in total, one PCB at cysteine residue 84 in CpcA and two PCB at cysteine residue 82 and 153 in CpcB (Marx & Adir 2013). In contrast, APC contains only two covalently attached PCBs. While the α -subunits carry a PCB at cysteine residue 81 (CpcA and CpcD), the β -subunits have one PCB covalently attached at position 82 (Peng *et al.*, 2014).

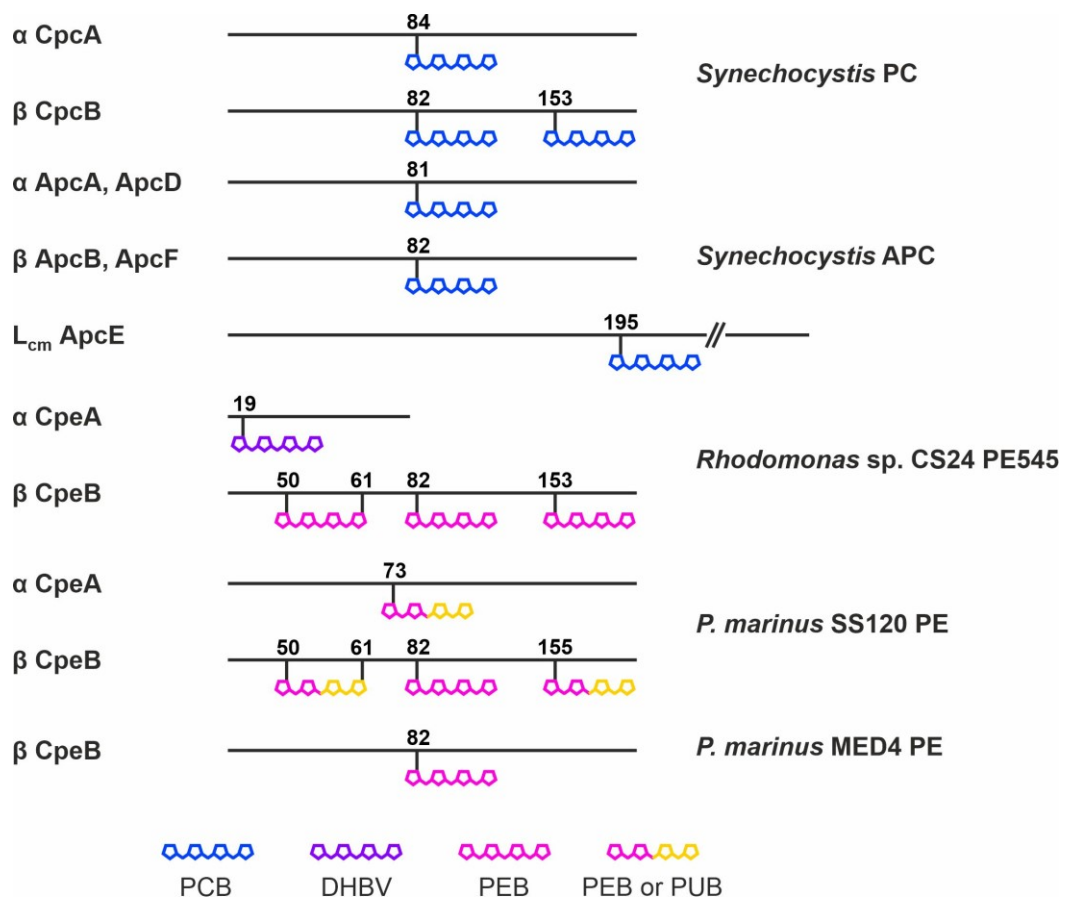


Figure 7: Post-translational modifications of PBPs in cyanobacteria and cryptophytes. Shown are the chromophorylation pattern of the *Synechocystis* APC and PC, the cryptophyte *Rhodomonas* sp. CS24 PE545 as well as the PEs of the *P. marinus* strains SS120 and MED4. Cysteine residues for covalent attachment of linear tetrapyrroles are indicated as numbers (according to their amino acid position within the protein sequence of the respective subunit) and the type of linked phycobilin is illustrated in colour (blue = PCB, purple = 15,16-dihydrobiliverdin (DHBV), pink = PEB, yellow = PUB). For *Synechocystis* APC, the α -subunits (ApcA, ApcD) and β -subunits (ApcB, ApcF) each harbour one PCB molecule at cysteine residues 81 and 82, respectively. In addition, the chromophorylated core-membrane linker L_{CM} contains one PCB at cysteine residue 195. In contrast to the characterized *Synechocystis* PBPs, the crystal structure of the *Rhodomonas* sp. CS24 PE545 serves as a model for cryptophyte PBPs as in *G. theta* (Wilk *et al.*, 1999). Although all homologous cysteine residues responsible for phycobilin binding are present, experimental data to elucidate the PE545 structure in *G. theta* remains elusive. The post-translational modifications of the *P. marinus* SS120 PE are mostly unknown, only a PUB to PEB ratio of 3:1 has been proposed (Steglich *et al.*, 2003). Therefore, potentially bound chromophores are labelled in multiple colours. In contrast, *in vitro* studies already showed the covalent attachment of PEB to cysteine residue 82 of the *P. marinus* MED4 CpeB by the PBP lyase CpeS (Wiethaus *et al.*, 2010).

After chromophore attachment, formation of PBSs is a step-wise process by successive addition of PBP-containing building blocks (Figure 8). Initially, the apo-proteins compete for the chromophores which are attached to specific cysteine residues by so-called PBP lyases. While attachment of chromophores is necessary for the formation of a stable $\alpha\beta$ heterodimer, accumulation to $(\alpha\beta)_3$ trimers occurs spontaneously. With the $(\alpha\beta)_3$ trimer as the basic module of PBSs, these units form the $(\alpha\beta)_6$ hexamer with a linker protein in its central cavity. Units of PBPs and linkers consequently form the final structure of a rod, which is attached to the core consisting of APC.

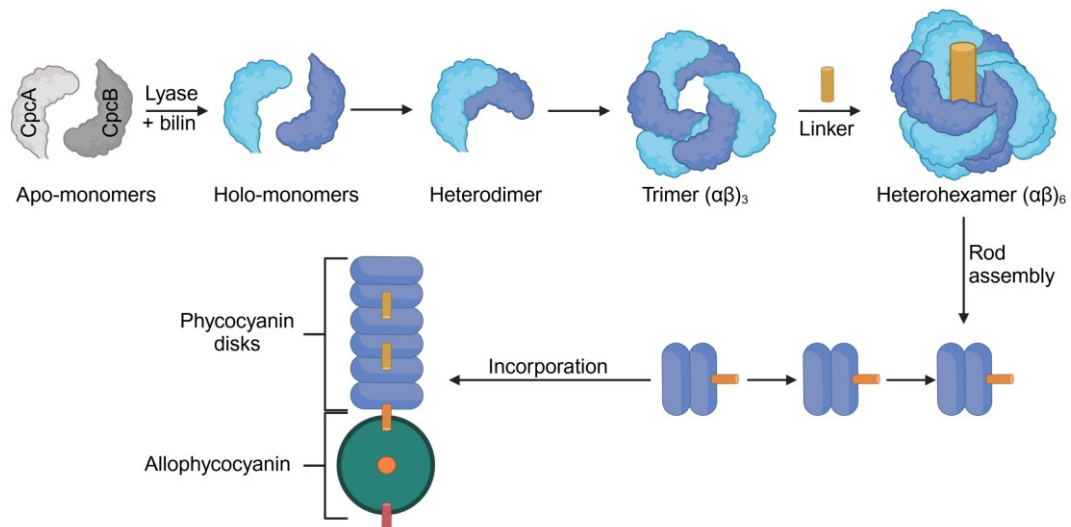


Figure 8: PBP and PBS rod assembly in *Synechocystis*. After chromophorylation of the Apo-monomers CpcA and CpcB, they form $\alpha\beta$ heterodimers and subsequently assemble to $(\alpha\beta)_3$ trimer. These accumulate to $(\alpha\beta)_6$ hexamers with a linker in its central cavity. They stack face to face to form the rods of the PBS and get attached to the APC core of the complex via linkers. Created with BioRender.com.

Compared to most cyanobacteria, cryptophyte PBPs reflect an interesting exception with respect to their structure. They carry some phycobilin chromophores which are not utilized for prokaryotic light-harvesting as 15,16-dihydrobiliverdin (15,16-DHBV) (Wedemayer *et al.*, 1992). 15,16-DHBV is only known as an intermediate molecule during cyanobacterial PEB biosynthesis (Frankenberg *et al.*, 2001). Consistent with unusual chromophores, cryptophytic PBPs assemble to rather atypical structures in a quite complex pathway (Glazer & Wedemayer 1995, Wilk *et al.*, 1999). In contrast to known cyanobacterial antenna complexes facing the cytosolic side of the thylakoid membrane, the cryptophyte *G. theta* harbours highly modified, soluble PBPs inside the thylakoid lumen (Broughton *et al.*, 2006, Gantt *et al.*, 1971, Laurel & Miller 1989). To facilitate efficient transfer of solar energy, these PBPs are densely packed inside the thylakoid lumen (Doust *et al.*, 2006, Lichtlé *et al.*, 1980, Scholes 2010). They consist of two very similar α -subunits of eukaryotic origin and two identical β -subunits of prokaryotic ancestry. Based on the complex architecture of the cryptophyte cell and the relocation of genes across all four genomes, the α -subunits (CpeA) of *G. theta* are subjected to an

elaborate transportation process (Figure 2B). While being encoded in the nucleus, CpeA has been postulated to be co-translationally transported (by the Sec secretion system) from the cytosol to the outer envelope of the complex plastid, the rough endoplasmic reticulum. Here, the first signal peptide of CpeA is cleaved and the accessible transit peptide is most likely responsible for the transport across the periplastidial membrane and the outer as well as inner plastid membrane (Gould *et al.*, 2006, Sommer *et al.*, 2007). Eventually, CpeA forms a heterodimer with the plastid-encoded β -subunit CpeB yielding the PBP PE545, which is very likely translocated (by the twin arginine translocation pathway) into the thylakoid lumen (Kieselbach *et al.*, 2018, Overkamp *et al.*, 2014). While the β -subunit shows high homology to the cyanobacterial equivalent, the α subunits are completely unrelated to any characterized PBPs, which also drives curiosity for the identification of the corresponding PBP lyase and its mode of action. According to studies on the close relative *Rhodomonas* sp. CS24, each of the α -holoproteins carry a conserved bilin-binding motive at a cysteine residue homologous to the Cys₁₉ location, which is occupied by one molecule of 15,16-DHBV (Figure 7) (Wilk *et al.*, 1999). In contrast, the β -subunit provides binding sites for three PEB molecules: the first chromophore is connected to the Cys₅₀ and Cys₆₁ sites via the A- and D-ring, whereas the others establish one covalent bond between the A-ring and the Cys₈₂ or Cys₁₅₈ residue (Doust *et al.*, 2004). Since most of the evidence is based on extraction and analysis of intact PBPs of some cryptomonad relatives, the mechanism of the post-translational assembly of the *G. theta* PE545 remains mostly elusive.

Unusual PBPs are not only found in cryptophytes, but also in some marine cyanobacterial species as in, e.g. the *Prochlorococcus* genus. In contrast to other prokaryotic light-harvesting systems, *Prochlorococcus* species lack PBSs but mainly employ divinyl-chlorophyll (DV) complexes, the *a*- and *b*-prochlorophyte chlorophyll-binding (Pcb) proteins (Moore *et al.*, 1998). However, they still possess genes encoding for a PE (PE class III) and most likely reflect a degenerate form of an ancestral PBS, rather than a complex acquired *de novo* by horizontal gene transfer. The genus of *Prochlorococcus* is divided into high-light (HL) and low-light (LL) adapted ecotypes based on their habitat, physiology and genetic attributes (Johnson *et al.*, 2006, Rocab *et al.*, 2002). HL strains occupy a niche close to the surface of the water column, while LL ecotypes dominate in depths below 100 m (Biller *et al.*, 2015). The genomes of both strains encode for PEs with operon sizes depending on their respective ecotype (Hess *et al.*, 1996, Steglich *et al.*, 2005). The HL SS120 strain possesses a PE consisting of α - (CpeA) and β -subunits (CpeB) and is most likely able to carry four phycobilins, namely PUB and PEB, in a ratio of 3:1 (Steglich *et al.*, 2003). Both subunits contain phycobilin-

binding cysteine residues at positions, which are homologues to other known cyanobacterial PEs. In *Prochlorococcus marinus* SS120 (*P. marinus* SS120), these cysteines are localized on CpeA at cysteine residue 73 and on CpeB at the cysteine residues 50, 61, 82 and 155 (Figure 7). However, the exact chromophorylation pattern remains elusive. In contrast, the *P. marinus* MED4 strain produces an even more degenerate PBP with only a single β -subunit. PE β -subunits typically contain four cysteines which are known to bind chromophores. However, in the strain MED4, two out of four cysteines are missing (Figure 7, position 61 and 155), which means that only a maximum of two phycobilins can be attached to the apo-protein. If a phycobilin is binding at position 50, a second cysteine at position 61 is required since the chromophore is attached via two thioether bonds. A different case has never been reported to date. Consequently, binding of a phycobilin at cysteine 50 is very unlikely. The CpeB of *P. marinus* MED4 was characterized using heterologous expression systems in *Escherichia coli* (*E. coli*) and has been proven to bind one PEB at the only phycobilin-binding cysteine residue at position 82. In a variety of cyanobacteria and algae, PEs demonstrate the function as highly abundant, photosynthetically active pigments. Although it cannot be excluded, CpeB of *P. marinus* MED4 probably does not capture solar energy as it is known for other PBP light-harvesting systems. Expression studies in their native hosts, the HL SS120 and the LL MED4 strains, show reduced expression levels of the genes responsible for PE assembly (Steglich *et al.*, 2005). While weak signals for some *cpeB* transcripts could be detected in the SS120, the signal was even more faint in MED4 indicating very low expression levels. Although this pigment might have increased expression levels under different cultivation conditions, evaluation of the SS120 PE light-harvesting capacity suggests very low contribution to photosynthesis (~1.8 %) (Steglich *et al.*, 2003). Consequently, photosynthetic activity of the MED4 CpeB, in a strain with about 100 times less phycoerythrin than in SS120, remains elusive.

Independent of the PBPs contribution to photosynthesis, spectroscopically active pigments require proper assembly with phycobilin chromophores. In cyanobacteria, four different phycobilins can be linked to PBPs: the orange PUB ($\lambda_{\max} = 495$ nm), the pink PEB ($\lambda_{\max} = 540$ nm), the violet PVB ($\lambda_{\max} = 590$ nm) and the blue PCB ($\lambda_{\max} = 620$ nm) chromophore (Figure 9). Cryptophytes typically employ PEB and PCB as well as their intermediates occurring in cyanobacterial phycobilin biosynthesis, 15,16-DHBV and 18¹,18²-DHBV, respectively. In addition, they synthesize chromophores which have not been described in other organisms, bilin 584 and bilin 618 (Wedemayer *et al.*, 1991, Wemmer *et al.*, 1993). Based on the variety of phycobilins and the number of reactive

cysteines in PBP subunits, covalent attachment of phycobilins is facilitated by targeted ligase reactions of PBP lyases.

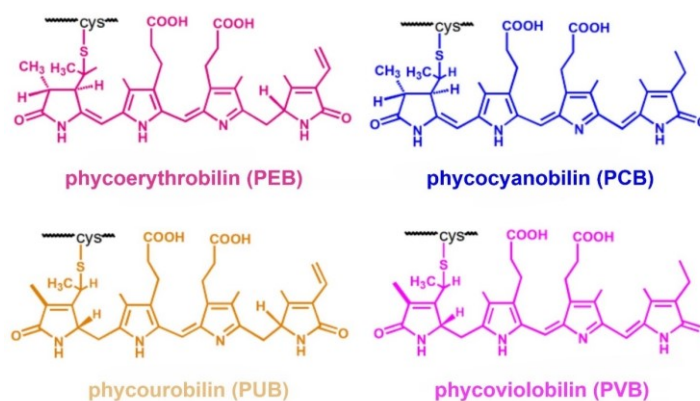


Figure 9: Phycobilins in cyanobacteria. Shown are the structures of the linear tetrapyrroles PEB (pink), PCB (blue), PUB (yellow) and PVB (purple) attached to PBP cysteine residues. Adapted from Gu (2023).

1.4. Phycobiliprotein assembly by phycobiliprotein lyases

Post-translational modification of PBP subunits requires a targeted ligase reaction mediated by PBP lyases. Although formation of covalent bonds between the chromophore and the PBP subunit has been proven to occur spontaneously *in vitro*, these reactions are prone to imprecise attachment based on an insufficient regiospecificity of the PBPs for the phycobilins (Fairchild & Glazer 1994b). One exception is exhibited by the chromophorylated core-membrane linker ApcE, which harbours an autocatalytic activity to attach the correct chromophore (Zhao *et al.*, 2005). In other cases, PBP lyases facilitate the attachment of the appropriate phycobilin to the correct cysteine residue within the corresponding PBP in a stereochemical accurate manner (Scheer & Zhao 2008). This is specifically important, as for the β -subunit CpcB of PCs, the PCB exists in two stereoisomeric forms at the C3¹ of the chromophore molecule. The *R*-isomer is the most prominent configuration (e.g. Cys₈₂). In contrast, the *S*-isomer has been detected at the Cys₁₅₃ position (Schirmer *et al.*, 1986). The tetrapyrrole chromophore can not only be attached to one specific cysteine residue at the C3¹ atom in the A-ring, but also via a second covalent linkage at the C18¹ position in the D-ring. The latter is connected to an additional cysteine residue inside the PBP, the second binding site is thereby in close proximity downstream of the first thioether linkage (Kronfel *et al.*, 2019). The process of chromophorylation has been postulated to be of chronological nature where linkage to one specific cysteine depends on the formation of other covalent bonds between the bilin and the PBP (Kronfel *et al.*, 2019, Zhao *et al.*, 2007). Based on structure and chromophorylation activity, PBP lyases have been organized in three different classes: E/F-, S(U)- and T-type lyases (Schluchter *et al.*, 2010) (Figure 10).

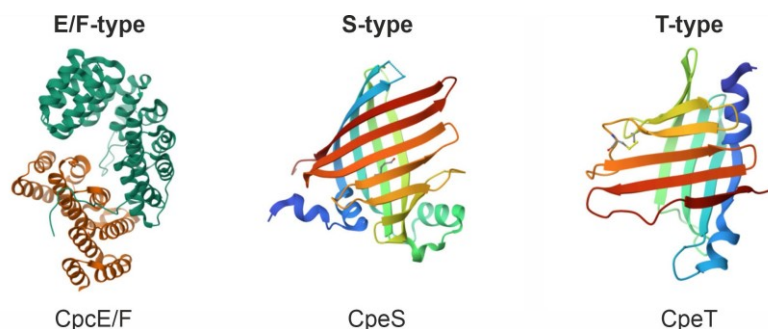


Figure 10: Structures of PBP lyases of the E/F-, S- and T-type family. The family of E/F-type lyases are typically composed of a heterodimeric complex as the PBP lyase CpcE/F from *Nostoc* sp. PCC 7120 (PDB: 5N3U, Zhao *et al.*, (2017)). They consist of an armadillo-like fold with numerous HEAT repeat motifs and covalently link phycobilins to cysteine residue 84 of PBP α -subunits. S-type PBP lyases, as CpeS from *G. theta* (PDB: 4TQ2, Overkamp *et al.*, (2014)), are responsible for phycobilin attachment to cysteine residue 82 of PBP β -subunits. Antiparallel β -sheets are connected with flexible loops and α -helices to form a barrel-like structure. Based on experimental design, the N-terminal α -helices (dark blue) are derived from the StrepII-tag for protein purification. PBP lyases of the T-type family exhibit similar structures as the S-type lyases and are responsible for the attachment of phycobilins to cysteine residue 155 of PBP β -subunits. Φ CpeT of the *Prochlorococcus* phage P-HM1 also adopts a barrel-like architecture consisting of antiparallel β -sheets to form a hydrophobic, central cavity for chromophore association (PDB: 5H18, Gasper *et al.*, (2017)).

The structure of E/F-type lyases demonstrates a characteristic domain architecture, consisting of an armadillo-type fold with HEAT (Huntington, elongation factor (EF3), protein phosphatase 2A (PP2A) and the yeast PI3-kinase TOR1) repeat motifs. These repeats contain antiparallel α -helical modules promoting protein-protein interactions as well as intracellular transportation (Andrade & Bork 1995). The class of E/F-type lyases consists of heterodimeric protein complexes and is further divided by their chromophore ligation activity. The most investigated E/F-type lyases are PCB: α -Cys₈₄ lyases like the heterodimer CpcE/CpcF in *Synechococcus* sp. PCC 7002 (hereafter *Synechococcus*). Both enzymes are required for accurate linkage of PCB to the α -Cys₈₄ site of PC and are responsible for the attachment as well as the release of the chromophore (Fairchild *et al.*, 1992). In general, E/F-type lyases possess a low specificity for the phycobilin chromophore, but high affinity for the α -Cys₈₄ site and its homologues. Alvey *et al.*, (2011a) demonstrated a universal mode of action for the lyase and its chromophore attachment to α -subunits using *E. coli* as the platform for heterologous protein production. Here, different bilin chromophores (PCB, PEB and phytochromobilin (P Φ B)) were attached to CpcA of *Synechocystis* and *Synechococcus* by the E/F-type lyase CpcE/F of *Synechococcus* yielding proteins with very high fluorescence quantum yields and photochemical activity. In addition, they could even produce three more variants using the lyase-isomerase PecE/F of *Nostoc* sp. PCC 7120 (hereafter *Nostoc*). This lyase-isomerase is able to isomerize PCB to PVB, PEB to PUB and P Φ B to phytoviolobilin. The mechanism of CpcE/F lyase-isomerases has been investigated by Storf *et al.*, (2001) for PecE/F in *Mastigocladus laminosus*. The lyase PecE binds PCB and attaches it to the PBP subunit, while its subsequent isomerization is performed by

PecF (Zhao *et al.*, 2002). E/F-type lyases also attach PEB to the appropriate PBP subunit as in *Fremyella diplosiphon* (hereafter *Fremyella*) via the CpeY/Z complex. Here, CpeZ lacks bilin transfer-activity and only supports the PEB: α -Cys₈₂ lyase CpeY (Biswas *et al.*, 2011) Recently, a new subdivision of E/F-type lyases have been characterized. Besides already investigated α -cysteine-lyases, Kronfel *et al.*, (2019) provide evidence for a structurally similar lyase called CpeF, facilitating covalent double-linkage of PEB to the β -subunit at positions equivalent to Cys₄₈ and Cys₅₉. In *Synechococcus* RS9916, the E/F-type lyase is able to attach PEB to both cysteines and isomerize it to PUB (Carrigee *et al.*, 2021). Although the E/F-type lyase family is known to form heterodimers to catalyse their reaction, Kumarapperuma *et al.*, (2022) identified an E/F-type lyase-isomerase in *Synechococcus* A15-62 called MpeQ which catalyses PEB attachment to cysteine residue 83 of the α -subunit MpeA and the following isomerization to PUB as one enzyme.

The family of S(U)-type lyases in general possess a low chromophore- and apo-protein specificity but are very specific for certain cysteine residues. S(U)-type lyases can be divided into two groups. One member is performing the covalent attachment of PEB to PE subunits. In *G. theta* and *P. marinus* MED4, the PBP lyase CpeS is responsible for the attachment of PEB to the cysteine residue 82 and homologues of the PE β -subunits (Tomazic *et al.*, 2021, Wiethaus *et al.*, 2010). The second member of the S(U)-type PBP lyases family is responsible for the phycobilin attachment to PC proteins and comprises of three subgroups (CpcS-I, CpcS-II and CpcS-III). Studies on the heterodimeric S(U)-type lyases CpcS-I/CpcU show covalent attachment of PCB to cysteine 82 of CpcB and cysteine 81 of both APC subunits, ApcA and ApcB (Saunée *et al.*, 2008). CpcS-II lyases were not characterized so far, it is only known that they are involved in PEB attachment to some PCs in marine *Synechococci* strains (Ong & Glazer 1988, Shen *et al.*, 2008). The last group of S(U)-type lyases is represented by, e.g. CpcS-III of *Thermosynechococcus elongatus*, which acts as a universal lyase capable of transferring PCB, PEB and P Φ B to a variety of PBP subunits. The active, dimeric form of CpcS-III is catalysing the covalent attachment to both subunits of APC and to the cysteine residue 82 of CpcB (PC) (Kronfel *et al.*, 2013).

The least characterized PBP lyases are T-type lyases, which form a calyx-shaped β -barrel fold in a homodimeric protein arrangement (Zhou *et al.*, 2014b) and mediate ligation of phycobilins to cysteine residues at position 155 (or homologues) of PC, PEC and PE β -subunits. Depending on the protein's context, CpcT catalyses the covalent attachment of PCB to PC (CpcB) and PEC (PecB) in *Nostoc* (Zhao *et al.*, 2007) and CpeT ligates PEB to PE (CpeB) as in *Fremyella* (Nguyen *et al.*, 2020). CpeT alone is

able to transfer PEB to CpeB, but its activity is greatly enhanced by the chaperone-like lyase CpeZ.

1.5. Bilin biosynthesis

Formation of linear tetrapyrroles

The linear tetrapyrrole chromophores attached to light-harvesting complexes by PBP lyases originate from the cyclic tetrapyrrole heme. In bacteria, plants and algae, formation of linear tetrapyrroles relies on the cleavage of heme, which is converted to the linear tetrapyrrole biliverdin IX α (BV IX α) via an oxidoreductase called heme oxygenase (HO, [E.C. 1.14.99.3]) (Frankenberg-Dinkel 2004, Wilks 2002). The cleavage of the α -methine bridge within the heme molecule is based on the enzymes regiospecificity (Wilks 2002, Wilks & Barker 2011). Besides BV IX α , there are other HOs with different regiospecificity for the catalysis into the other BV isomers IX β and BV IX δ (Gisk *et al.*, 2012, Ratliff *et al.*, 2001). The catalysis of heme to BV IX α by the HO is performed via several intermediates and involves the release of Fe(II) and carbon monoxide as well as the investment of seven electrons. Binding of heme to the heme oxygenase is potentially mediated by the initial coordination via a conserved histidine residue (Ishikawa *et al.*, 1992), which leads to the formation of a ferric [Fe(III)]-heme-HO complex (Figure 11).

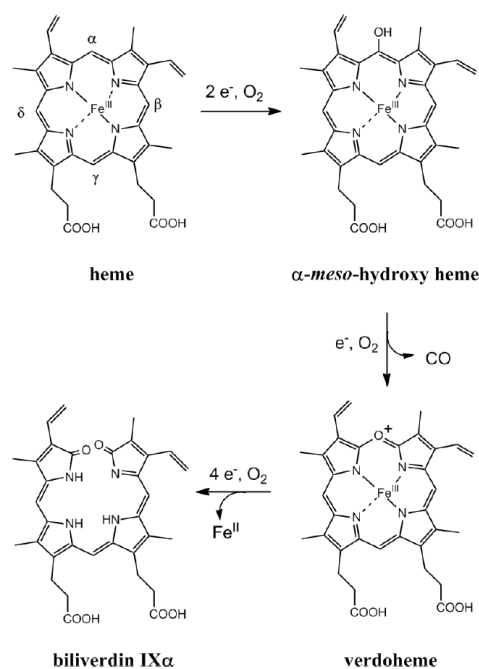


Figure 11: The reaction of the heme oxygenase to catalyze heme to biliverdin IX α . The reaction requires seven electrons as well as three molecules of molecular oxygen and is performed via several intermediates. Besides the product biliverdin IX α , one molecule of each Fe^{2+} and CO_2 is released. From Overkamp and Frankenberg-Dinkel (2013).

The first electron transfer yields a ferrous [Fe(II)]-heme-HO complex, which is then converted to a meta-stable oxy-complex upon binding of oxygen to the central iron. After cleavage of the α -meso-carbon, heme is subjected to self-hydroxylation, which yields the product α -meso-hydroxy heme. Following the consumption of an O_2 molecule and electrons, [Fe(II)]-containing verdoheme is generated. In prokaryotes, the final conversion to BV IX α requires four more electrons and one O_2 molecule. Release of the product is the rate-limiting step *in vitro* and is accelerated by the addition of chelators for divalent cations (Rhie & Beale 1995). It has been postulated that BV binding proteins as phytochromes and so-called ferredoxin-dependent bilin reductases (FDBRs) promote *in vivo* product release (Liu & Ortiz de Montellano 2000, Wegele *et al.*, 2004)

Ferredoxin-dependent bilin reductases

Processing of the open-chain tetrapyrrole BV IX α depends on FDBRs, which catalyse the substrate in a variety of bilin chromophores (Dammeyer *et al.*, 2008a, Frankenberg & Lagarias 2003, Kohchi *et al.*, 2001) (Figure 12).

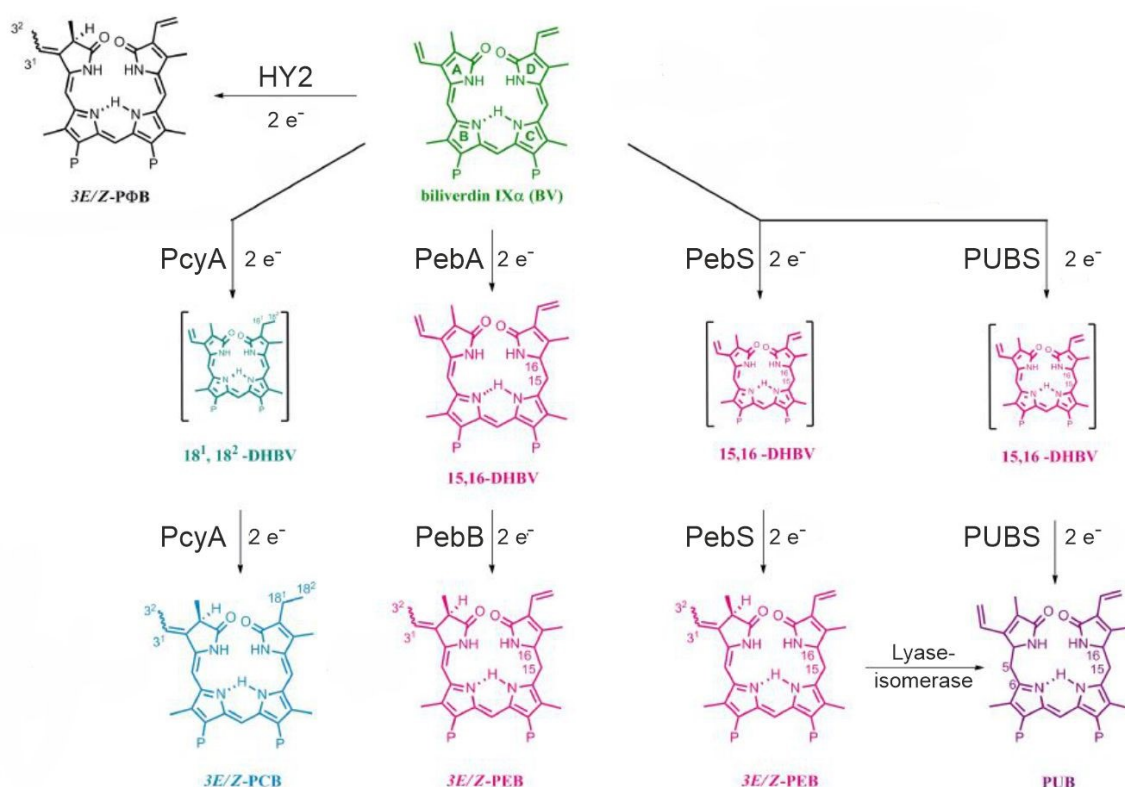


Figure 12: Ferredoxin-dependent bilin reductases and phycobilin biosynthesis. BV IX α is the substrate for all FDBR enzymes except PebB, which has a substrate specificity towards the intermediate DHBV. In cyanobacteria, PCB is produced via a four-electron reduction by PcyA. Formation of PEB in cyanobacteria thereby depends on a two-step reaction via PebA and PebB, each performing a two-electron reduction. Interestingly, the cyanophage derived PebS is able to perform a four-electron reaction as one enzyme. In accordance with PcyA and PebS, the most recently discovered PUBS enzyme performs a four-electron reduction to yield the PUB chromophore. Adapted from Overkamp and Frankenberg-Dinkel (2013).

The presence of FDBRs thereby depends on the hosts PBP composition. The PBP of e.g., the cryptophyte *G. theta* only binds the linear tetrapyrroles DHBV and PEB, consequently, the organism only employs the FDBRs PebA and PebB (Overkamp *et al.*, 2014). In contrast, the PBS of e.g., *Synechocystis* consists of the PBPs APC and PC, hence, the PCB-producing PcyA is the only present FDBR enzyme in that organism. Initially, in the red alga *Cyanidium caldarium* BV was found to be the precursor of PCB, one of the major phycobilin chromophores used in light-harvesting (Beale & Cornejo 1984). The reaction has been shown to be dependent on the electron donor Fd (Beale & Cornejo 1991). The first recombinant study for the characterization of FDBR enzymes was performed with a PΦB:ferredoxin-oxidoreductase (HY2, [E.C. 1.3.7.4]) which synthesizes the PΦB chromophore required for the plant phytochrome in *Arabidopsis thaliana*. HY2 catalyses a two-electron reduction of the BV molecules 2,3,3¹,3²-diene system at the A-ring which yields the PΦB chromophore (Kohchi *et al.*, 2001).

A prominent representative of the FDBR family is the PCB:ferredoxin oxidoreductase (PcyA, [E.C. 1.3.7.5]), which catalyses the conversion of BV IX α to the blue PCB chromophore by a four-electron reduction (Figure 12). In a vast number of cyanobacteria, PCB serves as the major chromophore in light-harvesting as it is the only phycobilin being covalently attached to the PBS core protein APC and to the PBS rod-protein PC (Chapman *et al.*, 1967, Marx & Adir 2013). Initially, the exo-vinyl group at the C18 atom of the D-ring in BV is reduced to an ethyl residue which forms the intermediate mesobiliverdin (18¹,18²-dihydrobiliverdin, MBV). After the first two-electron reduction, the 2,3,3¹,3²-diene of the A-ring is reduced yielding both isomers, 3E and 3Z, of PCB (Frankenberg & Lagarias 2003).

The PEB synthase PebS: an unusual FDBR enzyme derived from phages

In contrast to PCB biosynthesis, formation of the pink PEB chromophore in cyanobacteria is processed by two distinct FDBR enzymes (Dammeyer & Frankenberg-Dinkel 2006, Frankenberg *et al.*, 2001) (Figure 12). The 15,16-DHBV:ferredoxin oxidoreductase (PebA, [E.C. 1.3.7.2]) converts BV IX α to the intermediate 15,16-DHBV via a two-electron reduction at the double bond between the C15 and C16 atom. Based on metabolic channelling, the molecule is transferred to the second enzyme, the PEB:ferredoxin oxidoreductase (PebB, [E.C. 1.3.7.3]). Mediated by a second two-electron reduction, the final product PEB is formed (Dammeyer & Frankenberg-Dinkel 2006). A novel FDBR member has been identified in the genomes of phages as in, e.g. the *Prochlorococcus* infecting cyanophage (viruses that infect cyanobacteria) P-SSM2. The corresponding enzyme is a PEB synthase (PebS, [E.C. 1.3.7.6]) capable of

performing the four-electron reduction of BV to PEB as one enzyme (Dammeyer *et al.*, 2008a). Here, the intermediate 15,16-DHBV can also be utilized to form the final product PEB (Busch *et al.*, 2011). The structures of many FDBRs have been solved to date by X-ray crystallography, which enabled mechanistic insights of the enzymes' catalytic activities (Dammeyer *et al.*, 2008b, Hagiwara *et al.*, 2006, Sugishima *et al.*, 2020). Comparative analyses of the FDBRs PebS and PebA demonstrate the presence of a central seven-stranded β -sheet forming a hydrophobic substrate binding site (Figure 13).

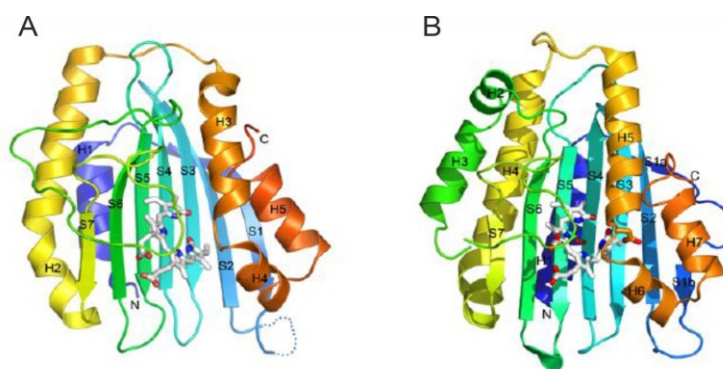


Figure 13: Crystal structures of PEB-forming FDBRs. The crystal structures of PebS from the cyanophage P-SSM2 (A) and PebA from *Synechococcus* sp. WH8020 (B) are shown coloured from blue (N-termini) to red (C-termini). The substrate biliverdin IX α is displayed in the central cavity of the enzymes as sticks. Seven central β -sheet strands are flanked by α -helices to form the hydrophobic substrate binding site. Adapted from Busch *et al.*, (2011a) and Dammeyer *et al.*, (2008b).

Furthermore, the binding pocket is always accompanied by two long, connected helices which form the central cavity for the substrate. After the formation of 15,16-DHBV by PebA, the product is immediately used by the enzyme PebB to yield the final product PEB (Aras *et al.*, 2020, Dammeyer & Frankenberg-Dinkel 2006). For the reduction of DHBV, substrate orientation in the binding pocket seems to play a key role in the specificity towards the phycobilins A- or D-ring (Sommerkamp *et al.*, 2019). Two central aspartate residues (99 and 219) have been identified and are crucial for the FDBR activity. Coordination of the substrate determines which 2,3,3¹,3²-diene system (A- or D-ring) is reduced.

The most recently discovered member of the FDBR family is the PUB synthase PUBS (E.C. classification not yet assigned) in the moss *Physcomitrella patens* which is affiliated with the phylogenetic lineage of PebA (Chen *et al.*, 2012, Rockwell *et al.*, 2017). Similar to the FDBR PebS, PUBS catalyses a four-electron reduction of BV to yield its product PUB via the intermediate 15,16-DHBV. While the catalysis of BV to the intermediate is performed as in PebS, the formation of PUB is facilitated by the transfer of two electron to the C4-C5 double bond of 15,16-DHBV instead of the C15-C16 double bond for PEB biosynthesis. Although PUB has been found in cyanobacteria (Ong & Glazer 1991), no PUBS homologue was identified until today.

1.6. Objectives of this work

Investigations of PBP assembly typically employ heterologous expression systems based on *E. coli*, which facilitate the biochemical study of phycobilin attachment to PBP subunits mediated by PBP lyases. Although significant progress has been made (Biswas *et al.*, 2010, Carrigee *et al.*, 2021), using this system for PBP investigations has several drawbacks. Challenges such as target protein insolubility impair proper PBP assembly characterization and complete PBP assembly (α - and β subunits) has not been reported to date. Moreover, this system only provides the basis for biochemical analyses but lacks the capability to assess the PBPs light-harvesting capacity *in vivo*. In contrast, cyanobacterial hosts present opportunities to characterize PBP assembly *in vitro* and their physiological relevance for photosynthesis *in vivo*. Previous studies demonstrated successful complementation of PBP-deficient strains with genes necessary for PBP assembly (Plank & Anderson 1995, Puzorjov *et al.*, 2021), highlighting the potential of cyanobacterial hosts for such investigations. However, only PBP genes were introduced, which depend on the model organism's native chromophore biosynthesis (as PCB). A vast number of PBPs rely on phycobilin biosynthesis pathways not present in commonly used cyanobacterial model systems like *Synechocystis*. PCs are widely studied since most model organisms exclusively employ that type of PBP as light-harvesting antennas. In contrast, marine cyanobacteria additionally synthesize the very abundant PE to fuel oxygenic photosynthesis. The challenges related to the investigation of PEs lies in difficulties associated with strain isolation, cultivation and their lack of amenability for genetic modifications which ultimately requires the utilization of alternative platforms.

Consequently, this work aimed for employing synthetic biology to reconstitute non-native PBPs, namely PEs, of normally inaccessible cyanobacteria in the routinely used cyanobacterial model organism *Synechocystis*. Introducing genes responsible for PE biosynthesis enables the study of both the biochemical assembly of heterologously produced PEs and their physiological contribution to light-harvesting. Therefore, PEB biosynthesis was introduced into the *Synechocystis* wildtype using the cyanophage gene *pebS* to expand the hosts repertoire of phycobilins. After evaluation of this novel chassis, additional genes responsible for the assembly of the *P. marinus* MED4 CpeB were introduced into *Synechocystis* to assess heterologous PE assembly in cyanobacterial hosts and to unravel the mechanism of such a light-harvesting apparatus.

2. Materials and methods

2.1. Microbial strains, materials, and chemicals

2.1.1. Microbial strains

Table 1: Microbial strains used in this study.

Strain	Genotype	Source/Reference
<i>E. coli</i> BL21 (DE3)	<i>E. coli</i> B F ⁻ <i>ompT hsdS_B</i> (r _B ⁻ , m _B ⁻) <i>gal dcm</i> ⁺ (DE3)	Studier & Moffatt (1986)
<i>E. coli</i> BL21 (DE3) pLysS	<i>E. coli</i> B F ⁻ <i>ompT hsdS_B</i> (r _B ⁻ , m _B ⁻) <i>gal dcm</i> ⁺ (DE3) pLysS Cam ^R	Invitrogen
<i>E. coli</i> BL21 (DE3) CodonPlus-RIL	<i>E. coli</i> B F ⁻ <i>ompT hsdS</i> (r _B ⁻ , m _B ⁻) <i>gal dcm</i> ⁺ Tet ^R (DE3) <i>endA Hte (argU ileY leuW)</i> Cam ^R	Stratagene
<i>E. coli</i> BL21 (DE3) pGro7	<i>E. coli</i> B F ⁻ <i>ompT hsdS_B</i> (r _B ⁻ , m _B ⁻) <i>gal dcm</i> ⁺ (DE3) pGro7 Cam ^R	TaKaRa
<i>E. coli</i> BL21 (DE3) Rosetta-Gami	<i>E. coli</i> B F ⁻ <i>ompT hsdS_B</i> (r _B ⁻ , m _B ⁻) <i>gal dcm</i> ⁺ <i>lacY1 ahpC</i> (DE3) <i>gor552::Tn10 trxB</i> pRARE (Cam ^R , Kan ^R , Tet ^R)	Novagen
<i>E. coli</i> BL21 AD494	<i>E. coli</i> K-12 F ⁻ <i>ompT hsdS_B</i> (r _B ⁻ , m _B ⁻) <i>gal dcm</i> ⁺ (DE3) <i>trxB15::Kan</i> ^R	Novagen
<i>E. coli</i> BL21 (DE3) C41	<i>E. coli</i> B F ⁻ <i>ompT hsdS_B</i> (r _B ⁻ , m _B ⁻) <i>gal dcm</i> ⁺ (DE3), uncharacterized mutation for conferring tolerance to toxic proteins	Sigma-Aldrich
<i>E. coli</i> BL21 (DE3) Arctic express RIL	<i>E. coli</i> B F ⁻ <i>ompT hsdS_B</i> (r _B ⁻ , m _B ⁻) <i>gal dcm</i> ⁺ Tet ^R (DE3) <i>endA Hte (cpn10, cpn60, Gm</i> ^R) (<i>argU, ileY, leuW, Str</i> ^R)	Agilent
<i>E. coli</i> BL21 (DE3) SHuffle T7 express	<i>E. coli</i> B F ⁻ <i>lac, pro, lacI^q / Δ(ara-leu)7697 araD139 fhuA2 lacZ::T7 gene1 Δ(phoA)Pvull phoR ahpC* galE (or U) galK λatt::pNEB3-r1-cDsbC (Spec</i> ^R , <i>lacI^q) ΔtrxB rpsL150(Str</i> ^R) <i>Δgor Δ(malF)3</i>	New England Biolabs
<i>E. coli</i> BL21 (DE3) Rosetta pLysS	<i>E. coli</i> B F ⁻ <i>ompT hsdS_B</i> (r _B ⁻ , m _B ⁻) <i>gal dcm</i> ⁺ (DE3) pLysSRARE, Cam ^R	Novagen
<i>E. coli</i> BL21 (DE3) Tuner	<i>E. coli</i> B F ⁻ <i>ompT hsdS_B</i> (r _B ⁻ , m _B ⁻) <i>gal dcm</i> ⁺ <i>lacY1</i> (DE3)	Novagen
<i>E. coli</i> TOP10	<i>E. coli</i> K-12 F ⁻ <i>mcrA Δ(mrr-hsdRMS-mcrBC) φ80lacZΔM15 ΔlacX74 nupG recA1 araD139 Δ(ara-leu)7697 galE15 galk16 rpsL(Str</i> ^R) <i>endA1</i>	Invitrogen, United States
<i>E. coli</i> J53 [RP4]	<i>E. coli</i> K-12 F ⁺ <i>met pro Azi</i> ^R pRP4 (Amp ^R Km ^R Tet ^R)	DSMZ, Germany (DSM 3876)
<i>Synechocystis</i> sp. PCC 6803	WT	Vasudevan <i>et al.</i> , (2019)
<i>Synechocystis</i> sp. PCC 6803 pCAT.000 (VC)	WT derived transconjugant harbouring pCAT.000, Kan ^R	This study
<i>Synechocystis</i> sp. PCC 6803 pCGT.STH02 (Syn-pPebS)	WT derived transconjugant harbouring pCGT.STH02, Kan ^R	This study
<i>Synechocystis</i> sp. PCC 6803 pCGT.STH10 (WT-PE)	WT derived transconjugant harbouring pCGT.STH10, Kan ^R	This study
<i>Synechocystis</i> sp. PCC 6803 pCGT.STH11 (WT-PE C82A)	WT derived transconjugant harbouring pCGT.STH11, Kan ^R	This study
<i>Synechocystis</i> sp. PCC 6803 pCGT.STH12 (WT-polyPE)	WT derived transconjugant harbouring pCGT.STH12, Kan ^R	This study
<i>Synechocystis</i> sp. PCC 6803 pCGT.STH13 (WT-polyPE C82A)	WT derived transconjugant harbouring pCGT.STH13, Kan ^R	This study

<i>Synechocystis</i> sp. PCC 6803 $\Delta cpcBA$ (<i>olive</i>)	$\Delta cpcBA$	Vasudevan <i>et al.</i> , (2019)
<i>Synechocystis</i> sp. PCC 6803 <i>olive</i> pCGT.STH10 (<i>Olive-PE</i>)	<i>Olive</i> derived transconjugant harbouring pCGT.STH10, Kan ^R	This study
<i>Synechocystis</i> sp. PCC 6803 <i>olive</i> pCGT.STH11 (<i>Olive-PE C82A</i>)	<i>Olive</i> derived transconjugant harbouring pCGT.STH11, Kan ^R	This study
<i>Synechocystis</i> sp. PCC 6803 <i>olive</i> pCGT.STH12 (<i>Olive-polyPE</i>)	<i>Olive</i> derived transconjugant harbouring pCGT.STH12, Kan ^R	This study
<i>Synechocystis</i> sp. PCC 6803 <i>olive</i> pCGT.STH13 (<i>Olive-polyPE C82A</i>)	<i>Olive</i> derived transconjugant harbouring pCGT.STH13, Kan ^R	This study

2.1.2. Plasmids

Table 2: Plasmids used for heterologous expression experiments in *E. coli*.

Plasmid	Features	Antibiotic	Reference
pET_Duet_Gt <i>cpcX</i> _oSA	pETDuet™-1 derivative harbouring the codon-adapted (for <i>E. coli</i>) gene <i>cpcX</i> of <i>Guillardia theta</i> yielding a His-tagged fusion protein	Amp ^R / Carb ^R	Tomazic (2020)
pASKIBA45+Gt <i>cpcX</i> _oSA	pASKIBA45+ derivative harbouring the codon-adapted (for <i>E. coli</i>) gene <i>cpcX</i> of <i>Guillardia theta</i> yielding a StrepII-tagged fusion protein	Amp ^R / Carb ^R	Tomazic (2020)
pMAL-c2	Vector for heterologous expression in <i>E. coli</i> allowing translational fusion of the <i>E. coli</i> maltose binding protein (encoded by <i>malE</i>) to the N-terminus of the cloned target protein	Amp ^R / Carb ^R	New England Biolabs
pMAL_FXa_ <i>cpcX</i> -StrepII	pMAL-c2 derivative harbouring the codon-adapted (for <i>E. coli</i>) gene <i>cpcX</i> of <i>Guillardia theta</i> with N-terminal MBP-tag and C-terminal StrepII-tag (MBP-FXa-CpcX-Strep)	Amp ^R / Carb ^R	This study
pMAL_HRV3C_ <i>cpcX</i> -StrepII	pMAL_FXa_ <i>cpcX</i> -StrepII derivative, Factor Xa recognition site was substituted by HRV3C protease recognition site via site directed mutagenesis (MBP-HRV3C-CpcX-Strep)	Amp ^R / Carb ^R	This study
pTD <i>ho1pebS</i>	pACYC derivative harbouring native cyanophage P-SSM2 genes for the expression of the heme oxygenase <i>ho1</i> and the phycoerythrobilin synthase <i>pebS</i>	Cam ^R	Dammeyer <i>et al.</i> , (2008a)
pCOLADuet MED4 <i>cpeB</i>	pCOLADuet-1 derivative harbouring the native <i>Prochlorococcus marinus</i> MED4 gene for <i>cpeB</i>	Kan ^R	Pauls (2014)
pASKIBA45+ <i>cpeSMED4</i>	pASKIBA45+ derivative harbouring native <i>Prochlorococcus marinus</i> MED4 gene for the phycobiliprotein lyase <i>cpeS</i>	Amp ^R / Carb ^R	Wiethaus <i>et al.</i> , (2010)

Table 3: Commercial library parts for modular cloning (MoClo). The restriction endonucleases (*Bbs*I-HF and *Bsa*I-HF^{®v2}) indicate the corresponding 4 bp overhangs of Golden-Gate-based cloning for directional assembly of DNA constructs. For the introduction of DNA fragments, acceptor vectors harbour a *lacZ* α gene for blue-white screening after transformation of the assembly reaction. Newly generated library parts in acceptor vectors for cloning into the next level are labelled as *insert* between the 4 bp overhangs.

Plasmid	Features	Antibiotic	Reference
pAGM1287	Level 0 acceptor vector for CDS parts, <i>Bbs</i> I: AATG- <i>lacZ</i> α -TTCG <i>Bsa</i> I: AATG-insert-TTCG	Spec ^R	Weber <i>et al.</i> , (2011)
pC0.005	Level 0 part, Strong and light responsive <i>cpc560</i> promoter of the <i>Synechocystis cpc</i> operon, <i>Bsa</i> I: GGAG-P _{<i>cpc560</i>} -AATG	Spec ^R	Vasudevan <i>et al.</i> , (2019)
p.C0049	Level 0 part, Constitutive <i>J23119</i> promoter, BioBrick derived promoter part, contains <i>lacO</i> repressor and the broad-range BBa_B0034 RBS. <i>Bsa</i> I: GGAG-P _{<i>J23119</i>} -AATG	Kan ^R	Vasudevan <i>et al.</i> , (2019)
p.C059	Level 0 part, Synthetic variant of the <i>trc</i> promoter from <i>E. coli</i> . <i>Bsa</i> I: GGAG-P _{<i>trc10</i>} -AATG	Kan ^R	Vasudevan <i>et al.</i> , (2019)
pC0.078	Level 0 part, Terminator of the <i>Synechocystis cpc</i> operon <i>Bsa</i> I: GCTT-T _{<i>cpc</i>} -CGCT	Spec ^R	Vasudevan <i>et al.</i> , (2019)
pC0.082	Level 0 part, Double terminator composed of <i>E. coli rrmB</i> T1 terminator (BBa_B0010) and T7 phage terminator (BBa_B0012), <i>Bsa</i> I:GCTT-T _{<i>rrmB</i>} -CGCT	Spec ^R	Vasudevan <i>et al.</i> , (2019)
pCM0-095	Level 0 part, C-terminal His tag <i>Bsa</i> I: TTCG-6xHis-GCTT	Spec ^R	Crozet <i>et al.</i> , (2018)
pCM0-096	Level 0 part, C-terminal Strep tag <i>Bsa</i> I: TTCG-StrepII-GCTT	Spec ^R	Crozet <i>et al.</i> , (2018)
pCM0-101	Level 0 part, Multi-Stop module (adds one stop codon for each reading frame) <i>Bsa</i> I: TTCG-multiStop-GCTT	Spec ^R	Crozet <i>et al.</i> , (2018)
pICH47732	Level 1 position 1 acceptor vector, <i>Bsa</i> I: GGAG- <i>lacZ</i> α -CGCT <i>Bbs</i> I: TGCC-insert-GCAA	Amp ^R /Carb ^R	Weber <i>et al.</i> , (2011)
pICH41722	Level 1 End-Linker 1 (EL1), <i>Bbs</i> I: GCAA-EL1-GGGA	Amp ^R /Carb ^R	Weber <i>et al.</i> , (2011)
pICH47742	Level 1 position 2 acceptor vector, <i>Bsa</i> I: GGAG- <i>lacZ</i> α -CGCT, <i>Bbs</i> I: GCAA-insert-ACTA	Amp ^R /Carb ^R	Weber <i>et al.</i> , (2011)
pICH47751	Level 1 position 3 acceptor vector, <i>Bsa</i> I: GGAG- <i>lacZ</i> α -CGCT, <i>Bbs</i> I: ACTA-insert-TTAC	Amp ^R /Carb ^R	Weber <i>et al.</i> , (2011)
pICH41766	Level 1 End-linker 3 (EL3), <i>Bbs</i> I: TTAC-EL3-GGGA	Amp ^R /Carb ^R	Weber <i>et al.</i> , (2011)
pCAT.000	Level T acceptor vector, conjugative, RSF1010 oriV and RSF1010 oriT, <i>Bbs</i> I: TGCC- <i>lacZ</i> α -GGGA	Amp ^R /Carb ^R , Kan ^R	Vasudevan <i>et al.</i> , (2019)

Table 4: Library parts generated in this study for Golde-Gate-based modular cloning (MoClo).

Plasmid	Features	Anti-biotic	Reference
pCG0.STH01	CDS of <i>Prochlorococcus</i> phage P-SSM2 phycoerythrobilin synthase gene <i>pebS</i> (P-SSM2) in pAGM1287	Spec ^R	This work
pCG0.STH11	CDS of <i>Prochlorococcus marinus</i> MED4 β-phycoerythrin lyase gene <i>PmcpeS</i> in pAGM1287	Spec ^R	This work
pCG0.STH12	CDS of native <i>Prochlorococcus marinus</i> MED4 β-phycoerythrin gene <i>PmcpeB</i> in pAGM1287	Spec ^R	This work
pCG0.STH13	CDS of <i>Prochlorococcus marinus</i> MED4 β-phycoerythrin gene mutant <i>PmcpeB</i> C82A in pAGM1287	Spec ^R	This work
pCG1.STH03	<i>pebS</i> (pCH0.STH01) under the control of the <i>cpc</i> operon promoter (pC0.005) and terminator (pC0.078) in pICH47732	Carb ^R	This work
pCG1.STH15	<i>PmcpeB</i> (pCG0.STH12) under the control of the <i>J23119</i> promoter (pC0.049) and <i>rrnB</i> terminator (pC0.082) in pICH47742	Carb ^R	This work
pCG1.STH16	<i>PmcpeB</i> C82A (pCG0.STH13) under the control of the <i>J23119</i> promoter (pC0.049) and <i>rrnB</i> terminator (pC0.082) in pICH47742	Carb ^R	This work
pCG1.STH17	<i>PmcpeS</i> (pCG0.STH11) under the control of the <i>trc10</i> promoter (pC0.059) and <i>rrnB</i> terminator (pC0.082) in pICH47751	Carb ^R	This work
pCGT.STH02	Expression construct consisting of <i>pebS</i> (pCG1.STH03) assembled in conjugative vector pCAT.000 via End-linker 1 (pICH41722)	Amp ^R , Kan ^R	This work
pCGT.STH10	Expression construct consisting of the three TUs of <i>pebS</i> (pCG1.STH03), <i>PmcpeB</i> (pCG1.STH16) and <i>PmcpeS</i> (pCG1.STH17) assembled in conjugative vector pCAT.000 via End-linker 3 (pICH41766)	Amp ^R , Kan ^R	This work
pCGT.STH11	Expression construct consisting of the three TUs of <i>pebS</i> (pCG1.STH03), <i>PmcpeB</i> C82A (pCG1.STH15) and <i>PmcpeS</i> (pCG1.STH17) assembled in conjugative vector pCAT.000 via End-linker 3 (pICH41766)	Amp ^R , Kan ^R	This work
pCGT.STH12	Polycistronic expression construct consisting of <i>pebS</i> , <i>PmcpeB</i> and <i>PmcpeS</i> under the control of the <i>cpc</i> operon promoter (pC0.005) and <i>rrnB</i> terminator (pC0.082). <i>P_{cpc560}-pebS</i> was amplified from pCGT.STH02 using the oligonucleotides TGCC- <i>P_{cpc}-pebS</i> -GCAA fw and rv. <i>PmcpeB</i> and <i>PmcpeS</i> - <i>T_{rrnB}</i> were amplified with GCAA- <i>PmcpeB</i> _Strep-ACTA fw and rv as well as ACTA- <i>PmcpeS</i> -His- <i>T_{rrnB}</i> -GGGA fw and rv from pCGT.STH10 to introduce RBSs from (Bentley <i>et al.</i> , 2014). Amplicons were assembled in conjugative vector pCAT.000	Amp ^R , Kan ^R	This work
pCGT.STH13	Polycistronic expression construct consisting of <i>pebS</i> , <i>PmcpeB</i> C82A and <i>PmcpeS</i> under the control of the <i>cpc</i> operon promoter (pC0.005) and <i>rrnB</i> terminator (pC0.082) <i>P_{cpc560}-pebS</i> was amplified from pCGT.STH02 using the oligonucleotides TGCC- <i>P_{cpc}-pebS</i> -GCAA fw and rv. <i>PmcpeB</i> C82A and <i>PmcpeS</i> - <i>T_{rrnB}</i> were amplified with GCAA- <i>PmcpeB</i> _Strep-ACTA fw and rv as well as ACTA- <i>PmcpeS</i> -His- <i>T_{rrnB}</i> -GGGA fw and rv from pCGT.STH11 to introduce RBSs from (Bentley <i>et al.</i> , 2014). Amplicons were assembled in conjugative vector pCAT.000	Amp ^R , Kan ^R	This work

2.1.3. Oligonucleotides

DNA oligonucleotides in this work were acquired from Eurofins Genomics GmbH (Ebersberg). For routine cloning and screening applications, oligos were ordered in salt-free purity. In case of side-directed mutagenesis the oligonucleotides were purchased in HPSF purity. In the following table 5 nucleotides for overlap extension PCR are shown in lowercase, restriction enzyme recognition sites are marked in blue, introduced translational fusion tags in red and the sticky ends for golden gate cloning are underlined. Nucleotides hybridizing with target sequences for amplification are shown in uppercase.

Table 5: Oligonucleotides used for PCR, site directed mutagenesis and sequencing. Bases in capital letters are homologue to the template for PCR, minor letters mark non-homologous region for either generation of compatible overhangs or the introduction of new nucleotides in the target DNA sequence. Introduction of translational fusion tags is marked in red. For Golden-Gate-based cloning, *BbsI* restriction enzyme recognition sites are marked in blue and the corresponding four base pair overhangs are underlined. Introduced ribosome binding sites with a 6 base pair spacer for polycistronic construct generation is highlighted in green.

Oligonucleotide	Sequence 5'-3'
pMAL_LB-EcoRI-cpcX fw	gatcgaggaaggattcagaattcAACTCTGCTTGTGTGAGAGAAG
pMAL_RB-HindIII-Strep-cpcX rv	taaaacgacggccagtgccaagctttat <u>ttttcgaactgcgggtggctcca</u> agcgctG CAGTCCCACGCTAGAGG
pMAL_cpcX-HRV3C sdm fw	ttccaggggcccATTTTCAGAATTTCAACTCTGCTTGT
pMAL_cpcX-HRV3C sdm rv	TAACAATAACAACAACCTCGGGctggaagtactg
pCOLA_LB-NdeI-MCS2-ho1 fw	gtataagaaggagatatacatatgATGACAGTAGCAGATTTTTTCAG
pCOLA_RB-XhoI-MCS2-ho1 rv	ctcgagtctgtaaagaaaccgGAACTCGAGTCTGGTAAAGAA
pCOLA_LB-EcoRI-MCS1-pebA fw	caccacagccaggatccgaattcgATGTTTGATTCATTTCTCAATGAG
pCOLA_RB-SacI-MCS1-pebA fw	gacctgcaggcgccgagctcgaTCATTTGTGAGAGGAGGAG
<i>pebS</i> (PSSM2) <i>BbsI</i> fw	ttgaagacaaaATGACTAAAAACCCAAGAAATAACAAAC
<i>pebS</i> (PSSM2) <i>BbsI</i> rv	ttgaagacaacgaaTTATTTGTATGAAAAAGGAAATCGTTTA
<i>PmcpeB</i> domestication fw	GAAGAtATAAAGAATTTATTAATACTGCAAAC
<i>PmcpeB</i> domestication rv	AATATTTTTATTACTTATATTTTTCTAAATCTCTATCATTTG
<i>PmcpeB</i> <i>BbsI</i> fw	ttgaagacaaaATGACAGTTTCAAAGAGTAATCAAAT
<i>PmcpeB</i> <i>BbsI</i> rv	ttgaagacaacgaaGCTCTTAAAAGATTAATTATTCTCTCAAATTG
<i>PmcpeB</i> C8A sdm fw	GAAGATATAAAGAATTTATTAATACTGCAAAC
<i>PmcpeB</i> C82A sdm rv	AATATTTTTATTACTTATATTTTTCTAAATCTCTATCATTTG
<i>PmcpeS</i> <i>BbsI</i> fw	ttgaagacaaaATGTTGACGAAGAATCTAATAACAATTAATC
<i>PmcpeS</i> <i>BbsI</i> rv	ttgaagacaacgaaTCTTTTAAGATAGACATATTTCTTATCTC
TGCC-P _{cpc} - <i>pebS</i> -GCAA fw	ttgaagacaatgcccCACCTGTAGAGAAGAGTCCC
TGCC-P _{cpc} - <i>pebS</i> -GCAA rv	ttgaagacaattgctTTATTTGTATGAAAAAGGAAATCGTT
GCAA- <i>PmcpeB</i> _Strep-ACTA fw	ttgaagacaagcaaaggaggaatatATGACAGTTTCAAAGAGTAATCA AAT
GCAA- <i>PmcpeB</i> _Strep-ACTA rv	ttgaagacaatagtTTACTTCTCGAACTGCGGGTGGCTCCAagaaG CTCTTAAAAGATTAATTATTCTCTCAAATTG
ACTA- <i>PmcpeS</i> -His-T _{rnb} -GGGA fw	ttgaagacaaaactaaggaggaatatATGTTGACGAAGAATCTAATAAC AATTAATC
ACTA- <i>PmcpeS</i> -His-T _{rnb} -GGGA rv	ttgaagacaatcccCGCAGAAAGGCCACC
Lvl1-LB-seq fw	GCAGGATATATTGTGGTGTAAAC
Lvl1-RB-seq rv	GTTTACCCGCCAATATATCCTG
L4440 fw	AGCGAGTCAGTGAGCGAG
pBRforEco rv	AATAGGCGTATCACGAGGC

2.1.4. Chemicals

All chemicals used in this study were ACS grade or higher and were acquired from AppliChem (Darmstadt), Carl Roth (Karlsruhe), Merck KGaA (Darmstadt) and Sigma-Aldrich (Munich) unless otherwise mentioned.

2.1.5. Culture media and supplements

Cultures of *E. coli* were routinely grown in lysogeny broth (LB) with appropriate antibiotics and supplements (Table 6), if necessary. For cultivation on solid LB medium, 1.5 % agar-agar were added to the medium prior to sterilization.

LB-Medium (Lennox)

Tryptone	10 g/l
Yeast extract	5 g/l
NaCl	5 g/l
Agar-Agar (if appropriate)	15 g/l

Cultivation of *Synechocystis* was performed in liquid- or on solid BG-11 medium supplemented with kanamycin (Table 6), if needed. BG-11 medium was prepared using the stock solutions listed below. The BG-11 (100x) solution was sterilized by autoclaving, the remaining solutions were filter-sterilized.

BG-11 (100x)

NaNO ₃	1.76 M
MgSO ₄ x 7 H ₂ O	30.39 mM
CaCl ₂ x 2 H ₂ O	24.48 mM
Citric acid x H ₂ O	3.12 mM
0.25 M Na ₂ EDTA, pH 8	1.12 ml/l

Trace elements (1000x)

H ₃ BO ₃	46.25 mM
MnCl ₂ x 4 H ₂ O	9.14 mM
ZnSO ₄ x 7 H ₂ O	0.76 mM
Na ₂ MoO ₄ x 2 H ₂ O	1.61 mM
CuSO ₄ x 5 H ₂ O	0.32 mM
Co(NO ₃) ₂ x 6 H ₂ O	0.17 mM

Iron solution (1000x)

Ferric ammonium citrate	41.88 mM
-------------------------	----------

Sodium carbonate solution (1000x)

Na ₂ CO ₃	188.69 mM
---------------------------------	-----------

Sodium bicarbonate solution (100x)

NaHCO ₃	1 M
--------------------	-----

TES solution (100x)

TES	1 M
-----	-----

Phosphate solution (1000x)

K ₂ HPO ₄	0.17 M
---------------------------------	--------

For liquid BG-11 medium, BG-11 (100x), trace elements and iron solution were added to MQ water and autoclaved. Solutions were cooled down to 60 °C and complemented with filter sterilized phosphate-, sodium carbonate-, sodium bicarbonate solution as well as kanamycin, if applicable. BG-11 solid medium was prepared using an agar- and BG-11 stock-solution. Both stock solutions were autoclaved, cooled down to 60 °C, combined and complemented with filter sterilized phosphate-, sodium carbonate-, sodium bicarbonate-, TES solution and kanamycin, if appropriate.

BG-11 (liquid, 1 l)		BG-11 (solid, 1 l)	
BG-11 (100x)	10 ml	Agar stock solution	
Trace elements	1 ml	MilliQ water	700 ml
Iron solution	1 ml	Agar-Agar	1.5 % (w/v)
MilliQ water	976 ml	BG-11 stock solution	
Autoclave and complement with:		BG-11 (100x)	10 ml
Phosphate solution	1 ml	Trace elements	1 ml
Sodium carbonate solution	1 ml	Iron stock solution	1 ml
Sodium bicarbonate solution	10 ml	MilliQ water	226 ml
		Na ₂ S ₂ O ₃	18.97 mM
		Autoclave, combine agar- and BG-11-stock solution and complement with:	
		Phosphate solution	1 ml
		Sodium carbonate solution	1 ml
		Sodium bicarbonate solution	10 ml
		TES solution	10 ml

Conjugation into *Synechocystis* (chapter 2.3.6) was performed using LB-BG11 solid medium containing 5 % of liquid LB medium (v/v). Therefore, an agar- and a BG-11-stock solution were prepared and autoclaved separately. After the stock solutions were cooled down to 60 °C, they were combined and supplemented with phosphate-, sodium carbonate- and sodium bicarbonate solution as well as sterile liquid LB medium.

LB-BG-11 (solid, 1 l)	
Agar stock solution	
MilliQ water	700 ml
Agar-Agar	1.5 %
BG-11 stock solution	
BG-11 (100x)	10 ml
Trace elements	1 ml
Iron stock solution	1 ml
MilliQ water	186 ml
Autoclave, combine stock solutions and complement with:	
Phosphate solution	1 ml
Sodium carbonate solution	1 ml
Sodium bicarbonate solution	10 ml
LB (Lennox, liquid)	50 ml

Solid and liquid media were complemented with antibiotics in concentrations as listed in Table 6, if necessary. For plasmid construction via Golden Gate assembly, X-Gal was added to solid LB-Medium in addition to appropriate antibiotic selection (Table 6).

Table 6: Antibiotics and media supplements.

Antibiotics / Supplements	Stock concentration	Solvent	Final conc. <i>E. coli</i>	Final conc. <i>Synechocystis</i>
Spectinomycin	50 mg/ml	H ₂ O	50 µg/ml	---
Carbenicillin	100 mg/ml	50 % EtOH in H ₂ O	100 µg/ml	---
Chloramphenicol	33 mg/ml	70 % EtOH in H ₂ O	33 µg/ml	---
Kanamycin	50 mg/ml	H ₂ O	50 µg/ml	50 µg/ml
Tetracycline	25 mg/ml	EtOH	25 µg/ml	---
X-Gal	20 mg/ml	DMF	200 µg/ml	---

2.1.6. Kits, enzymes and antibodies

All kits, enzymes and antibodies were used according to the manufacturers' instructions unless otherwise stated.

Table 7: Commercial Kits and enzymes.

Product	Name	Manufacturer/Reference
MoClo library parts (Golden Gate cloning)	CyanoGate Kit	Addgene, Kit #1000000146 Vasudevan <i>et al.</i> , (2019)
	MoClo Plant Parts Kit	Addgene, Kit #1000000047 Engler <i>et al.</i> , (2014)
	MoClo Toolkit (<i>Chlamydomonas reinhardtii</i>)	Chlamydomonas Resource Center (CRC) Crozet <i>et al.</i> , (2018)
PCR clean-up kit	DNA Clean & Concentrator-5	Zymo Research
Plasmid DNA extraction kit	E.Z.N.A.® Plasmid DNA Mini Kit I	Omega Bio-Tek™
	NucleoSpin® Plasmid EasyPure	Macherey-Nagel GmbH & Co. KG
Restriction endonucleases	Restriction endonucleases or high-fidelity endonucleases (HF®-line)	New England Biolabs
DNA Ligase	T4 DNA Ligase	New England Biolabs
DNA Polymerase	Phusion® High-Fidelity DNA Polymerase	New England Biolabs
Polynucleotide Kinase	T4 polynucleotide kinase	Thermo Scientific™
Trypsin	Trypsin from bovine pancreas	Sigma-Aldrich
	Pierce trypsin protease, MS grade	Thermo Scientific™
DNase I	DNase I	AppliChem
Lysozyme	Lysozyme	Carl Roth
Proteases	PreScission protease	Home-made
	Factor Xa	New England Biolabs
Gel Filtration Markers Kit 29 kDa – 700 kDa	Lysozyme	Sigma-Aldrich
	Carbonic anhydrase (~ 29 kDa)	Sigma-Aldrich
	Albumin (~ 66 kDa)	Sigma-Aldrich
	Alcohol dehydrogenase (~ 150 kDa)	Sigma-Aldrich
	β-Amylase (~ 200 kDa)	Sigma-Aldrich
	Blue Dextran (~2000 kDa)	Sigma-Aldrich

Table 8: Proteins and antibodies used for immunodetection of target proteins.

Antibody	Dilution	Antigen	Manufacturer
Strep-Tactin® AP conjugate	1:4000	Strep-tag®II	IBA Lifesciences GmbH
Anti-6xHis-tag antibody (mouse)	1:3000	Hexahistidine	Thermo Scientific™
Anti-Mouse IgG AP conjugate	1:10000	Mouse IgG	Sigma Aldrich

2.1.7. Equipment and consumables

Table 9: Devices and instruments used in this study.

Device / Consumable	Name	Manufacturer
Agarose gel electrophoresis chamber	Com Phor L Mini Com Phor L Midi	Biozym GmbH
Agarose gel electrophoresis power supply	EPS 601	GE Healthcare
Autoclave	VX 150	Systec
Blotting system	Semidry Blot Trans-Blot® SD	BioRad
Centrifuges	5415 D (Rotor F-45-24-11)	Eppendorf
	5810 R (Rotor A-4-62)	Eppendorf
	Z32HK (Rotor 12/002)	Hermle
	Sorvall LYNX 6000 (Rotors Fiberlite F9-6x1000 LEX, T29-8 x 50 fixed Angle)	ThermoFisher
	ECL ChemoStar V90D	Intas Science Imaging
Chemiluminescence imager	Optima L-80 XP (Rotor SW 40-Ti)	Beckman Coulter
Ultracentrifuge	Polyallomer tubes 14 ml, 14x95 mm, thin-walled	Laborgeräte Beranek GmbH
	iX20 Imager	Intas Science Imaging
Gel documentation	Minitron	Infors HT™
	Innova 44 Incubator Shaker Series	New Brunswick Scientific
Incubator	T6200	Heraeus Instruments
	Innova® 2300	New Brunswick™
Orbital shaker	Rocker 3D basic	IKA®
Vortex shaker	Basic pH Meter P-11	Sartorius
pH meter	Infinite® F200 PRO	Tecan
Plate reader	FluoStar Omega	BMG Labtech
	139 Primary Green	LEE Filters
Lighting filter	SimpLED, 1650 lm, 3000 K, warm-white (in Minitron, Infors HT™ incubator)	Paulmann Licht GmbH
	250-W 64663 Xenophot bulbs	Osram Licht AG
Scales	PB4000-2	Gottlieb KERN & Sohn
	R 300 S	Sartorius
SDS-PAGE chamber	Mini-PROTEAN® Tetra Cell	BioRad
SDS-PAGE power supply	PowerPac 300	BioRad
Thermo block	Thermocell CHB-202	Bioer
	ThermoStat plus	Eppendorf
Ultrasonic homogenizer	UW 2200 with tip KE 76	Bandelin
Ultrasonic bath	Sonorex Super RK 255	Bandelin
Thermocycler	Peqstar 2	Peqlab
	T1 Thermocycler	Biometra
Sterile bench	Tpersonal	Biometra
	Antares	Biohit
Vortex mixer	Vortex mixer	VWR
Fluorescence Spectrometer	FP-8300	Jasco
UV-Vis Spectrometer	8453 UV-Visible System	Agilent
Photometers	NanoDrop™ Lite	ThermoFisher
	Novaspec III	Amersham Biosciences
Dialysis tubing	Visking MWCO 14000	Carl Roth
DNA size standard	GeneRuler™ DNA Ladder	ThermoFisher
	Mix 1kb plus	

Protein size standard	Unstained Protein Standard, Broad Range (10-200 kDa) Color Prestained Protein Standard, Broad Range (10-250 kDa)	New England Biolabs New England Biolabs
Solid Phase Extraction material	Sep-Pak C18 3 cc Vac Cartridge (200 mg) Empore™ C18 Discs	Waters 3M™
Mass spectrometer	TripleTOF 6600 timsTOF Pro 2	AB Sciex Bruker
Nano(U)HPLC (coupled to mass spectrometers)	Eksigent Ekspert nanoLC 400 (coupled to TripleTOF 6600) nanoElute® (coupled to timsTOF Pro 2)	AB Sciex Bruker
Mixer mill	MM400	Retsch
Microscope	LSM880 confocal microscope	Zeiss
Photosynthesis Yield Analyzer	Mini-PAM-II	Walz
Oxygen sensor	OXR50-OI	PyroScience
FPLC systems	ÄKTA pure™ ÄKTApurifier	Cytiva GE Healthcare (now Cytiva)
FPLC accessories	F9-R (Fraction collector, connected to ÄKTA pure™) Frac-950 (Fraction collector, connected to ÄKTApurifier) Sample loop 500 µl Sample loop 5 ml	Cytiva GE Healthcare (now Cytiva) Cytiva Cytiva
FPLC columns	Superdex® 200 increase 10/300 GL Superdex® 75 10/300 GL HiTrap™ DEAE Sepharose Fast Flow	Cytiva Cytiva
HPLC system	Prominence LC-20A	Shimadzu
HPLC system Fraction collector	FRC-10A	Shimadzu
HPLC Column, Reversed Phase	Triart C18	YMC Europe
Ultra-pure water system	MilliQ® Integral Water Purification System	Merck KGaA
Transfer membrane	Roti®-PVDF-Membrane Nitrocellulose Membrane	Carl Roth Sartorius
Centrifugal concentrator	Amicon® Ultra 15-50 kDa MWCO Amicon® Ultra 15-10 kDa MWCO	Merck KGaA Merck KGaA
Beads (Mixer mill)	Zirconia/glass beads, 0.1mm	Carl Roth
Rotary Vacuum Concentrator	RVC 2-25 CDplus	Martin Christ
Lyophilizer	ALPHA 2-4 LSC <i>plus</i>	Gefriertrocknungsanlagen GmbH
Resin for gravity flow affinity chromatography	StrepTactin® Sepharose® Amylose Resin TALON® Superflow™ Ni-NTA Agarose	IBA Lifesciences GmbH New England Biolabs Cytiva Qiagen GmbH

2.1.8. Sterilization

Media and supplements used for cultivation of cells were autoclaved at 120 °C for 20 min at 1 bar. Temperature sensitive solutions were filter sterilized using syringe filters with a pore size of 0.22 µm. Glass ware was sterilized by dry heat at 180 °C for 3 h.

2.2. Molecular biological methods

2.2.1. Preparation of plasmid DNA

Plasmid DNA was extracted from *E. coli* TOP10 cells. Therefore, 5 ml of LB containing the appropriate antibiotic (Table 6) were inoculated with a single colony after transformation and cells were grown at 37°C and 160 rpm overnight. For cloning reactions, extraction of plasmid DNA was performed using the E.Z.N.A.® Plasmid DNA Mini Kit I according to the manufacturer's instructions. Purified plasmid DNA was stored at -20°C for further use.

Otherwise, plasmid DNA was isolated by alkaline lysis (Sambrook & Russell 2001). 2 ml of overnight cultures were harvested by centrifugation at 16000 g for 20 min. The cell pellet was resuspended in 200 µl of solution I supplemented with 100 µg/ml RNase A. After addition of 200 µl of solution II the tube was inverted several times and incubated for 2 min at RT. Subsequently, 200 µl of solution III was added and the tube was inverted several times. After incubation on ice for 10 min, the sample was centrifuged at 16000 g for 10 min at 4 °C. The supernatant was transferred in 500 µl of isopropanol (-20 °C) and the mixture was incubated at -20 °C for 20 min. Precipitated DNA was centrifuged at 16000 g for 10 min at 4 °C. The supernatant was discarded, and the pellet was air-dried at 50 °C. The DNA precipitate was washed with 70 % ethanol (v/v) followed by centrifugation at 16000 g for 10 min at 4 °C. The supernatant was discarded, and the pellet was air-dried at 50 °C. DNA was resuspended in 30 µl of MQ water and stored at -20 °C for further use.

Solution I

Tris/HCl pH 7.5	50 mM
EDTA	10 mM
RNase A	100 µg/ml

Solution II

NaOH	0.2 M
SDS	1 % (w/v)

Solution III

Potassium acetate pH 8	1.5 M
→ adjust pH with acetic acid	

2.2.2. Determination of nucleic acid concentrations

Concentrations of DNA in aqueous solutions were determined by measuring the absorbance at 260 nm with a NanoDrop™ Lite photometer (Thermo Fisher) using appropriate elution buffer as a reference. Sample purity was indicated by the ratio of absorbance values at 260 nm and 280 nm.

2.2.3. Agarose gel electrophoresis

Nucleic acids were separated according to their size by agarose gel electrophoresis. Agarose gels were prepared by dissolving 0.8 % (w/v) of agarose in 1x TAE buffer and boiling until the agarose in the solution was melted completely. Gels were casted into prepared gel chambers and polymerized at RT. Samples were prepared using 10x DNA loading dye in a 1x working concentration before loading the gel. The GeneRuler™ DNA Ladder mix was used as a reference standard according to the manufacturer's instructions. Gel electrophoresis was performed in 1x TAE at a constant voltage of 120 V for 35 min. Gels were immersed in ethidium bromide solution (0.05 % v/v ethidium bromide in MQ water) for 10 min. Visualization of nucleic acids was facilitated by excitation of DNA-ethidium bromide complex at 312 nm and documentation was performed via an iX20 imager (Intas).

1x TAE		10x DNA loading dye	
Tris/acetate pH 8	40 mM	Glycerol	40 % (v/v)
EDTA	50 mM	EDTA	10 mM
		SDS	0.5 % (w/v)
		Bromphenol blue	0.025 % (w/v)
		Xylene cyanol	0.025 % (w/v)

2.2.4. Polymerase chain reaction (PCR)

Amplification of specific DNA fragments was conducted by polymerase chain reaction (PCR) (Mullis & Faloona 1987). The Phusion™ High-Fidelity DNA Polymerase was used to reduce the introduction of mutations based on the polymerases 3'-5' exonuclease activity. The reaction was set up according to the manufacturer's instructions in a 50 µl reaction volume.

Table 10: Reaction setup for PCR reactions using Phusion® High-Fidelity DNA Polymerase.

Reagent	Final concentration
5x Phusion® HF Buffer	1x
dNTPs	200 µM each
Forward primer	0.5 µM
Reverse primer	0.5 µM
Phusion® DNA Polymerase	1 U
Template DNA	5-10 ng
H ₂ O	Ad 50 µl

Table 11: Reaction steps for PCRs using Phusion® High-Fidelity DNA Polymerase.

Reaction step	Temperature	Time	
Initial denaturation	98°C	3 min	} 30-35 cycles
Denaturation	98°C	30 s	
Annealing	T _m +3°C	30 s	
Elongation	72°C	2 kb/min	
Final elongation	72°C	Elongation time + 30 s	

After the PCR reaction, samples were analyzed by agarose gel electrophoresis (chapter 2.2.3). Therefore, 9 μ l of the reaction were complemented with 1 μ l of 10x DNA loading dye. For cloning purposes, the remaining 41 μ l were purified and concentrated according to chapter 2.2.5.

2.2.5. Purification of linear DNA

PCR products for cloning reactions were purified using the DNA Clean & Concentrator-5 kit (Zymo Research) according to the manufacturer's instructions. Concentrations of purified DNA fragments was determined as mentioned in chapter 2.2.2.

2.2.6. Restriction endonuclease digestion of nucleic acids

Restriction digest of DNA was conducted using restriction endonucleases in CutSmart™ buffer (New England Biolabs) according to the manufacturer's instructions. Following digestion at 37 °C, restriction endonucleases were thermally inactivated at the required temperature and time. The reaction was performed in a volume at least ten-fold higher than the volume of restriction endonucleases added. For plasmid DNA, digestion efficiency was analyzed by agarose gel electrophoresis (chapter 2.2.3)

2.2.7. Ligation of DNA fragments

Prior to ligation, DNA fragments and suitable vectors were digested by restriction endonucleases (chapter 2.2.6). Subsequently, ligation was performed using a T4 DNA Ligase (New England Biolabs). Vector- and insert DNA were added in a molar ratio of 1:3. The reaction was incubated for 1 h at RT prior to transformation into *E. coli* TOP10 cells (chapter 2.3.5).

2.2.8. Colony PCR

Colony PCR was routinely used to analyse either *E. coli* clones after transformation (chapter 2.3.5) or to verify *Synechocystis* strains after conjugation (chapter 2.3.6). The PCR reaction setup (chapter 2.2.4) was modified by increasing the initial denaturation step to 5 min.

For *E. coli*, single colonies were picked from transformation plates, maintained by streaking on a fresh LB-agar plate with appropriate antibiotics and submerged into the PCR reaction mixture (chapter 2.2.4). For *Synechocystis*, transconjugants after conjugation were transferred onto a fresh BG-11-agar plate containing kanamycin. After

several days of incubation, single colonies were resuspended in 15 μ l of resuspension buffer (5 mM Tris, 0.1 % Triton X-100, pH 7.5). Cyanobacterial suspensions were incubated at 98 °C for 5 min and centrifuged at 16000 *g* for 5 min. 1 to 2 μ l of the supernatant were used as a template for the PCR reaction.

2.2.9. Site-directed mutagenesis

Insertion of specific mutations into DNA sequences was performed by site directed mutagenesis via whole vector amplification using the inverse PCR technique with back-to-back primer orientation. Amino acid sequences were modified by introducing nucleotide mutations in the corresponding oligonucleotides used for amplification. Consequently, the PCR setup conditions using the Phusion™ High-Fidelity DNA Polymerase can be used as indicated in chapter 2.2.4. Following amplification, a so-called KLD- (kinase, ligase, *DpnI*) reaction was performed. Therefore, 1 μ l of the mixture was treated with an enzyme mix containing T4 Polynucleotide Kinase and T4 DNA Ligase to phosphorylate the 5'-ends of nucleotides and circularize the double stranded DNA. Removal of methylated template DNA was performed by *DpnI* restriction enzyme digestion (Table 12). After incubation for 1 h at RT, 10 μ l of the reaction was transformed in *E. coli* TOP10 cells (chapter 2.3.5).

Table 12: Setup for KLD reactions.

Reagent	Volume
10x T4 DNA Ligase buffer	1 μ L
T4 Polynucleotide Kinase	1 μ L
T4 DNA Ligase	1 μ L
<i>DpnI</i>	1 μ L
PCR product	1 μ l
H ₂ O	Ad 50 μ L

2.2.10. Gibson Assembly®

In contrast to T4 DNA ligase assisted cloning of target genes (chapter 2.2.7), DNA fragments were alternatively assembled via Gibson Assembly® (Gibson *et al.*, 2009). Therefore, primer containing a 16-25 bp homologous region to the vector backbone were designed manually. Initially, DNA fragments were amplified by PCR (chapter 2.2.4) and the target vector was prepared by restriction endonuclease digestion (chapter 2.2.6). 25 ng of vector DNA and a 3-fold molar excess of DNA fragments were adjusted with H₂O to a volume of 5 μ l. Subsequently, the DNA mix was added to 15 μ l of Gibson assembly master mix and incubated at 50 °C for 1 h. The homologous 5'-ends of double stranded DNA are digested by the T5-exonuclease (New England Biolabs) to facilitate annealing of DNA fragments. The Phusion® DNA Polymerase (New England Biolabs)

closes the nucleotide gaps at the annealing sites, which is followed by the ligation of nicks using the Taq DNA ligase (Biozym Scientific).

Stock solutions

NAD	50 mM
Tris (pH 7.5)	1 M
MgCl ₂	2 M
DTT	1 M

5x isothermal reaction buffer	Final concentration	Weight / Volume
PEG 8000	25 % (w/v)	0.25 g
Tris (pH 7.5)	500 mM	500 µl
MgCl ₂	50 mM	25 µl
DTT	50 mM	50 µl
NAD	5 mM	100 µl
dNTPs	1 mM (each)	4x 10 µl
H ₂ O		Ad 1 ml

Assembly master mix

5x isothermal reaction buffer	320 µl
T5 exonuclease (10U/µL)	0.64 µl
Phusion® DNA Polymerase (2 U/µL)	20 µl
Taq DNA Ligase (40 U/µL)	160 µl
H ₂ O	Ad 1.2 ml

After the assembly, 10 µl of the reaction were transformed into chemically competent *E. coli* TOP10 cells as mentioned in chapter 2.3.5.

2.2.11. Golden Gate assembly and modular cloning (MoClo)

DNA constructs prepared for the modification of *Synechocystis* cells were prepared by Golden Gate cloning. The method exploits the ability of Type IIS restriction endonucleases to cleave DNA outside of their recognition sequence. Cleavage by type IIS restriction endonucleases generates sticky ends consisting of four nucleotides, which facilitates directional assembly of one or multiple DNA fragments. Golden Gate cloning can be utilized for a hierarchical assembly strategy known as modular cloning (MoClo). The hierarchy of the MoClo syntax is based on plasmid-based sets of genetic parts and acceptor vectors (level 0, level 1 and level 2 or T) which facilitates one-pot assemblies in three successive steps. Every acceptor vector harbours a *lacZα* gene within the cloning site to facilitate initial selection of *E. coli* clones via blue-white screening. The level 0 vectors consist of basic parts (as promoters, UTRs, coding sequences, terminators, etc.), which are assembled in level 1 acceptor vectors and thereby typically form single transcriptional units. In the next step, multiple transcriptional units (level 1) are assembled in level 2 or level T acceptor vectors. While level 2 acceptor vectors were originally developed for genetic modifications in plants and predominantly serve clonal

purposes, the level T vectors for cyanobacterial hosts can additionally harbour genetic elements necessary for conjugation in cyanobacteria as well as an origin of replication for vector replication in the host.

All Golden Gate assembly reactions were performed according to Engler *et al.*, (2014) using a molar ratio between DNA fragments and acceptor vector of 2:1 (Table 13). Efficient performance of restriction endonucleases and the T4 DNA ligase was facilitated by alternating incubation steps at 37 °C and 16 °C, followed by a heat inactivation step after the reaction (Table 14). Eventually, reaction products were transformed in chemically competent *E. coli* (chapter 2.3.5). While level 0 library parts were confirmed by sequencing (chapter 2.2.12), level 1 and level T constructs were verified by colony PCR (chapter 2.2.8) and restriction endonuclease digestion (chapter 2.2.6).

Table 13: Level-dependent components for Golden Gate based modular Cloning reactions.

Level 0 and level T assembly	Concentration / volume	Level 1 assembly	Concentration / volume
PCR product / level 1 parts	50 fmol	Level 0 parts	50 fmol
End linker (level T only)	50 fmol	Acceptor vector	25 fmol
Acceptor vector	25 fmol	ATP (10 mM)	2 µl
ATP (10 mM)	2 µl	CutSmart® buffer	2 µl
CutSmart® buffer	2 µl	<i>Bsal</i> -HF ^{v2}	1 µl
<i>BbsI</i> -HF [®]	1 µl	T4 DNA Ligase	1 µl
T4 DNA Ligase	1 µl	MilliQ water	Ad 20 µl
MilliQ water	Ad 20 µl		

Table 14: Reaction setup for Golden Gate based modular cloning.

Temperature	Time	
37 °C	10 min	} 5 cycles
16 °C	10 min	
65 °C (<i>BbsI</i> -HF [®]) /	20 min	
80 °C (<i>Bsal</i> -HF ^{v2})		
8 °C	∞	

The genetic construct pCGT.STH02 in the strain Syn-pPebS was prepared as follows. Initially, the level 1 construct pCG1.STH03 was assembled into the acceptor vector pICH47732 using the level 0 library part of the strong, light responsive *cpc* promoter (in pC0.005), the level 0 library part containing the *pebS* gene (in pCG0.STH01) and the level 0 part of the *cpc* terminator (in pC0.078). The assembled level 1 construct (pCG1.STH03) was then cloned into the level T cargo vector pCAT.000 via the end linker 1 (in pICH41722) yielding the final construct pCGT.STH02.

The construct pCGT.STH10 in the *Synechocystis* strains WT-PE and Olive-PE were prepared using three level 1 constructs. As the first level 1 construct, pCG1.STH03 was used (as for Syn-pPebS). The second level 1 assembly (pCG1.STH15) into acceptor

vector pICH47742 consists of the strong, constitutive *J23119* promoter (in pC0.049), the *PmcpeB* coding sequence (in pCG0.STH12) and the *rrnB* terminator (in p0.082). The last level 1 assembly (pCG1.STH17) into the acceptor vector pICH47751 was carried out using the constitutive *trc10* promoter (in pC0.059), the *PmcpeS* coding sequence (in pCG0.STH12) and the *rrnB* terminator (in p0.082). All three level 1 constructs were assembled into the cargo vector pCAT.000 via the end-linker 3 (in pICH47751) which yielded the shuttle vector pCGT.STH10.

The construct pCGT.STH11 in WT-PE C82A and Olive-PE C82A was assembled as pCGT.STH10 with one exception. To generate a C82A variant of *PmCpeB*, the nucleotides encoding a cysteine at position 82 (AA numbering) were replaced to encode for an alanine, which yielded the plasmid pCG0.STH13. Using the same genetic parts as mentioned above, pCG0.STH13 was used instead of pCG0.STH12 to assemble the level 1 construct pCG1.STH16 into the acceptor vector pICH47742. To yield the final cargo vector pCGT.STH11, the level 1 vectors pCG1.STH03, pCG1.STH16 and pCG1.STH17 were assembled into pCAT.000 via the end-linker 3 (in pICH47751).

2.2.12. Sequencing of DNA

Constructs for heterologous expression in *E. coli* as well as level 0 library parts generated by Golden Gate assembly were verified by Sanger sequencing at Eurofins Genomics GmbH (Ebersberg). Samples were prepared according to the companies' instructions.

2.3. Microbiological methods

2.3.1. Cultivation of microorganisms

Liquid cultures of *E. coli* were grown in LB medium supplemented with appropriate antibiotics, if necessary, and incubated at 37 °C and 160 rpm (Innova 2300). Cell densities of liquid cultures were determined photometrically at 600 nm (Novaspec III) using sterile LB medium for blank measurements. Cultivation of *E. coli* strains on solid LB-agar medium was performed at 37 °C overnight. *Synechocystis* liquid cultures were grown in BG-11 medium at 30 °C under continuous warm-white LED light at a light intensity of 40 $\mu\text{mol}/\text{m}^2\cdot\text{s}$ and 120 rpm using an Infors Minitron incubator (Infors HT). Transconjugant strains were grown in BG-11 medium supplemented with 50 $\mu\text{g}/\text{ml}$ kanamycin. Densities of *Synechocystis* liquid cultures were measured by reading the absorbance value at 730 nm (Novaspec III) using the appropriate growth medium as a blank. *Synechocystis* strains were maintained on BG-11-agar (1.5 % w/v) supplemented with 50 $\mu\text{g}/\text{ml}$ kanamycin under continuous white light (10 $\mu\text{mol}/\text{m}^2\cdot\text{s}$) at RT.

2.3.2. Cyanobacterial growth experiments

Growth of cyanobacterial cultures were performed under standard cultivation conditions as mentioned in chapter 2.3.1 unless otherwise mentioned. Physiological characterization of the *Synechocystis* strain Syn-pPebS was conducted as biological triplicates in a total culture volume of 100 ml in 500 ml Erlenmeyer flasks. The *Synechocystis* WT and a vector control (VC) harbouring the conjugative vector pCAT.000 were used as a reference. Initially, cultures were adjusted to an OD_{730 nm} of 0.1 (~ 0.28 $\mu\text{g}/\text{ml}$ Chl *a*). During the experiment, growth was monitored by measuring the culture density at an OD_{730 nm} (chapter 2.3.1) and by chlorophyll *a* extraction (chapter 2.4.15). For further evaluation, additional samples were prepared by adjusting the culture density to a final OD_{730 nm} of 1 in 1 ml. Cells were harvested by centrifugation at 6000 *g* and RT for 5 min and the supernatant was discarded. A 100 mg of FastPrep 0.1 mm silica beads and 1 ml of PBS buffer (154 mM NaCl, 5.6 mM Na₂HPO₄, 1.058 mM KH₂PO₄, pH 7.4) were added prior to cell lysis by bead-beating at 30 beats per minutes for 2 min. Subsequently, samples were kept on ice in the dark for 1 h. Separation of the lysate into a soluble and insoluble fraction were performed by centrifugation at 15000 *g* and 4 °C for 5 min. The resulting supernatant was then used for protein (chapter 2.4.11), glycogen (chapter 2.4.16) and phycobiliprotein (chapter 2.4.17) content quantification.

For growth curve experiments under green light, cultures of Syn-pPebS, the *Synechocystis* WT and VC were adjusted to an OD_{730 nm} of 0.1 and grown as biological

duplicates in 100 ml Erlenmeyer flasks with a total culture volume of 30 ml. Cultures were incubated at RT, 100 rpm on a rotary shaker and a light intensity of 22 $\mu\text{mol}/(\text{m}^2\cdot\text{s}^1)$ (HLX 250W 64663). Green light was provided by a lighting filter foil (139 Primary Green, LEE Filters) and adjustment of light intensity for the control conditions under white light was facilitated using a white light transmission foil. Growth was monitored by reading the absorbance values at a wavelength of 730 nm as mentioned before (chapter 2.3.1).

Small scale growth experiments for the *Synechocystis* strains harbouring genes for the *P. marinus* MED4 CpeB assembly (WT-MED4, WT-MED4 C82A, WT-polyMED4, WT-polyMED4 C82A) were performed in biological triplicates. The *Synechocystis* WT and VC served as controls. Therefore, cultures with a total culture volume of 30 ml in 100 ml Erlenmeyer flasks were adjusted to an $\text{OD}_{730 \text{ nm}}$ of 0.1 and incubated under standard conditions (chapter 2.3.1). Growth of cultures was tracked by absorbance measurements as stated above.

Bacterial growth rates (μ) in all growth experiments were calculated as follows:

$$\mu = \frac{\ln N(t_x) - \ln N(t_{x-1})}{t_x - t_{x-1}}$$

$N(t_x)$ = chl *a* content or $\text{OD}_{730 \text{ nm}}$ at timepoint t_x

$N(t_{x-1})$: chl *a* content or $\text{OD}_{730 \text{ nm}}$ at timepoint t_{x-1}

The corresponding doubling (T_d) times were calculated according to the following formula:

$$T_d = \frac{\ln(2)}{\mu}$$

2.3.3. Cryopreservation of microorganisms

E. coli cells were stored in LB medium supplemented with 20 % glycerol (v/v) and appropriate antibiotics, if necessary. For *Synechocystis*, cells were conserved in BG-11 medium supplemented with 6 % DMSO and appropriate antibiotics, if applicable. All strains were flash frozen in liquid nitrogen and stored at -80 °C.

2.3.4. Preparation of chemically competent *E. coli* cells

Chemically competent *E. coli* cells were prepared by diluting an overnight culture of the corresponding strain 1:100 in 100 ml fresh LB medium. Cultures were incubated at 37 °C and 160 rpm to an $\text{OD}_{600 \text{ nm}}$ of ~ 0.5. Cells were collected by centrifugation at 1700 *g* and

4 °C for 10 min in 50 ml centrifugation tubes. Each pellet was resuspended in 50 ml of ice-cold 50 mM CaCl₂ solution and incubated for 1 h. Subsequently, cells were harvested as mentioned above and resuspended in 5 ml of ice-cold 50 mM CaCl₂ solution supplemented with 15 % glycerol (v/v). Aliquots of 200 µl chemically competent cells were flash-frozen in liquid nitrogen and stored at -80 °C until further use.

2.3.5. Transformation of chemically competent *E. coli* cells

Initially, chemically competent *E. coli* cells (chapter 2.3.4) were thawed at RT. Either 50-100 ng of plasmid DNA, 10 µl of ligation- (chapter 2.2.7), KLD- (chapter 2.2.9) or Gibson assembly (chapter 2.2.10) products or 5 µl of Golden Gate assembly reactions (chapter 2.2.11) were added to the cells and the mixture was incubated on ice for 30 min. Subsequently, cells were subjected to a heat shock at 42 °C for 2 min and 600 µl of LB medium were added. After incubation at 37 °C and 160 rpm for 1 h, the cells were collected by centrifugation at 16000 *g* and RT for 2 min. The supernatant was discarded by decanting and the remaining medium was used to resuspend the cells prior to plating on selective LB-agar and incubation at 37 °C overnight.

2.3.6. Conjugation of cyanobacteria via triparental mating

Generation of mutants by conjugation with plasmid DNA was performed via triparental mating by using *E. coli* J53 [RP4] as the helper- and *E. coli* TOP10 strains, harbouring the appropriate pCAT.000 derivatives, as the cargo strains. Prior to conjugation, overnight cultures of the helper (1 ml per conjugation) and cargo strain (5 ml per conjugation) were prepared. Therefore, colonies of *E. coli* J53 [RP4] were used for inoculation in LB medium supplemented with ampicillin (100 µg/ml) as well as kanamycin (40 µg/ml) and colonies of the TOP10 cargo strains were transferred in LB-medium supplemented with kanamycin (50 µg/ml). Both, the helper- and the cargo strains were incubated overnight at 37 °C and 160 rpm. Following overnight growth, cells were harvested at 3000 *g* and RT for 10 min. The pellets were washed three times with fresh LB medium in a volume identical to the initial harvesting volume to remove residual antibiotics. Subsequently, the supernatant was discarded, and the cells were resuspended in fresh LB medium in a half the volume of the initial culture volume. Both *E. coli* cultures were mixed 1:1 in a total volume of 900 µl and incubated at RT until further use. Following the preparation of helper- and cargo strains, *Synechocystis* cultures at an OD_{730 nm} of 0.5 – 1 (1 ml per conjugation) were harvested at 1500 *g* and RT for 10 min. The pellet was washed three times with fresh BG-11 in a volume identical to the initial culture volume. 900 µl of the washed *Synechocystis* cells was added to the combined *E. coli* strains. After incubation

at RT for 30 min, the mixture was centrifuged at 1500 g and RT for 10 min. 1.6 ml of the supernatant were discarded and the pellet was resuspended in the remaining ~200 μ l. The conjugation mixture was spread on 0.45 μ m nitrocellulose membrane (3 cm x 3 cm) placed on LB-BG-11 agar plates lacking antibiotics. Plates were incubated under illumination of warm-white light (80 μ mol/(m²·s¹) at 30 °C for 24 h. Following incubation on LB-BG-11 agar plates, the membranes were transferred onto BG-11 agar plates supplemented with kanamycin (50 μ g/ml), which were incubated in identical conditions until colonies appeared after 7 to 14 days. Transconjugant strains were confirmed by colony PCR (chapter 2.2.8).

2.3.7. Confocal laser scanning microscopy

For confocal laser scanning microscopy of liquid *Synechocystis* cultures, cells were immobilized on agarose pads. Therefore, 1 % low-melting agarose was solubilized in BG-11 medium and cast in SDS-Gel casting stands with 0.75 mm thickness. 5 μ l of exponentially grown cells were spotted on the agarose pads, airdried and covered with a coverslip. Images were obtained with a Zeiss LSM880 AxioObserver confocal laser scanning microscope equipped with a Zeiss C-Apochromat 63x/1.4 oil-immersion objective. For the detection of phycobilin-derived fluorescence, samples were excited with a helium-neon laser at 543 nm. Prior to analysis, single-cell fluorescence emission spectra were recorded (λ scan) to adjust the wavelength intervals for signal acquisition. Based on the observed spectral properties, phycobilin-derived fluorescence emission was recorded between 550-587 nm for PEB and between 607-624 nm for PCB. Chl a emission was detected between 701-721 nm. All images were acquired using identical settings for excitation and detection, pictures were processed utilizing the Zeiss software ZEN 2.3.

2.3.8. Light response curves and oxygen formation

Measurements of oxygen evolution can provide valuable insights into the photosynthetic activity of organisms performing oxygenic photosynthesis. Based on the splitting of water at PS II with oxygen as a byproduct, evaluation of oxygen levels in the surrounding medium can serve as a reporter for photosynthetic activity. Consequently, cells were illuminated using the Mini-Pam II (Heinz Waltz GmbH) as a light source and oxygen content in the medium was detected by an oxygen sensor (OXR50-OI, PyroScience).

Prior to measurements, oxygen sensors were calibrated in a two-step procedure using a 0 % and a 100 % oxygen reference. As a 0 % reference, dissolved oxygen in BG-11

medium was scavenged by the addition of 30 mM Na₂S₂O₄. The 100 % reference was prepared by enriching BG-11 medium with atmospheric air for 20 min using a conventional aquarium air pump.

Initially, cultures of *Synechocystis* in a total volume of 30 ml were grown as biological triplicates to an OD_{730 nm} of 0.4 under the conditions stated in chapter 2.3.1 and the chlorophyll *a* content per ml of culture was determined (chapter 2.4.15). Cyanobacterial suspensions were adjusted to a chlorophyll *a* concentration of 2.5 µg/ml. Therefore, cells were harvested by centrifugation at 3000 *g* for 5 min and resuspended in fresh BG-11 medium (supplemented with 10 mM NaHCO₃ and, kanamycin if applicable). 500 µl of the culture was transferred to a KS-2500 cuvette (Heinz Walz GmbH) with the oxygen sensor connected to it. Measurements were performed under stirring conditions (50 %). After adaptation to the dark for 20 min, cultures were illuminated with 7 progressively increasing light intensities (15, 28, 41, 56, 78, 119, 178 µmol/m²*s), where each illumination period lasted for 3 min to allow stable signal acquisition. After data collection, a moving average with a 17-point data interval was calculated to compensate for minor oscillations during the measurements. Eventually, the oxygen evolution rate per hour was normalized to mg chlorophyll *a*.

2.4. Biochemical and biophysical methods

2.4.1. Production and isolation of recombinant proteins in *E. coli*

2.4.1.1. Production of recombinant proteins – analytic scale

Production of recombinant *GtCpcX* was initially performed on analytical scale to assess protein abundance and solubility using *E. coli*-based expression systems. To identify suitable conditions for downstream protein purification and analyses, a number of key production parameters were evaluated including different *E. coli* strains, expression constructs, induction of gene expression, culturing conditions, media additives and extraction buffer composition. Initially, heterologous CpcX production was performed using short affinity tags as the His-tag encoded on pET_Duet_ *GtCpcX*_oSA (CpcX-His) or the Strep-tag encoded on pASKIBA45+*GtCpcX*_oSA (Strep-CpcX). Based on its solubility-enhancing properties, the additional maltose binding protein-(MBP) fusion constructs MBP-FXa-CpcX-Strep (pMAL_FXa_cpcX-StrepII) and MBP-HRV3C-CpcX-Strep (pMAL_HRV3C_cpcX-StrepII) were prepared to improve folding of the target protein.

All analytical scale expression studies were performed in a total culture volume of 20 ml in 100 ml Erlenmeyer flasks (with baffles) and non-induced cultures were grown under the conditions mentioned in chapter 2.3.1, unless otherwise stated. First, single colonies of *E. coli* strains harbouring the respective plasmid were used to inoculate an overnight culture in 5 ml LB medium with appropriate antibiotic selection. The next day, fresh LB medium supplemented with antibiotics was inoculated 1:100 with the overnight culture. After cultures reached an OD_{600 nm} of ~ 0.5, gene expression and subsequent protein production was induced by the addition of 0.1 mM IPTG (for pET_Duet-and pMAL derivatives) or 200 µg/l AHT (for pASK derivative). After induction, protein expression was performed at different incubation temperatures.

Following heterologous protein production, 2 ml of culture were harvested by centrifugation at 16.000 *g* for 2 min and the supernatant was discarded. To evaluate protein production and protein solubility, cells were lysed by a freeze-thaw approach using a modified procedure of Johnson & Hecht (1994). Cell pellets were frozen in liquid nitrogen for 2 min and subsequently thawed for 8 min by transferring samples in a water bath set to a temperature of 4 °C. The freeze-thaw procedure was repeated twice and the pellet was resuspended in 50 µl of lysis buffer (50 mM Tris, 300 mM NaCl) by scraping the microfuge tube against the openings of a microfuge tube rack for 30 s. Cell suspensions were further incubated in a water bath at 4 °C for 30 min to enhance protein extraction. Eventually, soluble and insoluble fractions were separated by centrifugation

at 10000 *g* and 4 °C for 10 min and each fraction was analyzed by SDS-PAGE (chapter 2.4.12). Initially, analytical scale of heterologous protein production using pET_Duet_GtcpcX_oSA (CpcX-His) and pASKIBA45+GtcpcX_oSA (Strep-CpcX) was performed to evaluate the influence of *E. coli* strains and temperatures after induction of gene expression (Table 15) on target protein solubility. For the production of MBP-CpcX fusion constructs (MPB-FXa-CpcX-Strep and MBP-HRV3C-CpcX-Strep), the *E. coli* strains BL21 and pLysS were used at 17 °C incubation temperature after the induction of gene expression.

Table 15: Analytical scale of heterologous protein production. Different *E. coli* strains and protein production temperatures were evaluated for pET_Duet_GtcpcX_oSA and pASKIBA45+GtcpcX_oSA regarding the yield and the solubility of the target protein. The '+' indicates soluble target protein and the '-' implies insoluble protein using the respective strains.

<i>E. coli</i> strain	BL21	pLysS	RIL	Shuffle	pGro	Rosetta-Gami	AD494	C41	Arctic express RIL	Rosetta pLysS	Tuner
Expression conditions											
30 °C 3 h	-	+	-	-	+	-	-	-	-	-	-
17 °C oN	-	+	-	-	++	-	-	-	-	-	-

The *E. coli* strains pLysS and pGro7 showed an efficient protein production at 17 °C and 30 °C. Further tests were conducted using both strains with an incubation temperature of 17 °C overnight after the induction of gene expression. To increase solubility of recombinant proteins, the lysis buffer (chapter 2.4.1.1) was complemented with various detergents (Table 16). Evaluation of enhanced protein solubility by complementing lysis buffers with detergents was only performed for the Strep- and His tagged CpcX variants using the *E. coli* strains *E. coli* BL21 pLysS and *E. coli* BL21 pGro7. Based on the MPB fusion proteins solubility, target gene expression was performed using *E. coli* pLysS at 17°C overnight and extraction of proteins was performed with lysis buffer without the addition of detergents.

Table 16: Complementation of lysis buffer with detergents to evaluate its effect on target protein solubility. Proteins encoded on pET_Duet_GtcpcX_oSA and pASKIBA45+GtcpcX_oSA were used to assess the usage of detergents for protein extraction. *E. coli* BL21 pLysS and pGro7 served as the platform for heterologous protein production. Target protein solubility was evaluated by categorization of protein abundance with a '+' (+ < ++ < +++).

Detergents	pLysS	pGro7
Chaps (0.5 %, w/v)		++
DDM (1 %, w/v)		++
Tween20 (0.2 %, v/v)	++	+
TritonX-100 (0.2 %, v/v)		++
NP-40 (0.2 %, v/v)		+

After evaluating conditions to yield promising amounts of soluble target protein, heterologous protein production was scaled-up to a total culture volume of 1 l as described in chapter 2.4.1.2.

2.4.1.2. Production of recombinant proteins – preparative scale

Following the evaluation of recombinant protein production parameters on analytical scale (chapter 2.4.1.1), heterologous protein production experiments on preparative scale were carried out using the *E. coli* pLysS and pGro7 strains and the constructs pET_Duet_GtcpcX_oSA, pASKIBA45+GtcpcX_oSA, pMAL_FXa_cpcX-StrepII as well as pMAL_HRV3C_cpcX-StrepII. Therefore, a total culture volume of 1 l in 5 l Erlenmeyer flasks (with baffles) was used and cells were cultivated under standard growth conditions (chapter 2.3.1) until gene expression was induced. Initially, a single colony of *E. coli* cells containing the respective expression plasmid was transferred into 20 ml of LB with appropriate antibiotics. After overnight incubation, the expression culture was inoculated 1:100 and incubated until the culture reached an OD_{600 nm} of ~ 0.5. Protein production was induced with 0.1 mM IPTG (for pET_Duet- and pMAL derivatives) or 200 µg/l AHT (for pASK derivative). Cells were further cultivated overnight at 17 °C and subsequently harvested at 17000 g and 4 °C for 15 min (Sorvall LYNX 6000 Centrifuge, rotor T9). The supernatant was discarded and the cell pellet was transferred into a 50 ml centrifugation tube. Pellets were flash-frozen in liquid nitrogen and stored at -20 °C for further use.

2.4.1.3. Lysis of cells and fractionation

Cell pellets containing recombinant proteins (chapter 2.4.1.2) were thawed on ice and resuspended in 40 ml of ice-cold lysis buffer (chapter 2.4.1.1). For further evaluation of protein solubility on a preparative scale, the lysis buffer was complemented with either 0.2 % TritonX-100 or 0.2 % Tween20 for Strep-CpcX and CpcX-His. Suspensions of *E. coli* strains in lysis buffer were mixed with a spatula tip of DNase I and lysozyme and incubated on ice for 30 min. Cells were routinely lysed using a high-pressure homogenizer (Microfluidizer LM10) for three rounds operated at 15000 psi. In other cases, lysis was performed using sonification (Bandelin Sonopuls HD 2200 with KE 76 tip, 50 % intensity, 9 x cycles) in an ice-water bath. Sonification was performed in three steps, where each step consisted of 30 s sonification and a 1 min lasting cool down phase. Subsequently, the insoluble and soluble fraction of the cell lysate were prepared by centrifugation at 50000 g and 4 °C for 1 h (Sorvall LYNX 6000 Centrifuge, rotor T29). After separation, samples of both fractions were prepared for SDS-PAGE (chapter 2.4.12) and Western Blot (chapter 2.4.13) analysis. The remaining soluble fraction (supernatant) was further used for protein purification via affinity chromatography (chapter 2.4.1.4).

Strep-lysis buffer (Strep-CpcX & MBP-CpcX-Strep variants)		His-lysis buffer (CpcX-His)	
Tris pH 7.9	50 mM	Tris pH 7.9	50 mM
NaCl	300 mM	NaCl	300 mM
		Imidazol	20 mM

2.4.1.4. Purification of recombinant proteins via affinity chromatography

Isolation of target proteins from the soluble lysate was performed via affinity chromatography using a gravity flow approach. The temperature of all buffers was adjusted to 4 °C and stored on ice during the purification procedure. With respect to the fused affinity tags, columns with a total volume of 2 ml containing either StrepTactin® Sepharose® (Strep-tag), Amylose Resin (MBP-tag) or TALON® Superflow™ (His-tag) were prepared according to the manufacturer's instructions.

Prior to sample application, columns were equilibrated with 5 column volumes (CV) of appropriate lysis buffer (as shown below). The supernatant was added to the column and the flowthrough was collected for further analysis. For Strep- or MBP- fused variants, the columns were washed with 10 CV Strep-lysis buffer (chapter 2.4.1.3). In case of protein purification using a His-tag, the resin was washed with 10 CV His-wash buffer. All washing steps were collected for further analysis. Proteins bound to the resin were eluted with 3 CVs of appropriate elution buffer (Strep-elution buffer for Strep fusion constructs, MBP-elution buffer for MBP variants and His-elution buffer for His-tagged proteins). Elution of proteins was collected in 0.5 ml fractions. All fractions collected during purification were analyzed by SDS-PAGE (chapter 2.4.12) and Western Blot (chapter 2.4.13) to evaluate the purification process. The summary of all purification procedures is shown in Table 17.

Strep-elution buffer (Strep-CpcX & MBP-CpcX-Strep variants)		His-wash buffer (CpcX-His)	
Tris pH 7.9	50 mM	Tris pH 7.9	50 mM
NaCl	300 mM	NaCl	300 mM
Desthiobiotin	2.5 mM	Imidazol	50 mM
MBP-elution buffer		His-elution buffer (CpcX-His)	
Tris pH 7.9	50 mM	Tris pH 7.9	50 mM
NaCl	300 mM	NaCl	300 mM
Maltose	10 mM	Imidazol	150 mM

Table 17: Summary of heterologous protein production of CpcX variants in *E. coli*. The '+' indicates the abundance of the target protein CpcX in the corresponding fractions produced during affinity chromatography purification (+ < ++ < +++). The '-' implies the lack of target protein in the marked fractions.

Affinity chromatography	pGro7 + Strep-cpcX			pLysS + His-cpcX	pLysS + MBP-cpcX-Strep
With detergent	NP-40	Tween20	Triton X-100	Tween20	
TALON					
Flowthrough				++	
Wash fraction				++	
Elution				-	
StrepTactin					
Flowthrough	+	+	+		+
Wash fraction	+	+	+		+
Elution	+++	++	+		++
Amylose					
Flowthrough					+
Wash fraction					+
Elution					+++

Elution fractions containing either Strep-CpcX or CpcX-His were combined for subsequent dialysis (chapter 2.4.1.6) and size exclusion chromatography (chapter 2.4.1.7). For MBP fusion proteins, cleavage by proteases to remove the MBP-tag was performed (chapter 2.4.1.5) prior to dialysis and size exclusion chromatography. After purification, all columns were regenerated according to the manufacturer's instructions and stored on 20 % (v/v) ethanol at 4 °C until further use.

2.4.1.5. Protease digestion of recombinant proteins

Protease cleavage of purified fusion proteins (chapter 2.4.1.4) was performed to remove the MBP-tag using either the Factor Xa- (MBP-FXa-CpcX-StrepII) or the PreScission® protease (MBP-HRV3C-cpcX-StrepII). Protein digestion using the Factor Xa protease was performed overnight at 4 °C under stirring conditions according to the manufacturer's instructions. Based on reduced digestion activity by the Factor Xa protease, the protease recognition site was replaced by the PreScission® protease recognition site using site-directed mutagenesis (chapter 2.2.9). Cleavage of MBP-HRV3C-CpcX-Strep by the PreScission® protease was performed overnight at 4 °C under stirring conditions. Therefore, 10 µl laboratory proprietary PreScission® protease (2 U/100 µg) per ml of elution fraction were added to the purified protein. After protein cleavage, a white precipitate was observed. The digestion reaction was performed with different concentrations of Tween20 (0.01 %, 0.025 %, 0.05 % and 0.1 %, v/v) in elution buffer to enhance protein solubility. Subsequently, the MBP-tag was removed by a second round of affinity chromatography (chapter 2.4.1.4) using amylose resin. Cleaved CpcX-Strep was collected in the flowthrough fraction and subjected to dialysis (chapter 2.4.1.6) as well as size-exclusion chromatography (chapter 2.4.1.7).

2.4.1.6. Dialysis and protein concentration

Purified Strep-CpcX and CpcX-His after affinity chromatography (chapter 2.4.1.4) and cleaved CpcX-Strep (prior MBP fusion protein, chapter 2.4.1.5) were dialyzed against the 250-fold sample volume of Lyase assay buffer (25.25 mM NaH₂PO₄, 34.75 mM Na₂HPO₃, 300 mM NaCl, pH 7.5). Therefore, elution fractions were transferred into a dialysis tubing with an exclusion limit of 14 kDa (Visking MWCO 14000). Dialysis was performed overnight at 4 °C under stirring conditions. Concentration of samples for size exclusion chromatography (chapter 2.4.1.7) was conducted by centrifugation at 1480 g and 4 °C using a centrifugal concentrator (Amicon® Ultra 15-10 kDa MWCO). Prior use, centrifugal concentrators were washed with MQ water and equilibrated with the appropriate lysis buffer.

2.4.1.7. Polishing and determination of protein oligomerization state

Size exclusion chromatography (SEC) is a chromatographic method to separate molecules based on their size, or more precisely based on their hydrodynamic radius, by filtration through a porous, gel-like column matrix. While smaller molecules tend to be retained longer in pores of the column, larger molecules migrate faster through the matrix. Consequently, large molecules have a lower retention time compared to small molecules, which leads to elution profiles correlating with the size of globular proteins. SEC can serve multiple purposes. On the one hand, proteins can be further purified and on the other hand, their oligomerization state can be determined. Therefore, the proteins apparent molecular weight was determined by using commercial standards (Gel Filtration Markers Kit 29 kDa-700 kDa) consisting of proteins with known relative molecular mass. SEC was performed at 4 °C and a flowrate of 0.2 ml/min using either a Superdex® 75 10/30 GL or a Superdex® 200 Increase 10/30 GL connected to an ÄKTA pure™ or ÄKTApurifier FPLC system. The column volume was 24 ml for each column. All buffers were filter sterilized (0.22 µm) and degassed by sonification for 15 min. Prior to use, columns were washed with 2 CV of MQ water and equilibrated with 2 CV of Lyase assay buffer (chapter 2.4.1.6). Protein solutions were filtered and centrifugated at 16000 g and 4 °C for 2 min. Subsequently, samples were applied using a 500 µl sample loop and eluted with 1.5 CV of the respective lysis buffer. Elution was monitored by reading the absorbance at 280 nm and fractions were collected in 0.5 ml volumes. Protein containing fractions were either subjected to precipitation (chapter 2.4.10) for SDS-PAGE (chapter 2.4.12) and Western Blot (chapter 2.4.13) analysis or combined and concentrated with centrifugal concentrators as mentioned in chapter 2.4.1.6 to perform phycobilin binding assays (chapter 2.4.1.8).

2.4.1.8. Phycobilin interaction assay

Phycobilins exhibit characteristic spectral properties based on their chemical nature. These properties typically change upon interactions between a phycobilin and a PBP lyase or through covalent linkage to a PBP. While interactions between phycobilins and PBP lyases are of non-covalent nature, binding of chromophores to PBPs is established via a thioether bond. Binding of such chromophores typically results in a conformational change of the phycobilin, which is reflected in altered spectroscopic properties. Therefore, chromophore binding to a PBP lyase can be monitored using UV-Vis spectroscopy (chapter 2.4.18). The phycobilins used in this assay originated from laboratory internal stock solutions. Prior to spectroscopic measurements, their purity was evaluated by HPLC analysis (data not shown).

Initially, absorbance spectra between 250 nm and 750 nm were recorded for free phycobilins (5 μ M) in Lyase assay buffer (chapter 2.4.1.6). After the addition of \sim 20 μ M CpcX, absorbance spectra were acquired every 2 min. The interaction between CpcX and PEB, PCB and DHBV were analyzed. Data was normalized to absorbance values at 750 nm.

2.4.2. Isolation of phycocyanin from *Synechocystis*

2.4.2.1. Cultivation of cells and lysis

For the purification of the native PC, cultures of *Synechocystis* were grown in a total culture volume of 500 ml in 2 l Erlenmeyer flasks. After adjusting the cultures' optical density at 730 nm to 0.1, cells were grown under indicated culture conditions (chapter 2.3.1) and collected at an OD_{730 nm} of 1 by centrifugation at 6000 g and RT for 15 min. The pellet was freeze-dried for 24 h (ALPHA 2-4 LSC plus) until further use. Freeze-dried samples were thawed on ice and resuspended (10 ml/100 mg cell dry weight) in Na-phosphate buffer (21.59 mM NaH₂PO₄, 28.41 mM Na₂HPO₄, pH 7). Cell lysis was performed for 2 min on ice with 30 s sonification pulse and 30 s cool down using sonification with 9 cycles and 50 % power at 4 °C (Tip KE 76, Sonopuls HD2200). Soluble and insoluble fractions were separated by centrifugation at 16000 g and 4 °C for 10 min.

2.4.2.2. Salting out of proteins via ammonium sulfate precipitation

A common technique to fractionate protein mixtures is salting out of proteins via ammonium sulfate precipitation. The addition of salt increases the surface tension of water, which increases the hydrophobic interactions between water and proteins. Consequently, the proteins surface area is reduced, which diminishes its contact with the solvent and eventually leads to protein precipitation. Based on each protein's individual properties, protein mixtures can be fractionated.

The supernatant of *Synechocystis* lysate (chapter 2.4.2.1) was subjected to ammonium sulfate precipitation at 30 % (w/v) and 70 % (w/v) saturation. Therefore, crystalline ammonium sulfate was gradually added at 4 °C under stirring conditions. Once the salt was dissolved, the samples were stirred under the same conditions for at least 2 h. After each step, samples were centrifuged at 50000 g and 4 °C for 30 min (Sorvall LYNX 6000 Centrifuge, rotor T29). The resulting pellet of the 70 % saturation step was resuspended in 5 ml of purification buffer (20 mM Bis-Tris, pH 7) and dialyzed overnight. For dialysis, tubing with a molecular weight cut-off of 14 kDa were used as mentioned in chapter 2.4.1.6.

2.4.2.3. Anion exchange chromatography

Ion exchange chromatography is a method, which is used to separate proteins according to their net surface charge. More specifically, anion exchange chromatography employs a positively charged ion exchange resin, here diethylaminoethyl (DEAE), which has an affinity for negatively charged molecules. After binding of the negatively charged proteins to the resin, they can be eluted by increasing salt concentrations. The ions in the salt solution (e.g., Cl⁻) will thereby compete with the negatively charged proteins in binding to the resin. Prior to sample application, the HiTrap™ DEAE Sepharose FF anion exchange column (1 ml CV) connected to an ÄktaPure FPLC system was equilibrated with 5 CV of purification buffer. All steps during anion exchange chromatography were performed at a flowrate of 1 ml/min. Subsequently, the dialyzed sample (chapter 2.4.2.2) was loaded onto the column via a 5 ml sample loop and the column with bound proteins washed with at least 10 CV of purification buffer. Elution of PC containing fractions was performed with a stepwise increasing concentration gradient of NaCl (0.1 M, 0.15 M, 0.2 M, 0.25 M and 0.3 M) in purification buffer (chapter 2.4.2.2). Elution of proteins was monitored via absorbance readings at 280 nm with a built-in UV detector and 0.5 ml fractions were collected with a fraction collector. The fractions containing PC were combined and concentrated to a maximum volume of 500 µl using centrifugal concentrators (chapter 2.4.1.6) with a molecular weight cut-off of 14 kDa.

2.4.2.4. Preparative size exclusion chromatography

Preparative size exclusion chromatography was performed using a Superdex 200 increase 10/300 GL connected to an ÄktaPure FPLC System. All steps were performed at 4 °C and a flowrate of 0.2 ml/min. Prior to injection of the sample, the column was equilibrated with 2 CV of purification buffer (chapter 2.4.2.2). The concentrated protein sample after anion exchange chromatography (chapter 2.4.2.3) was then applied onto the column via a 500 µl sample loop. The elution of proteins with 1.5 CV purification buffer was monitored via absorbance readings at 280 nm with a built-in UV detector and 0.5 ml fractions were collected with a fraction collector. The purity of all protein containing fractions was assessed by SDS-PAGE (chapter 2.4.12) and samples exclusively containing PC were combined and concentrated using a centrifugal concentrator with a molecular weight cut-off of 14 kDa. Concentrated samples were used for UV-Vis (chapter 2.4.18) and fluorescence emission (chapter 2.4.19) analysis or precipitated (chapter 2.4.10) for storage at -20 °C and subsequent buffer exchange.

2.4.3. Purification of recombinant proteins from *Synechocystis*

The genes *PmcpeB* and *PmcpeS* of *P. marinus* MED4 were expressed in *Synechocystis* under control of constitutive promoters P_{J23119} and P_{trc10} , respectively. The corresponding recombinant proteins were purified from the *Synechocystis* transconjugants WT-PE, WT-PE C82A, Olive-PE and Olive-PE C82A. To facilitate protein purification via affinity chromatography, a *PmCpeB* fusion protein containing a Strep-tag and a *PmCpeS* variant harboring a His-tag were prepared accordingly. Therefore, 500 ml of total culture volume in 2 l Erlenmeyer flasks were inoculated to an $OD_{730\text{ nm}}$ of 0.1 and grown under standard cultivation conditions (chapter 2.3.1). Cells were harvested at an $OD_{730\text{ nm}}$ of 1 by centrifugation at 6000 *g* and 4 °C for 20 min (Sorvall LYNX 6000 Centrifuge, rotor T9) and the supernatant was discarded. Prior to cell lysis by high-pressure homogenization as pointed out in chapter 2.4.1.3, the pellet was resuspended in sodium-phosphate buffer (60 mM sodium phosphate, 100 mM NaCl, pH 7.5). After homogenization, the lysate was separated in a soluble and insoluble fraction via centrifugation at 50000 *g* and 4 °C for 45 min (Sorvall LYNX 6000 Centrifuge, rotor T29).

For the purification of both recombinant proteins, gravity flow columns with a total CV of 1 ml were prepared according to the manufacturer's instructions using Strep-Tactin Sepharose for the Strep-tagged *PmCpeB* and Ni-NTA resin for the His-tagged *PmCpeS*. Prior to sample application, columns were equilibrated with 5 CV of sodium phosphate buffer. The supernatant was added to the Strep-Tactin column and the flowthrough was collected for subsequent application onto the Ni-NTA gravity flow column to purify

PmCpeS-His. For *PmCpeB*-Strep, the columns were washed with 10 CV sodium phosphate buffer and bound proteins were eluted with 3 CVs of sodium phosphate buffer complemented with 2.5 mM desthiobiotin. Elution of proteins was collected in 0.5 ml fractions. In case of protein purification using a His-tag, the Ni-NTA resin with the applied flowthrough of the Strep-Tactin column was washed with 10 CV Ni-Wash buffer 1 (sodium phosphate buffer with 10 mM imidazol). Subsequently, the column was washed again with 10 CV of Ni-Wash buffer 2 (sodium phosphate buffer complemented with 20 mM imidazol). Eventually, elution of proteins was performed with 4 CV of Ni-Elution buffer (sodium phosphate buffer with 250 mM imidazol) and fractions with a volume of 1 ml were collected. All fractions collected during purification were analyzed by SDS-PAGE (chapter 2.4.12) and fluorescence emission analysis after excitation at 550 nm (chapter 2.4.19). Elution fractions of each protein purification procedure were combined and subjected to protein precipitation (chapter 2.4.10) to concentrate the samples for subsequent SDS-PAGE (chapter 2.4.12) and tryptic in-gel digestion (chapter 2.4.5) for mass spectrometry analysis (chapter 2.4.8).

2.4.4. Tryptic digestion in solution

Identification and characterization of proteins by mass spectrometry is a common method in proteomic analyses. Prior to protein identification, endopeptidases as trypsin are commonly used to digest the proteins into peptides. Trypsin thereby cleaves at the carboxyl site of lysine and arginine residues, yielding predictable peptide fragments. The resulting tryptic peptides can then be analyzed based on their mass to charge ratio.

For HPLC and LC-MS analysis of chromopeptides, tryptic digest of proteins was performed in solution using trypsin from bovine pancreas (T4799, Sigma-Aldrich). Therefore, freeze-dried PC pellets after protein precipitation (chapter 2.4.10) were resuspended in 50 mM ammonium bicarbonate (pH 7.8). After the determination of the sample's protein content (chapter 2.4.11), trypsin was added in a ratio of 1:20 (w/w, trypsin to protein). Digestion by trypsin was performed in the dark at 37 °C overnight. The tryptic digest was inactivated by the addition of 30 % (v/v) acetic acid. Samples were desalted using a Sep-Pak[®] C18 3cc Vac cartridge (Waters Corporation). Prior to sample application, the sorbent was preconditioned with 4 ml of 100 % methanol (MeOH) and 4 ml of 0.1 % (v/v) trifluoroacetic acid (TFA) (in water). After adsorption of the tryptic peptide solution, the cartridge was washed four times with 4 ml of 0.1 % (v/v) TFA (in MQ water). Elution of sample was performed by the addition of 4 ml 100 % MeOH. The solvent containing desalted, tryptic peptides was evaporated (RVC 2-25 CDplus) for further HPLC analysis (chapter 2.4.6).

2.4.5. Tryptic in-gel digestion

Tryptic digest can be performed in solution (chapter 2.4.4) and in-gel with samples derived from SDS-PAGE separation. Tryptic in-gel digestion was employed to confirm heterologous protein biosynthesis in *Synechocystis*. Samples after SDS-PAGE were based on whole cell protein and soluble lysate preparations (chapter 2.4.12).

After separation of proteins by SDS-PAGE (chapter 2.4.12), the gel was immersed in MQ water for 5 min and stained with colloidal Coomassie solution (chapter 2.4.12) for 1 h under shaking conditions. Signals of interest were excised with a razor blade and cut into pieces of an approximate size of 1 mm². The gel pieces were transferred into a 1.5 ml microfuge tube and subsequently destained with 500 µl of destaining solution (40 % MeOH and 10 % acetic acid in MQ water) for 30 min using a rotary shaker. Subsequently, gel particles were equilibrated with 300 µl of 40 mM ammonium bicarbonate (ABC buffer) for 5 min while shaking thoroughly. The liquid was discarded and 300 µl of 70 % acetonitrile (ACN) were added. After shaking thoroughly for 10 min, the solvent was removed. Incubation in ABC buffer and 70 % ACN was repeated twice. Dehydration was performed by 300 µl of 100 % ACN for 10 min under shaking conditions. The solvent was discarded, and remaining liquids were removed by evaporation (RVC 2-25 CDplus) for 10 min. Rehydration was performed by covering the gel particles with 40 mM ammonium bicarbonate complemented with trypsin (Pierce trypsin protease, MS grade) at a final concentration of 10 ng/µl. Following incubation at RT for 15 min, small volumes of ABC buffer were added to completely cover the gel particles. Digestion of proteins was performed at 37 °C overnight. After incubation, condensed liquids were collected by centrifugation at 6000 g for 30 s and 20 % formic acid (FA) were added to a final concentration of 2 %. Extraction of peptides was facilitated by incubation for 10 min under shaking conditions. The peptide containing supernatant was transferred into a new 1.5 ml microfuge tube and solvents were evaporated (RVC 2-25 CDplus). Elution of tryptic peptides was promoted by the addition of 100 µl buffer 1 (10 % ACN and 2 % FA in water) to the gel particles and vigorous shaking for at least 30 min. The remaining supernatant was combined with the peptide containing supernatant subjected to evaporation. Lastly, gel particles were incubated in 200 µl of buffer 2 (60 % ACN and 2 % FA in water) under shaking conditions for at least 30 min. Eventually, the resulting supernatant was again combined with the peptide containing supernatant subjected to evaporation. After complete removal of liquids, dried samples were stored at -20 °C until further use.

2.4.6. Separation of chromopeptides by RP-HPLC

Separation of organic compounds including peptides was performed via reversed phase high performance liquid chromatography (RP-HPLC). RP-HPLC is a method of liquid chromatography that separates analytes depending on their polarity by using a non-polar stationary phase and a polar mobile phase. In reversed phase mode, the compounds are longer retained by the stationary phase the more hydrophobic they are.

Desalted, freeze-dried peptide samples (chapter 2.4.4) were resuspended in solvent A (0.1 % FA in MQ water) by sonification in a water bath. Peptides were applied onto a YMC-Triart C18 reverse phase column (10.0 x 2.1 mm) tempered to 40 °C, which was connected to a Shimadzu Prominence LC-20A HPLC system. The samples were eluted by a binary gradient of buffer B (0.1 % FA in ACN) from 15-60 % over 17 min and from 60-80 % over 5 min at a flowrate of 0.3 ml/min. Elution of peptides was followed by a built-in diode array detector and fractions were collected in a volume of 150 µl. Subsequently, all liquids of the collected fractions were removed by evaporation (RVC 2-25 CDplus) and the pellets were stored at -20 °C until further use.

2.4.7. Desalting of peptides via STAGE tips

STAGE tips for desalting of tryptic peptides were prepared by stamping out two stacks of Empore™ C18 SPE (solid phase extraction) discs using a blunt-tipped hypodermic needle attached to a retractable, spring-loaded syringe as demonstrated by Franz & Li (2015). The discs inside the needle tip were fixed at the tapering end of a 200 µl pipette tip. Conditioning of STAGE tips was performed by the addition of 50 µl solution B (0.1 % TFA, 1 % FA and 60 % ACN in water). The liquid was moved through the column via centrifugation at 300 g for 5 min by placing the pipette tip rack on a 96 deep well plate. Equilibration was performed by repeating the procedure with solution A (0.1 % TFA, 1 % FA, 2 % ACN in water). Dried samples of tryptic in-gel digestion (chapter 2.4.5) were resuspended in 50 µl of solution A by vigorous shaking and sonification. Prior to sample application on prepared STAGE tips, insoluble debris was removed by centrifugation at 15000 g for 3 min. After sample application, the column was washed four times by the addition of 50 µl solution A. Elution of samples was performed with 70 µl solution B. Eventually, the solvent of eluted peptides was evaporated and stored at -20 °C until further use.

2.4.8. Liquid Chromatography-Mass spectrometry (LC-MS) analysis

Tryptic, desalted peptides were resuspended in 30 μl of 0.1 % TFA, 1 % FA and 1 % ACN in MQ water (all solvents were LC-MS grade) by vigorous shaking and sonification. Samples derived from HPLC separation (chapter 2.4.6) were analyzed by LC-MS/MS using a Eksigent 425 HPLC coupled to a TripleTOF 6600 (AB Sciex). Initially, peptide samples were separated using a nanoHPLC with a flow rate of 4 $\mu\text{l}/\text{min}$ via a gradient from 5 % to 70 % of buffer B (buffer A: 0.1 % FA and 1 % ACN; buffer B: 0.1 % FA and 90 % ACN) over 11 min. The mass spectrometer was operated in positive ion mode. MS1 spectra between 350 m/z and 1500 m/z were acquired for 250 ms. Thereby, 20 MS/MS scans (between 100 m/z and 1500 m/z) were triggered in high sensitivity mode with a dwell time of 40 ms resulting in a total cycle time of 1100 ms. Exclusion of analyzed precursors was set for 7 s and singly charged precursors or precursors having a response below 300 cps were completely excluded from MS/MS analysis. Identification of PEB- and PCB-containing peptides was performed manually by filtering MS spectra for the CpcA-derived peptide C₈₄AR with an additional monoisotopic mass of 586.27 for the phycobilins PEB or PCB. Additionally, MS/MS spectra were filtered for PEB or PCB fragments. MS1 precursor masses and MS/MS fragment masses were assigned to the corresponding peaks using the PeakView2 software (AB Sciex).

Peptides derived from tryptic in-gel digestion (chapter 2.4.7) were analyzed by a nanoUHPLC-LC-MS system (nanoElute coupled to timsTOF Pro2, Bruker). Samples were applied onto a C18 column with an integrated emitter (25 cm, 75 μm ID, 1.6 μm particle size, Odyssey series, IonOpticks) tempered to 50 °C. Peptides were separated at a flow rate of 0.3 $\mu\text{l}/\text{min}$ using buffer A (0.1 % FA in water) and buffer B (0.1 % FA in ACN) using a linear gradient from 2 % B to 27 % B over 35 min, followed by an increase to 35 % within 3 min. After each run, the system was washed and equilibrated again. MS was performed in positive mode; electrospray voltage was set to 1.4 kV and spectra were recorded between a range of 100 – 1700 m/z . 10 MS/MS PASEF ramps (1/ K_0 – 1.43 $\text{V}^*\text{s}/\text{cm}^2$) with 100 ms duration were recorded per cycle and target intensity for MS/MS was set to 14500. Subsequently, precursors were excluded from fragmentation for 0.4 min. Recorded data was searched against the UniProt database for the *Synechocystis* sp. PCC 6803 proteome (Proteome ID: UP000001425) and against the *Prochlorococcus marinus* MED4 CpeB and CpeS amino acid sequences using the FragPipe v19.1 processing pipeline selecting the default LFQ-MBR workflow with minor modifications (Yu *et al.*, 2020). The peptide length was limited to a minimum of 6 amino acids, missed cleavages to 3 and normalization of intensities between different runs was omitted.

2.4.9. Isolation of intact phycobilisomes from *Synechocystis*

Intact phycobilisomes were isolated from *Synechocystis* cultures by sucrose density ultracentrifugation. All steps were performed at RT unless otherwise mentioned. Cells were cultivated under the conditions mentioned in 2.3.1 in a total volume of 200 ml using 1 l Erlenmeyer flasks. Cultures were harvested at an OD_{730 nm} of 0.7 at 6000 g for 15 min (Sorvall LYNX 6000 Centrifuge, rotor T9). The pellet was resuspended in 2 ml of 0.75 M potassium-phosphate buffer (pH 7) and transferred in a new 2 ml reaction tube. Following centrifugation at 3000 g for 5 min, the pellet was resuspended in 0.75 ml of potassium-phosphate buffer. Cells were disrupted after addition of ~ 200 mg of 0.1 mm FastPrep silica beads and bead beating at 30 bpm for 1 min. Mechanical lysis was performed four times with 1 min break after each bead beating interval. Separation of beads and insoluble cell debris from the soluble components was performed by a two-step centrifugation procedure with both being performed at 15000 g for 15 min. Between both steps, the supernatant was transferred to a new 1.5 ml microfuge tube. After the second centrifugation step, Triton X-100 was added to the supernatant to a final concentration of 2 % (v/v). After mixing for 15 min under shaking conditions, the sample was centrifuged at 15000 g for 10 min. The lower, aqueous phase contains PBSs and other soluble proteins and is transferred in a new 1.5 ml reaction tube. The remaining upper layer consisting of Triton X-100, chlorophyll *a* and other proteins was discarded. The PBSs were further enriched by sucrose density ultracentrifugation. Discontinuous sucrose gradients were prepared by layering the following rising concentrations of sucrose solution in ultracentrifugation tubes (Polyallomer tubes 14 ml): 2.8 ml of 1.5 M, 2.8 ml of 1 M, 2.3 ml of 0.75 M and 1.8 ml of 0.5 M sucrose solution. All sucrose solutions were prepared by dissolving the corresponding amount of sucrose in 0.75 M Potassium-phosphate buffer (pH 7). After preparation of the gradient, 3 mg of protein extract were applied on top of the gradient. PBS separation was performed via ultracentrifugation at 130000 g and 20 °C for 16 h (Optima L-80 XP centrifuge, SW40 Ti swinging-bucket rotor). Subsequently, coloured fractions were extracted from the gradient and transferred in new 1.5 ml reaction tubes for further analysis.

2.4.10. Protein precipitation

Precipitation of proteins was performed via two different methods based on protein abundance and downstream protein analysis. Acetone precipitation was used after the purification of PC from *Synechocystis* (chapter 2.4.2) for storage of the protein pellet at -20 °C and subsequent buffer exchange for tryptic protein digestion (chapter 2.4.4). Purified PC was precipitated by the addition of 80 % ice cold acetone (v/v) and incubated

overnight at -20 °C. Following incubation, precipitated proteins were collected by centrifugation at 16000 g and 4 °C for 15 min and the supernatant was discarded. Residual acetone was removed from the pellet by air drying. Precipitated and air-dried PC was stored at -20 °C until further use.

For *E. coli*-based expression studies on analytical scale, precipitation was performed by using a combination of trichloroacetic acid (TCA) and deoxycholate (DOC) according to Koontz (2014). DOC assists in precipitation of proteins by acting as a co-precipitant. Once DOC binds to the hydrophobic patches on the protein surface, its readily precipitating in acidic conditions (Bodzoń-Kuślakowska *et al.*, 2013). The following steps are based on 1 ml sample volume. Initially, 100 µl of 0.15 % DOC were added to the protein solution followed by brief vortexing. After incubation at RT for 10 min, 50 µl of 100 % TCA were added to the sample, which is then incubated on ice for 30 min. Precipitated protein was collected by centrifugation at 10000 g and 4 °C for 10 min and the supernatant was discarded. The remaining pellet was washed with 500 µl ice cold acetone and centrifuged as mentioned in the step before. After removal of the acetone, the pellet was air dried and resuspended in 1x SDS sample buffer (chapter 2.4.12).

2.4.11. Determination of protein concentration

The protein concentration of samples was determined via the Bradford assay (Bradford 1976) using the ROTI®Quant (5x) reagent. Therefore, 50 µl of protein solution were transferred in microtiter plates followed by the addition of 250 µl 1x ROTI®Quant. After incubation at RT for 20 min, absorbance values at 595 nm were recorded (Infinite F200 pro, Tecan). Protein concentrations were derived from a calibration curve consisting of a bovine serum albumin (BSA) dilution series in lysis buffer ($R^2 = 0.99$). As a reference, 50 µl of the corresponding lysis buffer were mixed with 250 µl 1x ROTI®Quant. Technical triplicates were employed for samples of the calibration curve and the blank measurements. Prior to data evaluation, sample values were normalized to blank measurements.

2.4.12. SDS-polyacrylamide gel electrophoresis (SDS-PAGE)

Purification procedures and purity of protein containing fractions were analyzed using denaturing SDS-polyacrylamide gel electrophoresis (SDS-PAGE). In this approach proteins are separated according to their molecular weight based on differential rates of migration through a matrix of polyacrylamide. Two different separation systems were used based on the desired resolution. For heterologous expression experiments in *E. coli* and protein identification in cyanobacterial cells or soluble lysates, Tris-glycine SDS-

PAGE was employed (Lämmli 1970). Here, a setup consisting of a separation gel (pH 8.8) with an acrylamide concentration of 12.5 % and a stacking gel (pH 6.8) with an acrylamide concentration of 5.25 % was used.

For (Tris-glycine) SDS-PAGE samples derived from cyanobacterial cells, cultures were adjusted to an OD_{730 nm} of ~ 2 in 1 ml and cells were harvested by centrifugation at 16000 g and RT for 5 min. The supernatant was discarded and the cell pellet was resuspended in 50 µl of 1x SDS loading dye. For samples of soluble lysates, 30 ml of culture were harvested at an OD₇₃₀ of 0.7 by centrifugation at 1480 g and 4 °C for 10 min. The supernatant was discarded and the cells were resuspended in 200 µl sodium-phosphate buffer (chapter 2.4.3). After the addition of 100 mg FastPrep silica beads (0.1 mm), cells were lysed by vortexing for 10 min. Following centrifugation at 16000 g for 5 min, the supernatants protein content was determined (chapter 2.4.11) and samples were resuspended in 1x SDS loading dye.

4x SDS stacking buffer		4x SDS separation buffer	
Tris-HCl pH 6.8	0.5 M	Tris-HCl pH 8.8	1.5 M
SDS	4 % (w/v)	SDS	0.4 % (w/v)
1x SDS running buffer		5x SDS sample buffer	
Tris-HCl pH 8.8	25 mM	Tris-HCl pH 6.8	250 mM
Glycine	192 mM	SDS	10 % (w/v)
SDS	1 % (w/v)	Glycerol	50 % (v/v)
		DTT	500 mM
		Bromphenol blue	0.025 % (w/v)
Stacking gel 5.25 % (4 mini gels)		Separating gel 12 %	
ROTIPHORESE®Gel 30	1.4 ml	ROTIPHORESE®Gel 30	6.7 ml
4x stacking buffer	2 ml	4x separation buffer	4 ml
H ₂ O	4.6 ml	H ₂ O	5.3 ml
APS (10 %)	0.03 ml	APS (10 %)	0.08 ml
TEMED	0.02 ml	TEMED	0.008 ml
Staining solution		Destaining solution	
Acetic acid	10 % (v/v)	Acetic acid	10 % (v/v)
Ethanol	30 % (v/v)	Ethanol	30 % (v/v)
Coomassie Brilliant Blue G-250	0.25 % (w/v)		
Colloidal Coomassie staining solution		Colloidal Coomassie Destaining solution	
H ₃ PO ₄	10 % (v/v)	Acetic acid	10 % (v/v)
(NH ₄) ₂ SO ₄	10 % (w/v)	Methanol	40 % (v/v)
Methanol	20 % (v/v)		
Coomassie Brilliant Blue G-250	0.12 % (w/v)		

For protein separation of samples collected during the purification of PC from Syn-pPebS (chapter 2.4.2), Bis-Tris SDS-PAGE with MES running buffer was employed to facilitate increased separation resolution of low molecular weight proteins with similar size.

7x Bis-Tris buffer		20x MES buffer	
Bis-Tris (HCl, pH 6.6)	2.5 M	MES	1 M
		Tris	1 M
Reducing agent stock solution		SDS	2 % (w/v)
Sodium bisulfite	1 M	EDTA	20 mM
Stacking gel 4 % (4 mini gels)		Separation gel 12 % (4 mini gels)	
ROTIPHORESE®Gel 30	1.32 ml	ROTIPHORESE®Gel 30	8 ml
7x Bis-Tris buffer	0.94 ml	7x Bis-Tris buffer	1.88 ml
H ₂ O	7.68 ml	H ₂ O	10.1 ml
TEMED	0.02 ml	TEMED	0.04 ml
APS (10 %)	0.04 ml	APS (10 %)	0.08 ml

Prior to protein separation, all samples in 1x SDS loading dye were incubated for 5 min at 98 °C and centrifuged at 16000 *g* and RT for 2 min (centrifuge 5415 D, rotor F-45-24-11). Tris-glycine SDS-PAGE was carried out at 200 V for 50 min, Bis-Tris SDS-PAGE was conducted at 150 V for 1.5 h. After SDS-PAGE separation, proteins were routinely visualized with staining solution. For peptide identification via tryptic in-gel digestion and subsequent LC-MS analysis, proteins were visualized using Colloidal Coomassie staining solution. Removal of background signals after staining was achieved by using the appropriate destaining solution until an optimal signal-to-background ratio was observed. All staining and destaining procedures were performed at RT under shaking conditions.

2.4.13. Western Blot and immunodetection of recombinant proteins

Western Blot analysis was employed to detect recombinant fusion proteins using antibody conjugates (Table 8) for either chromogenic or chemiluminescent detection (Towbin *et al.*, 1979). Initially, protein samples were separated by SDS-PAGE (chapter 2.4.12) and transferred onto a PVDF membrane via semi-dry blotting. Therefore, the PVDF membrane was activated in 100 % MeOH for 10 min, rinsed with water and equilibrated in Towbin buffer for 5 min. Additionally, two sheets of Whatman paper (3 mm thickness) and the SDS-gel were equilibrated in Towbin buffer for 5 min. After assembling a stack (from bottom to top) of Whatman paper, PVDF membrane, SDS-gel and a second Whatman paper, the electrophoretic transfer was performed at 15 V for 16 min. Following the protein transfer, the PVDF membrane was incubated in blocking buffer for either 1 hour at RT or overnight at 4 °C under shaking conditions. Blocked membranes were washed three times by incubation in PBS-T for 5 min at RT under shaking conditions. For detection of StrepII-tagged proteins, biotinylated proteins were additionally blocked with 2 µg/ml avidin in PBS-T for 10 min at RT under shaking conditions. Subsequently, antibodies at indicated dilution factors (Table 8) in PBS-T were applied for 1 h at RT under shaking conditions. After incubation, antibody solutions were

stored at -20 °C for further use. The membrane was washed three times in PBS-T as stated above.

For the detection of StrepII-tagged proteins, chemiluminescent detection was performed using the alkaline phosphatase substrate CPD-*Star*[®] at a concentration of 0.25 mM in AP buffer. The PVDF membrane was covered with the substrate solution and incubated for 10 min. Detection of chemiluminescent signals were performed using a chemiluminescence imager (ECL ChemoStar V90D) with sequential acquisition times of 2 min and a total exposure time of 24 min.

Immunodetection of His-tagged proteins was facilitated using an anti-mouse antibody coupled to an alkaline phosphate at the indicated dilution (Table 8) in PBS-T. After incubation for 1 h at RT under shaking conditions, secondary antibodies were stored at -20 °C for further use. Removal of residual secondary antibodies was performed by washing the membrane three times with PBS-T as stated above. Detection of chemiluminescent signals was conducted using the alkaline phosphatase substrate CPD-*Star*[®] as stated above.

Towbin buffer (pH 8.3)		Blocking buffer	
Tris	25 mM	Milk powder in PBS-T	3 % (w/v)
Glycine	192 mM		
PBS (pH 7.4)		AP buffer (pH 9.5)	
Na ₂ HPO ₄	10 mM	Tris	100 mM
KH ₂ PO ₄	1.8 mM	NaCl	100 mM
KCl	2.7 mM	MgCl ₂	5 mM
NaCl	137 mM		
PBS-T			
Tween-20 (in PBS)	0.05 % (v/v)		

2.4.14. Zinc-enhanced fluorescence

Covalent attachment of linear tetrapyrroles to protein residues was analyzed by zinc-enhanced fluorescence (Berkelman & Lagarias 1986). Zinc thereby forms a complex with the phycobilin-linked peptides, which can be visualized via excitation with UV-light. After SDS-PAGE (chapter 2.4.12) and protein transfer on a PVDF membrane (chapter 2.4.13), the membrane was incubated in a solution of 1.3 M zinc acetate at RT for 1 h. Excitation of samples was performed at a wavelength of 312 nm and signals were documented with an iX20 imager (Intas).

2.4.15. Chlorophyll a extraction from cyanobacterial cells

Growth of cyanobacterial cultures can be monitored not only using measurements of optical densities (chapter 2.3.1), but also by chlorophyll *a* extraction followed by an UV-Vis spectroscopy (chapter 2.4.18) based pigment quantification. Therefore, 1 ml of cyanobacterial culture was harvested in a 1.5 ml microfuge tube by centrifugation at 6000 *g* and RT for 5 min and the supernatant was discarded. A 100 mg of 0.1 mm FastPrep silica beads and 1 ml of 100 % methanol were added to the pellet. Lysis of cells was performed via bead-beating at 30 bpm for 2 min. The lysed sample was incubated overnight at 4 °C in the dark. The next day, the lysate was vortexed for 30 s and centrifuged at 15000 *g* and 4 °C for 15 min. The supernatant was transferred into a new 1.5 ml microfuge tube. Spectra of the cleared extract were measured in range between 250 nm and 800 nm by UV-Vis spectroscopy using 100 % MeOH as a reference. Data was normalized to absorbance values at 780 nm. The concentration of chlorophyll *a* was calculated with the Beer-Lambert law equation $A = c \cdot d \cdot \epsilon$. Here, the absorbance value (*A*) is directly proportional to the concentration (*c*) and the extinction coefficient (ϵ) of the analyte. Additionally, absorbance values depend on the path length of the cuvette (*d*). Consequently, quantification of chlorophyll *a* was performed using the normalized absorbance value at 665 nm, the path length of 1 cm and $\epsilon_{665 \text{ nm}} = 70.02 \cdot 10^3 \text{ l}/(\text{mol} \cdot \text{cm})$ as the molar extinction coefficient in 100 % MeOH (Li *et al.*, 2012). Conversion of the molar concentration (*c*) into mass concentration (g/l) was performed using the molecular weight of 893.51 g/mol of chlorophyll *a*. Eventually, the chlorophyll *a* content per ml of culture was calculated with respect to the volume of harvested cells and the volume of added 100 % methanol prior to cell lysis.

2.4.16. Determination of glycogen content

Glycogen is a main storage compound of carbohydrates, which gives the cell a remarkable plasticity when facing environmental cues. Photosynthesis provides the energy and metabolites required for, e.g. numerous biosynthetic processes and the excess energy is accumulated as glycogen. Therefore, quantification of cellular glycogen content can give insights into the carbon metabolism during phototrophic growth of cyanobacteria. The content of glycogen can be determined in microtiter plates by a colorimetric detection at 620 nm using a method based on anthrone and sulfuric acid (Laurentin & Edwards 2003). After cell lysis in an aqueous buffer system, the water-soluble glycogen is converted to a hydroxymethyl furfural product by sulfuric acid. Eventually, the anthrone binds the reaction product, thereby forming a blue-green complex, which is detectable by photometric measurements.

For the quantification of the glycogen content, 100 µl of the soluble lysate (chapter 2.3.2) were complemented with 250 µl anthrone solution (2 mg/ml anthrone in 98 % sulfuric acid) and incubated at 80 °C for 30 min. As a reference, 100 µl of soluble lysate were replaced by 100 µl of PBS buffer. For the determination of glycogen content, 250 µl of the reaction product were transferred into a microtiter plate and optical densities at 620 nm were measured in a microtiter plate reader (FluoStar Omega). Quantification was performed using a calibration curve ($R^2 = 0.99$) ranging from 1.95 µg/ml to 125 µg/ml of glycogen from oyster in PBS buffer. Technical triplicates were employed for samples of the calibration curve and the blank measurements.

2.4.17. Quantification of phycobiliproteins

Phycobiliproteins are the main light-harvesting complexes of most cyanobacteria and represent one significant factor of cyanobacterial viability under phototrophic conditions. Therefore, evaluation of the phycobiliprotein content reflects an approach to gain insight into the photosynthetic capacity of phototrophs. The quantification of phycobiliproteins is based on absorbance measurements of cleared cell extracts using specific wavelengths and absorption coefficients. These properties thereby depend on the species and chromophore composition of each phycobiliprotein.

Soluble lysates for the quantification of the phycobiliprotein content in *Synechocystis* cultures were derived from the supernatant used for the protein (chapter 2.4.11) and glycogen (chapter 2.4.16) content determination. The supernatants containing phycobiliproteins was analyzed by UV-Vis spectroscopy (chapter 2.4.18). The content of PC and APC was determined by reading the absorbance values at 615 nm and 652 nm, respectively, using the equations of Bennett & Bogorad (1973).

2.4.18. UV-Vis spectroscopy

Analysis of spectral properties derived from phycobilins and chlorophyll *a* was performed by reading absorbance spectra in a range of 250 nm to 750 nm using an UV-Vis spectrometer (8453 UV-Visible system) and a 10 mm quartz cuvette. Prior to sample measurements, blank spectra were recorded using the appropriate sample buffer or extraction solvent. Acquired data was normalized to absorbance values at 750 nm and, if appropriate, to the samples' protein content in mg.

2.4.19. Fluorescence spectroscopy

Fluorescence emission spectra were acquired between 555 nm and 750 nm using a fluorescence spectrometer (FP-8300) after sample excitation at a wavelength of 550 nm. Excitation and emission bandwidth were set to 5 nm and the response time was adjusted to 50 ms in high sensitivity mode. Acquired data was normalized to fluorescence intensities at 750 nm and, if applicable, to the samples' protein content in mg.

3. Results

PBPs represent a largely diverse class of photosynthetically active pigment-protein complexes, which are typically found in phototrophic organisms in terrestrial and aquatic environments. The study of PBPs is of increasing scientific interest in structural biology, ecology and biotechnology. PBPs exhibit important biological properties for humans and animals, which reflects a strong motivation in biotechnology for the development of new products and processes. Their biological mode of action ranges from anti-oxidant- (Romay & Gonzalez 2010) and anti-inflammatory- (Zhu *et al.*, 2016) to anti-cancer (Thangam *et al.*, 2013) activities. In ecology, PBPs play a crucial role in the composition of marine and freshwater habitats. They enable photosynthetic organisms to efficiently utilize light energy in habitats with low light penetration, such as deep ocean waters. Consequently, understanding the structure and function of PBPs can provide insights into ecosystem dynamics and the adaptation of photosynthetically active organisms to different light conditions. A commonly used approach for studying the assembly and the structure of PBPs involves heterologous protein production in *E. coli*, given the unavailability, uncultivability, or genetic inaccessibility of various, native hosts.

In parts of this work, the assembly of the unusual PBP, PE545, of the cryptophyte *G. theta* was investigated via heterologous expression in *E. coli* to gain insights into its atypical structural features to further elucidate the functional mechanisms behind the cryptophyte light-harvesting machinery. While phycobilin transfer has already been shown for the PBP lyase CpeS of *G. theta*, the mode of action for the putative lyase CpcX remains elusive. Therefore, the putative PBP lyase CpcX was characterized for chromophore interacting properties, which is a necessary step for subsequent attachment to the PBP.

In contrast to *E. coli*-based protein production and subsequent *in vitro* protein analysis, additional research was performed to establish a novel platform for the assembly and the characterization of PEB-containing PBPs. Here, the cyanobacterium *Synechocystis* sp. PCC 6803 was used as a model organism and reflects a promising approach to investigate PBPs not only *in vitro* but also *in vivo* based on its present light-harvesting machinery. Since the model organism exclusively synthesizes the PCB chromophore, PEB chromophore biosynthesis was introduced. Subsequently, heterologous chromophore biosynthesis was evaluated in physiological and biochemical aspects. As a proof of concept, the construct encoding for PEB biosynthesis was expanded by the most minimal construct for PE assembly, the genes for the PBP lyase *cpeS* and the standalone PBP β -subunit *cpeB* of *P. marinus* MED4.

3.1. The putative PBP lyase CpcX of *Guillardia theta*

The unusual arrangement of cryptophyte PBPs inside the thylakoid lumen raises questions about how they transfer light energy to the photosynthetic reaction centres. In contrast to known cyanobacterial light-harvesting systems, they do not assemble to phycobilisomes where a funnel-like energy transfer has already been described. To investigate cryptophyte light-harvesting, the model organism *G. theta* is widely used as all of its four genomes are completely sequenced. Therefore, necessary genes for PE545 assembly can be identified by bioinformatical analyses.

The function of the putative PBP lyase CpcX has not been elucidated to date. Based on preliminary sequencing studies, CpcX has been proposed as PCB:α-PC lyase-like protein (Gould *et al.*, 2006). Further bioinformatical analyses supports this hypothesis. Modelling approaches of CpcX revealed an armadillo-like protein fold consisting of HEAT-repeats, which reflects a typical structure for E/F-type PBP lyases (Overkamp 2014). Consequently, CpcX most likely attaches phycobilin chromophores to the cysteine 19 of CpeA or cysteines 50/61 of CpeB. To characterize the function of CpcX, heterologous protein production was performed in *E. coli* and the interaction between phycobilins and purified CpcX were analyzed by UV-Vis spectroscopy. Therefore, original sequences of *G. theta* were codon-adapted to the codon usage of *E. coli* K12 and expression constructs yielding differently tagged fusion proteins were prepared (pASKIBA45+*Gt*cpcX_oSA, pET_Duet_*Gt*cpcX_oSA, pMAL_FXa_cpcX-StrepII and pMAL_HRV3C_cpcX-StrepII). Derived from issues with protein solubility in preliminary studies, a variety of expression conditions, buffer compositions and purification strategies were evaluated. In addition, MBP-CpcX-Strep fusion constructs were prepared since MBP is known to exhibit solubility enhancing properties. A summary of all tested expression and purification conditions is shown in chapter 2.4.1.1 (Table 15 to Table 17). Using *E. coli* BL21 pLysS and the construct pMAL_HRV3C_cpcX-StrepII yielded a sufficient amount of MBP-HRV3C-CpcX-Strep after affinity chromatography purification (Appendix Figure A1A). To minimize potential interference of the high-molecular weight MBP-tag in CpcX activity assays, the fusion protein was cleaved. Although removal of free MBP could be accomplished almost completely using the described purification procedure, reduced amounts of MPB-CpcX-Strep fusion protein were still detected in the purified protein solution. Consequently, size-exclusion chromatography was performed to separate CpcX-Strep and MBP-HRV3C-CpcX-Strep according to their size and to analyse the oligomerization state of CpcX-Strep. The determination of the oligomerization state can provide insights into target protein folding and consequently, the protein stability. However, CpcX-Strep is most likely forming

aggregates with free MBP (Appendix Figure A2). Since the majority of free MBP was successfully removed by size-exclusion chromatography, phycobilin interaction assays were performed with PCB, PEB and DHBV. No significant change in the chromophores' spectroscopic properties could be detected (data not shown).

Consequently, the function of the putative lyase CpcX of *G. theta* remains elusive, which motivated the evaluation of different protein production parameters, including new host systems. PBP assembly typically involves multiple enzymes including appropriate FDBRs for phycobilin biosynthesis, PBP subunits as part of the functional light-harvesting protein and PBP lyases, which are responsible for chromophore attachment to the PBPs. Hence, investigations of PBPs using *E. coli*, which all require such elaborate biosynthesis pathways, often face difficulties in terms of target protein abundance, folding and functionality. Consequently, further motivations of this work focus on the establishment of a novel, suitable platform for PBP assembly while focusing on PEs which require the pink pigment PEB. Cyanobacteria reflect a promising opportunity to assemble foreign PBPs as they already employ similar PBP assembly machineries. Here, the widely studied cyanobacterial model organism *Synechocystis* with a well characterized light-harvesting complex was used. As a fundamental prerequisite for PE assembly, *Synechocystis* was modified to heterologously produce the chromophore PEB since the host exclusively synthesizes the blue PCB chromophore.

3.2. Phycoerythrobilin biosynthesis in *Synechocystis*

Evaluation of new platforms for heterologous protein production reflects a viable approach to facilitate proper biosynthesis of target proteins. In the field of PBP research, *E. coli* is routinely used as a host. However, such heterologous expression experiments as performed in this study represent a typical challenge in protein biochemistry including protein folding and solubility. In addition, PBPs can be exclusively investigated for their biochemical properties *in vitro*, completely neglecting the opportunity to study their light-harvesting capabilities *in vivo*. Employment of a photosynthesizing cyanobacterium, that naturally possesses a light-harvesting apparatus, as a host for heterologous PBP production, represents a promising approach to gain insights into the PBPs contribution to cellular physiology. It may be feasible to investigate the PBPs contribution to photosynthesis *in vivo* besides already established *in vitro* analyses as they are performed using *E. coli*-based systems. More specifically, the PBPs ability in harvesting light-energy and its subsequent energy transfer to the photosynthetic reaction centres may potentially be unravelled by *in vivo* analyses. Consequently, PEB biosynthesis was established in *Synechocystis* by introducing the *pebS* gene of the cyanophage P-SSM2 under the control of the strong *cpc* promoter on a replicative plasmid into the *Synechocystis* WT. The newly generated, *pebS*-complemented strain *Synechocystis* sp. PCC 6803 pCGT.STH02 (hereafter Syn-pPebS) already exhibited a phenotypic difference after genetic modification (Figure 14), suggesting production of PEB by the enzyme PebS.

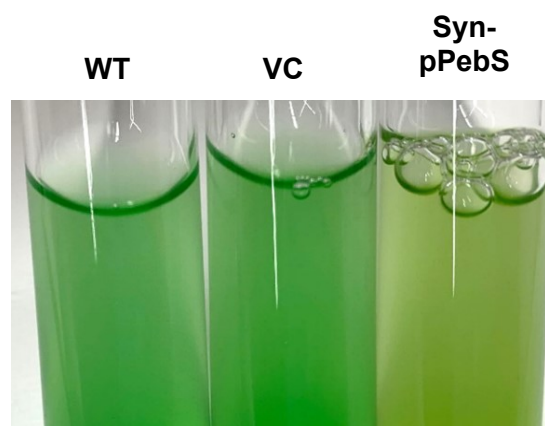


Figure 14: Phenotypes of *Synechocystis* WT (left), *Synechocystis* vector control (VC, middle) and the *pebS*-complemented strain Syn-pPebS (right). Growth of cultures was carried out at 30 °C and 120 rpm under continuous white light with an intensity of 40 $\mu\text{mol}/(\text{m}^2\cdot\text{s})$. For comparability, cultures were adjusted to an $\text{OD}_{730 \text{ nm}}$ of 1.

With the first, strong indication for successful chromophore production, the phototrophic growth was monitored to gain first insights into the effect of PEB biosynthesis on cell viability.

3.2.1. Biomass formation under modified phycobilin biosynthesis

Establishing a heterologous chromophore biosynthesis may interfere with cellular physiology, especially when grown under phototrophic conditions, since the introduced phycobilins potentially bind to endogenous PBPs. As a first approach, growth of Syn-pPebS was measured for approximately seven days (168 h) by reading the absorbance values at 730 nm and determining the chlorophyll a content per ml of culture.

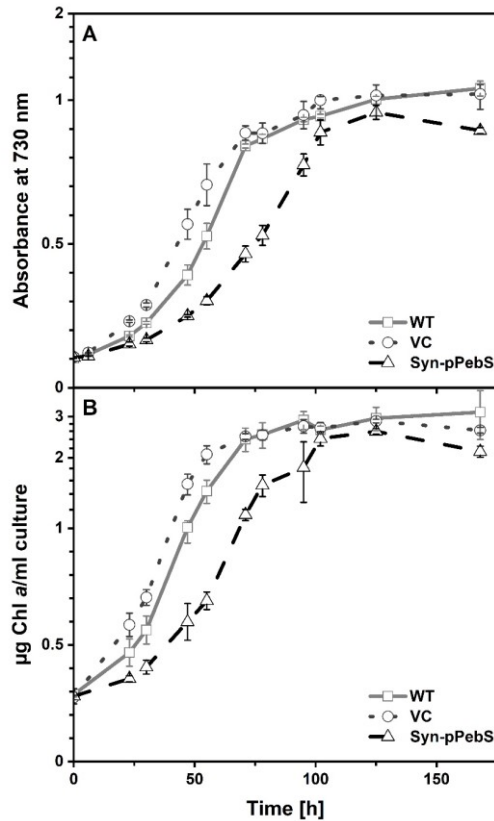


Figure 15: Phototrophic growth of *Synechocystis* WT (grey), VC (dotted line) and the *pebS*-complemented strain Syn-pPebS (dashed line). Shown are the mean values \pm SD of $n = 3$. (A) Absorbance measurements of culture densities at a wavelength of 730 nm. (B) Chl a content per ml of culture.

As shown in Figure 15, a significant increase of biomass to an $\text{OD}_{730 \text{ nm}}$ of ~ 0.9 and $2.5 \mu\text{g Chl } a/\text{ml}$ was observed within the first 75 h post inoculation for the WT (solid line) and the VC (dotted line) and growth reached stationary phase at an $\text{OD}_{730 \text{ nm}}$ of ~ 1 and a Chl a content of $\sim 2.8 \mu\text{g}/\text{ml}$ after 100 h. The *pebS*-complemented strain Syn-pPebS (dashed line) immediately exhibited slower culture growth. However, as the culture progressed towards stationary phase, the biomass accumulation remained comparable to both control strains although with a delay of ~ 25 h.

Quantitative evaluation of culture growth was performed using Chl *a* content during mid-exponential phase to determine the growth rates and doubling times. Included were timepoint measurements for the WT (between 55 h and 30 h), for the VC (between 47 h and 23 h) and for Syn-pPebS (between 71 h and 47 h) with statistical analyses carried out between the VC and the Syn-pPebS (Table 18).

Table 18: Growth rate and doubling time of *Synechocystis* WT, VC and Syn-pPebS. Shown are the mean values \pm SD of $n = 3$ and statistical significance was calculated between the VC and Syn-pPebS using a two-tailed Student's *t*-test. Asterisks indicate significant differences to the VC (* = $p \leq 0.05$). The calculations of growth rates in $\mu\text{g Chl } a \cdot \text{h}^{-1}$ and doubling times in h^{-1} were derived from Chl *a* content in mid-exponential phase between 55 h and 30 h for the WT, between 47 h and 23 h for the VC and between 71 h and 47 h for Syn-pPebS.

Strain	Growth rate $\mu\text{g Chl } a/\text{h} \pm \text{SD}$	Doubling time $/\text{h} \pm \text{SD}$
WT	0.038 ± 0.0004	18.47 ± 0.17
VC	0.046 ± 0.007	15.24 ± 2.39
Syn-pPebS	0.032 ± 0.003 (*)	22.11 ± 2.02 (*)

The WT exhibited a growth rate of $0.038 \mu\text{g Chl } a/\text{h}$ (± 0.0004) with a doubling time of $18.47/\text{h}$ (± 0.17). The VC showed the highest growth rate of $0.046 \mu\text{g Chl } a/\text{h}$ (± 0.007) and a doubling time of $15.24/\text{h}$ (± 2.39). Contrary to the control strains, Syn-pPebS demonstrated a growth rate of $0.032 \mu\text{g Chl } a/\text{h}$ (± 0.003) and a doubling time of $22.11/\text{h}$ (± 2.02). When compared to the WT, the PEB producing strain showed no significant difference in growth rate, however, its growth rate was significantly lower ($p \leq 0.05$) than that of the VC.

The change in growth rates under phototrophic conditions highly suggested a significant impact of PEB biosynthesis on the photosynthetic activity of *Synechocystis*. To draw further conclusions about the photosynthetic activity under modified phycobilin biosynthesis in the host, the light-harvesting proteins PC and APC were quantified and oxygen formation derived from water oxidation at PSII was measured.

3.2.2. Photosynthetic activity and nutrient accumulation

PBP abundance is highly responsive to environmental cues as depletion or excess of nutrients and ambient light conditions. The quantification of PBPs can give insights into the physiological conditions during phototrophic growth. In cultivation under high-light conditions, the content of PBP decreases to prevent oxidative stress by reactive oxygen species (ROS) due to an excessive amount of photonic energy being passed on to the photochemical reactions. In low-light conditions, however, PBP levels increase to enhance light-harvesting efficiency. To assess the reduced growth rate under modified phycobilin biosynthesis, light-harvesting efficiency was evaluated by the quantification of

the native PBPs, namely PC and APC. In addition, photosynthetic activity was analyzed by oxygen evolution measurements derived from water hydrolysis at PSII.

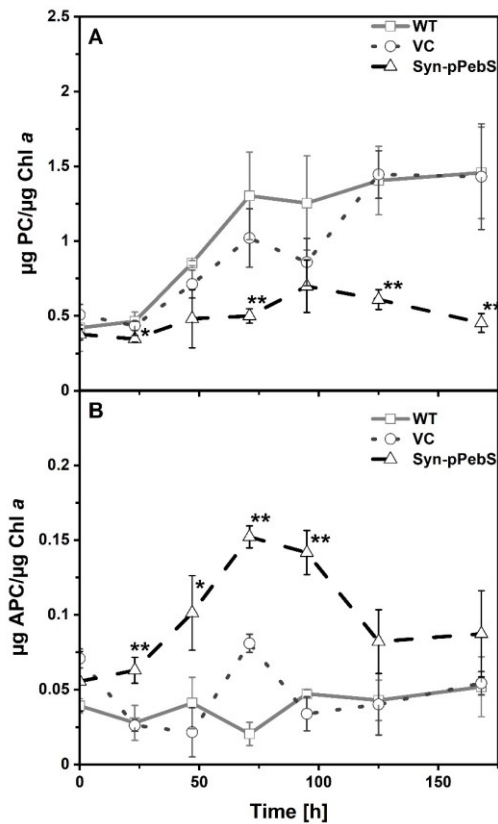


Figure 16: Evaluation of parameters reflecting cell health during phototrophic growth via quantification of the light-harvesting proteins PC and APC. Shown are mean values of $n = 3 \pm$ SD of the *Synechocystis* WT (solid line), VC (dotted line) and Syn-pPebS (dashed line). Soluble cell lysates during the growth curve experiment were analyzed by UV-Vis spectroscopy. PBP content was calculated according to Bennet and Bogorad (1973). Observed values were normalized to $\mu\text{g Chl } a$. Statistical significance was calculated between the VC and Syn-pPebS using a two-tailed Student's *t*-test. Asterisks indicate significant differences to the VC (* = $p \leq 0.05$, ** = $p \leq 0.01$). **(A)** Content of PC derived from absorbance maxima at 615 nm. **(B)** APC content calculated from absorbance values at 652 nm.

For PBP content determination, first significant differences in the content of PC were observed after 23 h of inoculation ($p \leq 0.05$) (Figure 16A). With a PC content of $\sim 0.34 \mu\text{g/ml}$, Syn-pPebS (dashed line) shows a reduction of approximately 20 % compared to $\sim 0.43 \mu\text{g/ml}$ in the VC (dotted line). This tendency was observed throughout the complete growth curve experiment. The PC contents in Syn-pPebS were $\sim 0.49 \mu\text{g/ml}$, $\sim 0.6 \mu\text{g/ml}$ and $0.45 \mu\text{g/ml}$ compared to $\sim 1.02 \mu\text{g/ml}$, $\sim 1.45 \mu\text{g/ml}$ and $\sim 1.43 \mu\text{g/ml}$ in the VC after 71 h, 125 h and 168 h, respectively ($p \leq 0.01$). Consequently, Syn-pPebS showed a reduction in PC content of $\sim 47 \%$, $\sim 41 \%$ and $\sim 32 \%$ compared to the VC with respect to the above mentioned timepoints. In summary, the reduced amount of PC in Syn-pPebS, with respect to Chl *a*, is persistent independent of the growth phase.

Since the quantification of PBPs relies on the endogenous PCB chromophore being attached to all potential cysteines, the reduced PC content implies either a change in abundance of native PC or a modification of the protein's chromophore composition. In contrast, the analysis of APC content shows an opposite effect. Here, protein abundance is significantly increased throughout the complete growth experiment. Initially, a 2.3-fold increase in APC content was observed after 23 h ($p \leq 0.01$) in Syn-pPebS. Here, the content of the PBS core protein were $\sim 0.062 \mu\text{g/ml}$ in Syn-pPebS, compared to $\sim 0.026 \mu\text{g/ml}$ in the VC. The amount of APC steadily increased until it exceeded the VCs APC content of $\sim 0.08 \mu\text{g/ml}$ by a factor of two and reached a value of $0.16 \mu\text{g APC}/\mu\text{g Chl } a$ ($p \leq 0.01$). As growth approached the stationary phase, the APC content of Syn-pPebS decreased to comparable levels at the beginning of the growth experiment ($\sim 0.08 \mu\text{g/ml}$) after 23 h. Independent of the APC's chromophore content, the PCB-derived measurements showed an increased protein abundance, even if a certain extend of phycobilin binding sites is occupied with the heterologously produced PEB instead of the native PCB.

In conclusion, the Chl *a*-dependent pigment contents are significantly modified in Syn-pPebS, which strengthens a PEB-related impairment of cell viability as already observed in the growth rate and doubling time during phototrophic growth (Table 18). Since the quantification of PBPs using the method stated above can only reliably be applied to native, unmodified PBPs, evaluating the consequences of changed abundances for the light-harvesting efficiency of Syn-pPebS remains challenging. Consequently, oxygen release measurements derived for water hydrolysis at PSII were performed over a range of light intensities to evaluate the utilization of light-energy *in vivo* (Figure 17).

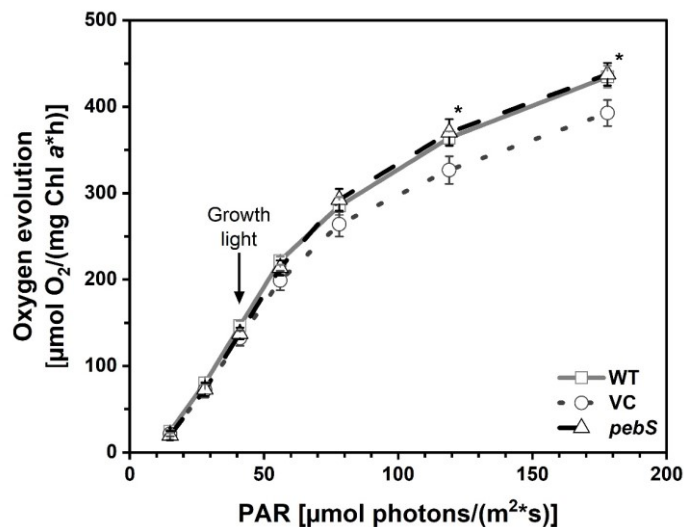


Figure 17: Photosynthetic activity under modified phycobilin biosynthesis. Oxygen evolution of *Synechocystis* WT (solid line), VC (dotted line) and Syn-pPebS (dashed line) under incrementally increasing light intensities (PAR: photosynthetically active radiation). Oxygen evolution was standardized to mg Chl *a* and statistical significance was calculated between the VC and Syn-pPebS using a two-tailed Student's *t*-test. Asterisks indicate significant differences to the VC (* = $p \leq 0.05$). Shown are mean values of $n = 3 \pm$ SD.

In oxygen evolution measurements, all three strains show comparable oxygen release rates ($\sim 135 \mu\text{mol O}_2/(\text{mg Chl a}\cdot\text{h})$) at the culture growth light intensity (PAR: photosynthetically active radiation) of $40 \mu\text{mol}/(\text{m}^2\cdot\text{s}^1)$ during growth curve experiments (Figure 17, arrow). After the light intensity rose above an intensity of $50 \mu\text{mol}/(\text{m}^2\cdot\text{s}^1)$, the WT (solid line) and Syn-pPebS (dashed line) release more O_2 into the growth medium as the VC (dotted line). Significant differences were observed at a light intensity of 119- and $178 \mu\text{mol}/(\text{m}^2\cdot\text{s}^1)$ ($p \leq 0.05$) with an oxygen evolution of ~ 365 - and $\sim 435 \mu\text{mol O}_2/(\text{mg Chl a}\cdot\text{h})$ in the WT as well as in Syn-pPebS compared to ~ 325 - and $395 \mu\text{mol O}_2/(\text{mg Chl a}\cdot\text{h})$ in the VC, respectively. Although Syn-pPebS exhibits an increased oxygen release rate when compared to the VC, light-energy utilization remains at similar levels with respect to the WT. Under the culturing light intensity, all three strains show no difference in PSII-derived activities. Based on the considerable changes in the growth rate and the PBP content of Syn-pPebS but negligible differences in oxygen evolution measurements, further assessment of cellular viability was performed by evaluating the content of accumulated nutrients.

Cell health is not only reflected by growth rate, pigment content and oxygen release, but also by the accumulation of nitrogen- and carbon rich nutrients. Depending on the growth conditions, nitrogen is stored up to $\sim 75\%$ in cellular proteins (González López *et al.*, 2010). Consequently, the strains' protein contents were used to determine nitrogen accumulation. For carbon-rich compounds, glycogen was used as a representative. Glycogen serves as a major energy-storage compound derived from CO_2 fixation by the

Calvin-Benson cycle and is a highly branched glucose polymer, which can accumulate to a content of 10 % to 50 % of cyanobacterial biomass (Möllers *et al.*, 2014).

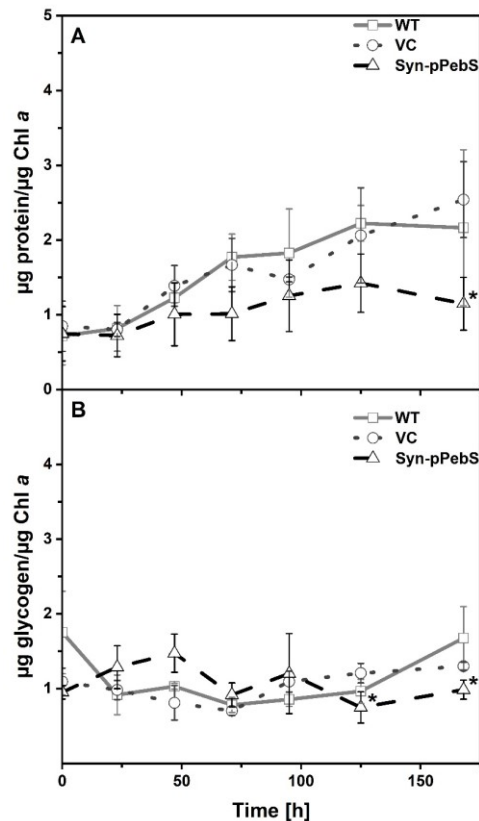


Figure 18: Nutrient accumulation under phototrophic growth of *Synechocystis* WT and transconjugants. Shown are mean values of $n = 3 \pm \text{SD}$ of the *Synechocystis* WT (solid line), VC (dotted line) and Syn-pPebS (dashed line). Soluble lysates prepared during the growth curve experiment were used to determine the protein (A) and glycogen (B) content. Observed values were normalized to $\mu\text{g Chl } a$ and statistical significance was calculated using a two-tailed Student's *t*-test between the VC and Syn-pPebS. Asterisks indicate significant differences to the VC (* = $p \leq 0.05$).

As shown in Figure 18A, minor changes in the protein content were observed after 50 h of inoculation between the VC (dotted line) and Syn-pPebS (dashed line) with $\sim 1.3 \mu\text{g/ml}$ and $1.0 \mu\text{g/ml}$ of protein, respectively. Apart from negligible discrepancies in the protein content of Syn-pPebS throughout the growth experiment, significant differences were observed when the cultures rested in stationary phase at 168 h ($p \leq 0.05$) with a protein content of $\sim 2.5 \mu\text{g/ml}$ for the VC and $\sim 1.1 \mu\text{g/ml}$ in Syn-pPebS. A similar trend was observed for the glycogen contents (Figure 18B). Here, the glycogen levels of all three strains remained at comparable levels between ~ 0.8 - and $1.0 \mu\text{g/ml}$ for every timepoint until 125 h post inoculation. Here, significant differences to the VC became noticeable ($p \leq 0.05$). Comparing the glycogen content of $\sim 1.2 \mu\text{g/ml}$ in the VC, Syn-pPebS shows a reduction of $\sim 38 \%$ ($0.75 \mu\text{g/ml}$). Similarly, the glycogen content in Syn-pPebS ($0.98 \mu\text{g/ml}$) is 24 % less than in the VC ($1.30 \mu\text{g/ml}$) after 168 h of inoculation. In summary, Syn-pPebS only exhibited significant differences in the relative levels of intracellular protein and glycogen, as the cultures rested in stationary phase.

Although reduces growth rates and a change of PBP abundance under modified phycobilin biosynthesis was observed, evaluation of nutrient accumulation and photosynthetic activity by oxygen evolution measurements demonstrate that *Synechocystis* has the capacity to efficiently manage the expression of *pebS* on a physiological level. Despite the phenotypic and physiological evidence, which clearly show a *pebS*-dependent effect on cell viability, biochemical proof for the formation of PEB is still required. In further studies, UV-Vis- and fluorescence emission analysis was performed to gather first evidence for heterologous PEB production.

3.2.3. PEB production induces PBP diffusion in *Synechocystis*

Based on its chemical nature, phycobilins as PEB and PCB have spectroscopic properties, which provides PBPs with the capability to process incoming light-energy, when the chromophores are covalently attached. While both free phycobilins and those covalently attached to PBPs exhibit spectral properties in UV-Vis analysis, free phycobilins demonstrate minimal fluorescence upon excitation. However, upon covalent attachment to PBPs, they yield highly fluorescent proteins (Isailovic *et al.*, 2006). To gather first evidence of heterologous PEB formation in *Synechocystis*, fractions of the soluble lysate were analyzed by UV-Vis spectroscopy and fluorescence emission measurements (Figure 19). Shown are absorbance spectra (A) and fluorescence emission spectra after excitation at 550 nm (B) of the *Synechocystis* WT (black), the VC (blue) and Syn-pPebS (red).

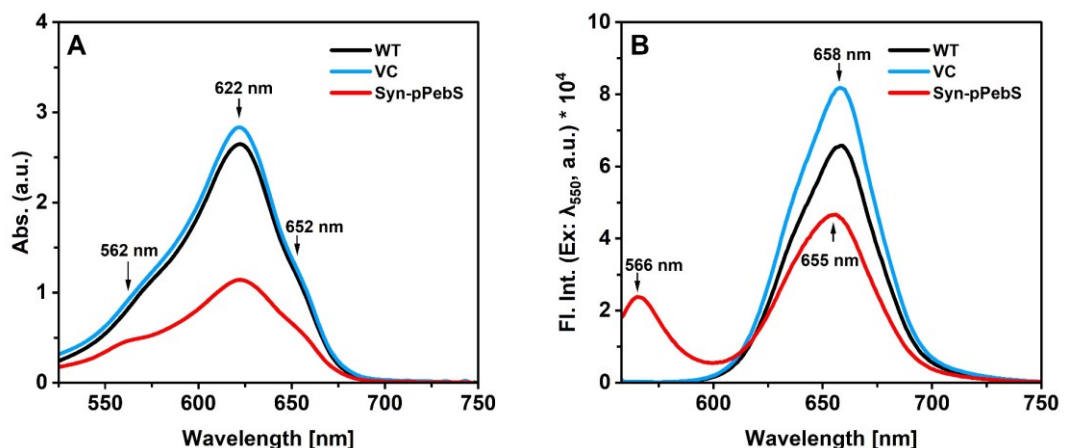


Figure 19: Heterologous PEB production in *Synechocystis* WT and transconjugants. Cells of the *Synechocystis* WT (black), VC (blue) and Syn-pPebS (red) from late-exponential phase were harvested and the soluble lysate was analyzed for spectroscopic properties. Data was normalized to values at 750 nm and mg protein. (A) UV-Vis spectra between 525 nm and 750 nm and (B) Fluorescence emission spectra of the soluble lysates. Shown is the fluorescence emission intensity between 558 nm and 750 nm after excitation at a wavelength of 550 nm.

The spectroscopic properties (Figure 19A) of the WT and the VC exhibited characteristic absorbance maxima for PC and APC at 622 nm and 652 nm, respectively. In the absorbance spectra of Syn-pPebS, a new signal at 562 nm, indicative for PEB, was observed in addition to the native absorbance maxima for PC and APC. Comparing the absorbance intensities per mg protein, Syn-pPebS exhibits reduced values by ~ 60 % for PC at 622 nm and by ~ 50 % for APC at 652 nm. In fluorescence emission analysis (Figure 19B), maxima in fluorescence intensity were observed at 658 nm in both control strains, which is indicative for APC-derived fluorescence. Since PC emission, typically observed at 640 nm, is absent, these spectra suggest an energy transfer of incoming light (here at 550 nm) from PC to APC. In contrast to the observed maximum at 658 nm in the control strains, measurements of Syn-pPebS exhibited a shift from 658 nm to 655 nm. The most significant difference between the emission spectra was observed at 566 nm. Here, a new signal occurred for Syn-pPebS, which is the commonly reported emission wavelength for PEB-derived fluorescence.

As this first spectroscopic analysis strongly indicates heterologous formation and covalent linkage of PEB, co-localization studies were performed via confocal laser scanning microscopy to study the potential association of PEB to the native PBSs. Prior to microscopic imaging, proper signal acquisition settings for phycobilin-derived fluorescence were evaluated by reading single cell fluorescence emission spectra of the WT (black), the VC (blue) and Syn-pPebS (red) between 500 nm and 700 nm after excitation at 543 nm (Figure 20).

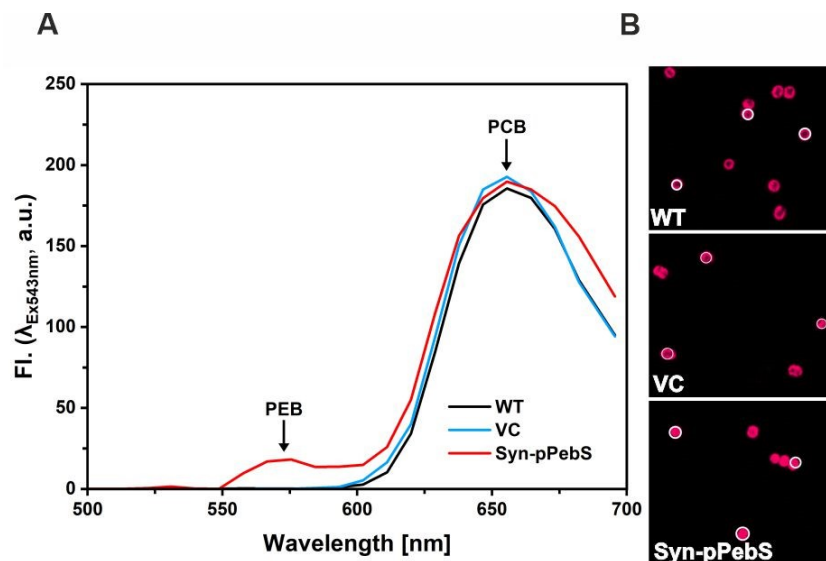


Figure 20: Fluorescence emission spectra of single *Synechocystis* cells. (A) Emission spectra between 500 nm and 700 nm after excitation at 543 nm of the *Synechocystis* WT (black), VC (blue) and Syn-pPebS (red). Maxima at ~ 560 nm and ~660 nm indicate PEB- and PCB-derived fluorescence, respectively. Shown are mean values of three technical replicates. (B) Fluorescent imaging of *Synechocystis* WT and transconjugants. White circles show the area of data acquisition for the fluorescence emission spectra shown in (A).

The fluorescence emission spectra of *Synechocystis* WT (black), VC (blue) and Syn-pPebS (red) single cells all exhibit a local maximum at ~ 660 nm, which is indicative for PCB-derived fluorescence of APC. In accordance with previous fluorescence measurements of soluble lysates, Syn-pPebS additionally shows a PEB-derived signal at ~ 560 nm. Based on the observed emission spectra, fluorescence imaging (Figure 21) was performed by setting the signal acquisition range between 550 nm and 587 nm for PEB and between 607 nm and 624 nm for PCB. Chl *a* derived fluorescence emission was detected between 701 nm and 721 nm.

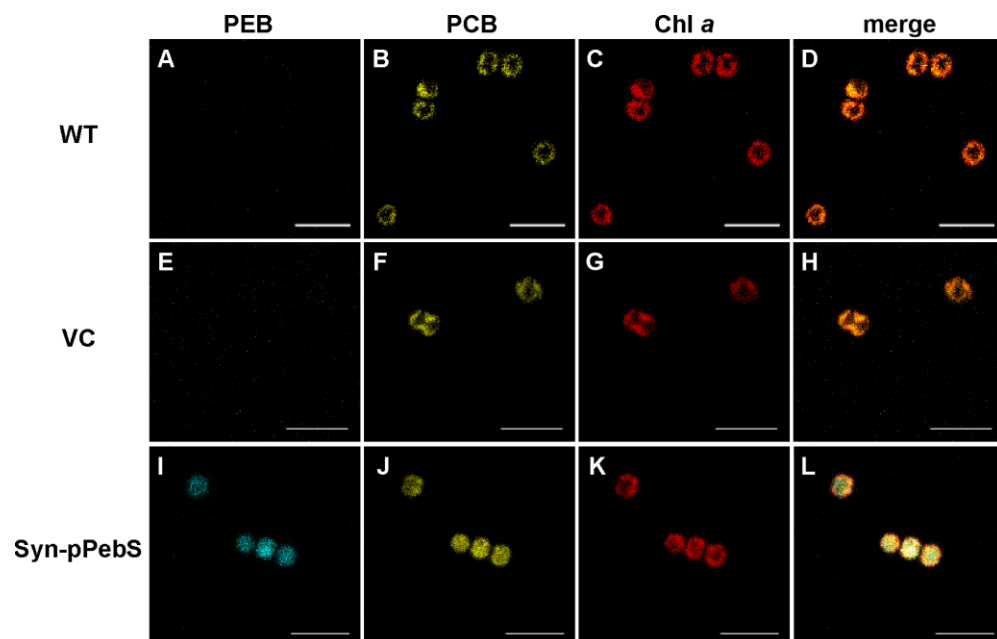


Figure 21: Confocal fluorescence imaging of *Synechocystis* WT and transconjugant cells, VC and Syn-pPebS cells. Shown are fluorescent images of *Synechocystis* WT (A to D), the VC (E to H) and Syn-pPebS (I to L) cells. Phycobilin-derived fluorescence after excitation at 543 nm was recorded for PEB between 550 nm and 587 nm (A, E, I), for PCB at 607 nm and 624 nm (B, F, J) and for Chl *a* between 701 nm and 721 nm (C, G, K). Merging of images was performed to visualize co-localization of signals (D, H, L). Images are shown in customized colours showing fluorescence derived from PEB (blue), PCB (yellow) and Chl *a* (red). The scale bar defines a length of 5 μ m.

As shown, the imaging profiles of the *Synechocystis* WT and the VC showed a defined co-localization pattern of PCB-derived PBP- (Figure 21B, F) and Chl *a* (Figure 21C, G) fluorescence. Consequently, both controls indicate the association of native PBs with the thylakoid membrane (Figure 21D, H). In contrast to the WT and the VC, Syn-pPebS demonstrates a new signal for PEB-derived fluorescence, which is dispersed across the whole cell (Figure 21I). A similar pattern was observed for the PCB-related fluorescence emission (Figure 21J). In contrast to the diffuse PBP signals in Syn-pPebS, the Chl *a*-derived fluorescence remained mostly localized in the cell periphery as in the control strains, which strongly indicates a highly reduced co-localization of PBPs with the thylakoid membrane (Figure 21L). Consequently, heterologously produced PEB seems to bind the native PBPs of *Synechocystis*, but leads to either impaired PBS assembly or

destabilization of already assembled PBSs. Intact PBSs could not reliably be detected in the CLSM profile of Syn-pPebS. Therefore, PBSs were isolated and their spectral properties as well as their protein composition were analyzed to evaluate PBS integrity and to identify potential PEB binding partners.

3.2.4. Modified PBPs are not incorporated into intact PBSs

Previous CLSM images of Syn-pPebS suggested covalent attachment of PEB to PBPs. Modified PBPs remain as cytosolic protein complexes, which seem to be not utilized for PBS assembly (chapter 3.2.3). Based on the strong diffuse fluorescence signals dispersed across the whole cell, intact PBSs as shown for the control strains were not clearly observed in Syn-pPebS. *In vitro* analysis of intact PBSs may further provide insights into the potential interaction partner of PEB and the integrity of the macromolecular antenna complexes. Therefore, intact PBSs were isolated via density gradient ultracentrifugation using a discontinuous sucrose gradient.

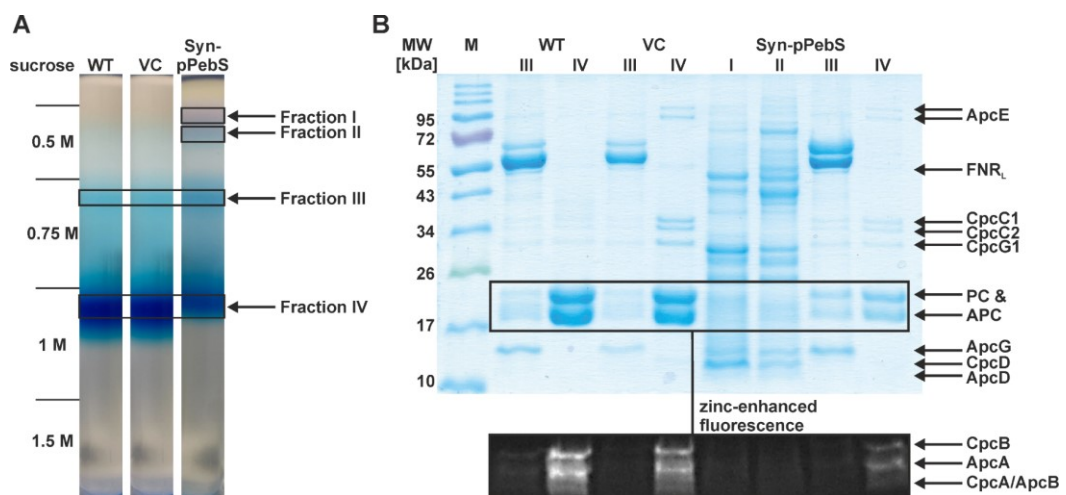


Figure 22: The impact of heterologous PEB biosynthesis on PBS isolation profiles and the fractions protein composition. (A) Shown are PBS isolation profiles of the *Synechocystis* WT (left), the VC (middle) and Syn-pPebS (right) with the corresponding sucrose concentration layers. Fractions for subsequent SDS-PAGE analysis and zinc-enhanced fluorescence are labelled on the right. (B) SDS-PAGE analysis of fractions marked in (A). After protein staining with Coomassie blue, obtained signals were designated based on reference samples analyzed by LC-MS/MS in Domínguez-Martín *et al.*, (2022). Following protein separation, proteins were transferred onto a PVDF membrane and incubated in zinc-acetate. Visualization of covalently bound phycobilins was facilitated by exposure at 312 nm (lower picture (B)). M: Molecular mass standard (Color Prestained Protein Standard, Broad Range, 10-250 kDa) with corresponding MW in kDa; ApcE: Chromophorylated core-membrane linker polypeptide; FNR_L: Ferredoxin-NADP reductase; CpcC1: PBS rod linker polypeptide; CpcC2: PBS rod linker polypeptide; CpcG1: PBS rod-core linker polypeptide; PC: Phycocyanin; APC: Allophycocyanin; ApcG: PBS core component; CpcD: PBS rod capping protein; ApcD: Allophycocyanin α subunit variant.; CpcB: Phycocyanin β subunit; ApcA: Allophycocyanin α subunit; CpcA: Phycocyanin α subunit; ApcB: Allophycocyanin β subunit.

The observed PBS isolation profiles consisted of a variety of pigment-based fractions, which were labelled Fraction I to IV (Figure 22A, from top to bottom). Typically, intact PBS complexes will remain in Fraction IV (1 M sucrose) after ultracentrifugation as

reported in previous studies (Wallner *et al.*, 2012). In this study, the *Synechocystis* WT, the VC and Syn-pPebS exhibit a strong blue signal in the reported gradient concentration. Although the complex in Fraction IV of Syn-pPebS seems to be present in a subjectively lower amount, SDS-PAGE and subsequent zinc-enhanced fluorescence analyses show the presence of the PC- and APC subunits (Figure 22B, Fraction IV of the WT, the VC and Syn-pPebS). Consequently, electrophoretic analysis of Fraction IV strongly suggests the presence of intact PBSs in all three strains. The blue-coloured signals in Fraction III (Figure 22, 0.75 M sucrose) consist of PC and APC but lack the core-membrane linker L_{CM} (ApcE, Figure 22B, Fraction III). ApcE is known to serve as the scaffolding protein responsible for the PBS core formation (Zhang *et al.*, 2017) and its truncation leads to disorganized PBS isolation profiles (Elanskaya *et al.*, 2018). In conclusion, the analysis of Fraction III indicates the presence of PBP complexes of lower molecular weight in the WT, the VC and Syn-pPebS. More interestingly, novel fractions in magenta and blue colour were observed in Fraction I and II of Syn-pPebS (Figure 22, 0.5 M sucrose). In this case, evaluation of the fractions' protein composition by SDS-PAGE remains challenging. The PBS extract which is applied onto the sucrose gradient consists of a large number of soluble, cellular proteins. Consequently, the poor resolution after ultracentrifugation-based separation yields an unidentifiable amount of protein signals after SDS-PAGE analysis. However, UV-Vis and fluorescence emission analyses of the fractions phycobilin-derived spectral properties potentially aid in the identification of the PBP type (PC or APC) as well as their chromophore composition (Figure 23).

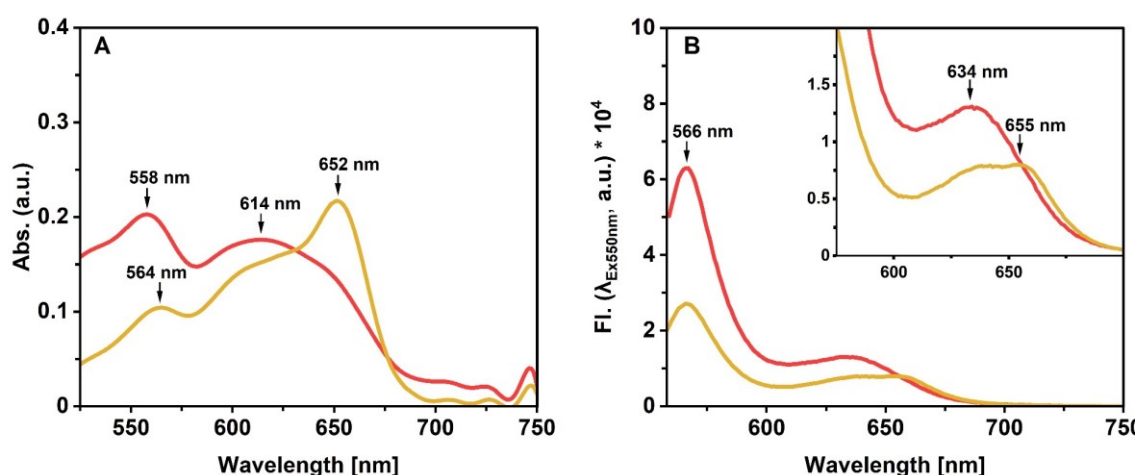


Figure 23: Spectroscopic analysis of the novel fraction I and II after PBS isolation of Syn-pPebS. After spectroscopic measurements, data was normalized to values at 750 nm and mg protein (A) UV-Vis spectra of fraction I (red line) and fraction II (orange line) between 525 nm and 750 nm. Absorbance maxima derived from PEB are indicated at 558 nm and 564 nm, from PCB at 614 nm (PC) and 652 nm (APC). (B) Fluorescence emission spectra of fractions I (red line) and II (orange line) in (A). Shown is the fluorescence emission intensity * 10^4 between 558 nm and 750 nm after excitation at 550 nm. Inset shows a magnification of the wavelength range between 575 nm and 700 nm to highlight PCB-derived fluorescence at 634 nm (PC) and 655 nm (APC).

In UV-Vis measurements (Figure 23A), fraction I and II of the PBS isolation profiles of Syn-pPebS both exhibit spectral properties characteristic for PC and APC with bound PCB chromophores at 614 nm and 652 nm, respectively. While fraction I mainly contains PC, the majority of PBPs in fraction II consists of APC. Interestingly, spectral data clearly shows two absorbance maxima at either 558 nm (fraction I) or 564 nm (fraction II) which both are in the range of commonly reported maxima for PEB-containing PBPs. The absorbance maxima derived from chromophores can vary slightly depending on the protein environment of phycobilins, as PBPs tailor their spectroscopic properties. Consequently, UV-Vis analysis suggests an association of PEB to multiple PBP subunits of PC, APC or both. To gather further implications for covalent linkage of PEB to proteins, fluorescence emission spectra were recorded (Figure 23B) for fraction I and fraction II of the Syn-pPebS PBS isolation profile. Here, a strong fluorescence signal at 566 nm was detected, which is representative for PEB-based emission and therefore strongly indicates covalent attachment of PEB to proteins, especially focusing on the PBPs subunits. In addition to the novel fractions in the 0.5 M sucrose layer, fraction III and IV of the WT (black), the VC (blue) and Syn-pPebS (red) were analyzed for their spectral properties to further characterize the fractions PBP contents and their chromophore composition (Figure 24).

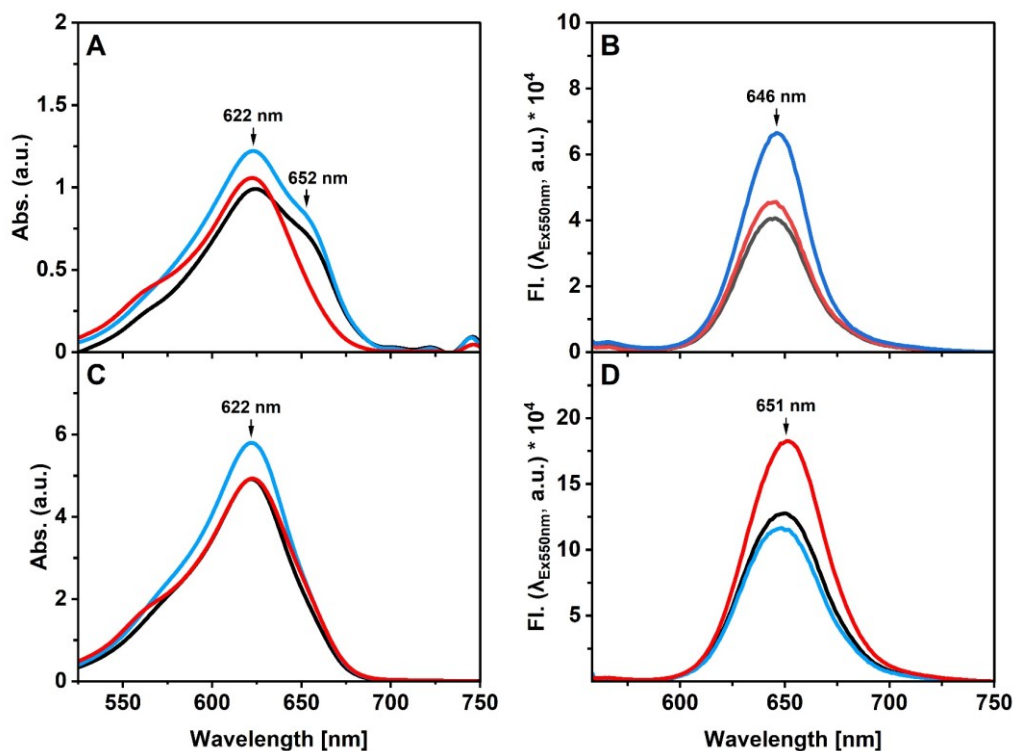


Figure 24: Spectroscopic analysis of the PBS fractions in the 0.75 M and 1 M sucrose gradient layer. Data for the *Synechocystis* WT (black), VC (blue) and Syn-pPebS (red) was normalized to mg protein. Shown are the fraction III (A, B) and fraction IV (C, D) UV-Vis spectra between 525 nm and 750 nm (A, C) with local maxima at 622 nm (PC) and 652 nm (APC) and fluorescence emission intensities * 10^4 between 558 nm and 750 nm (B, D) with peaks at 646 nm (PC) and 651 nm (APC).

Spectroscopic analysis of fractions III and IV (Figure 24A, B) are shown for the *Synechocystis* WT (blue), the VC (black) and Syn-pPebS (red). In accordance with SDS-PAGE analysis (Figure 22B), the UV-Vis measurements of fractions in the 0.75 M gradient (Figure 24A) exhibit spectral properties representative for PC at 622 nm and APC at 652 nm. However, absorbance maxima for APC are missing in Syn-pPebS, indicating the sole presence of PC in fraction III. Fluorescence emission readings thereby show PC-derived signals at 646 nm for fraction III of all three strains. As already indicated in electrophoretic protein content analysis, the scaffolding protein ApcE for PBS core formation is absent in the 0.75 M layer, which impairs the assembly of the APC core complex with the PC rods to form intact PBSs. Consequently, the shown fluorescence emission only shows PC-derived signals because the transfer of light-energy from PC to APC is most likely not feasible. In contrast, spectroscopic measurements of fraction IV show light energy-transfer from PC to APC (Figure 24C, D). As the UV-Vis data only shows an absorbance maximum for PC at 622 nm, the fluorescence emission maximum at 651 nm exhibits spectral properties characteristic for APC emission.

In conclusion, only the novel Fractions I and II exhibit PEB-characteristic spectral properties, these spectroscopic signals were absent in Fraction III and IV. However, data of the PBS isolation are in accordance with the co-localization studies using CLSM (Figure 21). As indicated by SDS-PAGE analysis of fraction I and II of Syn-pPebS, the present proteins most likely represent free cytosolic protein complexes, including the modified PBPs, which were observed as dispersed fluorescence signals across the whole cell during confocal imaging. In order to validate covalent linkage of PEB to PBPs, the highly abundant PC was purified by alternative purification methods due to the challenging nature in separating the two novel fractions I and II in the 0.5 M sucrose layer.

3.2.5. PEB binds to phycocyanin

In order to elucidate whether the recombinantly produced PEB is covalently attached to PC, the PBP was purified and subsequently analyzed using UV-Vis- and fluorescence spectroscopy.

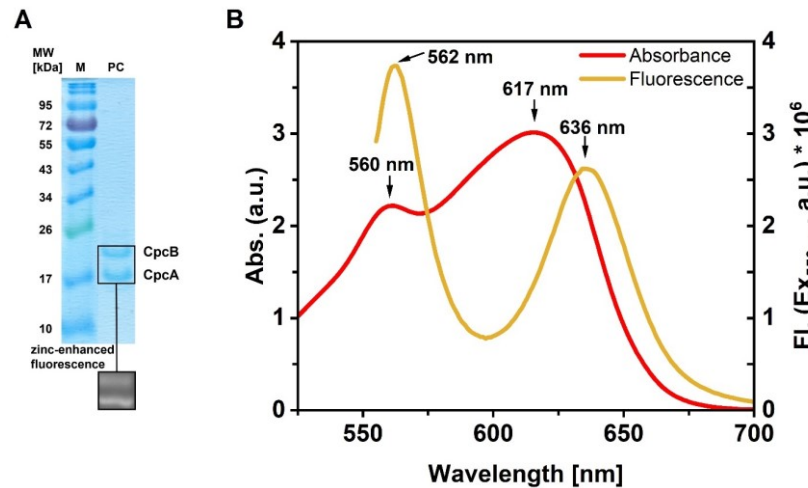


Figure 25: Modified PC from Syn-pPebS after purification. (A) SDS-PAGE analysis and zinc-enhanced fluorescence of purified PC. M: Molecular mass standard (Color Prestained Protein Standard, Broad Range, 10-250 kDa) with corresponding MW in kDa. The signals at ~21 kDa and ~18 kDa correlate with the PC subunits CpcB (β subunit) and CpcA (α subunit), respectively. Covalent attachment of phycobilins to proteins was visualized via zinc-enhanced fluorescence after excitation at 312 nm. (B) UV-Vis spectroscopy and fluorescence emission after excitation at 550 nm of purified PC in (A). For the UV-Vis spectrum, data of PC is shown between 525 nm and 700 nm (red). Local maxima at 560 nm and 617 nm are indicative for PEB and PCB-derived absorbance, respectively. The fluorescence emission intensity $\cdot 10^6$ is shown between 558 nm and 700 nm after excitation at 550 nm (yellow). Peaks at 562 nm and 636 nm correspond to PEB- and PCB-based fluorescence emission, respectively.

As shown in SDS-PAGE analysis (Figure 25A), purified fractions exclusively contained the PC-forming subunits CpcB and CpcA at an approximate molecular weight of ~20 kDa and ~18 kDa, respectively. In zinc-enhanced fluorescence analysis, both subunits demonstrate the expected fluorescence signals after excitation at 312 nm. With the following spectroscopic analyses, the type of covalently attached phycobilin was further evaluated (Figure 25B). In UV-Vis measurements (red), PC exhibits the native, PCB-derived absorbance maximum at 617 nm in addition to a PEB-characteristic peak at 560 nm. Fluorescence emission spectra of PC (yellow) show two distinct emission maxima at 562 nm and 656 nm, indicative for PEB and PCB, respectively. In summary, PC is capable of binding heterologously produced PEB in addition to the native PCB chromophore. As a consequence, potential binding sites were elucidated in further experiments.

3.2.6. PEB is covalently attached to cysteine 84 of CpcA

Since previous spectroscopic analyses of purified PC derived from Syn-pPebS provide evidence for covalent PEB attachment, tandem mass spectrometry (MS/MS) was performed to identify specific peptide sequences and their post-translational modification, PCB and PEB. In MS/MS analysis, selected ions (as peptides) are induced to fragmentation to enable the determination of the molecule's structure.

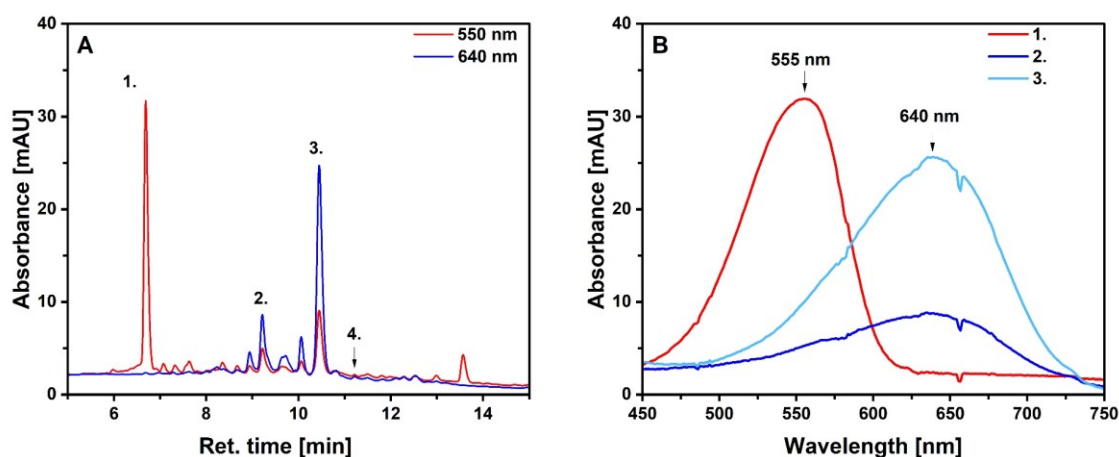


Figure 26: HPLC analysis and separation of tryptic peptides from purified PC of Syn-pPebS. (A) HPLC chromatogram of tryptic peptides with absorbance measurements at 550 nm (red) and 640 nm (blue) to monitor elution and fractionation of PEB- and PCB-containing peptides, respectively. Fractions of interest were labelled with numbers for further analysis. (B) UV-Vis spectra of fraction 1 (red), 2 (blue) and 3 (light blue) recorded during peptide separation in (A) are shown between 450 nm and 750 nm with absorbance maxima at 555 nm for PEB- and 640 nm for PCB-containing peptides.

Separation of tryptic peptides of PC yields a variety of chromopeptides (Figure 26A) with higher absorbance intensities at either 550 nm (red) and a retention time of ~ 6.8 min (fraction 1) or at 620 nm (blue) with a retention time of ~ 9.2 min and ~ 10.4 min (fraction 2 and 3), indicative for PEB- or PCB-containing chromopeptides. Analysis of the fractions UV-Vis measurements (Figure 26B) shows characteristic spectral features for PEB (fraction 1, red) with an absorbance maximum at 555 nm and for PCB (fraction 2 in blue, fraction 3 in light blue) at 640 nm. Although the peptide content of all fractions was analyzed by LC-MS/MS, the first analysis was focused on the PEB-containing fraction 1 to identify the peptide where PEB is attached to. Subsequently, small proportions of the same peptide with attached PCB were found in fraction 4 (Figure 26A, fraction 4).

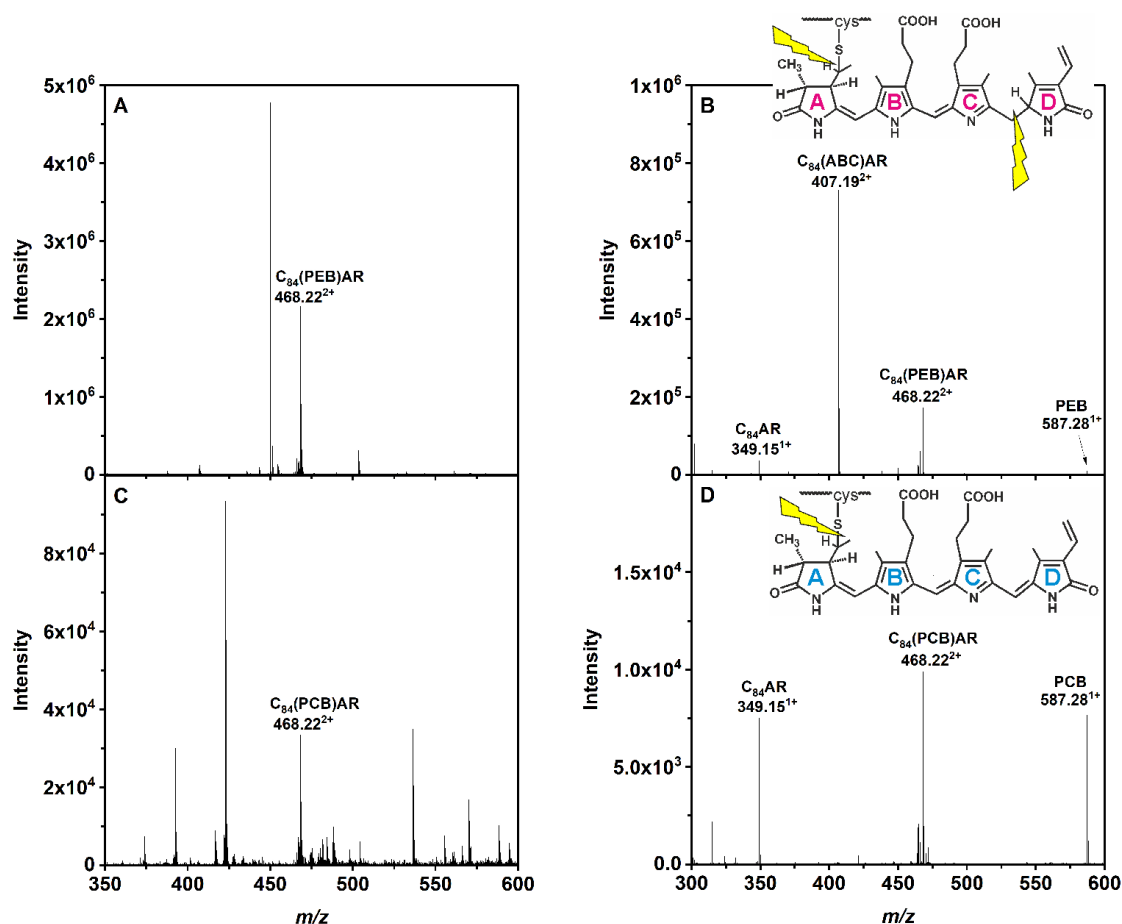


Figure 27: Tandem mass spectrometry analysis of chromopeptides after the HPLC separation of tryptic PC peptides. Shown are the MS¹ (A, C) and MS² (B, D) spectra of the peptides in fraction 1 (A, B) and fraction 4 (C, D) after HPLC separation. For MS² spectra, the most abundant peaks with fragmentation products assigned according to their calculated *m/z* are shown. (A) MS¹ of fraction 1 (Figure 26) for the peptide C₈₄AR with attached PEB at a *m/z* of 468.222⁺ [M+2H]²⁺ (calc. *m/z* = 468.232⁺ [M+2H]²⁺). (B) MS² spectrum of the precursor ion at *m/z* = 468.222⁺ in (A). C₈₄AR (calc. *m/z*: 349.161⁺ [M+1H]¹⁺): peptide without PEB chromophore. C₈₄(ABC)AR (calc. *m/z*: 407.202⁺ [M+2H]²⁺): chromopeptide with dissociated D-ring of PEB. C₈₄(PEB)AR: precursor ion. PEB (calc. *m/z*: 587.281⁺ [M+1H]¹⁺): phycobilin dissociated from the peptide. (C) MS¹ of fraction 4 (Figure 26A) for the peptide C₈₄AR with attached PCB at a *m/z* = 468.222⁺ [M+2H]²⁺ (calc. *m/z*: 468.232⁺ [M+2H]²⁺). (D) MS² of the precursor ion at a *m/z* = 468.222⁺ in (C). C₈₄AR¹⁺ (calc. *m/z*: 349.161⁺ [M+1H]¹⁺): peptide without PCB chromophore. C₈₄(PCB)AR: precursor ion. PCB (calc. *m/z*: 587.281⁺ [M+1H]¹⁺): phycobilin dissociated from the peptide. An example of *m/z* calculations is given as follows: Derived from the monoisotopic molecular mass of 934.42 g/mol of the C₈₄AR-PEB peptide (348.147 g/mol for the peptide C₈₄AR and 586.279 g/mol for PEB), the *m/z* is calculated by adding the mass of two protons (2·1.008 g/mol) since the chromopeptide is twice positively charged and by dividing the resulting mass by the number of charges.

In LC-MS/MS analysis of the PEB-containing fraction 1 (Figure 27A), an *m/z* of 468.222⁺ was found (example of *m/z* calculations in description of Fig. 27), which aligns with the theoretically calculated *m/z* of the CpcA derived peptide C₈₄AR with an additional mass of PEB (theor. calc. *m/z* = 468.222⁺ [M+2H]²⁺). Fragmentation of that peptide generated four abundant signals in the corresponding MS² spectrum (Figure 27B). Besides the parent ion at a *m/z* of 468.222⁺, the C₈₄AR amino acid sequence without post-translational modification was identified at an *m/z* of 349.151⁺ (theor. calc. *m/z* = 349.161⁺ [M+1H]¹⁺). In accordance with the dissociation of the peptide from the chromophore, small proportions of free PEB were found at a *m/z* of 587.281⁺ (theor. calc. *m/z* = 587.281⁺

[M+1H]¹⁺). More interestingly, the most abundant signal exhibits a $m/z = 407.19^{2+}$ which correlates with the m/z of the chromopeptide PEB- C₈₄AR where the D-ring of the PEB dissociated from the parent ion (C₈₄(ABC)AR) (theor. calc. $m/z = 407.20^{2+}$ [M+2H]²⁺). In the following LC-MS/MS analysis of all fractions derived from HPLC separation, the naturally occurring CpcA derived peptide C₈₄AR with a bound PCB was identified in fraction 4 (Figure 26A). Here, the PCB-containing chromopeptide exhibited a m/z of 468.22²⁺ (Figure 27C) (theor. calc. $m/z = 468.23^{2+}$ [M+2H]²⁺), as already observed for the same peptide with the isomeric PEB bound to it. Notably, when compared to the PEB-containing peptide, fragmentation of that parent ion yields a different signal pattern in the MS² spectrum (Figure 27D). Here, three predominant peaks were detected and assigned according to their calculated m/z . While the parent ion at a m/z of 468.22²⁺ is present in high proportions, fragmentation yields only two fragments which correlate with the peptide C₈₄AR without chromophore at a m/z of 349.15¹⁺ (theor. calc. $m/z = 349.16^{1+}$ [M+1H]¹⁺) and the free phycobilin PCB at a m/z of 587.28¹⁺ (theor. calc. $m/z = 587.28^{1+}$ [M+1H]¹⁺).

In conclusion, mass spectrometry analysis shows the presence of two populations of the PC subunit CpcA. The subunit is able to bind both phycobilins, PCB or the heterologously produced PEB, at cysteine 84 which indicates a competition of both chromophores for the attachment site. Interestingly, the fragmentation pattern seems to be highly dependent on the location of double bonds between the phycobilins pyrrole rings and the presence of the thioether bond between the chromophore and the peptide. While PCB contains a double bond between the C- and the D-ring, PEB exhibits only a single bond between both mentioned pyrrole rings. Consequently, the preferential fragmentation product is the chromopeptide with a dissociated D-ring for the PEB-containing chromopeptide. In contrast, the PCB-containing peptide splits up into nearly equal proportions of free PCB chromophore and unmodified C₈₄AR peptide due to the only present single bond positioned at the thioether bond between the phycobilin and the peptide.

Engineering *Synechocystis* as a platform for phycoerythrin assembly reflects a promising approach to investigate PBPs both *in vitro* and, more interestingly, *in vivo*. To provide the required chromophore for proper post-translational modification of the PBP subunits, the phycoerythrobilin synthase gene *pebS* was introduced into *Synechocystis*. This study shows successful formation of the phycobilin PEB by spectroscopic measurements and its covalent attachment to the CpcA subunit of the native PC by mass spectrometry analysis. Based on the new spectral properties of the modified PC, the protein and consequently the engineered *Synechocystis* strain Syn-pPebS may exhibit an increase

in its light-harvesting capacity under green light. Therefore, growth of Syn-pPebS was evaluated under green light to assess light-energy utilization derived from the heterologously produced PEB (Appendix Figure A4), but differences in growth were not observed. This is probably derived from the modified PC, which is not utilized for PBS assembly as shown by confocal fluorescence microscopy and *in vitro* analyses after PBS isolation. Although the structure of the native light-harvesting complex was strongly affected by the heterologously produced chromophore, its impact on cellular physiology remains minimal. While PEB production does not affect intracellular protein- and glycogen- levels as well as photosynthetic activity shown by oxygen evolution measurements, the reduced growth rate still indicates minor physiological effects on the host. Consequently, *Synechocystis* is amenable to the modified phycobilin biosynthesis, motivating further studies to assemble a PEB-containing PBP. In the following, assembly of a heterologously produced PE was evaluated by expanding the currently used genetic construct with additional genes involved in the biosynthesis of a complete phycoerythrin from *P. marinus* MED4.

3.3. Assembly of phycoerythrin from *P. marinus* MED4

3.3.1. Heterologous expression of phycoerythrin biosynthesis genes

The formation of photosynthetically active PBPs requires the action of several proteins, including FDBR enzymes for phycobilin biosynthesis and PBP lyases for targeted chromophore attachment to specific cysteine residues within the PBP subunits. As the previous experiments of this work show successful production of the PEB chromophore in the cyanobacterium *Synechocystis*, the fundamental prerequisite for subsequent PE assembly is provided. Consequently, the genetic construct used for the engineered *Synechocystis* strain Syn-pPebS was expanded with genes encoding for a PBP lyase and a PBP subunit. Assessment of heterologous PE assembly was performed using the minimalistic PE from the marine cyanobacterium *P. marinus* MED4. The degenerate PBP of this strain only consists of one subunit, namely *PmCpeB*, with one reactive cysteine capable of binding PEB (Steglich *et al.*, 2005). Consequently, its endogenous PBP biosynthesis machinery exclusively requires, besides chromophore biosynthesis and the PBP subunit *PmCpeB*, one PBP lyase called *PmCpeS*. This PBP lyase is responsible for the attachment of PEB to the cysteine residue 82 of the subunit (Wiethaus *et al.*, 2010). These minimal genetic requirements to form a functional PE resulted in a genetic construct consisting of the cyanophage gene *pebS*, *PmcpeS* and *PmcpeB* to evaluate heterologous phycoerythrin assembly in *Synechocystis*. Two different constructs were prepared to introduce PBP biosynthesis, one consisting of three separate transcription units and one polycistronic operon. In the following sections, PE assembly was assessed using the construct with three transcription units (Figure 28). Since the recombinant proteins were not detected in the strains harbouring the polycistronic constructs, the corresponding experiments are listed in the appendix of this work (Appendix Figure A5 to A7).



Figure 28: Synthetic construct in pCGT.STH10 for the assembly of the *Prochlorococcus marinus* MED4 PE in *Synechocystis*. The expression construct is composed of three transcription units consisting of *pebS* from the cyanophage P-SSM2 and the *P. marinus* MED4 genes *cpeB* and *cpeS*. Expression of *pebS* is controlled by the strong, light-responsive *cpc* promoter and the corresponding terminator, which also regulate the endogenous phycocyanin operon of *Synechocystis*. In contrast, *cpeB* and *cpeS* are controlled by the BioBrick-derived, constitutive *J23119* promoter and the synthetic variant of *P_{trc}* from *E. coli*, respectively. The *trc* promoter normally is an inducible promoter based on binding of the Lac repressor LacI to the operator sequence *lacO*. The coding sequence *lacI* is absent in the construct used for *Synechocystis*. Consequently, using the *P_{trc10}* leads to constitutive expression of *cpeS*. Transcription of both *P. marinus* MED4 genes is terminated by the *E. coli*-derived double terminator *T_{rmb}*, which has been characterized in Gale *et al.*, (2021). Promoters were characterized in Vasudevan *et al.*, (2019). The vector pCGT.STH10 was introduced into the *Synechocystis* WT leading to the transconjugant WT-PE. To generate a control strain, a similar construct has been introduced in WT-PE C82A using the vector pCGT.STH11. Here, the cysteine residue 82 of *PmcpeB*-Strep, the attachment site of PEB, was exchanged to an alanine by site directed mutagenesis of the corresponding DNA fragment. The vector pCGT.STH11 was also introduced into the *Synechocystis* WT yielding the WT-PE C82A strain. Created with BioRender.com

In the construct consisting of three separate transcription units, expression of *PmcpeB* and *PmcpeS* are under control of the constitutive, strong promoters P_{J23119} and P_{trc10} , respectively, which have been characterized in Vasudevan *et al.*, (2019). In addition, *PmcpeB* was fused with a Strep-tag and *PmcpeS* with a His-tag for immunodetection of recombinant proteins and their purification via affinity chromatography. Termination of transcription is provided by using the terminator T_{cpc} for *pebS*- and T_{rmb} for *PmcpeB* as well as *PmcpeS* expression. While T_{cpc} represents the endogenous terminator of the PC operon in *Synechocystis*, efficiency of T_{rmb} in *Synechocystis* was characterized in Gale *et al.*, (2021). As a control for *PmCpeB* (in the vector pCGT.STH10), the reactive cysteine for PEB attachment was altered to an alanine by site directed mutagenesis to yield a *PmCpeB* variant C82A (pCGT.STH11). In addition to the WT, these two constructs were introduced into the so-called olive mutant of *Synechocystis*. The olive mutant is a PC-deficient strain incapable of assembling PBS rods, or in other words, it is only able to form the PBS core consisting of APC (Lea-Smith *et al.*, 2014, Vasudevan *et al.*, 2019). Since most of PBP subunits exhibit similar molecular masses and demonstrate intense spectral properties, the absence of PC, the most-abundant protein in *Synechocystis*, may assist in proper characterization of phycoerythrin assembly. While conjugation of the construct pCGT.STH10 yielded the strains WT-PE and Olive-PE, the strains WT-PE C82A as well as Olive-PE C82A were generated with the vector containing the *CpeB* C82A variant (pCGT.STH11). After confirmation of transconjugants, heterologous protein production was assessed by SDS-PAGE-, Western blot- and mass spectrometry analysis. After verification of recombinant protein biosynthesis, *PmCpeS* and *PmCpeB* were purified by affinity chromatography and *PmCpeB* was analyzed for its spectroscopic properties to evaluate heterologous PE assembly.

3.3.2. Production of *PmCpeB* and *PmCpeS*

To gather first evidence for heterologous protein production, the presence of *PmCpeB* and *PmCpeS* in the transconjugant strains Olive-PE, Olive-PE C82A, WT-PE and WT-PE C82A was assessed by SDS-PAGE- and Western blot analysis (Figure 29). Subsequently, separated proteins were transferred to a PVDF membrane and visualized by chemiluminescent immunodetection (Figure 29B, C).

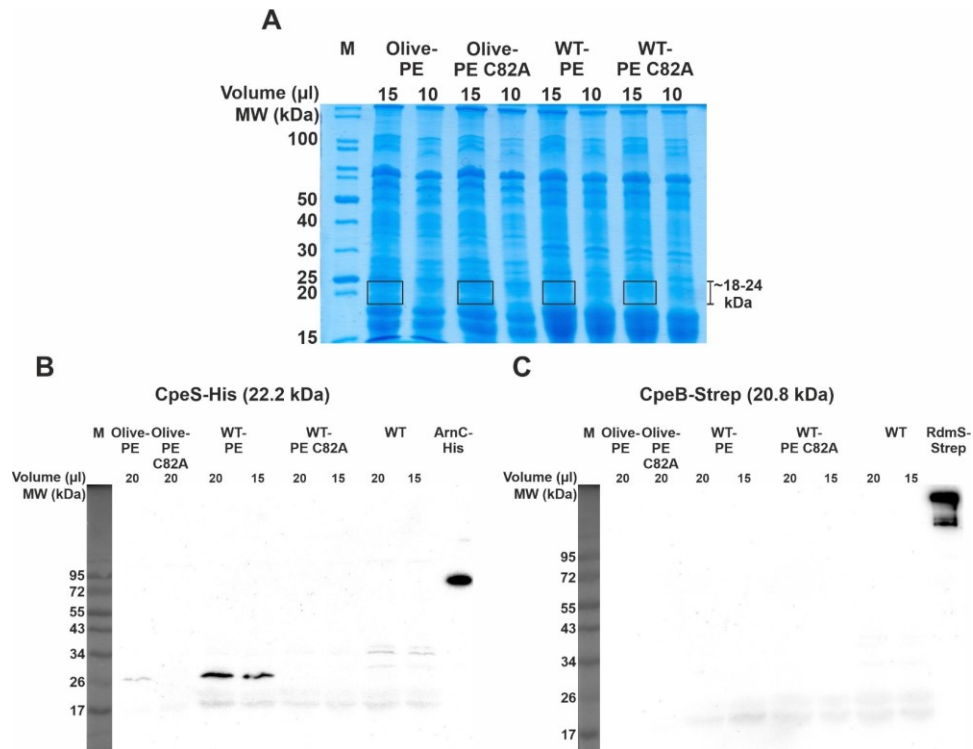


Figure 29: SDS-PAGE and WB analysis of proteins derived from whole cells of different *Synechocystis* strains. Cultures of Olive-PE, Olive-PE C82A, WT-PE and WT-PE C82A were adjusted to an $OD_{730\text{ nm}}$ of ~ 2 in 1 mL, harvested and prepared for electrophoretic protein separation at 150 V for 1.5 h. The recombinant proteins CpeS-His and CpeB-Strep exhibit calculated molecular weights of 22.2 kDa and 20.8 kDa, respectively. **(A)** Samples for SDS-PAGE analysis were applied using volumes of 15 μ l and 10 μ l. After visualization of proteins by Coomassie blue, samples were extracted from the indicated area between ~ 18 kDa and ~ 24 kDa (black boxes) for subsequent identification of tryptic peptides by LC-MS. M: Molecular mass standard (Unstained Protein Standard, Broad Range, 10-200 kDa) **(B/C)** Western blot analysis of samples derived from whole cells. Prior to immunodetection of CpeS-His and CpeB-Strep, 20 μ l and 15 μ l of protein samples were separated by SDS-PAGE and transferred onto PVDF membranes. Proteins were visualized by chemiluminescence. M: Molecular mass standard (Color Prestained Protein Standard, Broad Range, 10-250 kDa); ArnC-His: positive control for the detection of His-tagged proteins; RdmS-Strep: positive control for the detection of Strep-tagged proteins.

Recombinant protein production could not reliably be detected using Western blot analysis. Although there is a signal present in WT-PE cells for *PmCpeS*-His, and probably to some extent in Olive-PE cells (Figure 29B), the corresponding size of the detected proteins with a molecular weight of ~ 30 kDa do not correlate with the theoretically calculated mass of ~ 22.2 kDa. Curiously, the signal at ~ 30 kDa is missing completely in the strains Olive-PE C82A and WT-PE C82A harbouring the *PmCpeB*-Strep variant incapable of binding PEB. In contrast to immunolabeling of *PmCpeS*-His, no signals were detected for the Strep-tagged *PmCpeB* (Figure 29C) with a theoretical

molecular weight of ~ 20.8 kDa. The observed weak chemiluminescence observed at ~ 18 kDa and ~ 24 kDa most likely originates from the endogenous PC subunits. Since no clear evidence could be provided using this method, proteins after SDS-PAGE between a molecular weight of ~18 kDa and ~24 kDa were extracted from the gel (Figure 29A, black boxes) and analyzed by mass spectrometry (Table 19).

Table 19: Identification of recombinant *PmCpeB* and *PmCpeS* in *Synechocystis* cells by mass spectrometry analysis. A selection of host proteins is shown as a reference for intensity values.

Peptides (rel. intensities)	Olive-PE	Olive-PE C82A	WT-PE	WT-PE C82A
<i>PmCpeB</i>	3.90 * e ⁶	6.32 * e ⁴	1.05 * e ⁵	0
<i>PmCpeS</i>	1.13 * e ⁷	1.23 * e ⁵	2.79 * e ⁷	2.68 * e ⁵
ApcA (Allophycocyanin α chain)	1.36 * e ⁸	1.36 * e ⁸	8.36 * e ⁷	7.81 * e ⁷
ApcB (Allophycocyanin β chain)	3.09 * e ⁷	3.59 * e ⁷	1.29 * e ⁷	6.53 * e ⁶
CpcT (Chromophore lyase)	1.26 * e ⁷	1.36 * e ⁷	1.19 * e ⁷	9.42 * e ⁶
CpcS2 (Chromophore lyase)	2.38 * e ⁶	1.14 * e ⁶	2.85 * e ⁶	2.28 * e ⁶
PetE (Plastocyanin)	1.44 * e ⁶	1.14 * e ⁶	4.68 * e ⁵	3.87 * e ⁵
psbA2 (PS II protein D1)	1.20 * e ⁶	5.43 * e ⁵	4.38 * e ⁵	5.36 * e ⁵
AtpA (ATP synthase α-subunit)	6.49 * e ⁶	4.52 * e ⁶	3.45 * e ⁶	3.07 * e ⁶
RpoE (RNA polymerase σ-E factor)	9.78 * e ⁴	4.30 * e ⁴	1.80 * e ⁵	3.98 * e ⁵

In contrast to Western blot analysis, mass spectrometric measurements of samples derived from whole-cell protein separation provided evidence for the production of the recombinant proteins *PmCpeB* and *PmCpeS* in *Synechocystis*. Although it remains challenging to perform a total quantification of both proteins, corresponding signal intensities within the sample indicate increased levels of CpeS when compared to CpeB, which correlate with the previously shown Western blot analysis.

Utilizing *Synechocystis* as a platform for heterologous PE assembly requires proper separation from native PBPs to characterize *PmCpeB* biochemically. Prior to the purification of recombinant proteins, the solubility of *PmCpeB* after cell lysis was assessed using SDS-PAGE and Western blot (Figure 30).

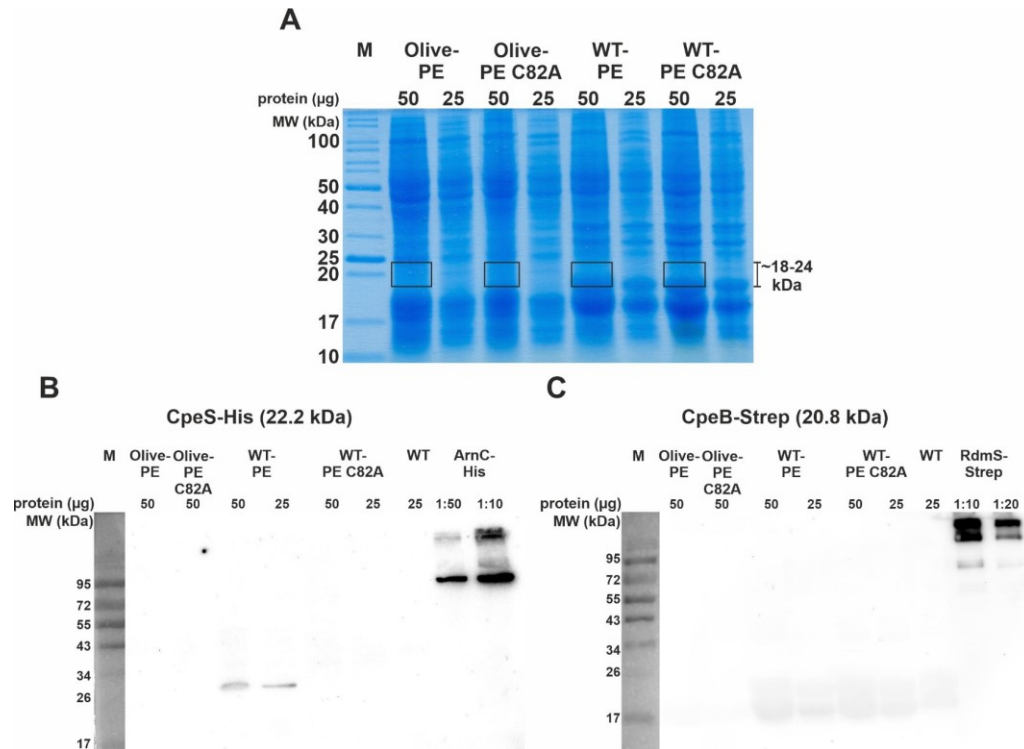


Figure 30: SDS-PAGE and WB analysis of proteins from the soluble fraction of cell lysates from different *Synechocystis* strains. Cultures of Olive-PE, Olive-PE C82A, WT-PE and WT-PE C82A were harvested and subjected to cell lysis. Soluble and insoluble fractions of cell lysates were separated at 150 V for 1.5 h. For SDS-PAGE- and Western blot analysis, 50 µg and 25 µg of soluble protein were applied. The recombinant proteins CpeS-His and CpeB-Strep exhibit calculated molecular weights of 22.2 kDa and 20.8 kDa, respectively. **(A)** Protein content analysis after SDS-PAGE. Following visualization of proteins by Coomassie blue, samples were extracted from the indicated area between ~ 18 kDa and ~ 24 kDa (black boxes) for subsequent identification of tryptic peptides by LC-MS. M: Molecular mass standard (Unstained Protein Standard, Broad Range, 10-200 kDa) **(B/C)** Western blot analysis of proteins derived from soluble lysates. Prior to immunodetection of CpeS-His and CpeB-Strep, protein samples were separated by SDS-PAGE and transferred onto PVDF membranes. Recombinant proteins were visualized by chemiluminescence. M: Molecular mass standard (Color Prestained Protein Standard, Broad Range, 10-250 kDa); ArnC-His: positive control for the detection of His-tagged proteins; RdmS-Strep: positive control for the detection of Strep-tagged proteins.

As already observed in previous Western blot analyses, *PmCpeS*-His detection exhibits a chemiluminescent signal at ~ 30 kDa in the WT-PE strain (Figure 30B). This signal could not be detected in all remaining strains. For *PmCpeB*-Strep (Figure 30C), no signals, except the endogenous PC subunits, could be detected. Consequently, proteins between ~ 18 kDa and ~24 kDa were extracted after SDS-PAGE (Figure 30A, black boxes) to assess the solubility of the recombinant proteins, *PmCpeB* and *PmCpeS*, using mass spectrometry (Table 20).

Table 20: Assessment of recombinant *PmCpeB* and *PmCpeS* solubility by mass spectrometry analysis. A selection of host proteins is shown as a reference for intensity values.

Peptides (rel. intensities)	Olive-PE	Olive-PE C82A	WT-PE	WT-PE C82A
<i>PmCpeB</i>	2.78 * e ⁵	0	1.75 * e ⁴	0
<i>PmCpeS</i>	3.64 * e ⁶	9.00 * e ³	4.44 * e ⁶	2.11 * e ⁴
ApcA (Allophycocyanin α chain)	3.87 * e ⁷	4.81 * e ⁷	2.07 * e ⁷	1.98 * e ⁷
ApcB (Allophycocyanin β chain)	7.07 * e ⁷	5.47 * e ⁷	6.17 * e ⁷	5.15 * e ⁷
CpcT (Chromophore lyase)	9.56 * e ⁶	1.04 * e ⁷	2.26 * e ⁷	1.87 * e ⁷
CpcS2 (Chromophore lyase)	9.69 * e ⁶	6.65 * e ⁶	4.88 * e ⁶	4.85 * e ⁶
PetE (Plastocyanin)	6.60 * e ⁶	6.66 * e ⁶	1.02 * e ⁷	4.95 * e ⁶
psbA2 (PS II protein D1)	6.11 * e ⁵	3.09 * e ⁵	2.59 * e ⁵	1.17 * e ⁵
AtpA (ATP synthase α -subunit)	3.03 * e ⁵	1.40 * e ⁵	1.02 * e ⁵	2.14 * e ⁵

Similar to MS analysis of samples derived from whole cells, both recombinant proteins could be detected in the soluble fraction of the lysate. Although the PBP lyase *PmCpeS* was detected across all strains, the presence of *PmCpeB* was limited to the strains Olive-PE and WT-PE, implying a crucial role of the *PmCpeB*'s reactive cysteine in the protein solubility. After assessing the production and solubility of *PmCpeB*-Strep and *PmCpeS*-His, they were purified by affinity chromatography to biochemically evaluate the ability of phycobilin transfer and chromophore attachment to *PmCpeB* using the strain WT-PE.

3.3.3. Heterologous phycoerythrin assembly

The recombinant proteins *PmCpeB* and *PmCpeS* are both under control of constitutive promoters and fused to sequences for a C-terminal Strep- and His-tag, respectively. Evaluation of the purification procedure was performed by SDS-PAGE analysis for *PmCpeB* (Figure 31A) and *PmCpeS* (Appendix Figure 6A) produced in the strain WT-PE. Based on reduced signal intensity after protein visualization with Coomassie blue, protein signals in the combined and concentrated elution fractions were subjected to mass spectrometry analysis (Appendix Figure A6B, CpeS C and CpeB C). During *PmCpeB*-Strep affinity chromatography, fluorescence emission measurements were performed to analyse the presence of PEB-derived signals in the protein fractions (Figure 31B to D).

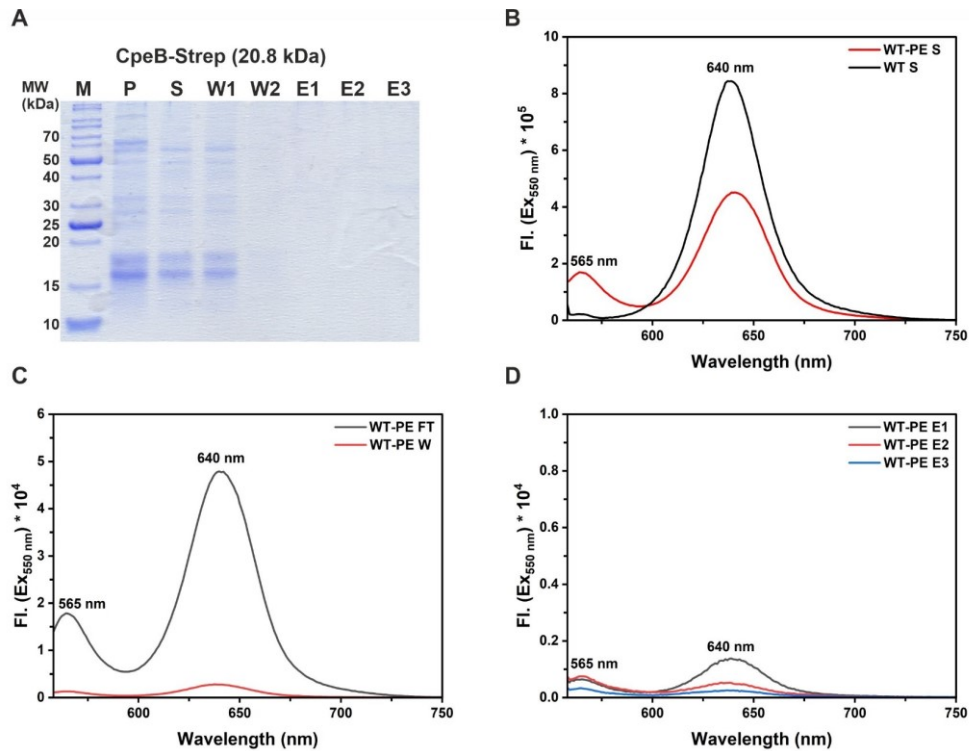


Figure 31: SDS-PAGE and fluorescence emission analysis of the CpeB-Strep purification via affinity chromatography. Cells of WT-PE were harvested, lysed and the lysate was separated in a soluble and insoluble fraction. The resulting soluble fraction was subjected to affinity chromatography using Strep-Tactin Sepharose resin. M: Molecular mass standard (Unstained Protein Standard, Broad Range, 10-200 kDa); P: insoluble fraction; S: soluble fraction; W1: Column wash step 1; W2: Column wash step 2; E1-3: Elution fractions. (A) SDS-PAGE analysis of the fractions after the purification of CpeB-Strep (calc. molecular mass of 20.8 kDa). (B-D) Fluorescence emission spectra between 558 nm and 750 nm of fractions after affinity chromatography upon excitation at 550 nm. Local maxima at 565 nm and 640 nm indicate PEB- and PCB-derived fluorescence signals, respectively.

The purification of *PmCpeB*-Strep did not yield detectable amounts of target protein in the elution fractions after electrophoretic protein separation (Figure 31A). Consequently, elution fractions were combined, concentrated and again subjected to SDS-PAGE (Appendix Figure A6B, CpeB C). There was still no protein signal observed corresponding to the molecular weight of ~ 20.8 kDa for *PmCpeB*-Strep. As a final step,

proteins below the detection limit of the Coomassie stain were extracted between ~ 18 kDa and ~ 24 kDa, digested with trypsin and subjected to mass spectrometry analysis. Eventually, *PmCpeB*-Step could not be identified by mass spectrometry and therefore motivates further studies to optimize recombinant protein production. In accordance with the lack of *PmCpeB*-Strep signals after SDS-PAGE, fluorescence emission signals representative for PEB at 565 nm were only detected in the soluble fraction after cell lysis (Figure 31B, red), the flowthrough (Figure 31C, black) and in the wash fractions of the column (Figure 31C, red). In the elution fractions, however, no significant PEB-derived fluorescence was observed (Figure 31D). In contrast, *PmCpeS*-His could be purified to a minimal amount (Appendix Figure A6B) but did not exhibit any spectroscopic features indicating an interaction with phycobilins (data not shown).

To complement the biochemical investigations of PE assembly in WT-PE with physiological analysis, a growth experiment was performed to evaluate the impact of the observed minimal recombinant protein production *in vivo* under phototrophic conditions (Figure 32).

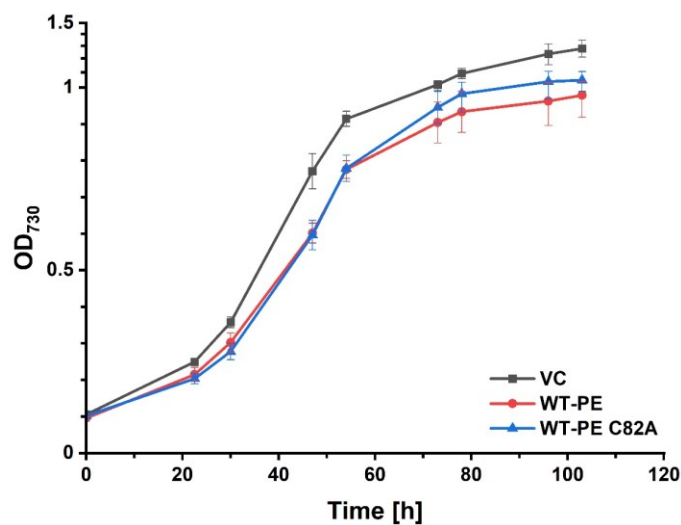


Figure 32: Phototrophic growth of *Synechocystis* WT transconjugants harbouring the constructs for the phycoerythrin assembly of *P. marinus* MED4. Absorbance measurements of *Synechocystis* VC (black), WT-PE (red) and WT-PE C82A (blue) culture densities at a wavelength of 730 nm. Shown are the mean values \pm SD of $n = 3$.

Differences in growth between the VC (grey) and both PE strains, WT-PE (red) and WT-PE C82A (blue), become noticeable 30 hours after inoculation. While the VC progressed towards stationary phase after ~80 h at an OD_{730 nm} of ~ 1, both PE strains reached optical densities of ~ 0.8. When comparing WT-PE with WT-PE C82A, no differences in growth were observed. The growth rates of the VC, WT-PE and WT-PE C82A were 1.03, 0.93 and 0.94 OD_{730 nm}/d, respectively, and showed no significant differences. Consequently, the reduced biomass formation as well as the slightly lower growth rate

of both PE strains, WT-PE and WT-PE C82A, is most likely derived from PEB formation as already observed in Syn-pPebS.

Biochemical analyses of heterologous PE assembly in *Synechocystis* provide evidence for the production of the recombinant proteins. While *PmCpeB* is produced in a soluble state in WT-PE and therefore complies with requirements for subsequent purification to evaluate its phycobilin content, the cysteine variant *PmCpeB* C82A in WT-PE C82A exclusively serves as a control for whole-cell analyses based on its insolubility after cell lysis. Implementing *PmCpeB* C82A as a control for biochemical investigations requires further optimization in the gene expression and protein extraction procedure. Previous studies already demonstrated the utilization of the CpeB cysteine variant C82A for *in vitro* PE assembly using *E. coli* as a platform for heterologous protein production (Steglich *et al.*, 2005). Considering the abundance of recombinant proteins and the challenging purification procedure of *PmCpeB* and *PmCpeS*, engineering of *Synechocystis* as a platform for heterologous PE assembly requires further optimization in terms of target protein abundance to investigate the attachment of PEB to *PmCpeB*. Once PE assembly has been shown *in vitro*, physiological studies as already performed for Syn-pPebS, are required to analyse the PBPs light-harvesting capability and its contribution to photosynthesis.

4. Discussion

4.1. Phycobiliprotein assembly in heterologous hosts

Investigations of PBPs often rely on recombinant overexpression systems since their native host often is either not isolated, challenging to cultivate in laboratory environments or genetically inaccessible. To enable the study of these light-harvesting proteins, engineered *E. coli* strains are commonly utilized as production platforms. Significant progress has been made using these systems but they are restricted to the analysis of PBP assembly by the evaluation of structural features and biochemical properties (Biswas *et al.*, 2010, Guo *et al.*, 2020, Saunée *et al.*, 2008). Based on covalently attached phycobilin chromophores, PBPs exhibit spectroscopically active properties which enable the proteins' function in light-harvesting. PBP assembly requires multiple enzymes consisting of suitable phycobilin biosynthesis pathways, PBP lyases for chromophore attachment and apo-PBP subunits as phycobilin acceptors to form the functional light-harvesting holo-proteins. Investigating PBP assembly also involves the biochemical characterization of respective PBP lyases to gain insights into their phycobilin-associating and transfer activities which reflects a necessary prerequisite for subsequent PBP subunit chromophorylation.

Assembly of PE545 in *G. theta*

Cryptophytes possess unusual PEs besides their chlorophyll containing light-harvesting complexes (Zhang *et al.*, 2024). Although cryptophytes are descendants of red algae, they employ quite different light-harvesting systems in terms of localization, organization, structure and chromophore composition. Red algae capture solar energy via light-harvesting complexes comparable to cyanobacteria. They employ both membrane-bound chlorophyll *a*-binding protein complexes and PBSs associated with the outer membrane of the thylakoid (Green 2019). In contrast, cryptophytes harvest light-energy via membrane-embedded chlorophyll *a/c*₂-binding proteins as well as PE PBPs, which are densely packed inside the thylakoid lumen (van der Weij-De Wit *et al.*, 2006, Zhao *et al.*, 2023). The cryptophyte model organism *G. theta* only employs the PBP PE545 which has the linear tetrapyrroles 15,16-DHBV and PEB attached to it as it is known from the crystal structure of its close relative *Rhodomonas* sp. CS24 (Wilk *et al.*, 1999). Here, 15,16-DHBV is bound to cysteine residue 19 of CpeA and three molecules of PEB are bound to the β -subunit CpeB. In CpeB, one PEB is doubly linked to cysteine 50 and 61 and two more PEB molecules are attached to cysteines 82 as well as 158, respectively. Two putative lyases already have been characterized to bind and transfer phycobilins to apo-PBP subunits.

The GtCPET lyase has been shown to attach phycobilins to reactive cysteines at position 158 (and homologues) of PBP β -subunits by successfully complementing a *Synechocystis* T-type lyase deletion mutant (Bolte *et al.*, 2008). The lyase GtCPES was proven to bind PEB and covalently attach the phycobilin to cysteine residue 82 of the *P. marinus* MED4 CpeB (Tomazic *et al.*, 2021). Since the assembly of the *PmCpeB* was already characterized using its native lyase *PmCpeS* (Steglich *et al.*, 2005, Wiethaus *et al.*, 2010), this *in vitro* system was adapted for GtCPES. In contrast, transfer of PEB by GtCPES to the native PBP β -subunit of *G. theta* remains challenging based on protein insolubility of GtCpeB (Overkamp 2014). Based on cryptophyte evolution, CpeB of *G. theta* exhibits high homology to cyanobacterial β -subunits which provides a strong foundation for the identification of the respective PBP lyases. In contrast to a single β -subunit, sequencing of the *G. theta* nucleus genome (Curtis *et al.*, 2012) revealed 16 α -subunits (Overkamp & Frankenberg-Dinkel 2013). It has been postulated that cryptophyte α -subunits evolved from red algal scaffolding proteins (Rathbone *et al.*, 2021) by outcompeting the cyanobacteria-derived CpeA. Despite the complex evolution of cryptophyte α -subunits, bioinformatic analyses revealed a putative E/F-type lyase for either CpeA (cysteine 19) or CpeB (cysteine 50 and 61) chromophore attachment called GtCpcX (Gould *et al.*, 2006). This sequence was derived from ESTs (expressed sequence tags) and the respective protein sequence shows low homology to other known E/F-type lyases. However, structural prediction and domain analysis revealed a protein architecture consisting of HEAT-repeats which is typically observed for E/F-type lyases and therefore strengthens the potential role of CpcX as a 15,16-DHBV:CpeA- or PEB:CpeB lyase in *G. theta* (Overkamp *et al.*, 2014). First approaches to produce CpcX were already performed in previous work to confirm its PBP lyase activity, but protein insolubility prevented subsequent biochemical *in vitro* analyses (Tomazic 2020).

The putative E/F-type PBP lyase CpcX

In this study, CpcX production conditions in *E. coli* were optimized to yield soluble protein for the biochemical characterization of the putative PBP lyase to gain insights into the assembly and the light-harvesting mechanism of the cryptophytic PBP PE545. The putative lyase CpcX could be produced in *E. coli* as a soluble protein by either co-expression with the chaperones GroES-EL or as a fusion construct with MBP. The latter yielded sufficient amounts of CpcX after protein purification (Appendix Figure A1). However, size-exclusion chromatography after MBP removal suggests higher aggregates of CpcX which, often implies improper protein folding (Appendix Figure A2). Since HEAT-repeat containing E/F-type lyases are known to be involved in chromophore attachment to α - and β -subunits (Carrigee *et al.*, 2020, Kronfel *et al.*, 2019), purified

CpcX was evaluated for its 15,16-DHBV and PEB associating activity. However, the lack of spectroscopic activity during phycobilin binding assays further supports impaired protein biosynthesis as already indicated by protein aggregation and the necessity of solubility enhancers during gene expression. Based on these results, the function of CpcX remains elusive. Proper CpcX activity could rely on heterodimer formation as it is known for other E/F-type lyases responsible for chromophore attachment to PBP α -subunits of PCs and PEs (Fairchild & Glazer 1994a, Zhao *et al.*, 2000). Crystallization studies of CpcE/F in *Nostoc* strongly suggest that both PBP lyase subunits are necessary for its activity since the cavity for phycobilin association is generated upon heterodimerization (Zhao *et al.*, 2017).

Formation of heterodimers are not only mandatory for the chromophore associating activity of most E/F-type lyases, but also for subsequent phycobilin attachment to PBP subunits. In *Synechococcus*, the deletion of genes necessary for the formation of the heterodimeric CpcE/F-lyase, specifically *cpcE*, *cpcF*, or both, leads to a significant impairment of phycobilin attachment to cysteine residue 84 of CpcA (Zhou *et al.*, 1992). Not only heterodimer formation of the putative PBP lyase CpcX may be required for proper PBP assembly, but also a chaperone-like PBP lyase called CpeZ which lacks intrinsic phycobilin associating properties. In *Fremyella*, covalent attachment of PEB to CpeA is facilitated by CpeY alone, but co-expression with CpeZ leads to enhanced levels of Holo-CpeA (Biswas *et al.*, 2011). Not only chromophore attachment to CpeA is supported by CpeZ, but also PEB addition to CpeB by the CpeT lyase is greatly improved by the chaperone-like PBP lyase (Nguyen *et al.*, 2020). In conclusion, CpeZ seems to be a universal keyplayer for PBP assembly by enhancing holo-protein formation which could also improve CpcX activity. In *G. theta*, a sequence for a putative chaperone-like PBP lyase have been identified and exhibits ~ 30 % sequence identity to CpeZ of *Fremyella* (Overkamp 2014). Consequently, further studies using a *GtccpcX* and *GtcpeZ* co-expression system reflects a reasonable approach to evaluate CpcX activity. However, there is also the possibility that the gene for the putative CpcX lyase does not encode for a functional PBP lyase protein. The evolution of cryptophyte α -subunits is rather complex since these subunits are derived from red algae scaffolding proteins. Here, scaffolding proteins most likely outcompeted the PE α -subunit, the primary binding partner of the red algae β -subunit (Rathbone *et al.*, 2021). This event may have led to the loss of the red algae phycobilisome and the evolution of the cryptophytic light-harvesting antenna. Consequently, the cryptophyte PBP lyase responsible for the phycobilin attachment to the evolved α -subunit may also show no homology to known α -

subunit lyases. Therefore, proper PBP lyase identification most likely requires more extensive bioinformatical investigations.

In conclusion, heterologous protein production in *E. coli* is a versatile and helpful tool to understand structural and biochemical features of PBPs but faces limitations. Not only challenging protein purification procedures as observed for CpcX of *G. theta* provides a motivation for the utilization of alternative hosts, but also the inability to evaluate the light-harvesting capacity of PBPs on a physiological level in this system. Consequently, employing a host with an appropriate physiological background including a photosynthetic machinery may enable the analysis of the PBPs contribution to photosynthesis.

4.2. Modified phycobilin biosynthesis in *Synechocystis*

The studies in this work based on expression systems in *E. coli* reflect the challenging nature of biochemical PBP analyses using such platforms. In contrast, utilization of cyanobacterial model organisms such as *Synechocystis* for the heterologous production of PBPs reflects a promising approach to assemble these light-harvesting proteins and investigate their physiological role *in vivo*. In addition to providing an alternative platform for the biochemical characterization of PBPs, this approach may allow the evaluation of their contribution to photosynthesis. *Synechocystis* provides a suitable physiological and molecular background to heterologously synthesize PBPs based on its native assembly machinery consisting of PBP lyases, a methyl transferase and appropriate chaperones which enable and support the sequential post-translational modification during PBP biosynthesis.

Consequently, this study aimed at expanding the toolbox for PBP research by genetically modifying *Synechocystis* to serve as a chassis for the investigation of light-harvesting proteins containing PEB as a chromophore, namely PEs. To establish a cyanobacterial platform for studying unusual PEB-containing PBPs, the cyanophage gene *pebS* was introduced to expand the phycobilin repertoire of *Synechocystis* which leads to the formation of both phycobilins, the natively synthesized PCB and the heterologously produced PEB.

4.2.1. The physiology of *Synechocystis* under heterologous PEB biosynthesis

The transconjugant Syn-pPebS harbouring the *pebS* expression construct already showed a phenotypic difference to the WT by a change of colony colour, which already suggested successful production of PEB (Figure 14). Interestingly, the observed phenotype closely resembles that of a *Synechocystis* strain called olive, a PBS truncation mutant (Vasudevan *et al.*, 2019). As previous studies already reported unstable, heterologous PEB formation in cyanobacterial hosts (Alvey *et al.*, 2011b), consistent PEB biosynthesis in Syn-pPebS was confirmed by spectroscopic measurements (Figure 19) after several rounds of sub-cultivation.

Photosynthetic activity during PEB formation

In this study, formation of PEB reduced the growth rate of Syn-pPebS compared to both control strains (Figure 15), suggesting a reduced viability if phycobilin biosynthesis pathways are modified in cyanobacterial hosts. Expanding the phycobilin repertoire of cyanobacteria potentially leads to an enhanced light-harvesting efficiency if the newly

introduced phycobilin is bound by endogenous PBPs and if the modified PBPs are able to form functional PBS complexes. However, studies in the PCB-, and therefore PC- and APC-producing strain *Synechococcus* sp. 7942 show covalent attachment of heterologously synthesized PEB to the endogenous PC. The assembly of modified PBPs to hybrid PBSs antenna complexes thereby depends on the degree of PEB chromophorylation (Sato *et al.*, 2024). The PEB-producing *Synechococcus* sp. 7942 shows impaired phototrophic growth under strong, heterologous expression of *pebA* and *pebB* and is very likely derived from gradual replacement of PCB- with PEB-bound PBPs, which shifts the ratio between free PBPs and assembled PBSs to rather free, cytosolic PBP complexes. A similar case has been observed in Syn-pPebS of this study via CLSM and PBS isolation experiments (Figure 21 and Figure 22). Free PBPs in the cytosol, as it was shown in *Synechocystis* antenna truncation mutants, also absorb light (Ughy & Ajlani 2004). But the free PBPs in such strains rather dissipate the energy as heat and fluorescence than forward the solar energy to fuel oxygenic photosynthesis (Ajlani *et al.*, 1995, Reuter *et al.*, 1994). To assess if the reduced viability in Syn-pPebS is derived from modified PBPs, and therefore potentially impaired light-harvesting capacity, photosynthetic activity was evaluated.

While the light saturation curve of the WT aligns with reported values (Wang *et al.*, 2010), the kanamycin resistant VC exhibits reduced oxygen evolution rates at light intensities above approximately $75 \mu\text{mol}/(\text{m}^2 \cdot \text{s})$ (Figure 17). Previous research has already demonstrated that certain antibiotics, including ampicillin, can impair oxygen production derived from photosynthesis as in the β -lactam resistant strain *Fremyella diplosiphon* B481-SD (Yalcin *et al.*, 2022). However, it remains unclear whether this observation applies to kanamycin-based selection systems in *Synechocystis*. Curiously, the oxygen evolution rates of Syn-pPebS resemble that from the WT, which suggests negligible effects of PEB biosynthesis on the photosynthetic activity of *Synechocystis*. Compared to the proper control strain, namely the VC, Syn-pPebS even shows an increase in oxygen evolution. Earlier studies have shown enhanced oxygen production through different modifications on PBSs as reducing the abundance of the antenna light-harvesting complex (Joseph *et al.*, 2014, Kwon *et al.*, 2013, Lea-Smith *et al.*, 2014). Similarly, Syn-pPebS exhibits a lower content of intact PBSs per cellular protein content (Figure 22). The photosynthetic activity seems to depend not only on the abundance but also on the size of the light-harvesting complex. *Synechocystis* PBS mutants show increasing levels of PSII reaction centres to compensate for antenna modifications (Nagarajan *et al.*, 2014). The increasing abundance of PSII complexes thereby leads to progressively higher oxygen production rates. Comparably, the reduced PBS levels in

Syn-pPebS potentially result in elevated PSII levels, which might contribute to the enhanced photosynthetic activity represented by increased oxygen evolution rates (Figure 17). However, the abundance of PSII reaction centres in Syn-pPebS was not evaluated in this study.

PEB biosynthesis regulated PBP abundance and PBS integrity

The abundance of intact PBSs in this study is mainly based on visual signal density in PBS isolation profiles because a quantification is not feasible by using the applied method. Why a reduced abundance of PBSs per cellular protein was observed, remains uncertain. However, previous *in vitro* analysis showed a complete loss of intact PBSs under strong expression of *pebA* and *pebB* in *Synechocystis* since significant replacement of native PCB with PEB, which is bound to endogenous PBPs, leads to either improper PBS assembly or even disassembly of intact PBSs (Sato *et al.*, 2024). The quantification of PBSs or PBPs can provide valuable insights into the hosts photosynthetic activity and is often derived from spectroscopic measurements of the soluble lysate. The absorbance maxima of the PCB-containing PC and APC in combination with their appropriate extinction coefficient is used to determine PBP abundance (Zavřel *et al.*, 2018). However, introducing PEB biosynthesis into *Synechocystis* yields PBPs with attached PEB (Figure 23 and Figure 25), which changes the quantity of covalently bound PCB and therefore impedes a reliable determination of the PBP content. Although there are first implications for the covalent attachment of PEB to APC, a significant increase in APC levels was still observed in Syn-pPebS (Figure 16). Regardless of its chromophore composition, PCB-derived values still illustrate elevated levels of APC. By increasing the cellular APC abundance, potentially reduced levels of intact PBSs are compensated. Leganés *et al.*, (2014) already demonstrated increased APC levels in a strain of *Nostoc* with a truncated PBS antenna complex (LC1 mutant). Decreased PBS antenna sizes in the LC1 mutant are further overcompensated by increasing the effective quantum yield of the PSII photochemistry, which also results in elevated oxygen evolution. This strongly suggests a more efficient energy conversion in PBS truncation mutants and further strengthens the observed increase in oxygen production in Syn-pPebS as already discussed earlier.

In contrast to APC, the PC content is reduced in Syn-pPebS and is derived from a mixture of PC proteins with either only PCB or PEB bound to it. Consequently, exact quantification of the modified PBPs derived from soluble lysates remains challenging and only provides a rough estimate of PBP abundance in Syn-pPebS. The reduced PC levels in Syn-pPebS could also be derived from the native regulation of PBP biosynthesis.

PBPs are typically degraded when the formation of the native ($\alpha\beta$)-monomers is impaired. In strain 4R of *Synechocystis*, CpcB is truncated by an insertional mutation which leads to an early termination of translation (Plank *et al.*, 1995). Here, the abundance of CpcA, the interaction partner of (the missing) CpcB, is reduced to levels beyond the limit of immunodetection. Consequently, $\alpha\beta$ -monomer formation potentially confers protection against proteolysis. Also the phycobilins attached to both subunits plays a vital role in PC stability (Toole *et al.*, 1998). Deletions of phycobilin binding sites by site directed mutagenesis can lead to a reduction of PBPs up to ~ 50 %. These results imply, in combination with steady-state PBP transcript levels, that the number of error-prone PCs and therefore their stability is regulated on post-translational level since transcript levels do not correlate with protein abundance. A similar case regarding PBP stability may be observed for the PC assembly in Syn-pPebS. The dispersed signals in CLSM imaging (Figure 21) provides first insights into a potential instability of the modified PC having both phycobilins PCB and PEB bound to it. Binding of the heterologously produced PEB may influence the PC subunit structures to prevent proper assembly of higher molecular weight complexes. PCB and PEB are isomeric molecules and only differ in the length of their conjugated π -electron system between the A- and D-ring of the linear tetrapyrrole. While the C-C double bond between C15 and C16 in PCB gives the molecule its rigidity, the linkage is reduced in PEB which provides the molecule with increased flexibility (Tomazic *et al.*, 2021). As a consequence, the flexible D-ring of PEB may prevent the utilization of the modified PC for PBS assembly based on steric hindrance, if the protein-protein interface necessary for antenna formation is disturbed.

In conclusion, the formation of both PCB and PEB, demonstrate overall negligible effects on the cellular physiology of *Synechocystis*. The only negative impact of the modified phycobilin biosynthesis in *Synechocystis* was detected by the reduction of the growth rate and PBS integrity. In contrast, Syn-pPebS demonstrates stable and steady formation of PEB without strongly interfering with phenotypic and genetic stability as the opposite effect has been observed in a *Synechococcus* strain expressing *pebAB* (Alvey *et al.*, 2011b). The impact of the modified phycobilin biosynthesis on cellular nitrogen reserves remains minimal suggesting no influence on general protein biosynthesis. In addition, Syn-pPebS stably performs oxygenic photosynthesis as shown by reasonable oxygen release, which is further supported by steady glycogen levels. Consequently, physiological data strengthens the feasibility of this platform and provides a motivation for the introduction of the remaining genes necessary for phycoerythrin assembly.

4.2.2. Assembly of modified phycobiliproteins

The biosynthesis of PebS in *Synechocystis* results in the production of PEB (Figure 19), which is covalently attached to CpcA, the α -subunit of PC, in addition to its native chromophore PCB (Figure 26 and Figure 27). Although this study provides first implications for covalent attachment of PEB to APC (Figure 23), investigations were focused on the highly abundant PBS rod protein PC. The ability of APC to bind PEB has been already shown in a *Synechocystis* PebS- Δ Rod mutant that lacks endogenous PCB biosynthesis (Guo *et al.*, 2022). Substitution of the APCs native chromophore PCB with PEB has drastic effects on the structure of the PBS core complex. While native APC forms trimeric aggregates, PEB-containing APC did not exceed the monomeric stage. Curiously, the trimeric aggregation typically observed in native APC could be recovered in an APC complex with covalently attached PEB and P Φ B. In conclusion, this study reveals the broad chromophore specificity of PBP subunits *in vivo*, here of APC subunits, which suggests a similar phenomenon for the rod protein PC.

This case was observed in this work for PC. Following the isolation of PC, the proteins spectroscopic properties provide evidence for the covalent attachment of both PCB and PEB. Since both PC subunits combined, CpcA and CpcB, harbour three attachment sites for phycobilin chromophores, tryptic peptides were separated and one PEB-containing peptide was identified by LC-MS/MS. Consequently, covalent attachment of PEB to the CpcA-derived peptide C₈₄AR was observed (Figure 27). These observations agree with previously reported studies that demonstrated covalent attachment of PEB to CpcA in an engineered *Synechococcus* strain (Alvey *et al.*, 2011b). Additionally, *in vitro* analyses based on heterologous expression systems in *E. coli* demonstrate very efficient attachment of PEB to CpcA (from *Synechocystis*) by the E/F-type lyases CpcE and CpcF from *Synechococcus* (Alvey *et al.*, 2011a). These findings, together with the data of this study, suggest a broad chromophore specificity of E/F-type lyases responsible for phycobilin attachment to cysteine residue 84 homologues of CpcA. Here, the *Synechocystis* CpcE/F lyases are most likely responsible for the attachment of PEB to cysteine residue 84 of CpcA. Interestingly, mass spectrometry analysis of the modified CpcA shows a chromophore-dependent fragmentation pattern in MS² spectra (Figure 27B, D). While PEB-C₈₄AR mainly dissociates to the peptide containing only the A, B and C pyrrole rings of PEB, the PCB chromophore in PCB-C₈₄AR is completely cleaved off from the peptide after fragmentation. This observation follows a predictable pattern determined by the location of C-C single bonds between each pyrrole ring within the phycobilin molecule as well as the thioether bond between the chromophore and the reactive cysteine of the peptide. While the carbon-carbon bond between C15 and C16 in

PEB is reduced, and therefore only has a single bond between the C- and the D-pyrrole ring, PCB harbours a double bond at that location. Dissociation of the phycobilin is derived from the average bond energy of double- ($D = 602 \text{ kJ}\cdot\text{mol}^{-1}$) and single C-C bonds ($D = 346 \text{ kJ}\cdot\text{mol}^{-1}$) (Huheey *et al.*, 1993) and therefore seems to be mainly dependent on the length of the phycobilins π -electron system. Consequently, this mass spectrometry approach may assist in the characterization of novel PBPs to identify its covalently bound phycobilins. While this study provides the first evidence for these phycobilin-dependent fragmentation patterns employing the exact same peptide, previous work already reported similar observations in MS/MS analyses using a commercial phycoerythrin (B-PE) derived from the red alga *Porphyridium purpureum* (Tamara *et al.*, 2019). B-PE consists of α -, β - and γ -subunits, the latter stabilizes the $(\alpha\beta)_3$ -hemaxers. While α - and β -subunits carry PEB as chromophores, the γ -subunit has one molecule of PUB attached to it. By subjecting the peptides of the corresponding subunits to fragmentation, the authors could demonstrate distinct signature peaks in MS² spectra which were highly dependent on either PUB or PEB. This study therefore further supports the utilization of mass spectrometry approaches to support the identification of phycobilin chromophores attached to PBPs.

In Syn-pPebS, the heterodimeric E/F-type lyase CpcE/F is most likely responsible for covalent attachment of PEB to CpcA. The remaining two candidates of PBP lyases, namely CpcS and CpcT, are also known to attach PEB to Apo-PBPs although they only bind and transfer PCB in their native host (Chen *et al.*, 2020). However, these observations are based on heterologous expression systems in *E. coli* with PEB being the only available chromophore. Replication of such studies in cyanobacterial systems has not been reported. Even less is known about their chromophore specificity in an artificial environment as in this study, a *Synechocystis* strain producing both phycobilins, PCB and PEB.

In summary, production of PEB in *Synechocystis* causes significant changes in the light-harvesting machinery by generating a mixture of native PC with attached PCB and modified PC with PEB attached to cysteine residue 84 of CpcA. Substitution of PCB with PEB most likely reduces the stability of PC and impairs the incorporation of the modified PC into the PBS antenna complex based on a reduced protein-protein interaction. Considering both physiological and biochemical assessment of heterologous PEB biosynthesis, the engineered *Synechocystis* strain presents a promising novel platform to investigate unusual phycoerythrins.

4.3. Assembly of the *P. marinus* MED4 phycoerythrin in *Synechocystis*

This study demonstrates the amenability of *Synechocystis* to modifications in phycobilin biosynthesis by introducing PEB biosynthesis via the *pebS* gene from the *Prochlorococcus* phage P-SSM2. Since the PEB chromophore is stably produced in this host, the remaining genes required for appropriate PE assembly were introduced. As a proof of concept for heterologous PE assembly and to elucidate the function of the degenerate *P. marinus* MED4 PBP β -subunit, the genetic construct of Syn-pPebS was extended by *PmCpeB* and its corresponding PBP lyase *PmCpeS*, which is responsible for the covalent attachment of PEB to cysteine residue 82 of the PBP. Prior to assessing the light-harvesting capacity of the *P. marinus* MED4 CpeB in *Synechocystis*, proper assembly of the heterologously produced PBP is required. Therefore, evidence for target protein production was provided. Uncertain or lacking Western Blot signals (Figure 29 and Figure 30) thereby indicate low target protein abundance which necessitated a more sensitive detection method as mass spectrometry (Table 19 and Table 20). Despite the successful production of *PmCpeS* and *PmCpeB*, assembly of *PmCpeB* was not confirmed by spectroscopic analyses for PEB-derived fluorescence in this study (Figure 31). A reduced abundance of both recombinant proteins and improper *PmCpeB* assembly is further supported by the unaffected growth rate of WT-PE (Figure 32).

Although earlier studies demonstrate efficient production and assembly of the *P. marinus* MED4 PE using heterologous expression systems in *E. coli* (Steglich *et al.*, 2005, Wiethaus *et al.*, 2010), a similar approach in *Synechocystis* requires further optimization. Both recombinant proteins, *PmCpeS* and *PmCpeB*, are encoded by the native *P. marinus* MED4 DNA sequences and have not been adapted to the codon-usage of *Synechocystis*. Although bioinformatical analysis of both DNA sequences demonstrates a feasible relative adaptiveness (distribution of codons for each amino acid) to the *Synechocystis* codon-usage, a reduced number of codons falls below a frequency of 10 % suggesting impaired tRNA availability for translation. Therefore, adaptation of the coding sequences for *PmcppeB* and *PmcppeS* to the codon-usage of *Synechocystis* potentially leads to an increased recombinant protein production. While some proteins are heterologously produced in a higher abundance using their native DNA sequence as the phage-derived FDBR enzyme PcyX (Ledermann 2018), adaptation to the expression hosts codon-usage significantly promotes target protein production in a considerable amount of studies (Karaođlan & Erden-Karaođlan 2020, Yadava & Ockenhouse 2003, Yu *et al.*, 2022). While these studies employ the commonly used protein production platforms *E. coli* and *Pichia pastoris*, codon optimization strategies also have been

successfully employed in *Synechocystis* (Lindberg *et al.*, 2010, Sebesta & Peebles 2020) and therefore reflects a promising approach to increase the protein abundance of *PmCpeS* and *PmCpeB* in the WT-PE strain of this study. In addition to the adaptation to the codon-usage of *Synechocystis*, different promoters controlling the expression of both target genes should be considered for optimization. The *J23119* promoter controlling *PmcpeB*- and the *trc10* promoter controlling *PmcpeS*- expression were proven to act as strong, constitutive promoters (Vasudevan *et al.*, 2019), using an eYFP reporter system. However, other studies show that the coding sequence downstream of the corresponding promoter has significant effects on the expression strength in *Synechocystis* as shown for the ethylene-forming enzyme EFE from *Pseudomonas syringae*. The *cpc560* promoter, which is also used for *pebS* expression in Syn-pPebS of this study, is well characterized and can yield target proteins up to 15 % of the total soluble protein (Zhou *et al.*, 2014a). For EFE, controlling expression strength with this promoter only yields a reduced amount of protein when compared to the light-responsive *psbA* promoter (natively drives PS II protein D1 expression in *Synechocystis*) and its synthetic derivative *psbA** which show a three- and ten-fold increase in *efe* gene expression, respectively (Wang *et al.*, 2018). Consequently, improving heterologous protein production of *PmCpeS* and *PmCpeB* involves the utilization of different promoters to evaluate a more efficient target gene expression. In addition to fine-tuning expression strength of target genes, translational efficiency can also be optimized by assessing different ribosome binding sites. Although translation of both *PmCpeS* and *PmCpeB* are under control of a strong, broad-range RBS (Geerts *et al.*, 1995, Huang *et al.*, 2010), efficiency is significantly affected by their genetic environment as investigated by Thiel *et al.*, (2018) using a system consisting of two different, but coupled fluorescent reporters. Consequently, transcription and translation depend on their genetic context and the evaluation of both promoters and RBSs reflect an opportunity to improve heterologous protein production of *PmCpeS* and *PmCpeB*. Based on increasing interest in *Synechocystis* for biotechnological applications, various promoters and RBSs are already characterized and may be considered for further optimization strategies (Englund *et al.*, 2016, Ferreira *et al.*, 2018, Sebesta & Peebles 2020, Veetil *et al.*, 2017). To investigate the relative protein abundance between the different expression constructs during optimization approaches, fusion proteins consisting of target- and fluorescent proteins (as eYFP fusion proteins) may be utilized as a convenient reporter system.

Despite the technical strategies to provide a chassis for heterologous PE assembly in *Synechocystis*, an established platform serving such research motivations may shed

light onto their physiological function *in vivo*. The PE of *P. marinus* is of great scientific interest because its biochemical properties suggest either a light-harvesting- or a photoreceptor-like function. Enrichment experiments of the native PE from *P. marinus* and studies using recombinant protein unambiguously show covalent attachment of PEB to β -phycoerythrin. Curiously, *P. marinus* produces the two phycobilins PEB and PCB and both were shown to bind to *PmCpeB* (Steglich *et al.*, 2005). While stereochemical correct phycobilin attachment occurs autocatalytically for phytochrome photoreceptors (Hübschmann *et al.*, 2001), proper covalently linkage of the phycobilins to the β -subunit requires PBP lyases such as *PmCpeS* (Wiethaus *et al.*, 2010). Interestingly, the genome of *P. marinus* MED4 lacks sequences for a functional phytochrome which raises the question of the PCB chromophores function *in vivo*. On the one hand, the highly fluorescent PEB-CpeB complex suggests a PBP-like function in *P. marinus*. On the other hand, PCB-CpeB shows rather phytochrome-like properties which indicates a potential photoreceptor function (Steglich *et al.*, 2005, Terry *et al.*, 1993). Another promising interaction partner for PCB is the GENOMES UNCOUPLED4 (GUN4) protein, which was originally found in *Arabidopsis thaliana*. GUN4, which is also present in various cyanobacteria, plays a vital role in retrograde signalling by binding porphyrins as well as the ChlH subunit of the magnesium chelatase, an enzyme catalysing the first committed step in chlorophyll biosynthesis (Larkin *et al.*, 2003, Wilde *et al.*, 2004). The reduction of the chlorophyll content in *Arabidopsis* and *Synechocystis gun4* knockout strains and their inability to further grow photoautotrophically strongly suggests an essential role of GUN4 in the cell metabolism (Peter & Grimm 2009, Sobotka *et al.*, 2008). Interestingly, besides being able to bind various porphyrins, GUN4 is also capable of binding PCB as shown in *in vitro* analyses (Zhang *et al.*, 2021). Consequently, PCB biosynthesis might contribute to the regulation of chlorophyll biosynthesis in *P. marinus* MED4.

To understand the possible function of the *P. marinus* β -phycoerythrin, it is essential to have an appropriate *in vivo* platform, such as an engineered *Synechocystis* strain capable of assembling phycobilin-containing proteins, to assess the physiological significance of the PBP. The *P. marinus* MED4 PE addressed in this study is only one of many examples of interesting, unusual PBPs, especially of hosts with limitations in strain isolation, cultivation and in amenability for genetic modifications. These challenges are also applicable to PEs of various cyanobacteria including other *Prochlorococci* strains (e.g., *P. marinus* SS120) as well as to eukaryotic algae as the cryptophyte *G. theta*. The findings of this study serve as an opportunity to further understand oxygenic photosynthesis driven by accessory light-harvesting complexes on a structural, mechanistic and evolutionary level.

5. Summary

A variety of organisms, including cyanobacteria, red algae and cryptophytes, perform oxygenic photosynthesis using chlorophyll-containing protein complexes and phycobiliproteins for light-harvesting. The most prominent phycobiliproteins described in literature assemble to macromolecular antenna complexes, called the phycobilisomes, to enhance oxygenic photosynthesis. Phycobiliproteins are categorized according their chromophore composition, with phycocyanins and allophycocyanins binding phycocyanobilin, while phycoerythrins can bind various bilins, such as 15,16-dihydrobiliverdin and phycoerythrobilin. Investigations of phycoerythrins often involves heterologous expression systems based on *E. coli* but only allow for biochemical characterization. In contrast, the utilization of expression systems in cyanobacteria, such as *Synechocystis* sp. PCC 6803, offer the opportunity to study phycoerythrins on a physiological level.

Consequently, this work aimed at providing a platform for heterologous phycoerythrin assembly using the cyanobacterium *Synechocystis* sp. PCC 6803, which naturally synthesizes allophycocyanin and phycocyanin with covalently attached phycocyanobilin. As a necessary prerequisite, phycoerythrobilin biosynthesis was established to provide the chromophore for phycoerythrin assembly. The impact of heterologous phycoerythrobilin production on the cellular physiology was assessed by growth curve experiments, oxygen evolution measurements as well as nutrient- and phycobiliprotein content determination. Despite a reduction in the growth rate, physiological effects were negligible. In addition, the influence of phycoerythrobilin formation on the biochemical properties of endogenous phycobiliproteins and its consequences for phycobilisome assembly were evaluated and show covalent attachment of phycoerythrobilin to CpcA of phycocyanin. The modified phycocyanin is unable to assemble into the phycobilisome complex leading to free cytosolic phycobiliproteins. Eventually, the remaining genes necessary for the assembly of the *P. marinus* MED4 phycoerythrin were introduced in *Synechocystis* sp. PCC 6803. Although in a rather low abundance, evidence for recombinant protein production is provided. However, proper assembly of the phycoerythrin was not confirmed in this study which motivates for further optimization strategies to increase the yield of target proteins.

In summary, this work demonstrates the amenability of *Synechocystis* sp. PCC 6803 to modifications in its biosynthetic phycobilin pathways by heterologously producing the chromophore phycoerythrobilin. Consequently, a promising foundation for the assembly of phycoerythrins is provided. Although proper phycoerythrin assembly was not confirmed in this study, the remaining challenges are most likely of technical nature.

These findings still strengthen the potential of utilizing cyanobacteria as a platform for the biochemical and physiological evaluation of phycoerythrins from otherwise inaccessible oxygenic phototrophs. Consequently, using such a platform may strongly contribute to the understanding of the structure and the mechanism of accessory light-harvesting machineries contributing to oxygenic photosynthesis.

6. Zusammenfassung

Eine Vielzahl an Organismen, die oxygene Photosynthese betreiben, darunter Cyanobakterien, Rotalgen und Kryptophyten, verwenden Chlorophyll-haltige Proteinkomplexe und Phycobiliproteine zur Lichtsammlung. Die bekanntesten in der Literatur beschriebenen Phycobiliproteine lagern sich zu makromolekularen Antennenkomplexen zusammen, um die oxygene Photosynthese anzutreiben. Phycobiliproteine werden nach ihrer Chromophor-Zusammensetzung kategorisiert. Während Phycocyanine und Allophycocyanine den Chromophor Phycocyanobilin binden, können Phycoerythrine viele verschiedene Biline binden, wie zum Beispiel 15,16-dihydrobiliverdin und Phycoerythrobin. Bei der Untersuchung von Phycoerythrinen werden häufig heterologe Expressionssysteme auf der Basis von *E. coli* eingesetzt, die jedoch nur eine biochemische Charakterisierung erlauben. Im Gegensatz dazu bietet die Verwendung von Expressionssystemen in Cyanobakterien, wie in *Synechocystis* sp. PCC 6803, die Möglichkeit, Phycoerythrine auf physiologischer Ebene zu untersuchen.

Folglich war es Ziel dieser Arbeit, eine Plattform für die heterologe Assemblierung von Phycoerythrinen mit Hilfe des Cyanobakteriums *Synechocystis* sp. PCC 6803 zu generieren. Dieser Wirt synthetisiert ausschließlich Phycocyanin und Allophycocyanin mit kovalent gebundenen Phycocyanobilin. Als Voraussetzung wurde die Biosynthese von Phycoerythrobin etabliert, um das notwendige Chromophor für den Aufbau von Phycoerythrinen bereitzustellen. Die Auswirkungen der heterologen Produktion von Phycoerythrobin auf die Zellphysiologie wurden durch Wachstumsexperimente, Messung der Sauerstoffentwicklung sowie die Bestimmung des Nährstoff- und Phycobiliprotein-Gehalts untersucht. Trotz einer Verringerung der Wachstumsrate, waren die physiologischen Auswirkungen vernachlässigbar. Zusätzlich wurde der Einfluss der PEB-Bildung auf die biochemischen Eigenschaften der endogenen Phycobiliproteine und ihre Auswirkungen auf den Aufbau von Phycobilisomen untersucht. Die Ergebnisse zeigen, dass PEB kovalent an CpcA des Phycocyanins gebunden ist. Das modifizierte Phycocyanin kann folglich nicht in den Phycobilisomkomplex eingebaut werden, was zu freien cytosolischen Phycobiliproteinen führt. Schließlich wurden die restlichen Gene, die für den Aufbau des Phycoerythrins von *P. marinus* MED4 erforderlich sind, in *Synechocystis* sp. PCC 6803 eingebracht. Wenn auch in einer eher geringen Menge, wurde die rekombinante Produktion von Proteinen, die für die Phycoerythrin-Assemblierung notwendig sind, bewiesen. Der Assemblierung des Phycoerythrins mit dem PEB Chromophor wurde in dieser Arbeit jedoch nicht

bestätigt, was zu weiteren Optimierungsstrategien motiviert, um die Ausbeute an Zielproteinen zu erhöhen.

Zusammenfassend zeigt diese Arbeit, dass *Synechocystis* sp. PCC 6803 durch die heterologe Produktion von PEB zugänglich für Modifikationen im Phycobilin-Biosyntheseweg ist und stellt damit eine vielversprechende Grundlage für die Assemblierung von Phycoerythrinen dar. Obwohl der korrekte Aufbau des Phycoerythrins von *P. marinus* MED4 nicht bestätigt werden konnte, sind die Herausforderungen wahrscheinlich technischen Ursprungs. Diese Ergebnisse stärken dennoch das Potenzial, Cyanobakterien wie *Synechocystis* sp. PCC 6803 als Plattform für die biochemische und physiologische Bewertung von Phycoerythrinen aus ansonsten unzugänglichen oxygenen phototrophen Organismen zu nutzen, um den Aufbau und die Funktionsweise der oxygenen Photosynthese und von akzessorischen Lichtsammelkomplexen näher zu verstehen.

References

- Ajlani G, Vernotte C, DiMagno L, Haselkorn R.** 1995. Phycobilisome core mutants of *Synechocystis* PCC 6803. *Biochim Biophys Acta Bioenerg* **1231**(2):189-196.
- Alvey RM, Biswas A, Schluchter WM, Bryant DA.** 2011a. Attachment of noncognate chromophores to CpcA of *Synechocystis* sp. PCC 6803 and *Synechococcus* sp. PCC 7002 by heterologous expression in *Escherichia coli*. *Biochem* **50**(22):4890–4902.
- Alvey RM, Biswas A, Schluchter WM, Bryant DA.** 2011b. Effects of modified phycobilin biosynthesis in the cyanobacterium *Synechococcus* sp. strain PCC 7002. *J Bacteriol* **193**(7):1663–1671.
- Andrade MA, Bork P.** 1995. HEAT repeats in the huntington's disease protein. *Nat Genet* **11**(2):115–116.
- Apt KE, Collier JL, Grossman AR.** 1995. Evolution of the phycobiliproteins. *J Mol Biol* **248**(1):79–96.
- Aras M, Hartmann V, Hartmann J, Nowaczyk MM, Frankenberg-Dinkel N.** 2020. Proximity channeling during cyanobacterial phycoerythrobilin synthesis. *FEBS J* **287**(2):284-294.
- Arteni AA, Ajlani G, Boekema EJ.** 2009. Structural organisation of phycobilisomes from *Synechocystis* sp. strain PCC6803 and their interaction with the membrane. *Biochim Biophys Acta Bioenerg* **1787**(4):272–279.
- Battchikova N, Wei L, Du L, Bersanini L, Aro E-M, Ma W.** 2011. Identification of novel ssl0352 protein (NdhS), essential for efficient operation of cyclic electron transport around photosystem I, in NADPH:plastoquinone oxidoreductase (NDH-1) complexes of *Synechocystis* sp. PCC 6803. *J Biol Chem* **286**(42):36992-37001.
- Beale SI, Cornejo J.** 1984. Enzymic transformation of biliverdin to phycocyanobilin by extracts of the unicellular red alga *Cyanidium caldarium*. *Plant Physiol* **76**(1):7-15.
- Beale SI, Cornejo J.** 1991. Biosynthesis of phycobilins. Ferredoxin-mediated reduction of biliverdin catalyzed by extracts of *Cyanidium caldarium*. *J Biol Chem* **266**(33):22328-22332.
- Bengtson S.** 1994. Early life on Earth. Columbia University Press.
- Bennett A, Bogorad L.** 1973. Complementary chromatic adaptation in a filamentous blue-green alga. *J Cell Biol* **58**(2):419–435.

- Bentley FK, Zurbriggen A, Melis A.** 2014. Heterologous expression of the mevalonic acid pathway in cyanobacteria enhances endogenous carbon partitioning to isoprene. *Mol Plant* **7**(1):71–86.
- Berkelman TR, Lagarias JC.** 1986. Visualization of bilin-linked peptides and proteins in polyacrylamide gels. *Anal Biochem* **156**(1):194-201.
- Biller SJ, Berube PM, Lindell D, Chisholm SW.** 2015. *Prochlorococcus*: the structure and function of collective diversity. *Nat Rev Microbiol* **13**(1):13-27.
- Biswas A, Vasquez YM, Dragomani TM, Kronfel ML, Williams SR, Alvey RM, Bryant DA, Schluchter WM.** 2010. Biosynthesis of cyanobacterial phycobiliproteins in *Escherichia coli*: Chromophorylation efficiency and specificity of all bilin lyases from *Synechococcus* sp. strain PCC 7002. *Appl Environ Microbiol* **76**(9):2729–2739.
- Biswas A, Boutaghou MN, Alvey RM, Kronfel CM, Cole RB, Bryant DA, Schluchter WM.** 2011. Characterization of the activities of the CpeY, CpeZ, and CpeS bilin lyases in phycoerythrin biosynthesis in *Fremyella diplosiphon* strain UTEX 481. *J Biol Chem* **286**(41):35509–35521.
- Blank CE.** 2004. Evolutionary timing of the origins of mesophilic sulphate reduction and oxygenic photosynthesis: a phylogenomic dating approach. *Geobiology* **2**(1):1-20.
- Bodzoń-Kuślakowska A, Drabik A, Mielczarek P, Sucharski F, Smoluch M, Suder P, Silberring J.** 2013. Fundamental strategies of protein and peptide sample preparation, p 25-77. *In* Ciborowski P, Silberring J (ed), *Proteomic Profiling and Analytical Chemistry*. Elsevier, Amsterdam.
- Bolte K, Kawach O, Prectl J, Gruenheit N, Nyalwidhe J, Maier UG.** 2008. Complementation of a phycocyanin-bilin lyase from *Synechocystis* sp. PCC 6803 with a nucleomorph-encoded open reading frame from the cryptophyte *Guillardia theta*. *BMC Plant Biol* **8**:1–12.
- Bolte K, Bullmann L, Hempel F, Bozarth A, Zauner S, Maier U-G.** 2009. Protein targeting into secondary plastids. *J Eukaryot Microbiol* **56**(1):9-15.
- Bradford MM.** 1976. A rapid and sensitive method for the quantitation of microgram quantities of protein utilizing the principle of protein-dye binding. *Anal Biochem* **72**(1):248-254.
- Broughton MJ, Howe CJ, Hiller RG.** 2006. Distinctive organization of genes for light-harvesting proteins in the cryptophyte alga *Rhodomonas*. *Gene* **369**:72–79.
- Burki F, Okamoto N, Pombert J-F, Keeling PJ.** 2012. The evolutionary history of haptophytes and cryptophytes: phylogenomic evidence for separate origins. *Proc R Soc B Biol Sci* **279**(1736):2246-2254.

- Busch AWU, Reijerse EJ, Lubitz W, Hofmann E, Frankenberg-Dinkel N.** 2011. Radical mechanism of cyanophage phycoerythrobilin synthase (PebS). *Biochem J* **433**(3):469–476.
- Calzadilla PI, Muzzopappa F, Sétif P, Kirilovsky D.** 2019. Different roles for ApcD and ApcF in *Synechococcus elongatus* and *Synechocystis* sp. PCC 6803 phycobilisomes. *Biochim Biophys Acta Bioenerg* **1860**(6):488-498.
- Carrigee LA, Mahmoud RM, Sanfilippo JE, Frick JP, Strnat JA, Karty JA, Chen B, Kehoe DM, Schluchter WM.** 2020. CpeY is a phycoerythrobilin lyase for cysteine 82 of the phycoerythrin I α -subunit in marine *Synechococcus*. *Biochim Biophys Acta Bioenerg* **1861**(8):148215.
- Carrigee LA, Frick JP, Karty JA, Garczarek L, Partensky F, Schluchter WM.** 2021. MpeV is a lyase isomerase that ligates a doubly linked phycourobilin on the β -subunit of phycoerythrin I and II in marine *Synechococcus*. *J Biol Chem* **296**(504):100031.
- Chapman D, Cole W, Siegelman H.** 1967. Chromophores of allophycocyanin and R-phycocyanin. *Biochem J* **105**(3):903-905.
- Chen H, Zheng C, Jiang P, Ji G.** 2020. Biosynthesis of a phycocyanin beta subunit with two noncognate chromophores in *Escherichia coli*. *Appl Biochem Biotechnol* **191**(2):763–771.
- Chen Y-R, Su Y-s, Tu S-L.** 2012. Distinct phytochrome actions in nonvascular plants revealed by targeted inactivation of phytyl biosynthesis. *Proc Natl Acad Sci* **109**(21):8310-8315.
- Cheng YC, Fleming GR.** 2009. Dynamics of light harvesting in photosynthesis. *Annu Rev Phys Chem* **60**:241–262.
- Chisholm SW.** 1992. Phytoplankton size, p 213-237. *In* Falkowski PG, Woodhead AD, Vivirito K (ed), Primary productivity and biogeochemical cycles in the sea, vol 43. Springer, Boston, MA.
- Cooley JW, Vermaas WFJ.** 2001. Succinate dehydrogenase and other respiratory pathways in thylakoid membranes of *Synechocystis* sp. strain PCC 6803: capacity comparisons and physiological function. *J Bacteriol* **183**(14):4251-4258.
- Crozet P, Navarro FJ, Willmund F, Mehrshahi P, Bakowski K, Lauersen KJ, Pérez-Pérez ME, Auroy P, Gorchs Rovira A, Sauret-Gueto S, Niemeyer J, Spaniol B, Theis J, Trösch R, Westrich LD, Vavitsas K, Baier T, Hübner W, Carpentier Fd, Cassarini M, Danon A, Henri J, Marchand CH, Mia Md, Sarkissian K, Baulcombe DC, Peltier G, Crespo JL, Kruse O, Jensen PE, Schroda M, Smith AG, Lemaire SD.** 2018. Birth of a photosynthetic chassis: a

moclo toolkit enabling synthetic biology in the microalga *Chlamydomonas reinhardtii*. *ACS Synth Biol* **7**(9):2074–2086.

- Csatorday K, MacColl R, Guard-Friar D, Hanzlik CA.** 1987. Excitation energy transfer between sensitizing chromophores of phycocyanin 612. *Photochem Photobiol* **45**(S1):845-848.
- Curtis BA, Tanifuji G, Burki F, Gruber A, Irimia M, Maruyama S, Arias MC, Ball SG, Gile GH, Hirakawa Y, Hopkins JF, Kuo A, Rensing SA, Schmutz J, Symeonidi A, Elias M, Eveleigh RJM, Herman EK, Klute MJ, Nakayama T, Oborník M, Reyes-Prieto A, Armbrust EV, Aves SJ, Beiko RG, Coutinho P, Dacks JB, Durnford DG, Fast NM, Green BR, Grisdale CJ, Hempel F, Henrissat B, Höppner MP, Ishida K-I, Kim E, Kořený L, Kroth PG, Liu Y, Malik S-B, Maier UG, McRose D, Mock T, Neilson JAD, Onodera NT, Poole AM, Pritham EJ, Richards TA, Rocap G, Roy SW, Sarai C, Schaack S, Shirato S, Slamovits CH, Spencer DF, Suzuki S, Worden AZ, Zauner S, Barry K, Bell C, Bharti AK, Crow JA, Grimwood J, Kramer R, Lindquist E, Lucas S, Salamov A, McFadden GI, Lane CE, Keeling PJ, Gray MW, Grigoriev IV, Archibald JM.** 2012. Algal genomes reveal evolutionary mosaicism and the fate of nucleomorphs. *Nature* **492**(7427):59-65.
- Dadheech PK, Glöckner G, Casper P, Kotut K, Mazzoni CJ, Mbedi S, Krienitz L.** 2013. Cyanobacterial diversity in the hot spring, pelagic and benthic habitats of a tropical soda lake. *FEMS Microbiol Ecol* **85**(2):389-401.
- Dammeyer T, Frankenberg-Dinkel N.** 2006. Insights into phycoerythrobilin biosynthesis point toward metabolic channeling. *J Biol Chem* **281**(37):27081–27089.
- Dammeyer T, Bagby SC, Sullivan MB, Chisholm SW, Frankenberg-Dinkel N.** 2008a. Efficient phage-mediated pigment biosynthesis in oceanic cyanobacteria. *Curr Biol* **18**(6):442–448.
- Dammeyer T, Hofmann E, Frankenberg-Dinkel N.** 2008b. Phycoerythrobilin synthase (PebS) of a marine virus: crystal structures of the biliverdin complex and the substrate-free form. *J Biol Chem* **283**(41):27547-27554.
- Domínguez-Martín MA, Sauer PV, Kirst H, Sutter M, Bina D, Greber BJ, Nogales E, Polívka T, Kerfeld CA.** 2022. Structures of a phycobilisome in light-harvesting and photoprotected states. *Nature* **609**(7928):835-845.
- Douglas S, Zauner S, Fraunholz M, Beaton M, Penny S, Deng L-T, Wu X, Reith M, Cavalier-Smith T, Maier U-G.** 2001. The highly reduced genome of an enslaved algal nucleus. *Nature* **410**(6832):1091-1096.

- Doust AB, Marai CNJ, Harrop SJ, Wilk KE, Curmi PMG, Scholes GD.** 2004. Developing a structure-function model for the cryptophyte phycoerythrin 545 using ultrahigh resolution crystallography and ultrafast laser spectroscopy. *J Mol Biol* **344**(1):135–153.
- Doust AB, Wilk KE, Curmi PMG, Scholes GD.** 2006. The photophysics of cryptophyte light-harvesting. *J Photochem Photobiol A Chem* **184**(1-2):1–17.
- Durán RV, Hervás M, Miguel A, Navarro JA.** 2004. The efficient functioning of photosynthesis and respiration in *Synechocystis* sp. PCC 6803 strictly requires the presence of either cytochrome c_6 or plastocyanin. *J Biol Chem* **279**(8):7229–7233.
- Elanskaya IV, Zlenko DV, Lukashev EP, Suzina NE, Kononova IA, Stadnichuk IN.** 2018. Phycobilisomes from the mutant cyanobacterium *Synechocystis* sp. PCC 6803 missing chromophore domain of ApcE. *Biochim Biophys Acta Bioenerg* **1859**(4):280–291.
- Engler C, Youles M, Gruetzner R, Ehnert TM, Werner S, Jones JDG, Patron NJ, Marillonnet S.** 2014. A Golden Gate modular cloning toolbox for plants. *ACS Synth Biol* **3**(11):839–843.
- Englund E, Liang F, Lindberg P.** 2016. Evaluation of promoters and ribosome binding sites for biotechnological applications in the unicellular cyanobacterium *Synechocystis* sp. PCC 6803. *Sci Rep* **6**(1):1–12.
- Fairchild CD, Zhaot J, Zhouti J, Colson SUEE, Bryantt DA, Glazer AN.** 1992. Phycocyanin α -subunit phycocyanobilin lyase. *Proc Natl Acad Sci* **89**(15):7017–7021.
- Fairchild CD, Glazer AN.** 1994a. Oligomeric structure, enzyme kinetics, and substrate specificity of the phycocyanin α subunit phycocyanobilin lyase. *J Biol Chem* **269**(12):8686–8694.
- Fairchild CD, Glazer AN.** 1994b. Nonenzymatic bilin addition to the α subunit of an apophytoerythrin. *J Biol Chem* **269**(46):28988–28996.
- Farhat D.** 2020. Developmental barriers in *T. gondii*: MORC at the onset of epigenetic rewiring of the parasite's cell fate. Dissertation. Université Grenoble Alpes.
- Farquhar GD, von Caemmerer Sv, Berry JA.** 1980. A biochemical model of photosynthetic CO_2 assimilation in leaves of C_3 species. *Planta* **149**:78–90.
- Ferreira EA, Pacheco CC, Pinto F, Pereira J, Lamosa P, Oliveira P, Kirov B, Jaramillo A, Tamagnini P.** 2018. Expanding the toolbox for *Synechocystis* sp. PCC 6803: validation of replicative vectors and characterization of a novel set of promoters. *Synth Biol* **3**(1):1–15.

- Flombaum P, Gallegos JL, Gordillo RA, Rincón J, Zabala LL, Jiao N, Karl DM, Li WKW, Lomas MW, Veneziano D, Vera CS, Vrugt JA, Martiny AC.** 2013. Present and future global distributions of the marine cyanobacteria *Prochlorococcus* and *Synechococcus*. *Proc Natl Acad Sci* **110**(24):9824-9829.
- Frankenberg-Dinkel N.** 2004. Bacterial heme oxygenases. *Antioxid Redox Signal* **6**(5):825–834.
- Frankenberg N, Mukougawa K, Kohchi T, Lagarias JC.** 2001. Functional genomic analysis of the HY2 family of ferredoxin-dependent bilin reductases from oxygenic photosynthetic organisms. *Plant Cell* **13**(4):965–978.
- Frankenberg N, Lagarias JC.** 2003. Phycocyanobilin: ferredoxin oxidoreductase of *Anabaena* sp. PCC 7120: biochemical and spectroscopic characterization. *J Biol Chem* **278**(11):9219-9226.
- Franz T, Li X.** 2015. Step-by-step preparation of proteins for mass spectrometric analysis, p 235-247. *In* Posch A (ed), *Proteomic profiling: methods and protocols*. Springer New York, New York, NY.
- Gale GAR, Wang B, McCormick AJ.** 2021. Evaluation and comparison of the efficiency of transcription terminators in different cyanobacterial species. *Front Microbiol* **11**:624011.
- Gallon JR.** 1981. The oxygen sensitivity of nitrogenase: a problem for biochemists and micro-organisms. *Trends Biochem Sci* **6**:19-23.
- Galloway JN, Dentener FJ, Capone DG, Boyer EW, Howarth RW, Seitzinger SP, Asner GP, Cleveland CC, Green P, Holland EA.** 2004. Nitrogen cycles: past, present, and future. *Biogeochem* **70**:153-226.
- Gantt E, Edwards MR, Provasoli L.** 1971. Chloroplast structure of the cryptophyceae: evidence for phycobiliproteins within intrathylakoidal spaces. *J Cell Biol* **48**(2):280–290.
- Gasper R, Schwach J, Hartmann J, Holtkamp A, Wiethaus J, Riedel N, Hofmann E, Frankenberg-Dinkel N.** 2017. Distinct features of cyanophage-encoded T-type phycobiliprotein lyase Φ CpeT: The role of auxiliary metabolic genes. *J Biol Chem* **292**(8):3089–3098.
- Geerts D, Bovy A, de Vrieze G, Borrias M, Weisbeek P.** 1995. Inducible expression of heterologous genes targeted to a chromosomal platform in the cyanobacterium *Synechococcus* sp. PCC 7942. *Microbiol* **141**(4):831-841.
- Gibson DG, Young L, Chuang R-Y, Venter JC, Hutchison CA, Smith HO.** 2009. Enzymatic assembly of DNA molecules up to several hundred kilobases. *Nat Methods* **6**(5):343-345.

- Gisk B, Wiethaus J, Aras M, Frankenberg-Dinkel N.** 2012. Variable composition of heme oxygenases with different regiospecificities in *Pseudomonas* species. *Arch Microbiol* **194**:597-606.
- Glazer A, Wedemayer G.** 1995. Cryptomonad biliproteins - an evolutionary perspective. *Photosynth Res* **46**:93–105.
- Glazer AN.** 1977. Structure and molecular organization of the photosynthetic accessory pigments of cyanobacteria and red algae. *Mol Cell Biochem* **18**(2):125–140.
- González López CV, García MdCC, Fernández FGA, Bustos CS, Chisti Y, Sevilla JMF.** 2010. Protein measurements of microalgal and cyanobacterial biomass. *Bioresour Technol* **101**(19):7587-7591.
- Gould SB, Sommer MS, Kroth PG, Gile GH, Keeling PJ, Maier UG.** 2006. Nucleus-to-nucleus gene transfer and protein retargeting into a remnant cytoplasm of cryptophytes and diatoms. *Mol Biol Evol* **23**(12):2413–2422.
- Green BR.** 2019. What happened to the phycobilisome? *Biomolecules* **9**(11):748.
- Grossman AR, Schaefer MR, Chiang GG, Collier JL.** 1993. The phycobilisome, a light-harvesting complex responsive to environmental conditions. *Microbiol Rev* **57**(3):725-749.
- Gu B.** 2023. Assembly and characterization of phycoerythrin-III from *Prochlorococcus marinus* SS120. Dissertation. Rheinland-Pfälzische Technische Universität Kaiserslautern-Landau.
- Guo R, Wang S, Niu N-N, Xu Y-L, Zhu J-X, Scheer H, Noy D, Zhao K-H.** 2022. Dichromic allophycocyanin trimer covering a broad spectral range (550-660 nm). *Chem Eur J* **29**(9):e202203367.
- Guo Y, Zang X, Cao X, Zhang F, Sun D, Shang M, Li R, Yangzong Z, Wei X, Zhang X.** 2020. Cloning and expression of allophycocyanin gene from *Gracilariopsis lemaneiformis* and studying the binding sites of phycocyanobilin on its α and β subunits. *J Appl Phycol* **32**(4):2657-2671.
- Hagiwara Y, Sugishima M, Takahashi Y, Fukuyama K.** 2006. Crystal structure of phycocyanobilin:ferredoxin oxidoreductase in complex with biliverdin IX α , a key enzyme in the biosynthesis of phycocyanobilin. *Proc Natl Acad Sci* **103**(1):27-32.
- Hauth AM, Maier UG, Lang BF, Burger G.** 2005. The *Rhodomonas salina* mitochondrial genome: bacteria-like operons, compact gene arrangement and complex repeat region. *Nucleic Acid Res* **33**(14):4433-4442.
- Hess WR, Partensky F, Van der Staay G, Garcia-Fernandez JM, Börner T, Vaultot D.** 1996. Coexistence of phycoerythrin and a chlorophyll a/b antenna in a marine prokaryote. *Proc Natl Acad Sci* **93**(20):11126-11130.

- Howe CJ, Barbrook AC, Nisbet RER, Lockhart PJ, Larkum AWD.** 2008. The origin of plastids. *Philos Trans R Soc B Biol Sci* **363**(1504):2675-2685.
- Huang HH, Camsund D, Lindblad P, Heidorn T.** 2010. Design and characterization of molecular tools for a synthetic biology approach towards developing cyanobacterial biotechnology. *Nucleic Acid Res* **38**(8):2577–2593.
- Hübschmann T, Börner T, Hartmann E, Lamparter T.** 2001. Characterization of the Cph1 holo-phytochrome from *Synechocystis* sp. PCC 6803. *Eur J Biochem* **268**(7):2055-2063.
- Huheey JE, Keiter EA, Keiter RL.** 1993. *Inorganic chemistry : principles of structure and reactivity*, Fourth edition ed. HarperCollins College Publishers, New York, NY.
- Iñiguez C, Capó-Bauçà S, Niinemets Ü, Stoll H, Aguiló-Nicolau P, Galmés J.** 2020. Evolutionary trends in RuBisCO kinetics and their co-evolution with CO₂ concentrating mechanisms. *Plant J* **101**(4):897-918.
- Isailovic D, Sultana I, Phillips GJ, Yeung ES.** 2006. Formation of fluorescent proteins by the attachment of phycoerythrin to R-phycoerythrin alpha and beta apo-subunits. *Anal Biochem* **358**(1):38-50.
- Ishikawa K, Sato M, Ito M, Yoshida T.** 1992. Importance of histidine residue 25 of rat heme oxygenase for its catalytic activity. *Biochem Biophys Res Commun* **182**(3):981-986.
- Johnson BH, Hecht MH.** 1994. Recombinant proteins can be isolated from *E. coli* cells by repeated cycles of freezing and thawing. *Nat Biotechnol* **12**(12):1357-1360.
- Johnson ZI, Zinser ER, Coe A, McNulty NP, Woodward EMS, Chisholm SW.** 2006. Niche partitioning among *Prochlorococcus* ecotypes along ocean-scale environmental gradients. *Science* **311**(5768):1737-1740.
- Jordan P, Fromme P, Witt HT, Klukas O, Saenger W, Krauß N.** 2001. Three-dimensional structure of cyanobacterial photosystem I at 2.5 Å resolution. *Nature* **411**(6840):909-917.
- Joseph A, Aikawa S, Sasaki K, Matsuda F, Hasunuma T, Kondo A.** 2014. Increased biomass production and glycogen accumulation in *apcE* gene deleted *Synechocystis* sp. PCC 6803. *AMB Express* **4**(1):17.
- Kachel B.** 2021. Metabolic engineering of *Synechococcus* sp. strain PCC 7002 for the photoautotrophic production of riboflavin (vitamin B2). Dissertation. Ruperto Carola Universität Heidelberg.
- Karaođlan M, Erden-Karaođlan F.** 2020. Effect of codon optimization and promoter choice on recombinant endo-polygalacturonase production in *Pichia pastoris*. *Enzyme Microb Technol* **139**:109589.

- Katayama N, Osanai T.** 2024. Arginine inhibits the arginine biosynthesis rate-limiting enzyme and leads to the accumulation of intracellular aspartate in *Synechocystis* sp. PCC 6803. *Plant Mol Biol* **114**(2):27.
- Keeling PJ.** 2009. Chromalveolates and the evolution of plastids by secondary endosymbiosis. *J Eukaryot Microbiol* **56**(1):1-8.
- Kehoe DM.** 2010. Chromatic adaptation and the evolution of light color sensing in cyanobacteria. *Proc Natl Acad Sci* **107**(20):9029–9030.
- Kieselbach T, Cheregi O, Green BR, Funk C.** 2018. Proteomic analysis of the phycobiliprotein antenna of the cryptophyte alga *Guillardia theta* cultured under different light intensities. *Photosynth Res* **135**(1):149-163.
- Kohchi T, Mukougawa K, Frankenberg N, Masuda M, Yokota A, Lagarias JC.** 2001. The *Arabidopsis* HY2 gene encodes phytochromobilin synthase, a ferredoxin-dependent biliverdin reductase. *Plant Cell* **13**(2):425–436.
- Kondo K, Geng XX, Katayama M, Ikeuchi M.** 2005. Distinct roles of CpcG1 and CpcG2 in phycobilisome assembly in the cyanobacterium *Synechocystis* sp. PCC 6803. *Photosynth Res* **84**:269-273.
- Koontz L.** 2014. TCA Precipitation, p 3-10. *In* Lorsch J (ed), *Methods in Enzymology*, vol 541. Academic Press.
- Kossalbayev BD, Tomo T, Zayadan BK, Sadvakasova AK, Bolatkhan K, Alwasel S, Allakhverdiev SI.** 2020. Determination of the potential of cyanobacterial strains for hydrogen production. *Int J Hydrog Energy* **45**(4):2627-2639.
- Kronfel CM, Kuzin AP, Forouhar F, Biswas A, Su M, Lew S, Seetharaman J, Xiao R, Everett JK, Ma LC, Acton TB, Montelione GT, Hunt JF, Paul CEC, Dragomani TM, Boutaghou MN, Cole RB, Rimi C, Alvey RM, Bryant DA, Schluchter WM.** 2013. Structural and biochemical characterization of the bilin lyase CpcS from *Thermosynechococcus elongatus*. *Biochem* **52**(48):8663–8676.
- Kronfel CM, Hernandez CV, Frick JP, Hernandez LS, Gutu A, Karty JA, Boutaghou MN, Kehoe DM, Cole RB, Schluchter WM.** 2019. CpeF is the bilin lyase that ligates the doubly linked phycoerythrobilin on phycoerythrin in the cyanobacterium *Fremyella diplosiphon*. *J Biol Chem* **294**(11):3987–3999.
- Kugrens P, Lee RE.** 1992. Organization of cryptomonads. *In* Patterson DJ, Larsen J (ed), *The biology of free-living heterotrophic flagellates*. Oxford University Press.
- Kumarapperuma I, Joseph KL, Wang C, Biju LM, Tom IP, Weaver KD, Grébert T, Partensky F, Schluchter WM, Yang X.** 2022. Crystal structure and molecular mechanism of an E/F type bilin lyase-isomerase. *Structure* **30**(4):1–11.

- Kurisu G, Zhang H, Smith JL, Cramer WA.** 2003. Structure of the cytochrome b_6/f complex of oxygenic photosynthesis: Tuning the cavity. *Science* **302**(5647):1009-1014.
- Kwon J-H, Bernát G, Wagner H, Rögner M, Rexroth S.** 2013. Reduced light-harvesting antenna: consequences on cyanobacterial metabolism and photosynthetic productivity. *Algal Res* **2**(3):188–195.
- Lämmli UK.** 1970. Cleavage of structural proteins during the assembly of the head of bacteriophage T4. *Nature* **227**(5259):680-685.
- Lane CE, van den Heuvel K, Kožera C, Curtis BA, Parsons BJ, Bowman S, Archibald JM.** 2007. Nucleomorph genome of *Hemiselmis andersenii* reveals complete intron loss and compaction as a driver of protein structure and function. *Proc Natl Acad Sci* **104**(50):19908-19913.
- Larkin RM, Alonso JM, Ecker JR, Chory J.** 2003. GUN4, a regulator of chlorophyll synthesis and intracellular signaling. *Science* **299**(5608):902-906.
- Laurel KRS-B, Miller.** 1989. Unique location of the phycobiliprotein light-harvesting pigment in the cryptophyceae. *J Phycol* **25**(3):412–419.
- Laurentin A, Edwards CA.** 2003. A microtiter modification of the anthrone-sulfuric acid colorimetric assay for glucose-based carbohydrates. *Anal Biochem* **315**(1):143-145.
- Lea-Smith DJ, Bombelli P, Dennis JS, Scott SA, Smith AG, Howe CJ.** 2014. Phycobilisome-deficient strains of *Synechocystis* sp. PCC 6803 have reduced size and require carbon-limiting conditions to exhibit enhanced productivity. *Plant Physiol* **165**(2):705–714.
- Ledermann B.** 2018. From metagenomes to green algae - the biochemical variety of bilin biosynthesis enzymes. Dissertation. Technische Universität Kaiserslautern.
- Leganés F, Martínez-Granero F, Muñoz-Martín MÁ, Marco E, Jorge A, Carvajal L, Vida T, González-Pleiter M, Fernández-Piñas F.** 2014. Characterization and responses to environmental cues of a photosynthetic antenna-deficient mutant of the filamentous cyanobacterium *Anabaena* sp. PCC 7120. *J Plant Physiol* **171**(11):915-926.
- Li Y, Scales N, Blankenship RE, Willows RD, Chen M.** 2012. Extinction coefficient for red-shifted chlorophylls: chlorophyll *d* and chlorophyll *f*. *Biochim Biophys Acta Bioenerg* **1817**(8):1292–1298.
- Lichtlé C, Jupin H, Duval JC.** 1980. Energy transfers from photosystem II to photosystem I in *Cryptomonas rufescens* (Cryptophyceae). *Biochim Biophys Acta Bioenerg* **591**(1):104–112.

- Lin S, Li S, Ouyang T, Chen G.** 2023. Site-2 protease Slr1821 regulates carbon/nitrogen homeostasis during ammonium stress acclimation in cyanobacterium *Synechocystis* sp. PCC 6803. *Int J Mol Sci* **24**(7):6606.
- Lindberg P, Park S, Melis A.** 2010. Engineering a platform for photosynthetic isoprene production in cyanobacteria, using *Synechocystis* as the model organism. *Metab Eng* **12**(1):70-79.
- Liu Y, Ortiz de Montellano PR.** 2000. Reaction intermediates and single turnover rate constants for the oxidation of heme by human heme oxygenase-1. *J Biol Chem* **275**(8):5297-5307.
- Lu K-J, Chang C-W, Wang C-H, Chen FYH, Huang IY, Huang P-H, Yang C-H, Wu H-Y, Wu W-J, Hsu K-C, Ho M-C, Tsai M-D, Liao JC.** 2023. An ATP-sensitive phosphoketolase regulates carbon fixation in cyanobacteria. *Nat Metab* **5**(7):1111-1126.
- Machingura MC, Moroney JV.** 2018. Closing the circle. *eLife* **7**:e42507.
- Martin-Cereceda M, Roberts EC, Wootton EC, Bonaccorso E, Dyal P, Guinea A, Rogers D, Wright CJ, Novarino G.** 2010. Morphology, ultrastructure, and small subunit rDNA phylogeny of the marine heterotrophic flagellate *Goniomonas* aff. *amphinema*. *J Eukaryot Microbiol* **57**(2):159-170.
- Marx A, Adir N.** 2013. Allophycocyanin and phycocyanin crystal structures reveal facets of phycobilisome assembly. *Biochim Biophys Acta Bioenerg* **1827**(3):311–318.
- Moisander P.** 2017. Chasing after non-cyanobacterial nitrogen fixation in marine pelagic environments. *Front Microbiol* **8**(1736):286758.
- Möllers KB, Cannella D, Jørgensen H, Frigaard N-U.** 2014. Cyanobacterial biomass as carbohydrate and nutrient feedstock for bioethanol production by yeast fermentation. *Biotechnol Biofuels* **7**(1):64.
- Moore LR, Rocap G, Chisholm SW.** 1998. Physiology and molecular phylogeny of coexisting *Prochlorococcus* ecotypes. *Nature* **393**(6684):464-467.
- Mullineaux CW.** 2014. Co-existence of photosynthetic and respiratory activities in cyanobacterial thylakoid membranes. *Biochim Biophys Acta Bioenerg* **1837**(4):503-511.
- Mullis KB, Faloona FA.** 1987. Specific synthesis of DNA *in vitro* via a polymerase-catalyzed chain reaction, p 335-350, *Methods in Enzymology*, vol 155. Academic Press.
- Nagarajan A, Page LE, Liberton M, Pakrasi HB.** 2014. Consequences of decreased light harvesting capability on photosystem II function in *Synechocystis* sp. PCC 6803. *Life* **4**(4):903-914.

- Nagarajan A, Pakrasi HB.** 2016. Membrane-bound protein complexes for photosynthesis and respiration in cyanobacteria, p 1-8, Encyclopedia of Life Sciences. John Wiley & Sons, Ltd. (Ed.).
- Nguyen AA, Joseph KL, Bussell AN, Pokhrel S, Karty JA, Kronfel CM, Kehoe DM, Schluchter WM.** 2020. CpeT is the phycoerythrobilin lyase for Cys-165 on β -phycoerythrin from *Fremyella diplosiphon* and the chaperone-like protein CpeZ greatly improves its activity. *Biochim Biophys Acta Bioenerg* **1861**(12):148284.
- Ong L, Glazer AN.** 1988. Structural studies of phycobiliproteins in unicellular marine cyanobacteria, p 388 pp. *In* (ed), Light-energy transduction in photosynthesis: higher plant and bacterial models. Am Soc Plant Physiol
- Ong L, Glazer A.** 1991. Phycoerythrins of marine unicellular cyanobacteria. I. Bilin types and locations and energy transfer pathways in *Synechococcus* spp. phycoerythrins. *J Biol Chem* **266**(15):9515-9527.
- Ortega-Martínez P, Roldán M, Díaz-Troya S, Florencio FJ.** 2022. Stress response requires an efficient connection between glycogen and central carbon metabolism by phosphoglucomutases in cyanobacteria. *J Exp Bot* **74**(5):1532-1550.
- Overkamp KE, Frankenberg-Dinkel N.** 2013. Phycobiliproteins — biosynthesis, assembly and applications, p 187–226, Handbook of Porphyrin Science, vol 28. World Scientific.
- Overkamp KE.** 2014. Biosynthese offenkettiger Tetrapyrrole und Assemblierung von Phycobiliproteinen in der Cryptophyte *Guillardia theta*. Dissertation. Ruhr-Universität Bochum.
- Overkamp KE, Gasper R, Kock K, Herrmann C, Hofmann E, Frankenberg-Dinkel N.** 2014. Insights into the biosynthesis and assembly of cryptophycean phycobiliproteins. *J Biol Chem* **289**(39):26691-26707.
- Palmer JD, Soltis DE, Chase MW.** 2004. The plant tree of life: an overview and some points of view. *Am J Bot* **91**(10):1437-1445.
- Pandey KD, Shukla SP, Shukla PN, Giri DD, Singh JS, Singh P, Kashyap AK.** 2004. Cyanobacteria in antarctica: Ecology, physiology and cold adaptation. *Cell Mol Biol* **50**(5):575-84.
- Pauls J.** 2014. Charakterisierung von Phycobiliproteinlyasen aus marinen Cyanophagen. Master thesis. Ruhr University Bochum.
- Peng P-P, Dong L-L, Sun Y-F, Zeng X-L, Ding W-L, Scheer H, Yang X, Zhao K-H.** 2014. The structure of allophycocyanin B from *Synechocystis* PCC 6803 reveals the structural basis for the extreme redshift of the terminal emitter in phycobilisomes. *Acta Crystallogr D* **70**(10):2558-2569.

- Peter E, Grimm B.** 2009. GUN4 is required for posttranslational control of plant tetrapyrrole biosynthesis. *Mol Plant* **2**(6):1198-1210.
- Pittera J.** 2015. Adaptations des cyanobactéries marines du genre *Synechococcus* au gradient latitudinal de température. Dissertation. Université Pierre et Marie Curie.
- Plank T, Anderson LK.** 1995. Heterologous assembly and rescue of stranded phycocyanin subunits by expression of a foreign *cpcBA* operon in *Synechocystis* sp. strain 6803. *J Bacteriol* **177**(23):6804–6809.
- Plank T, Toole C, Anderson LK.** 1995. Subunit interactions and protein stability in the cyanobacterial light-harvesting proteins. *J Bacteriol* **177**(23):6798-6803.
- Puzorjov A, Dunn KE, McCormick AJ.** 2021. Production of thermostable phycocyanin in a mesophilic cyanobacterium. *Metab Eng Commun* **13**:e00175.
- Rathbone HW, Michie KA, Landsberg MJ, Green BR, Curmi PMG.** 2021. Scaffolding proteins guide the evolution of algal light harvesting antennas. *Nat Commun* **12**(1):1890.
- Ratliff M, Zhu W, Deshmukh R, Wilks A, Stojiljkovic I.** 2001. Homologues of neisserial heme oxygenase in gram-negative bacteria: degradation of heme by the product of the *pigA* gene of *Pseudomonas aeruginosa*. *J Bacteriol* **183**(21):6394-6403.
- Raven JA, Evans MCW, Korb RE.** 1999. The role of trace metals in photosynthetic electron transport in O₂-evolving organisms. *Photosynth Res* **60**(2):111-150.
- Reuter W, Westermann M, Brass S, Ernst A, Boger P, Wehrmeyer W.** 1994. Structure, composition, and assembly of paracrystalline phycobiliproteins in *Synechocystis* sp. strain BO 8402 and of phycobilisomes in the derivative strain BO 9201. *J Bacteriol* **176**(3):896–904.
- Rhie GE, Beale SI.** 1995. Phycobilin biosynthesis: reductant requirements and product identification for heme oxygenase from *Cyanidium caldarium*. *Arch Biochem Biophys* **320**(1):182-194.
- Rocap G, Distel DL, Waterbury JB, Chisholm SW.** 2002. Resolution of *Prochlorococcus* and *Synechococcus* ecotypes by using 16S-23S ribosomal DNA internal transcribed spacer sequences. *Appl Environ Microbiol* **68**(3):1180-1191.
- Rockwell NC, Martin SS, Li F-W, Mathews S, Lagarias JC.** 2017. The phycocyanobilin chromophore of streptophyte algal phytochromes is synthesized by HY2. *New Phytol* **214**(3):1145-1157.
- Rogers MB, Gilson PR, Su V, McFadden GI, Keeling PJ.** 2006. The complete chloroplast genome of the chlorarachniophyte *Bigeloviella natans*: evidence for independent origins of chlorarachniophyte and euglenid secondary endosymbionts. *Mol Biol Evol* **24**(1):54-62.

- Romay C, Gonzalez R.** 2010. Phycocyanin is an antioxidant protector of human erythrocytes against lysis by peroxy radicals. *J Pharm Pharmacol* **52**(4):367-368.
- Sambrook J, Russell DW.** 2001. *In Vitro* amplification of DNA by the polymerase chain reaction., *Molecular cloning: a laboratory manual*, vol 2. Cold Spring Harbor Laboratory Press.
- Sato M, Kawaguchi T, Maeda K, Watanabe M, Ikeuchi M, Narikawa R, Watanabe S.** 2024. Functional modification of cyanobacterial phycobiliprotein and phycobilisomes through bilin metabolism control. *ACS Synth Biol* **13**(8):2391-2401.
- Saunée NA, Williams SR, Bryant DA, Schluchter WM.** 2008. Biogenesis of phycobiliproteins: II. CpcS-I and CpcU comprise the heterodimeric bilin lyase that attaches phycocyanobilin to CYS-82 of β -phycocyanin and CYS-81 of allophycocyanin subunits in *Synechococcus* sp. PCC 7002. *J Biol Chem* **283**(12):7513–7522.
- Scheer H, Zhao KH.** 2008. Biliprotein maturation: the chromophore attachment. *Mol Microbiol* **68**(2):263–276.
- Schirmer T, Huber R, Schneider M, Bode W, Miller M, Hackert ML.** 1986. Crystal structure analysis and refinement at 2.5 Å of hexameric C-phycocyanin from the cyanobacterium *Agmenellum quadruplicatum*. The molecular model and its implications for light-harvesting. *J Mol Biol* **188**(4):651–676.
- Schluchter WM, Shen G, Alvey RM, Biswas A, Saunée NA, Williams SR, Mille CA, Bryant DA.** 2010. Phycobiliprotein biosynthesis in cyanobacteria: structure and function of enzymes involved in post-translational modification. *Adv Exp Med Biol* **675**:211–228.
- Scholes GD.** 2010. Quantum-coherent electronic energy transfer: did nature think of it first? *J Phys Chem Lett* **1**(1):2–8.
- Searle GFW, Barber J, Porter G, Tredwell CJ.** 1978. Picosecond time-resolved energy transfer in *Porphyridium cruentum*. Part II. In the isolated light harvesting complex (phycobilisomes). *Biochim Biophys Acta Bioenerg* **501**(2):246-256.
- Sebesta J, Peebles CAM.** 2020. Improving heterologous protein expression in *Synechocystis* sp. PCC 6803 for alpha-bisabolene production. *Metab Eng Commun* **10**:e00117.
- Shen G, Schluchter WM, Bryant DA.** 2008. Biogenesis of phycobiliproteins: I. *cpcS-I* and *cpcU* mutants of the cyanobacterium *Synechococcus* sp. PCC 7002 define a heterodimeric phycocyanobilin lyase specific for β -phycocyanin and allophycocyanin subunits. *J Biol Chem* **283**(12):7503–7512.

- Six C, Thomas JC, Garczarek L, Ostrowski M, Dufresne A, Blot N, Scanlan DJ, Partensky F.** 2007. Diversity and evolution of phycobilisomes in marine *Synechococcus* spp.: a comparative genomics study. *Genome Biol* **8**(12):1-22.
- Sobotka R, Dühning U, Komenda J, Peter E, Gardian Z, Tichy M, Grimm B, Wilde A.** 2008. Importance of the cyanobacterial gun4 protein for chlorophyll metabolism and assembly of photosynthetic complexes. *J Biol Chem* **283**(38):25794-25802.
- Sommer MS, Gould SB, Lehmann P, Gruber A, Przyborski JM, Maier U-G.** 2007. Der1-mediated preprotein import into the periplastid compartment of chromalveolates? *Mol Biol Evol* **24**(4):918-928.
- Sommerkamp JA, Frankenberg-Dinkel N, Hofmann E.** 2019. Crystal structure of the first eukaryotic bilin reductase GtPEBB reveals a flipped binding mode of dihydrobiliverdin. *J Biol Chem* **294**(38):13889-13901.
- Stanier RY, Kunisawa R, Mandel M, Cohen-Bazire G.** 1971. Purification and properties of unicellular blue-green algae (order Chroococcales). *Bacteriol Rev* **35**(2):171-205.
- Steglich C, Mullineaux CW, Teuchner K, Hess WR, Lokstein H.** 2003. Photophysical properties of *Prochlorococcus* marinus SS120 divinyl chlorophylls and phycoerythrin *in vitro* and *in vivo*. *FEBS Lett* **553**(1-2):79-84.
- Steglich C, Frankenberg-Dinkel N, Penno S, Hess WR.** 2005. A green light-absorbing phycoerythrin is present in the high-light-adapted marine cyanobacterium *Prochlorococcus* sp. MED4. *Environ Microbiol* **7**(10):1611–1618.
- Steiner JM, Pompe JA, Löffelhardt W.** 2003. Characterization of *apcC*, the nuclear gene for the phycobilisome core linker polypeptide L_{C7.8} from the glaucocystophyte alga *Cyanophora paradoxa*. Import of the precursor into isolated cyanelles and integration of the mature protein into intact phycobilisomes. *Curr Genet* **44**(3):132-137.
- Stoebe B, Maier U-G.** 2002. One, two, three: nature's tool box for building plastids. *Protoplasma* **219**(3):123-130.
- Storf M, Parbel A, Meyer M, Strohmam B, Scheer H, Deng MG, Zheng M, Zhou M, Zhao KH.** 2001. Chromophore attachment to biliproteins: specificity of PecE/PecF, a lyase-isomerase for the photoactive 31-Cys- α 84-phycoviolobilin chromophore of phycoerythrocyanin. *Biochem* **40**(41):12444–12456.
- Studier FW, Moffatt BA.** 1986. Use of bacteriophage T7 RNA polymerase to direct selective high-level expression of cloned genes. *J Mol Biol* **189**(1):113-130.
- Sugishima M, Wada K, Fukuyama K, Yamamoto K.** 2020. Crystal structure of phytochromobilin synthase in complex with biliverdin IX α , a key enzyme in the biosynthesis of phytochrome. *J Biol Chem* **295**(3):771-782.

- Sui SF.** 2021. Structure of phycobilisomes. *Annu Rev Biophys* **50**:53-72.
- Tamara S, Hoek M, Scheltema RA, Leney AC, Heck AJR.** 2019. A colorful pallet of B-phycoerythrin proteoforms exposed by a multimodal mass spectrometry approach. *Chem* **5**(5):1302-1317.
- Terry MJ, Wahleithner JA, Lagarias JC.** 1993. Biosynthesis of the plant photoreceptor phytochrome. *Arch Biochem Biophys* **306**(1):1-15.
- Thangam R, Suresh V, Asenath Princy W, Rajkumar M, SenthilKumar N, Gunasekaran P, Rengasamy R, Anbazhagan C, Kaveri K, Kannan S.** 2013. C-phycoerythrin from *Oscillatoria tenuis* exhibited an antioxidant and *in vitro* antiproliferative activity through induction of apoptosis and G0/G1 cell cycle arrest. *Food Chem* **140**(1):262-272.
- Thiel K, Mulaku E, Dandapani H, Nagy C, Aro EM, Kallio P.** 2018. Translation efficiency of heterologous proteins is significantly affected by the genetic context of RBS sequences in engineered cyanobacterium *Synechocystis* sp. PCC 6803. *Microb Cell Fact* **17**(1):1–12.
- Timmis JN, Ayliffe MA, Huang CY, Martin W.** 2004. Endosymbiotic gene transfer: organelle genomes forge eukaryotic chromosomes. *Nat Rev Genet* **5**(2):123-135.
- Tomazic N.** 2020. Untersuchungen zur Struktur und Spezifität der Phycobiliproteinlyase CPES aus *Guillardia theta*. Dissertation. Technische Universität Kaiserslautern.
- Tomazic N, Overkamp KE, Wegner H, Gu B, Mahler F, Aras M, Keller S, Pierik AJ, Hofmann E, Frankenberg-Dinkel N.** 2021. Exchange of a single amino acid residue in the cryptophyte phycobiliprotein lyase GtCPES expands its substrate specificity. *Biochim Biophys Acta Bioenerg* **1862**(12):148493.
- Toole CM, Plank TL, Grossman AR, Anderson LK.** 1998. Bilin deletions and subunit stability in cyanobacterial light-harvesting proteins. *Mol Microbiol* **30**(3):475-486.
- Towbin H, Staehelin T, Gordon J.** 1979. Electrophoretic transfer of proteins from polyacrylamide gels to nitrocellulose sheets: procedure and some applications. *Proc Natl Acad Sci* **76**(9):4350-4354.
- Ughy B, Ajlani G.** 2004. Phycobilisome rod mutants in *Synechocystis* sp. strain PCC6803. *Microbiol* **150**(12):4147-4156.
- Ungerer J, Tao L, Davis M, Ghirardi M, Maness P-C, Yu J.** 2012. Sustained photosynthetic conversion of CO₂ to ethylene in recombinant cyanobacterium *Synechocystis* 6803. *Energ Environ Sci* **5**(10):8998-9006.
- van der Weij-De Wit CD, Doust AB, van Stokkum IHM, Dekker JP, Wilk KE, Curmi PMG, Scholes GD, van Grondelle R.** 2006. How energy funnels from the phycoerythrin antenna complex to photosystem I and photosystem II in cryptophyte *Rhodomonas* CS24 cells. *J Phys Chem B* **110**(49):25066-25073.

- Varman AM, Xiao Y, Pakrasi HB, Tang YJ.** 2013. Metabolic engineering of *Synechocystis* sp. strain PCC 6803 for isobutanol production. *Appl Environ Microbiol* **79**(3):908-914.
- Vasudevan R, Gale GAR, Schiavon AA, Puzorjov A, Malin J, Gillespie MD, Vavitsas K, Zulkower V, Wang B, Howe CJ, Lea-Smith DJ, McCormick AJ.** 2019. Cyanogate: a modular cloning suite for engineering cyanobacteria based on the plant moclo syntax. *Plant Physiol* **180**(1):39–55.
- Veetil VP, Angermayr SA, Hellingwerf KJ.** 2017. Ethylene production with engineered *Synechocystis* sp. PCC 6803 strains. *Microb Cell Fact* **16**(1):1–11.
- Vinyard DJ, Ananyev GM, Dismukes CG.** 2013. Photosystem II: the reaction center of oxygenic photosynthesis. *Annu Rev Biochem* **82**(1):577-606.
- Wallner T, Hagiwara Y, Bernát G, Sobotka R, Reijerse EJ, Frankenberg-Dinkel N, Wilde A.** 2012. Inactivation of the conserved open reading frame *ycf34* of *Synechocystis* sp. PCC 6803 interferes with the photosynthetic electron transport chain. *Biochim Biophys Acta Bioenerg* **1817**(11):2016–2026.
- Wang B, Eckert C, Maness PC, Yu J.** 2018. A genetic toolbox for modulating the expression of heterologous genes in the cyanobacterium *Synechocystis* sp. PCC 6803. *ACS Synth Biol* **7**(1):276–286.
- Wang Q, Hall CL, Al-Adami MZ, He Q.** 2010. IsiA is required for the formation of photosystem I supercomplexes and for efficient state transition in *Synechocystis* PCC 6803. *PLoS ONE* **5**(5):e10432.
- Ward DM, Ferris MJ, Nold SC, Bateson MM.** 1998. A natural view of microbial biodiversity within hot spring cyanobacterial mat communities. *Microbiol Mol Biol Rev* **62**(4):1353-1370.
- Weber E, Engler C, Gruetzner R, Werner S, Marillonnet S.** 2011. A modular cloning system for standardized assembly of multigene constructs. *PLoS ONE* **6**(2):e16765.
- Wedemayer GJ, Wemmer DE, Glazer AN.** 1991. Phycobilins of cryptophycean algae: structures of novel bilins with acryloyl substituents from phycoerythrin 566. *J Biol Chem* **266**(8):4731–4741.
- Wedemayer GJ, Kidd DG, Wemmer DE, Glazer AN.** 1992. Phycobilins of cryptophycean algae. Occurrence of dihydrobiliverdin and mesobiliverdin in cryptomonad biliproteins. *J Biol Chem* **267**(11):7315–7331.
- Wegele R, Tasler R, Zeng Y, Rivera M, Frankenberg-Dinkel N.** 2004. The heme oxygenase (s)-phytochrome system of *Pseudomonas aeruginosa*. *J Biol Chem* **279**(44):45791-45802.

- Wemmer DE, Wedemayer GJ, Glazer AN.** 1993. Phycobilins of cryptophycean algae. Novel linkage of dihydrobiliverdin in a phycoerythrin 555 and a phycocyanin 645. *J Biol Chem* **268**(3):1658–1669.
- Wiethaus J, Busch AWU, Kock K, Leichert LI, Herrmann C, Frankenberg-Dinkel N.** 2010. CpeS is a lyase specific for attachment of 3Z-PEB to Cys82 of β -phycoerythrin from *Prochlorococcus marinus* MED4. *J Biol Chem* **285**(48):37561–37569.
- Wijffels RH, Kruse O, Hellingwerf KJ.** 2013. Potential of industrial biotechnology with cyanobacteria and eukaryotic microalgae. *Curr Opin Biotechnol* **24**(3):405-413.
- Wilde A, Mikolajczyk S, Alawady A, Lokstein H, Grimm B.** 2004. The *gun4* gene is essential for cyanobacterial porphyrin metabolism. *FEBS Lett* **571**(1):119-123.
- Wilk KE, Harrop SJ, Jankova L, Edler D, Keenan G, Sharples F, Hiller RG, Curmi PMG.** 1999. Evolution of a light-harvesting protein by addition of new subunits and rearrangement of conserved elements: crystal structure of a cryptophyte phycoerythrin at 1.63-Å resolution. *Proc Natl Acad Sci* **96**(16):8901–8906.
- Wilks A.** 2002. Heme oxygenase: evolution, structure, and mechanism. *Antioxid Redox Signal* **4**(4):603-14.
- Wilks A, Barker KD.** 2011. Mechanisms of heme uptake and utilization in bacterial pathogens, p 357–398, *Handbook of Porphyrin Science*, vol 15. World Scientific.
- Williams JGK.** 1988. Construction of specific mutations in photosystem II photosynthetic reaction center by genetic engineering methods in *Synechocystis* 6803, p 766-778, *Methods in Enzymology*, vol 167. Academic Press.
- Yadava A, Ockenhouse CF.** 2003. Effect of codon optimization on expression levels of a functionally folded malaria vaccine candidate in prokaryotic and eukaryotic expression systems. *Infect Immun* **71**(9):4961-4969.
- Yalcin YS, Aydin BN, Sayadujhara M, Sittler V.** 2022. Antibiotic-induced changes in pigment accumulation, photosystem II, and membrane permeability in a model cyanobacterium. *Front Microbiol* **13**:930357.
- Yu F, Haynes SE, Teo GC, Avtonomov DM, Polasky DA, Nesvizhskii AI.** 2020. Fast quantitative analysis of timsTOF PASEF data with MSFragger and IonQuant. *Mol Cell Proteomics* **19**(9):1575-1585.
- Yu T-H, Tan S-I, Yi Y-C, Xue C, Ting W-W, Chang J-J, Ng IS.** 2022. New insight into the codon usage and medium optimization toward stable and high-level 5-aminolevulinic acid production in *Escherichia coli*. *Biochem Eng J* **177**:108259.
- Zavřel T, Chmelík D, Sinetova MA, Červený J.** 2018. Spectrophotometric determination of phycobiliprotein content in cyanobacterium *Synechocystis*. *J Vis Exp* **2018**(139):1–9.

- Zhang J, Ma J, Liu D, Qin S, Sun S, Zhao J, Sui S-F.** 2017. Structure of phycobilisome from the red alga *Griffithsia pacifica*. *Nature* **551**(7678):57-63.
- Zhang W, Willows RD, Deng R, Li Z, Li M, Wang Y, Guo Y, Shi W, Fan Q, Martin SS, Rockwell NC, Lagarias JC, Duanmu D.** 2021. Bilin-dependent regulation of chlorophyll biosynthesis by GUN4. *Proc Natl Acad Sci* **118**(20):e2104443118.
- Zhang Y-Z, Li K, Qin B-Y, Guo J-P, Zhang Q-B, Zhao D-L, Chen X-L, Gao J, Liu L-N, Zhao L-S.** 2024. Structure of cryptophyte photosystem II–light-harvesting antennae supercomplex. *Nat Commun* **15**(1):4999.
- Zhao C, Hoppner A, Xu QZ, Gartner W, Scheer H, Zhou M, Zhao KH.** 2017. Structures and enzymatic mechanisms of phycobiliprotein lyases CpcE/F and PecE/F. *Proc Natl Acad Sci U S A* **114**(50):13170-13175.
- Zhao K-H, Deng M-G, Zheng M, Zhou M, Parbel A, Storf M, Meyer M, Strohmann B, Scheer H.** 2000. Novel activity of a phycobiliprotein lyase: both the attachment of phycocyanobilin and the isomerization to phycoviolobilin are catalyzed by the proteins PecE and PecF encoded by the phycoerythrocyanin operon. *FEBS Lett* **469**(1):9-13.
- Zhao K-H, Wu D, Wang L, Zhou M, Storf M, Bubenzer C, Strohmann B, Scheer H.** 2002. Characterization of phycoviolobilin phycoerythrocyanin- α 84-cystein-lyase- (isomerizing) from *Mastigocladus laminosus*. *Eur J Biochem* **269**(18):4542-4550.
- Zhao K-H, Su P, Böhm S, Song B, Zhou M, Bubenzer C, Scheer H.** 2005. Reconstitution of phycobilisome core–membrane linker, L_{CM}, by autocatalytic chromophore binding to ApcE. *Biochim Biophys Acta Bioenerg* **1706**(1):81-87.
- Zhao KH, Zhang J, Tu JM, Böhm S, Plöschner M, Eichacker L, Bubenzer C, Scheer H, Wang X, Zhou M.** 2007. Lyase activities of CpcS- and CpcT-like proteins from *Nostoc* PCC7120 and sequential reconstitution of binding sites of phycoerythrocyanin and phycocyanin β -subunits. *J Biol Chem* **282**(47):34093–34103.
- Zhao L-S, Wang P, Li K, Zhang Q-B, He F-Y, Li C-Y, Su H-N, Chen X-L, Liu L-N, Zhang Y-Z.** 2023. Structural basis and evolution of the photosystem I–light-harvesting supercomplex of cryptophyte algae. *The Plant Cell* **35**(7):2449-2463.
- Zhou J, Gasparich GE, Stirewalt VL, Lorimier Rd, Bryant DA.** 1992. The *cpcE* and *cpcF* genes of *Synechococcus* sp. PCC 7002. Construction and phenotypic characterization of interposon mutants. *J Biol Chem* **267**(23):16138–16145.
- Zhou J, Zhang H, Zhang Y, Li Y, Ma Y.** 2012. Designing and creating a modularized synthetic pathway in cyanobacterium *Synechocystis* enables production of acetone from carbon dioxide. *Metab Eng* **14**(4):394-400.

- Zhou J, Zhang H, Meng H, Zhu Y, Bao G, Zhang Y, Li Y, Ma Y.** 2014a. Discovery of a super-strong promoter enables efficient production of heterologous proteins in cyanobacteria. *Sci Rep* **4**(1):4500.
- Zhou W, Ding W-L, Zeng X-L, Dong L-L, Zhao B, Zhou M, Scheer H, Zhao K-H, Yang X.** 2014b. Structure and mechanism of the phycobiliprotein lyase CpcT. *J Biol Chem* **289**(39):26677-26689.
- Zhu C, Ling Q, Cai Z, Wang Y, Zhang Y, Hoffmann PR, Zheng W, Zhou T, Huang Z.** 2016. Selenium-containing phycocyanin from Se-enriched *Spirulina platensis* reduces inflammation in dextran sulfate sodium-induced colitis by inhibiting NF- κ B activation. *J Agric Food Chem* **64**(24):5060-5070.
- Zwirgmaier K, Jardillier L, Ostrowski M, Mazard S, Garczarek L, Vaultot D, Not F, Massana R, Ulloa O, Scanlan DJ.** 2008. Global phylogeography of marine *Synechococcus* and *Prochlorococcus* reveals a distinct partitioning of lineages among oceanic biomes. *Environ Microbiol* **10**(1):147-161.

Appendix

DNA sequences (5'-3') used for heterologous expression in *E. coli*:

>*cpcX* of the cryptophyte *Guillardia theta*

```
AACTCTGCTTGTGTGAGAGAAGCGGCGGTGAAGGGCTTGGCGATGATATCGGAGAAGGGAAACCGC
AACGTTGTGCTCGCCATGGCCGAAGTGGTCGAGGAGGAGAGAGCCATCACTGTGAGGAGTGCAGCG
CTGCAAGCTCTGACAAGGGTGGCTGAGAGGGGGGACGAGGTAGCTGTGCGCCTGTGCTGAAGCTG
CTGCGGCGGGTTGAGGGCACAGAGAGAGGAGATTTCTTCTCCCCTCACCTCTCCCCATCATCAGCA
AGAATGCTGCCAAGGCCCTAGGTAGCCTAGCAGAGTACGGAGACCTCAAGGCCCTCAAGGCGCTTC
ACCTGCGCGTATTGGACGATCCGAACCCTGTGGTGAGGGAAGCAGCTGCGCGAGCACTTGGGAGCA
TTGCGAACATGGGTGACCGGCAAGTGATCTTCGCCCTCACGATCTGCCTGGAGGACGAGGACGAGG
GAGTTGACGGTCAGCGATGAGGAGCCTCAAGTCGTTGAAGAAGAAGGAGAAGGACGACGGAAGCC
TGAGCGACTTACTTGCGGAGGAGGACGACATGCTCGAGTGGTACGCGACGTGGTTGTGGCTGGTTC
CTCTAGCGTGGGACTGC
```

DNA sequences used for heterologous expression in *Synechocystis*:

>*pebS* of the *Prochlorococcus* phage P-SSM2

```
ATGACTAAAAACCCAAGAAATAACAAACCAAAAAAGATTTAGATTCATCTTATAAATCTAAAACAATCT
GGCAAAATTATATTGATGCTCTATTTGAAACATTTCCACAGTTAGAAATATCTGAGGTATGGGCAAAAT
GGGATGGTGGGAACGTCACTAAGGACGGTGGAGATGCTAAACTTACAGCAAAATATCCGTACAGGAGA
ACACTTTCTAAAGGCAAGAGAGGCACACATAGTAGATCCTAACTCTGACATATAACAATACCATACTCTA
TCCTAAAACAGGAGCAGATCTGCCTTGTGTTTGGTATGGATCTGATGAAGTTTAGTGATAAGAAGGTCA
TTATAGTATTTGACTTCCAGCATCCAAGAGAGAAGTATCTGTTCTCTGTTGATGGACTACCCGAAGATG
ATGGTAAGTATAGATTCTTTGAAATGGGTAATCATTCTCTAAGAATATCTTTGTAAGATACTGTAAACC
TGATGAAGTGGATCAATATCTTGATACCTTTAAATTATACTTGACAAAGTATAAAGAGATGATAGATAAC
AATAAACCTGTTGGTGAAGATACCACAGTCTATAGTACTTTGATACTTATATGACTGAACTTGATCCT
GTTAGAGGATATATGAAGAATAAGTTTGGTGGAGGGTAGATCAGAGGCATTTGTAACGATTTCCTTTTT
TCATACAAATAA
```

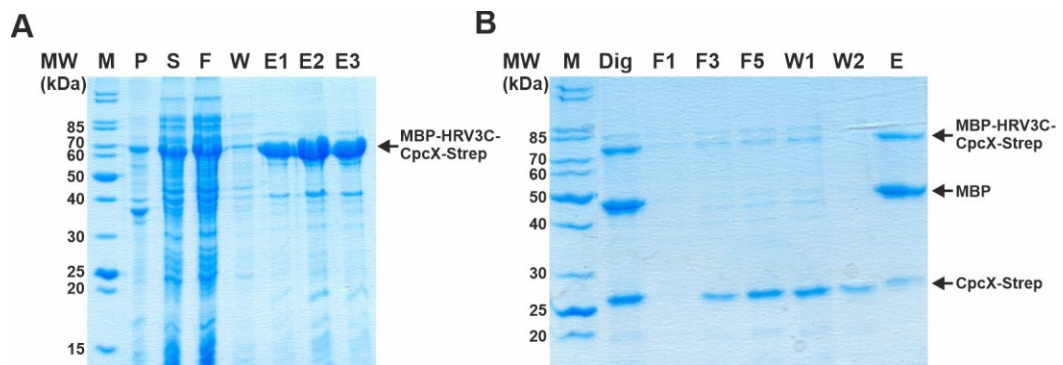
>*cpeB* of *Prochlorococcus marinus* MED4 (*PmcpeB*)

```
ATGACAGTTTCAAAGAGTAATCAAATTTATCAAATGATAGAGATTTAGAAAATATAAGTAATAAAAAATA
TTGAAGATATAAAAGAATTTATTAATACTGCAAACTCAAGATTAGATGCAATAGATTCAATAACAAATAA
TTCTCACGCAATTGCCGCTGATGCTGTGACTGCAATGATTTGTGAAAATCAAGATTCAGTTAATACAAA
AATATCTTTAGATACCACCAATAAGATGTCTGTTTGTCTAAGAGATGGAGAAAATAATTTTAAGGATTGTT
TCTTACCTTTTGATTTCTGATGACGAATCAGTTTTATCTAAAACTGTTTAAAGGATCTTAAAAATACTTA
TTTGGCCCTTGGTGTACCTCTGAAAAATGCTATCCGAGTTTTTGAATTGATGAGAGATGCAACGATTTTC
TGATTTAAAGTCTACTGTAAATTCTATGAAAGGAGAAAAAGAATTTCTTCTGATTTAATTTCTAATACA
GAGTTTCAATTTGAGAGAATAATTAATCTTTTAAG
```

>*cpeS* of *Prochlorococcus marinus* MED4 (*PmcpeS*)

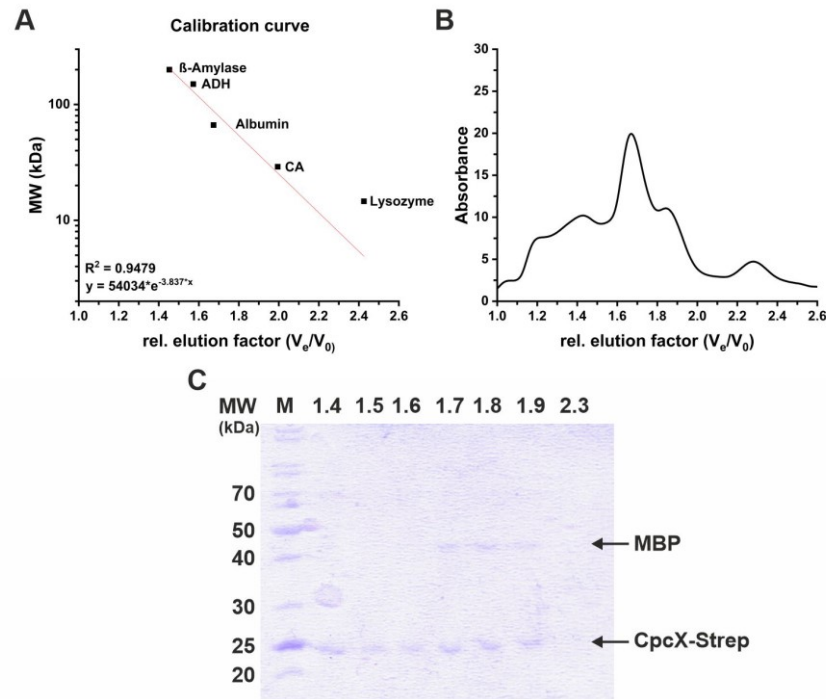
ATGTTGACGAAGAATCTAATAACAATTAATCAATTTATTCAAAAAAGTTTAGGAGAGTGGAATCCATAA
 GAAGCACTCACTCTTTGGCTTTTCAGGAAGTTGAAAATTCAGCAAAATAGAAATAAAAGAGTTAG
 AAAGCAATAATAAAAAATGTTTTAGGACTTTTAGAAAAATATAATTACACCTCTAACCTTCTTTTATTGCA
 TTATCAATAAGTTGGAAGGCAATAAGTGATTGGGAGATTGATCAAAAAATTGAACAAGATAAACTATA
 TTATTATTTTTACCAAAGGATAAAAATAAGGGGATTGTTCTACGTAATAAGGGATATACTGAATCCGTG
 ATTTTCATCATCAGAATATTTGATTGATGAAAATGAGAACTTAAATATTTAAACTATTTATAGTTCAACAG
 CTTCTGAAGAGAGAATTTGTTTTTATCAAATCATATTAGATCCAGATATTCAGTAATTAGAAATAATGA
 AAACAATACCGTAATACAAACCTCACACACATCAGAGATAAGAAATATGTCTATCTTAAAAGAT

Production of recombinant CpcX from *G. theta* in *E. coli* and protein isolation



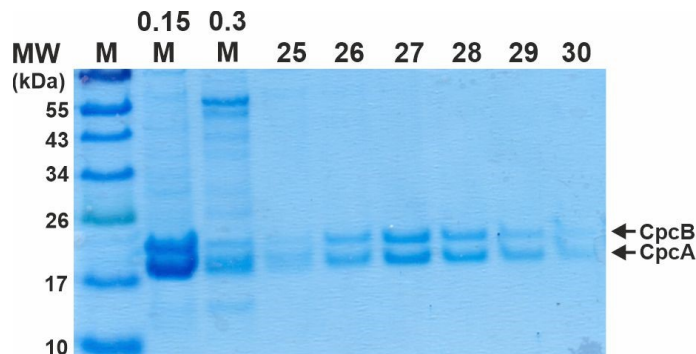
Appendix Figure A1: SDS-PAGE analysis of the purification of recombinant CpcX from *G. theta* in *E. coli*. The protein fusion variant MBP-HRV3C-CpcX-Strep was produced in *E. coli* pLysS and purified via two rounds of affinity chromatography. The theoretical molecular masses for MBP-HRV3C-CpcX-Strep, MBP and CpcX-Strep are ~66.9 kDa, ~42.8 kDa and ~24.2 kDa, respectively. As a reference, the molecular mass standard Unstained Protein Standard, Broad Range (10 – 200 kDa) was applied (M) (A) Following cell lysis, MBP-HRV3C-CpcX-Strep was purified via the StrepII-tag using Strep-Tactin® Sepharose. P: insoluble lysate fraction (pellet); S: soluble lysate fraction (supernatant); F: Flowthrough; W: Washing fraction; E: Elution fractions. (B) After the purification via Strep-Tactin® Sepharose, the recombinant protein (E1-E3) was digested with PreScission® Protease to remove the MPB-tag from the MBP-HRV3C-CpcX-Strep protein variant (Dig). Removal of the free MBP-tag was performed via a second round of affinity chromatography using amylose resin. While the free MBP-tag and the remaining full-length protein variant bind to the column resin, cleaved CpcX-Strep was collected in the Flowthrough (F1 to F3) and Washing fractions (W1 and W2). Eventually, residual proteins were eluted from the amylose resin (E).

Determination of the CpcX oligomerization state by size-exclusion chromatography



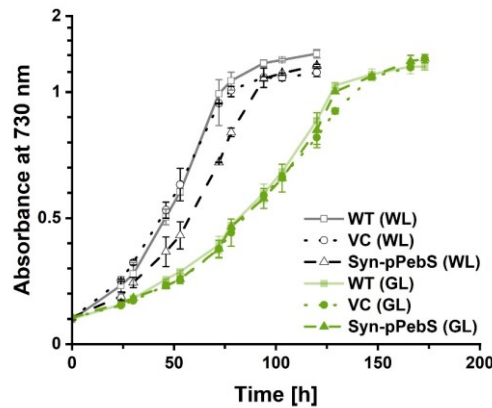
Appendix Figure A2: Determination of CpcX oligomerization state. After the purification of CpcX-Strep (Appendix Figure A1B), the protein was analyzed for its oligomerization state via size-exclusion chromatography. The theoretical molecular masses for MBP and CpcX-Strep are ~42.8 kDa and ~24.2 kDa, respectively (**A**) For recombinant protein analysis, a calibration curve with a R^2 of 0.9479 was recorded using commercial proteins with known molecular masses (Gel Filtration Markers Kit 29 – 700 kDa). ADH: alcohol dehydrogenase, CA: carbonic anhydrase; V_e : Elution volume; V_0 : Void volume. (**B**) Chromatogram of recombinant CpcX-Strep (Appendix Figure A1B, combined fractions F3, F5, W1 and W2) after size-exclusion chromatography by absorbance readings at 280 nm plotted against the relative elution factor V_e/V_0 . (**C**) SDS-PAGE analysis of elution fractions after size-exclusion chromatography. M: Unstained Protein Standard, Broad Range (10 – 200 kDa); 1.4 to 2.3: Elution fractions according to the relative elution factor V_e/V_0 .

Purification of PC from the *Synechocystis* transconjugant Syn-pPebS



Appendix Figure A3: Purification of native PC from the *pebS*-complemented *Synechocystis* strain Syn-pPebS. Shown is the protein content analysis via SDS-PAGE of fractions after ion-exchange- (0.15 M and 0.3 M NaCl elution fractions) and size-exclusion chromatography (25 to 30). PC is composed of the CpcB -subunit and the CpcA -subunit, their molecular masses are ~19.3 kDa and ~18.2 kDa, respectively. The molecular mass standard Color Prestained Protein Standard, Broad Range (10 – 250 kDa) was used as a reference.

Growth of Syn-pPebS under green light illumination



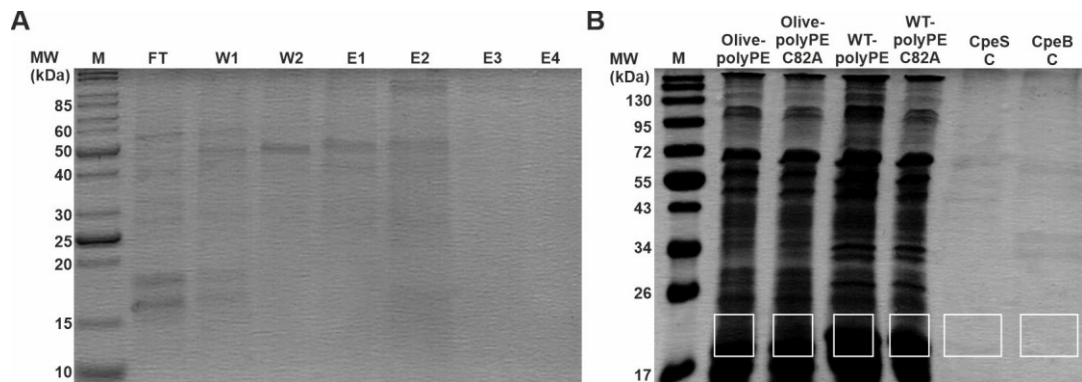
Appendix Figure A4: Growth of *Synechocystis* strains under green light illumination. Shown is the absorbance at 730 nm for the *Synechocystis* WT (solid lines), the VC (dotted lines) and Syn-pPebS (dashed lines) measured during growth under white- (WL) and green (GL) light. Cultures were grown at a light intensity of $22 \mu\text{mol}/(\text{m}^2\cdot\text{s})$, 100 rpm and RT. Data is displayed as means \pm SD of $n = 2$.

Polycistronic expression construct for the assembly of the *P. marinus* MED4 PE in *Synechocystis*



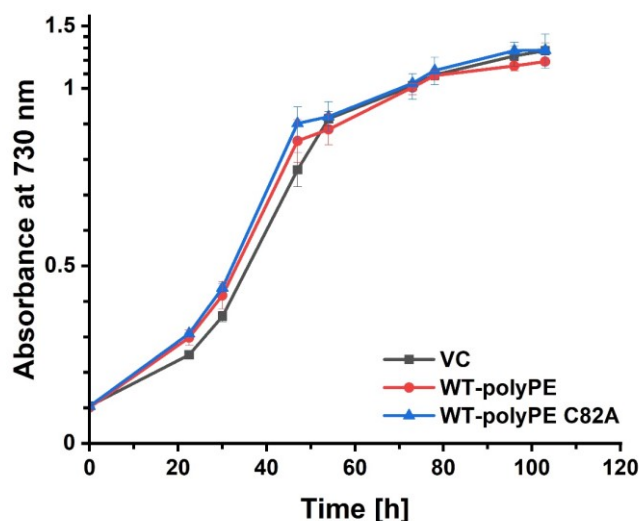
Appendix Figure A5: Polycistronic construct in pCGT.STH12 for the assembly of the *Prochlorococcus marinus* MED4 phycoerythrin in *Synechocystis*. The expression construct is composed of three genes consisting of *pebS* from the cyanophage P-SSM2 and the *P. marinus* MED4 genes *cpeB* and *cpeS*. Transcription of all three genes is controlled by the strong, light-responsive *cpc* promoter characterized in Vasudevan *et al.*, (2019). Termination of transcription is regulated by the *rnb* terminator from Gale *et al.*, (2021). DNA fragments for Golden-Gate assembly into the acceptor vector pCAT.000 were prepared by PCR (chapter 2.2.4) using the following oligonucleotides to generate compatible overhangs which include the RBSs for *PmcpeB-Strep* and *PmcpeS-His*: TGCC- P_{cpc} -*pebS*-GCAA fw and rv; GCAA-*PmcpeB-Strep*-ACTA fw and rv; ACTA-*PmcpeS-His*- T_{rnb} -GGGA fw and rv. The final construct, pCGT.STH10 was introduced into the *Synechocystis* WT and the olive mutant yielding the strains WT-polyPE and Olive-polyPE, respectively. As a control, the cysteine residue 82 of *PmcpeB-Strep* was substituted in pCGT.STH13 by an alanine via side directed mutagenesis of the corresponding DNA fragment. The construct was introduced into the *Synechocystis* WT and the olive mutant leading to the transconjugants WT-polyPE C82A and Olive-polyPE C82A, respectively. Created with BioRender.com

Purification of recombinant *PmCpeS*-His from WT-PE and evaluation of recombinant protein production in transconjugants harbouring polycistronic expression constructs.



Appendix Figure A6: Purification of *PmCpeS*-His from WT-PE and assessment of recombinant protein production derived from polycistronic expression constructs. The theoretical molecular weight for *PmCpeS*-His and *PmCpeB*-Strep are 22.2 kDa and 20.8 kDa, respectively. **(A)** SDS-PAGE analysis of the purification of *PmCpeS*-His via affinity chromatography. FT: Flowthrough; W1 and W2: Washing fractions; E1 to E4: Elution fractions. As a reference for molecular masses, the Unstained Protein Standard, Broad Range (10 – 200 kDa) was used (M). **(B)** Electrophoretic protein separation of transconjugant *Synechocystis* strains Olive polyPE and WT polyPE as well as Olive polyPE C82A and WT polyPE C82A harboring the vectors pCGT.STH12 and pCGT.STH13, respectively. In addition, concentrated elution fractions of the purification of *PmCpeS*-His (CpeS C) in (A) and *PmCpeB*-Strep (CpeB C) (in Figure 31A) derived from WT-PE were analyzed for their protein content via SDS-PAGE. The Blue Prestained Protein Standard, Broad Range (11 – 250 kDa) was used as a reference (M). White boxes covering the molecular masses between ~19 kDa and ~23 kDa indicate the area of sample extraction for peptide-derived protein identification via LC-MS. In the extracted sample of CpeS C, the protein *PmCpeS*-His was detected. No recombinant proteins were detected in the remaining samples. Consequently, *PmCpeB*-Strep from WT-PE was not purified and no recombinant proteins were produced in the strains containing polycistronic constructs for PE assembly (Olive-polyPE, Olive-polyPE C82A, WT-polyPE and WT-polyPE C82A).

Growth of transconjugant *Synechocystis* WT harbouring polycistronic constructs for PE assembly



Appendix Figure A7: Phototrophic growth of *Synechocystis* WT transconjugants harbouring polycistronic constructs for the phycoerythrin assembly of *P. marinus* MED4. Absorbance measurements of *Synechocystis* VC (black), WT-polyPE (red) and WT-polyPE C82A (blue) culture densities at a wavelength of 730 nm. Shown are the mean values \pm SD of $n = 3$.

Curriculum vitae

Persönliche Daten

Steffen Heck

Studium und schulische Laufbahn

Seit 06/2024	Naturwissenschaftler (MVZ Dr. Limbach & Kollegen, Heidelberg)
10/2020 – 03/2024	Doktorand/Wissenschaftlicher Mitarbeiter (TU Kaiserslautern; ab 01/2023 RPTU Kaiserslautern) in der Abteilung für Mikrobiologie von Prof. Dr. Nicole Frankenberg-Dinkel
09/2017 - 07/2020	Studium der Biologie (Karlsruher Institut für Technologie) Abschluss: Master of Science
09/2013 - 04/2017	Studium der Angewandten Biologie (Karlsruher Institut für Technologie) Abschluss: Bachelor of Science
09.2004 – 09.2013	Abitur Humboldt-Gymnasium (Karlsruhe)

Präsentationen

04/2023	Vortrag	MibiNeXt Seminarreihe, Heinrich-Heine-Universität (Düsseldorf)
08/2022	Poster	International Symposium on Phototrophic Prokaryotes (Liverpool, UK)
02/2022	Poster	VAAM Jahrestagung (digital)

Publikationen

Heck, S., Sommer, F., Zehner, S., Schroda, M., Gehringer, M.M. & Frankenberg-Dinkel, N. (2024) Expanding the toolbox for phycobiliprotein assembly: phycoerythrobilin biosynthesis in *Synechocystis*. *Physiol Plant*, **176**(1), e14137.

Schuhmacher, L., **Heck, S.**, Pitz, M., Mathey, E., Lamparter, T., Blumhofer, A., Leister, K. & Fischer, R. (2024) The LOV-domain blue-light receptor *LreA* of *Alternaria alternata* binds predominantly FAD as chromophore and acts as light and temperature sensor. *J Biol Chem*, **300**: 107238

Eingeworbene Drittmittel

07/2022	Drittmittel	Scottish Universities Life Sciences Alliance (SULSA), 10.000€
---------	-------------	--

Eidesstattliche Erklärung

Erklärungen lt. § 6 (4) der Promotionsordnung des Fachbereichs Biologie vom 28.11.2018:

Ich erkläre wahrheitsgemäß, dass ich die eingereichte Dissertation selbst angefertigt und alle für die Arbeit benutzten Hilfsmittel und Hilfestellungen in der Arbeit angegeben habe. Die Dissertation oder Teile hiervon habe ich bisher nicht als Prüfungsarbeit für eine staatliche oder andere wissenschaftliche Prüfung eingereicht.

Ebenso habe ich die gleiche oder eine andere Abhandlung nicht bei einem anderen Fachbereich oder einer anderen Universität als Dissertation eingereicht.

Datum, Unterschrift Doktorand

Darlegung des Eigenanteil

Steffen Heck

Establishing a novel platform for phycobiliprotein assembly: biosynthesis of the pink pigment phycoerythrobilin in *Synechocystis*

Die Konzeption, die Planung, das Versuchsdesign und die Methodenentwicklung der vorliegenden Arbeit wurde in Teilen von Prof. Dr. Nicole Frankenberg-Dinkel, PD Dr. Susanne Zehner und Dr. Michelle Gehringer unterstützt. Die Literaturrecherche, die Datenerhebung, die Datenanalyse, die Interpretation und die Diskussion der Ergebnisse wurden, sofern im Folgenden nicht anders dargelegt, nicht von Dritten unterstützt.

Die Datenerhebung der in dieser Arbeit durchgeführten Fluoreszenzmikroskopie (CLSM) wurde durch die Bedienung des Zeiss LSM880 AxioObserver konfokalen laser-scanning Mikroskops von PD Dr. Susanne Zehner in Teilen ermöglicht. Die Datenerhebung der in dieser Arbeit durchgeführten massenspektrometrischen Analyse wurde durch die Bedienung des TripleTOF 6600 (gekoppelt an Eksigent Ekspert nanoLC 400) und des timsTOF Pro2 (gekoppelt an nanoElute) von Dr. Frederik Sommer (RPTU, Molekulare Biotechnologie und Systembiologie) in Teilen ermöglicht.

Der Wildtyp- und die Olive Mutante von *Synechocystis* sp. PCC 6803 wurden freundlicherweise von Alistair McCormick vom Institut für Molekulare Pflanzenwissenschaften (Universität von Edinburgh, Vereinigtes Königreich) zur Verfügung gestellt. Alle daraus resultierenden Konjugationsstämme wurden vom Autor dieser Arbeit generiert.

Teile dieser Arbeit wurden unter folgender Referenz veröffentlicht:

Heck, S., Sommer, F., Zehner, S., Schroda, M., Gehringer, M.M. & Frankenberg-Dinkel, N. (2024) Expanding the toolbox for phycobiliprotein assembly: phycoerythrobilin biosynthesis in *Synechocystis*. *Physiol Plant*, **176**(1), e14137.

Die ersten Entwürfe für diese Veröffentlichung wurden vom Autor dieser Dissertation angefertigt, die Fertigstellung des Manuskripts bis zur Einreichung wurde von Prof. Dr. Nicole Frankenberg-Dinkel und Dr. Michelle Gehringer in Teilen unterstützt.

Die vorliegende Einschätzung über die erbrachte Leistung von Dritten wurde mit den genannten Personen einvernehmlich abgestimmt.

Darlegung aller benutzten Hilfsmittel und Hilfestellungen

Steffen Heck

Establishing a novel platform for phycobiliprotein assembly: biosynthesis of the pink pigment phycoerythrobilin in *Synechocystis*

Die Analyse und Visualisierung der meisten Daten erfolgte mit Hilfe von Microsoft Excel (Microsoft, Version 2021), Origin (OriginLab, Version 2022) und Corel DRAW Graphics Suite (Corel Corporation, Version 2023). Für einige Abbildungen wurde BioRender.com verwendet und entsprechend in der Bildbeschreibung aufgeführt. Die Analyse und Visualisierung der Mikroskopie-bilder (CLSM) wurden über das Programm Zen (Zeiss, Version 2.3) durchgeführt. Alle folgenden Programme für die Analyse von massenspektrometrischen Daten wurde von Prof. Dr. Michael Schroda (RPTU, Molekulare Biotechnologie und Systembiologie) zur Verfügung gestellt. Die manuelle Analyse von massenspektrometrischen Daten erfolgte durch den Autor dieser Dissertation mit Hilfe von PeakView (ABSciex, Version 2.2). Die Zuordnung der Rohdaten über MS-Datenbanken wurde mit MaxQuant (Version 2.5.1.0) und der FragPipe Analysepipeline (Version 19.1) von Dr. Frederik Sommer (RPTU, Molekulare Biotechnologie und Systembiologie) durchgeführt. Die daraus resultierende Analyse wurde wiederum vom Autor dieser Dissertation durchgeführt.

Diese Arbeit wurde von Helen Wegner (Doktorandin, RPTU, Mikrobiologie) in Teilen Korrektur gelesen.

Datum, Unterschrift Doktorand

Datum, Unterschrift Betreuerin

Danksagung

An dieser Stelle möchte ich einen herzlichen Dank an meine Doktormutter Frau Prof. Dr. Nicole Frankenberg-Dinkel aussprechen. Ich bedanke mich für die Vergabe dieses spannenden Projektes, für viele hilfreiche Anregungen und die konstruktiven Vorschläge, die zur Form dieser Arbeit deutlich beigetragen haben. Ebenso möchte ich mich für die intensiven fachlichen Diskussionen und die Möglichkeiten außerhalb dieser Dissertation, wie das Anfertigen und Einreichen eines Forschungsantrags, bedanken.

Bei Prof. Dr. Matthias Hahn bedanke ich mich für die freundliche Übernahme des Korreferats. Außerdem möchte ich mich bei Prof. Dr. Michael Schroda für die Bereitschaft der Übernahme des Vorsitzes der Prüfungskommission bedanken.

Weiterhin gilt mein Dank PD Dr. Susanne Zehner für die tatkräftige Unterstützung bei der Aufnahme der schönen mikroskopischen Aufnahmen und Dr. Michelle Gehringer für die Vielzahl an Anregungen zur physiologischen Charakterisierung.

Bedanken möchte ich mich auch bei der kompletten Arbeitsgruppe Mikrobiologie an der RPTU für die spannende Zeit und eine entspannte Arbeitsatmosphäre. Am meisten möchte ich mich bei Helen Wegner bedanken, die meine Zeit als Doktorand noch schöner gemacht hat und mich hoffentlich noch für eine lange Zeit weiter begleitet.

Auch meiner Familie möchte ich für die stetige Unterstützung bei meiner Doktorarbeit und allen anderen Vorhaben danken. Ihr seid immer eine große Stütze, auf die ich zählen kann.